



HAL
open science

Activation of homogeneous and heterogeneous Fenton processes by ultrasound and ultraviolet/visible irradiations for the removal of ibuprofen in water

Sandyanto Adityosulindro

► **To cite this version:**

Sandyanto Adityosulindro. Activation of homogeneous and heterogeneous Fenton processes by ultrasound and ultraviolet/visible irradiations for the removal of ibuprofen in water. Chemical engineering. Institut National Polytechnique de Toulouse - INPT, 2017. English. NNT : 2017INPT0027 . tel-04221776

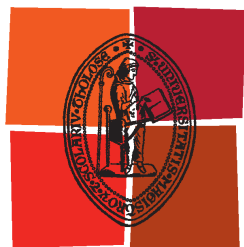
HAL Id: tel-04221776

<https://theses.hal.science/tel-04221776>

Submitted on 28 Sep 2023

HAL is a multi-disciplinary open access archive for the deposit and dissemination of scientific research documents, whether they are published or not. The documents may come from teaching and research institutions in France or abroad, or from public or private research centers.

L'archive ouverte pluridisciplinaire **HAL**, est destinée au dépôt et à la diffusion de documents scientifiques de niveau recherche, publiés ou non, émanant des établissements d'enseignement et de recherche français ou étrangers, des laboratoires publics ou privés.



Université
de Toulouse

THÈSE

En vue de l'obtention du

DOCTORAT DE L'UNIVERSITÉ DE TOULOUSE

Délivré par :

Institut National Polytechnique de Toulouse (INP Toulouse)

Discipline ou spécialité :

Génie des Procédés et de l'Environnement

Présentée et soutenue par :

M. SANDYANTO ADITYOSULINDRO

le vendredi 7 avril 2017

Titre :

Activation of homogeneous and heterogeneous Fenton processes by ultrasound and ultraviolet/visible irradiations for the removal of ibuprofen in water

Ecole doctorale :

Mécanique, Energétique, Génie civil, Procédés (MEGeP)

Unité de recherche :

Laboratoire de Génie Chimique (L.G.C.)

Directrices de Thèse :

MME CARINE JULCOUR

MME LAURIE BARTHE

Rapporteurs :

M. FRANK ERICH STUBER, UNIVERSITAT ROVIRA I VIRGILI TARRAGONA

M. STEPHANE BAUP, UNIVERSITE GRENOBLE ALPES

Membres du jury :

M. FRANK ERICH STUBER, UNIVERSITAT ROVIRA I VIRGILI TARRAGONA, Président
M. DOMINIQUE WOLBERT, ECOLE NATIONALE SUP DE CHIMIE DE RENNES, Membre

M. HENRI DELMAS, INP TOULOUSE, Membre

Mme CARINE JULCOUR, INP TOULOUSE, Membre

Mme LAURIE BARTHE, INP TOULOUSE, Membre

Author: Sandyanto ADITYOSULINDRO

Director of thesis: Dr. Carine JULCOUR-LEBIGUE and Dr. Laurie BARTHE

Title:

Activation of homogeneous and heterogeneous Fenton processes by ultrasound and ultraviolet/visible irradiations for the removal of ibuprofen in water

Abstract:

Due to booming consumption and only partial removal by conventional water treatment processes, ibuprofen, a non-steroidal anti-inflammatory drug, has been detected in water resources, raising increasing concerns for possible environmental and health impact. On the other hand, advanced oxidation processes (AOPs), among which Fenton reaction, have shown successful results for removal of various organic compounds. Traditionally based on the use of hydrogen peroxide and ferrous ions in solution, large-scale application of this AOP is still limited by narrow pH window (2 to 4) and uneasy recovery of iron catalyst.

This work investigated Fenton-based oxidation of ibuprofen, and reaction activation by ultrasound (US) irradiation and ultraviolet/visible light (UV/Vis) so as to lower the required concentration of dissolved iron catalyst or improve the activity of heterogeneous counterparts.

To that purpose, the efficacy of individual homogeneous AOPs (sonolysis, photolysis, ultrasound/H₂O₂, light/H₂O₂, Fenton oxidation) was evaluated first, varying operating parameters such as light wavelength and ultrasound frequency. Then, their two-by-two and overall combinations (sonophotolysis, sono-Fenton, photo-Fenton and sono-photo-Fenton oxidation) were examined with emphasis on the identification of synergistic effects. In particular, combined US/Fenton and Vis/Fenton oxidation were found more effective than the sum of individual processes due to sono- and photo-regeneration of ferrous ions. These results also served as a reference for the assessment of heterogeneous systems. Among tested solids, iron-containing zeolite (Fe-ZSM5 type) was shown to be a promising catalyst for peroxide oxidation of ibuprofen due to high efficiency at natural pH and low iron leaching. However, in this case, no more than additive effects was observed between ultrasound/light irradiation and heterogeneous Fenton oxidation. Beside pollutant and Total Organic Carbon conversion, main degradation products were monitored for different processes and some plausible degradation pathways were proposed. Water matrix impact was also addressed using wastewater plant effluent, which resulted into hindered performance of all oxidation processes either due to alkaline buffer or light attenuation effect.

Keywords: Water treatment, Advanced oxidation processes, Pharmaceuticals, Water matrix

This page is intentionally left blank

Auteur: Sandyanto ADITYOSULINDRO

Directrice de thèse: Dr. Carine JULCOUR-LEBIGUE et Dr. Laurie BARTHE

Titre:

Activation du procédé Fenton (homogène et hétérogène) par irradiation ultrasonore et rayonnement ultraviolet/visible pour l'élimination de l'ibuprofène dans l'eau

Résumé :

Du fait de sa consommation en plein essor et d'une élimination partielle par les procédés conventionnels de traitement des eaux, l'ibuprofène, un médicament anti-inflammatoire non stéroïdien, a été détecté dans les ressources en eau, suscitant de plus en plus d'inquiétude quant à son impact possible sur l'environnement et la santé. Par ailleurs, les procédés d'oxydation avancée (POA), parmi lesquels la réaction Fenton, ont montré d'excellents résultats pour l'élimination de divers composés organiques. Traditionnellement basé sur l'utilisation du peroxyde d'hydrogène et des ions ferreux en solution, l'application à grande échelle de ce POA est encore limitée par une fenêtre de pH étroite (2 à 4) et une récupération difficile du catalyseur à base de fer.

Ce travail a étudié l'oxydation Fenton de l'ibuprofène et l'activation de la réaction par irradiation ultrasonore (US) et rayonnement ultraviolet/visible (UV/Vis) et de manière à abaisser la concentration de fer dissous ou à améliorer l'activité de catalyseurs hétérogènes.

A cet effet, on a d'abord évalué l'efficacité des POA individuels homogènes (sonolyse, photolyse, sono- et photo-oxydation avec H_2O_2 , oxydation Fenton), en fonction de paramètres opératoires tels que la longueur d'onde lumineuse et la fréquence ultrasonore. Ensuite, on a examiné leurs combinaisons deux-par-deux et globale (sonophotolyse, oxydation sono-, photo- et sono-photo-Fenton) en mettant l'accent sur l'identification d'effets synergiques. En particulier, les oxydations US/Fenton et Vis/Fenton se sont révélées plus efficaces que la somme des procédés individuels grâce à la sono- et photo-régénération des ions ferreux. Ces résultats ont également servi de référence pour l'évaluation des systèmes hétérogènes. Parmi les solides testés, on a montré qu'une zéolite dopée au fer (de type Fe/ZSM5) était un catalyseur prometteur pour l'oxydation de l'ibuprofène par le peroxyde, en raison d'une efficacité élevée à pH naturel et d'une faible lixiviation du fer. Cependant, dans ce cas, on n'a observé au mieux qu'une addition d'effets des ultrasons ou de la lumière et de l'oxydation Fenton hétérogène. Outre la conversion du polluant et du carbone organique total (COT), la formation des principaux produits de dégradation a été suivie pour différents procédés et des voies possibles de dégradation ont été proposées. L'effet matrice a également été examiné en utilisant un effluent de station, qui a eu pour conséquence de réduire la performance de tous les procédés d'oxydation, en raison d'un pH tampon alcalin ou de l'atténuation de la lumière.

Mots-clés: Traitement d'eau, Procédés d'oxydation avancée, Médicaments, Effets matrice

This page is intentionally left blank

ACKNOWLEDGEMENT

This work was conducted at Laboratoire de Génie Chimique (LGC), INP-ENSIACET in Toulouse. Take a look behind the scenes, there are many people contributing in this successful work. First, I would like to express my sincere gratitude to my supervisors, Dr. Carine JULCOUR-LEBIGUE, and Dr. Laurie BARTHE for all the guidance, knowledge, patience and countless supports during my doctorate.

My deep gratitude also goes to the members of the jury: Prof. Frank STÜBER, Dr. Stéphane BAUP, Prof. Dominique WOLBERT and Prof. Henri DELMAS for spending your precious time reading my manuscript and also for the valuable advices and suggestions. Go back to 2013, a special word of gratitude must go to Prof. Henri DELMAS who was proposing an interesting research subject and supporting me to get the scholarship for my doctoral study.

A scholarship provided by Ministry of Research, Technology and Higher Education of the Republic of Indonesia is gratefully acknowledged. I also express my gratitude to Prof. Irwan KATILI, Prof. Djoko HARTONO, Prof. Widjojo PRAKOSO and Dr. Setyo MOERSIDIK from Civil Engineering Department Universitas Indonesia for their supports on the candidacy and extension of my scholarship. The financial supports from French National Agency for Research and Campus France are also acknowledged.

I would like to appreciate the contribution of Prof. Ulises Javier JAUREGUI-HAZA, Katia GONZALEZ-LABRADA and Michel MANDUCA-ARTILES from InSTEC Cuba in this work. My appreciation also extends to David RIBOUL, Marie-line DE SOLAN BETHMALE, Marie-line PERN, Gwenaëlle GUITTIER, Christine REY-ROUCH, Jean-louis LABAT, Ignazio COGHE, Jean-Pierre ESCAFIT, Vincent LOISEL, Alain PHILIP, Daniele BOUSCARY and Claudine LORENZON from LGC Toulouse for their analytical, technical and administrative support.

I would like to thank my colleagues: German, Imane, Sylvie, Leticia, Pei San, Lindy, Freddy, Pedro, Filipa, Séda, Rihab, Vincent, Benjamin, Bi, Sebastien, Sebastien, Jaouher, Sid Ahmed, Isabelle, Usman and all doctoral students for their help and encouragement during my stay at LGC. I thank Bpk. Robert and Ibu Septi from Consulate General of Indonesia in Marseille for their help during my stay in France. I also appreciate the kindness and supports from my

Indonesian friends in France: Bastian, Aziz, Mba Winda, Mas Deni, Mas Yoga, Mba Munky, Mas Harris, Mas Pai, Pak Aloysius, Bu Natalia, Bu Nelly, Bang Yusrizal, Fito, Amie,

Last but not least my sincere gratitude goes to my wife and my parents, thanks to their infinite moral and spiritual supports I can successfully pass one of the most exceptional and challenging period in my life: doing a doctoral study and becoming a “Papa” of a baby boy in a foreign country at the age of 27.

Thank you / Merci / Gracias / Obrigado / Danke / شُكْرًا / 谢谢 / Terima kasih / Matur nuwun

*"Gantungkan cita-cita mu setinggi langit, bermimpilah setinggi langit.
Jika engkau jatuh, engkau akan jatuh di antara bintang-bintang."*

*("Aim the sky as your goal, dream as high as the sky.
Even if you fall, you will fall among the stars")*

Soekarno (first President of Republic of Indonesia)

This page is intentionally left blank

TABLE OF CONTENTS

Abstract.....	1
Résumé.....	3
Acknowledgement	5
INTRODUCTION.....	15
CHAPTER 1 LITERATURE REVIEW.....	19
1.1. CONTAMINATION OF AQUATIC ENVIRONMENTS BY PHARMACEUTICAL COMPOUNDS.....	21
1.1.1. Removal of pharmaceuticals by conventional treatment processes.....	21
1.1.2. Sources and environmental fate.....	23
1.1.3. Possible adverse effect.....	24
1.2. ADVANCED OXIDATION PROCESSES	25
1.2.1. Principle	25
1.2.2. Ibuprofen removal by AOPs	27
1.2.3. Transformation products of ibuprofen	29
1.3. FENTON REACTION.....	31
1.3.1. Principle and mechanism	31
1.3.1.1. Homogeneous system.....	31
1.3.1.2. Heterogeneous system	34
1.3.2. Review of recent studies on Fenton oxidation.....	37
1.4. SONOLYSIS AND SONO-FENTON PROCESSES	40
1.4.1. Principle and mechanisms.....	40
1.4.1.1. Ultrasound process	40
1.4.1.2. Activation of Fenton reaction by ultrasound	42
1.4.2. Review of recent studies	44
1.5. PHOTOLYSIS AND PHOTO-FENTON PROCESSES	46
1.5.1. Principle and mechanisms.....	46
1.5.1.1. Photo-degradation.....	46

1.5.1.2.	Activation of Fenton reaction by (UV/Vis) light.....	48
1.5.2.	Review of recent studies	50
1.6.	SONO-PHOTO-FENTON PROCESSES	52
1.6.1.	Principle and mechanisms.....	52
1.6.2.	Review of recent studies	54
1.7.	EFFECT OF OPERATING PARAMETERS	56
1.7.1.	Hydrogen peroxide concentration.....	56
1.7.2.	Effect of iron catalyst concentration	57
1.7.3.	Effect of temperature	57
1.7.4.	Effect of pH.....	58
1.7.5.	Effect of initial concentration of pollutant.....	59
1.7.6.	Effect of dissolved gas	59
1.7.7.	Effect of ultrasound power and frequency.....	60
1.7.8.	Effect of lamp type (wavelength) and power.....	61
1.8.	CONCLUSION	62
CHAPTER 2 METHODS AND MATERIALS.....		63
2.1.	ANALYTICAL METHODS.....	66
2.1.1.	Analysis of liquid phase.....	66
2.1.1.1.	Quantification of ibuprofen by HPLC/UV	66
2.1.1.2.	Analysis of reaction intermediates by HPLC/MS	67
2.1.1.3.	Analysis of Total Organic Carbon (TOC)	69
2.1.1.4.	Analysis of (residual) hydrogen peroxide by spectrophotometry	71
2.1.1.5.	Analysis of total dissolved iron by ICP-AES	71
2.1.2.	Analysis of solid phase (heterogeneous catalyst)	72
2.1.2.1.	Laser diffraction	72
2.1.2.2.	SEM and EDX Spectroscopy	73
2.1.2.3.	X-ray diffraction	74

2.1.2.4.	Gas porosimetry.....	76
2.1.2.5.	CO chemisorption.....	76
2.1.2.6.	Identification of the pH at the point of zero charge.....	77
2.1.2.7.	Carbon trace analysis.....	77
2.2.	CHEMICALS AND CATALYSTS	78
2.2.1.	Ibuprofen.....	78
2.2.2.	Hydrogen peroxide.....	80
2.2.3.	Soluble catalysts.....	81
2.2.4.	Heterogeneous catalysts.....	82
2.2.4.1.	Iron containing zeolite (Fe-MFI).....	82
2.2.4.2.	Zero-valent iron (ZVI).....	85
2.3.	EXPERIMENTAL SETUP	88
2.3.1.	Sono-reactor.....	88
2.3.2.	Photo-reactor.....	91
2.4.	EXPERIMENTAL PROCEDURE	95
2.4.1.	Homogeneous processes	95
2.4.2.	Heterogeneous processes	95
2.4.3.	Sample preparation for HPLC/UV and TOC analysis.....	96
2.4.4.	Experimental data analysis	97
2.5.	CONCLUSION	97
CHAPTER 3 HOMOGENEOUS PROCESSES.....		99
3.1.	IBUPROFEN REMOVAL BY SINGLE PROCESSES.....	101
3.1.1.	Preliminary considerations: reference conditions of the study.....	101
3.1.2.	Ultrasound irradiation	102
3.1.2.1.	IBP degradation by ultrasound and its mechanisms	102
3.1.2.2.	pH effect	104
3.1.2.3.	Effect of ultrasound density.....	105

3.1.2.4.	Effect of sonication frequency.....	98
3.1.2.5.	Effect of H ₂ O ₂ addition on 20 kHz sonolysis.....	109
3.1.3.	Light irradiation (UV, Vis and UV-Vis).....	111
3.1.3.1.	IBP degradation under monochromatic UV light (254 nm) irradiation and its mechanisms.....	111
3.1.3.2.	pH effect.....	114
3.1.3.3.	Effect of irradiated volume fraction.....	115
3.1.3.4.	Effect of lamp type (irradiation spectrum).....	116
3.1.3.5.	Effect of H ₂ O ₂ addition.....	117
3.1.4.	Fenton oxidation.....	121
3.2.	IBUPROFEN REMOVAL BY COMBINED PROCESSES.....	125
3.2.1.	Sonophotolysis and sonophoto-oxidation with H ₂ O ₂	125
3.2.2.	Sono-Fenton oxidation.....	128
3.2.2.1.	Effect of Fenton's reagent concentration on sonolysis (20 kHz).....	128
3.2.2.2.	Effect of ultrasound density.....	131
3.2.2.3.	Effect of sonication frequency.....	133
3.2.3.	Photo-Fenton oxidation.....	135
3.2.3.1.	Effect of lamp type on photo-Fenton oxidation.....	136
3.2.3.2.	Effect of Fenton's reagent concentration (Xe lamp).....	138
3.2.4.	Sono-Photo-Fenton oxidation (20 kHz US / Xe lamp).....	139
3.3.	EVALUATION OF TRANSFORMATION PRODUCTS.....	145
3.3.1.	Identified intermediates and general IBP degradation scheme.....	145
3.3.2.	Comparison of different homogeneous processes.....	148
3.3.3.	Evolution of selected intermediates during homogeneous processes.....	151
3.4.	EFFECT OF WATER MATRIX.....	155
3.5.	CONCLUSIONS.....	160
CHAPTER 4 HETEROGENEOUS PROCESSES.....		161

4.1.	PRE-SELECTION OF THE HETEROGENEOUS CATALYST	163
4.1.1.	Adsorption of ibuprofen over Fe-MFI and ZVI catalysts	163
4.1.2.	Fenton oxidation of ibuprofen over Fe-MFI and ZVI catalysts.....	165
4.1.3.	Evaluation of Fe-MFI and ZVI catalysts after reaction	167
4.1.4.	Mechanisms of Fenton reaction over investigated catalysts	170
4.2.	PARAMETRIC STUDY	173
4.2.1.	Effect of solid catalyst concentration.....	173
4.2.2.	Effect of H ₂ O ₂ concentration	175
4.2.3.	Effect of H ₂ O ₂ / Fe molar ratio	177
4.2.4.	Effect of temperature	179
4.2.5.	pH effect.....	181
4.2.6.	Activity of leached iron	184
4.3.	HETEROGENEOUS SONO-FENTON PROCESSES	187
4.3.1.	Investigation of 20 kHz sono-Fenton oxidation.....	187
4.3.1.1.	Effect of catalyst particles on sonolysis	187
4.3.1.2.	Comparison of Fenton and sono-Fenton oxidation with Fe/MFI.....	189
4.3.2.	Effect of US application mode.....	191
4.3.3.	Effect of ultrasound intensity	191
4.3.4.	Effect of ultrasound power density	194
4.3.5.	Effect of ultrasound frequency.....	196
4.4.	HETEROGENEOUS PHOTO-FENTON PROCESSES	198
4.4.1.	Heterogeneous photo-Fenton oxidation under UV light (LP Hg lamp)	198
4.4.2.	Heterogeneous photo-Fenton oxidation under visible light (Xe lamp)	200
4.5.	HETEROGENEOUS SONO-PHOTO-FENTON PROCESSES.....	202
4.6.	EVOLUTION OF THE HETEROGENEOUS CATALYST	205
4.6.1.	Particle size distribution.....	205
4.6.2.	Catalyst morphology and iron content.....	206

4.6.3.	Activity of leached iron in sono-Fenton and photo(Vis)-Fenton oxidation.....	208
4.6.4.	Effect of ultrasound and light irradiation on residual carbon content	209
4.7.	EVALUATION OF TRANSFORMATION PRODUCTS	211
4.8.	EFFECT OF WATER MATRIX	214
4.9.	CONCLUSIONS	219
	CONCLUSIONS AND PERSPECTIVES	221
	REFERENCES	227

INTRODUCTION

Contaminated water is a world concern, and threatens both quality of life and public health. The oldest water pollution was that due to organic matter, followed in the beginning of twentieth century by metal pollution caused by the industrial development. With the increase of population, urbanization, industrialization and agriculture intensification, new types of pollutants have arisen such as organic solvents, fertilizers, pesticides and pharmaceuticals. It is now well-known that after medication, drugs can reach the aquatic environment via excreta and have an impact on non-target organisms. Thousands tons of pharmaceutical compounds (PCs) are commercially produced each year. Following their increasing use, numerous studies have demonstrated the presence of pharmaceuticals in various wastewater treatment effluents, typically at concentration levels from nanogram to few micrograms per liter. Possible risks associated to the release of pharmaceuticals are still unclear and require further research to better characterize their long-term effects for environment and human health. Regarding ecosystems, impacts can be blooms of microorganisms or apparition of mutant species. For humans, potential consequences of chronic exposure via drinking-water range from allergy to cancer through loss of fertility. Therefore those emerging pollutants have become an important issue due to their recognized occurrence in wastewater and probable harmful effects on environment and health.

Due to their complex molecular structure, low concentration in water and possible toxicity to microorganisms, most of these molecules cannot be completely removed by conventional wastewater treatment (*e.g.* chemical precipitation and activated sludge) due to their complex molecular structure, low concentration in water and possible toxicity to microorganisms. Thus environmental and health concerns are driving wastewater treatment plants to develop different techniques and to come up with advanced technologies. Moreover, current researches on the remediation of bio-recalcitrant and/or toxic compounds are moving towards a coupling of processes, either traditional or more innovative.

Advanced Oxidation Processes (AOPs) are promising techniques for the degradation of refractory organic compounds, including drugs. AOPs are based on the generation of reactive oxygen species (ROS), especially hydroxyl radical ($\bullet\text{OH}$) a powerful and non-selective oxidant and other strong oxidant species (*e.g.* $\bullet\text{OOH}$, $\bullet\text{O}_2^-$) that are capable to degrade and

INTRODUCTION

mineralize organic compounds into water (H₂O) and carbon dioxide (CO₂) as final products. AOPs are classified according to the reactive system (homogeneous or heterogeneous) and the radical generation methods (chemical, electrochemical, sonochemical or photochemical).

Fenton oxidation is one of the most popular AOPs. It classically involves the reaction of ferrous ions and hydrogen peroxide under acidic condition to form hydroxyl radicals. However, the relatively high iron concentration needed (50-500 ppm) with respect to discharge limit (2 ppm in EU) and the difficulty in recovering dissolved iron promote the development of heterogeneous systems. Heterogeneous Fenton oxidation uses an iron containing solid as catalyst in order to facilitate its recovery, for instance by using membrane filtration.

Unfortunately, degradation rates in heterogeneous process are usually lower than that of homogeneous counterpart. In order to enhance the reaction, several activation methods have been proposed, the most popular being UV/Vis light in the so-called photo-Fenton process. This irradiation enhances the regeneration of ferrous species (limiting step in dark Fenton process) by photo-reduction, while generating additional radicals. It also promotes the direct decomposition of H₂O₂ into •OH and eventually the direct photolysis of the molecule depending on the applied wavelengths.

More recently, increasing attention has also been paid to the application of ultrasound (“sono-Fenton process”) with nearly one hundred publications and two thirds of them from the last five years. In solution, a synergetic effect between Fenton reaction and ultrasound has been proven, in which US also improves Fe²⁺ regeneration and subsequent formation of radicals. Moreover, acoustic cavitation gives rise to extreme conditions inside and around the collapsing bubble, which can result in the thermal cleavage of the organic pollutants. Low frequency ultrasound also induces mechanical effects, including particle aggregate disruption and possible surface activation and/or regeneration of the heterogeneous catalysts. Still, scarce information is available on the exact role of US enhancement in heterogeneous Fenton reaction (mechanical vs. chemical effects).

The aim of this study is to investigate the coupling of both homogeneous and heterogeneous Fenton reaction with these activation techniques (ultrasound and/or ultraviolet/visible) for the degradation of pharmaceutical compounds. Reaction tests are performed in a batch mode and investigate the effects of irradiation spectrum (sound frequency / light wavelength), power input, irradiation time and modulation, as well as oxidant and catalyst doses. Despite efficacies of these combined techniques are probably

INTRODUCTION

greater, interactions could also be not so advantageous. Therefore the study progresses from the separate processes, via their two-by-two associations towards overall combination.

For this work, ibuprofen has been selected as model drug contaminant owing to its high consumption (for self-medication) and reported occurrence in the environment.

The manuscript starts with a review on pharmaceutical contaminants in aquatic systems, particularly ibuprofen, and advanced oxidation processes (AOPs) proposed to reduce this pollution. This literature survey focuses on homogeneous and heterogeneous Fenton reaction, as well as sonolysis, photolysis and their combination (sono-Fenton, photo-Fenton, sono-photo-Fenton). Finally, main operating parameters of these different AOPs are reviewed.

Description of materials, experimental equipment and procedures involved in this study is gathered in chapter 2. Liquid chromatography, analysis of Total Organic Carbon and residual hydrogen peroxide have been used as routine measurements for liquid samples so as to evaluate the process performance. Solid catalysts have been characterized by a range of techniques for their morphological and textural properties, as well iron species type, content and dispersion. For these heterogeneous systems, iron leaching in solution has also been monitored to evaluate possible contribution of homogeneous mechanism. Different types of ultrasound equipment and lamps have been used whose characteristics are also given in this chapter.

Chapter 3 is dedicated to the degradation of ibuprofen by homogeneous oxidation treatments: a parametric study is first carried out on the separate processes (sonolysis, photolysis, and Fenton oxidation) to highlight the involved mechanisms, prior to the investigation of their combinations.

Chapter 4 focuses on the heterogeneous Fenton reaction. The activity of two different catalysts (zero-valent iron particles and iron-containing zeolite) is first evaluated with respect to the homogeneous system. Then possible activation of selected catalyst by ultrasound and/or light irradiation is examined. In these two chapters, effect of water matrix and identification of degradation intermediates are also addressed in order to assess the feasibility and relevance of such advanced processes.

This page is intentionally left blank

CHAPTER 1 LITERATURE REVIEW

This chapter provides a literature survey about pharmaceutical emerging pollutants and advanced oxidation processes as possible treatment for their remediation.

This page is intentionally left blank

1.1. CONTAMINATION OF AQUATIC ENVIRONMENTS BY PHARMACEUTICAL COMPOUNDS

1.1.1. Removal of pharmaceuticals by conventional treatment processes

Water is an indispensable resource for human life. Drinking water consumption and wastewater generation are directly related to the population growth and human activities. Since the last decades, the characteristics of wastewater have become more complex along with increasing and diversifying industrial activities. At the same time, the development of analytical techniques has provided an overview of current conditions in which many refractory contaminants have been identified in the environment.

Among the organic pollutants, pharmaceutical and personal care products are of particular concern. For instance, in France, more than 3 milliards drug boxes are sold annually [1] with paracetamol, codeine and ibuprofen as the most used products. This high (and increasing) consumption should explain the accumulation of these molecules in the aquatic environment. Indeed, 24 pharmaceutical compounds were found in various water resources in France during national survey (2009-2010), caffeine, oxazepam and paracetamol being the most frequently detected [2]. This finding indicates that some pharmaceutical compounds are not fully degraded by conventional precipitation-biological treatments or by natural degradation process and follow complex pathway in the environment. According to the extensive review conducted by Deblonde et al. [3], anti-epileptics, contrast agents, analgesic and anti-inflammatories are reported as the most refractory pharmaceutical compounds. Example of anti-inflammatory removal in various conventional wastewater treatment plants is given in [table 1.1](#) [4]. It can be seen that, if ibuprofen can be eliminated by conventional treatments processes, this molecule however may be not fully degraded, but only transformed into other by-products [5] or even may be only adsorbed on suspended solids and accumulated in settling tank [6,7].

Several classic chemical oxidants, such as chlorine and chlorine dioxide, have shown capacity for the removal of pharmaceuticals, but their reaction is relatively slow, limited to only a few compounds and could form toxic intermediate substances, such as chloroform [8,9]. Physical techniques like adsorption on activated carbon [10] or membrane separation [11] are also applied, either as individual treatment or as integrated treatment with oxidation processes [12,13]. However, after adsorption of toxic compounds, activated carbon itself

becomes a hazardous waste that must be regenerated, treated or disposed properly. Similarly, even though nanofiltration and reverse osmosis have proved to remove most of the pharmaceutical compounds, these techniques require a post-destructive process increasing the operation costs.

Table 1.1. Example of pharmaceuticals removal in conventional treatment

Drugs	Unit operations	Removal (%)	Region
IBP	AcS/phosphate removal	78-100	Aura, Tampere, Harjavalta (Finland)
	AcS/N/DeN/phosphate removal	92-99	Helsinki, Seinajoki, Turku (Finland)
	1 ^o settling, AcS, 2 ^o	60-70	Galicia (Spain)
	1 ^o Settling, AcS/N/DeN, 2 ^o settling	86	S. England
	1 ^o Settling, AcS	75	Rio de Janeiro (Brazil)
	AcS, ppt with FeCl ₃	62-79	on Lake Geneva (W. Switzerland)
DCF	Conventional WWTP	17	Berlin (Germany)
	AcS, P removal	23-60	Aura, Tampere, Harjavalta (Finland)
	AcS/N/DeN/phosphate removal	9-25	Helsinki, Seinajoki, Turku (Finland)
	1 ^o Settling, AcS	75	Rio de Janeiro (Brazil)
	AcS, disinfection	18	Baltimore (USA)
NPX	AcS/phosphate removal	55-98	Aura, Tampere, Harjavalta (Finland)
	AcS/N/DeN/phosphate removal	69-94	Helsinki, Seinajoki, Turku (Finland)
	1 ^o Settling, AcS	78	Rio de Janeiro (Brazil)
	AcS/N/DeN, sand filtration	50-80	Kloten/Opfikon (Switzerland)
KTF	AcS/phosphate removal	51-100	Aura, Tampere, Harjavalta (Finland)
	AcS/N/DeN/phosphate removal	63-98	Helsinki, Seinajoki, Turku (Finland)
	AcS, ppt with FeCl ₃	15-72	on Lake Geneva (W. Switzerland)
	1 ^o Settling, AcS	69	Rio de Janeiro (Brazil)
MEF	1 ^o Settling, AcS/N/DeN, 2 ^o settling	91	S. England
	1 ^o Settling, AcS, ppt with FeCl ₃ , 2 ^o settling	28-74	on Lake Geneva (W. Switzerland)
	AcS, ppt with FeCl ₃	19-69	on Lake Geneva (W. Switzerland)

AcS: activated sludge, N: nitrification, DeN: denitrification, 1^o: primary settling tank, 2^o: secondary settling tank, ppt: chemical precipitation, IBP: Ibuprofen, DCF: Diclofenac, NPX: Naproxen, KTF: Ketoprofen, MEF: Mefenamic acid

These facts lead pharmaceutical compounds to become emerging pollutants. Emerging pollutants are new products or chemicals without regulatory status and whose (cumulative)

effects on environment and human health are unknown [3]. The concentration of the pharmaceutical products was not monitored in European waters until the revision of the Directive 2000/60/EC in 2013, when the European Commission has proposed to include on a "watch list" three pharmaceuticals (a painkiller **and** two hormones), namely diclofenac, α -ethinylestradiol, and β -estradiol.

1.1.2. Sources and environmental fate

It is widely accepted that pharmaceutical compounds are introduced into the environment mainly through wastewater effluent from pharmaceutical industries, hospitals, live-stock and household activities, as shown in [figure 1.1](#) [14]. Pharmaceutical wastewater generated from industry is more easily measured and managed than that derived from domestic source. The latter has been identified as the main contamination pathway of ibuprofen in the aquatic environment [15]. In aquatic environment, the possible removal processes of organic compounds are biodegradation, sorption and photo-degradation (direct and indirect). However, since pharmaceuticals contain active ingredients are designed to have pharmacological effects on humans and animals, they are usually resistant to biodegradation [16,17]. Photo-degradation might be also not efficient considering the spectral absorption of pharmaceuticals, which is usually in UV-C region [18–20]. On the other hand, removal by sorption process is both soil (or site)- and molecule- specific, so it cannot be generalized on a global basis and it may be only a liquid-solid phase transfer without significant degradation process.

In the case of ibuprofen (IBP), several studies reported its presence in effluents from wastewater treatment plants (0.002 - 95 $\mu\text{g/L}$), in surface water (0.01 - 0.4 $\mu\text{g/L}$) and in drinking water (0.0002 - 0.0013 $\mu\text{g/L}$) [4,21]. After excretion by human body or treatment by biological process, IBP can enter the water bodies under unaltered parent compound, as metabolized hydroxy-ibuprofen and as carboxy-ibuprofen [22–24]. In all cases, IBP also tends to adsorb onto suspended solids and sediments leading to an underestimation of its measured concentration in aquatic environment [25].

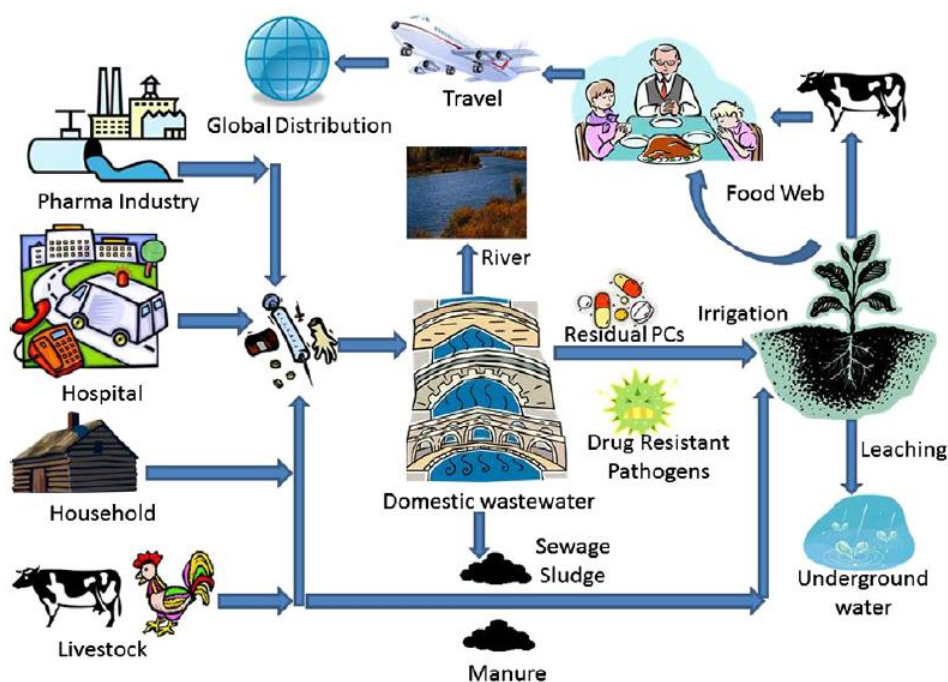


Figure 1.1. Possible sources and pathways of pharmaceutical compounds in the environment (adapted from reference [14])

1.1.3. Possible adverse effect

Regardless of its function as a medicine, the presence of pharmaceuticals in the environment may have negative impacts, especially for microorganisms and aquatic organisms. Carlsson et al. [26] evaluated hazard and risk assessments of 27 pharmaceuticals based on some parameters such as daily dose, acute toxicity, degradation, and octanol-water partition coefficient (K_{OW}) and they found diclofenac, ethinylestradiol, ibuprofen, metoprolol, norethisterone, and oxytetracycline as having the potential for toxic and/or long-term effects. Ecological risk assessment of 33 pharmaceutical compounds detected in French water resources was also carried out by Bouissou-Schurtz et al (2014). The results suggest that only ibuprofen was identified as posing real environmental risk based on its measured environmental concentration (Risk Quotient = 1.9) [25].

Despite the unclear effect on human health [3,27], ibuprofen has been shown to significantly affect the growth of several fishes, microorganisms, algae, bacterial and fungal species [28–32] (Table 1.2). Chronic exposure to ibuprofen at 0.1 - 1 $\mu\text{g/L}$ affects several endpoints related to the reproduction of the fish, including induction of vitellogenin in male fish, fewer broods per pair, and more eggs per brood [32].

Table 1.2. Environmental toxicity of ibuprofen

Species	Duration / endpoint	Concentration (mg/L)
P. carinatus	21 d / Growth (wet weight) NOEC	1.02
P. carinatus	21 d / Reproduction (hatching success) NOEC	2.43
P. carinatus	21 d / Survival NOEC	5.36
D. magna	21 d / Reproduction NOEC	20
D. magna	21 d / Reproduction NOEC	< 1.23
D. magna	21 d / Survival NOEC	33.3
D. magna	14 d / Reproduction EC50	13.4
D. magna	14 d / Survival NOEC	20
D. magna	14 d / Population growth rate NOEC	< 20
M. macrocopa	7 d / Reproduction NOEC	25
M. macrocopa	7 d / Survival NOEC	>50
H. vulgaris	10 d / Bud formation NOEC	>10
H. attenuata	96 h / Morphology EC50	1.65
H. attenuata	96 h / Morphology NOEC	0.1
H. attenuata	96 h / Feeding EC50	3.85
O. latipes	30 dph / Survival NOEC	0.1
O. latipes	90 dph / Survival NOEC	0.001
O. latipes	120 dph / Survival NOEC	0.0001
O. latipes	120 dph / Reproduction NOEC	0.001

EC₅₀: Half maximal effective concentration, LC₅₀: Half lethal concentration, NOEC: No observed effect concentration

1.2. ADVANCED OXIDATION PROCESSES

1.2.1. Principle

Advanced Oxidation Processes (AOPs) are oxidative processes applied for the elimination of contaminants in water, soils and air, which are based on the formation of highly reactive and non-selective species, such as hydroxyl radical ($\bullet\text{OH}$), superoxide radical ($\bullet\text{O}_2$), hydroperoxyl radical ($\bullet\text{O}_2\text{H}$) and peroxy radical ($\text{ROO}\bullet$). These reactive radicals are generated in atmospheric or subcritical conditions of temperature and pressure, with or without catalyst and/or energy (electrochemical, UV-Vis or ultrasound) [33]. Among reactive oxidant species, $\bullet\text{OH}$ is usually considered as the main oxidant since it possesses high standard oxidation potential ($E^0 = 2.8 \text{ V}$ in acidic medium) that would be able to oxidize almost all organic compounds to carbon dioxide and water through different mechanisms, *i.e.* electron transfer reaction (as oxidizing agent), abstraction of protons producing organic

radicals (R^\bullet) and electrophilic addition on a double bond or aromatic ring (figure 1.2) [34,35]. However, some of the simplest organic compounds, such as acetic, maleic, oxalic acids, acetone are more difficult to degrade by this process [36].

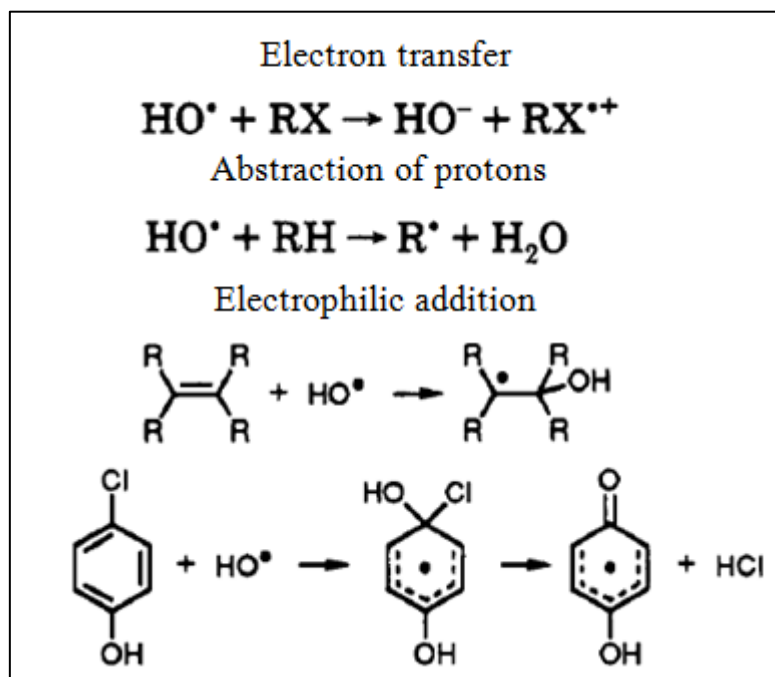


Figure 1.2. General scheme of hydroxyl radical based reactions (adapted from reference [34])

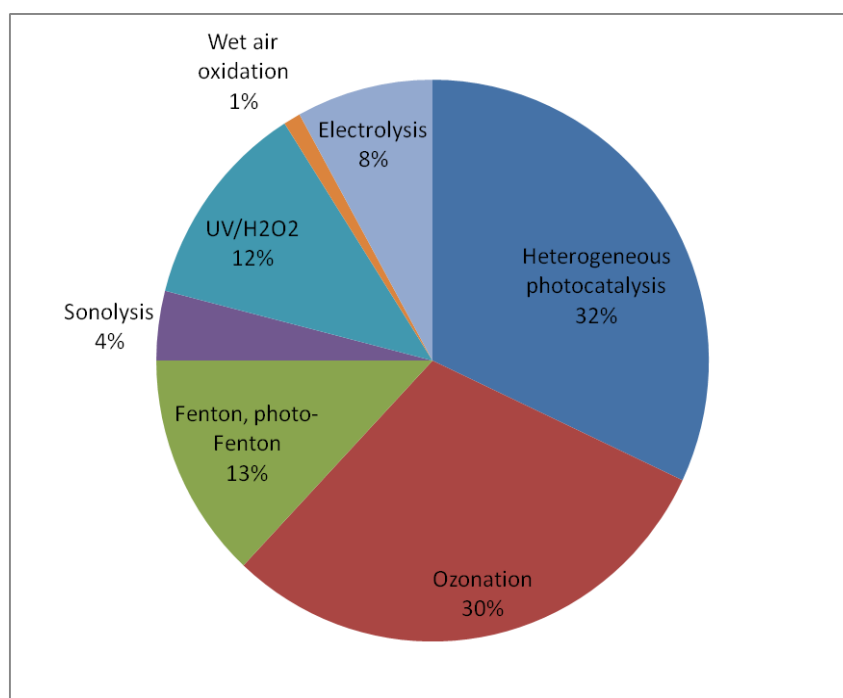


Figure 1.3. Distribution of studies on pharmaceuticals removal by AOPs (adapted from reference [37])

Numerous types of AOPs are known such as ozonation (O₃), Fenton reaction (H₂O₂ and iron-based catalyst), UV photolysis, photo-peroxide oxidation (UV/H₂O₂), photo-catalysis (UV/TiO₂), ultrasound (US), electrochemical oxidation, wet-air oxidation, pulse plasma and also their possible combination (such as UV/O₃, UV/Fenton, US/Fenton, Electro-Fenton, etc.). Considering pharmaceutical compounds as model pollutants, ozonation and heterogeneous photocatalysis using TiO₂ are the most studied [37] (figure 1.3).

1.2.2. Ibuprofen removal by AOPs

Various AOPs such as ozonation (O₃), O₃/H₂O₂, photolysis, sonolysis, photo-Fenton... have been applied for IBP removal from water. Table 1.3 summarizes the main results and conclusions of the corresponding studies, where X stands for (IBP or total organic carbon) removal efficiency (%) and k is the pseudo first-order rate constant (min⁻¹).

Table 1.3. Ibuprofen removal by several AOPs

Processes [Ref.]	Experimental conditions	Remarks
Homogeneous and heterogeneous Fenton [38]	[IBP] = 0.1 mM; T = 20°C; pH = 3; [H ₂ O ₂] = 1 mM; [Fe(II)] = 1 mM; [Fe ₃ O ₄] = 1 g/L (13 mM Fe); T = 20°C; pH = 6.6; under N ₂ injection	Homogeneous Fenton: X _{IBP} > 90% in 5 min. Heterogeneous Fenton: X _{IBP} = 50 % in 60 min. Heterogeneous Fenton reaction was much slower than homogeneous Fenton reaction.
Heterogeneous Fenton [39]	[IBP] = 0.07 mM; [Fe ₃ O ₄] = 1.84 g/L; [H ₂ O ₂] = 600 mM; T = 23°C; pH = 7	X _{IBP} = 30% in 180 min. Degradation of ibuprofen was very influenced by pH. Poor degradation of ibuprofen at neutral pH could be compensated with high concentration of catalyst and oxidant.
Sonolysis [40]	[IBP] = 0.1 mM; T = 25°C; pH = 5; f _{US} = 300 kHz; P _{US} = 80 W; I _{US} = 6.7 W/cm ² ; D _{US} = 270 W/L	X _{IBP} = 98% in 30 min. The reaction between radicals and IBP would be enhanced if IBP in molecular form (pH < pKa).
Sonolysis [41]	[IBP] = 0.1 mM; T = 25°C; pH = 8.5; f _{US} = 20 and 620 kHz; D _{US} = 400 W/L	k = 0.67 μM/min (20 kHz) and 16.3 μM/min (620 kHz). A more hydrophobic target compound with higher diffusivity is less impacted by the presence of organic compounds from water matrix.
Photolysis [42]	[IBP] = 0.1 mM; V = 220 mL; T = 25°C; UV (254 nm; 3.45x10 ⁻⁵ E/s) and VUV/UV lamp (185/254 nm; 3.66x10 ⁻⁵ E/s); Q _{gas} = 855 mL/min	X _{IBP} = 100%, X _{TOC} = 60% in 60 min (UV lamp); X _{IBP} = 100%, X _{TOC} = 50% in 10 min (VUV/UV lamp). The presence of nitrogen negatively affects the degradation kinetics.

Homogeneous photo-Fenton oxidation [43]	Sono-	[IBP] = 0.09 mM; [Fe(NO ₃) ₃] = 0.05 mM; T = 20±2°C; pH = 2.7; f _{US} = 213 kHz; P _{US} = 55 W/L; Xenon lamp; P _{UV} = 450 W	X _{IBP} = 100% in 60 min, X _{TOC} = 70% in 240 min. A slight synergy was observed when combining ultrasound and photo-Fenton oxidation.
Photolysis UV/H ₂ O ₂ [18]	and	[IBP] = 0.19 mM; T = 22±0.3°C; pH = 7; [H ₂ O ₂] = 1.5 mM; MP Hg lamp; P _{UV} = 60 W; λ _{UV} = 200-320 nm	k _{IBP} = 0.097 min ⁻¹ (UV); k _{IBP} = 0.56 min ⁻¹ (UV/H ₂ O ₂). UV and UV/H ₂ O ₂ processes using MP Hg lamp were effective for IBP removal.
Photolysis photocatalytic oxidation [44]	and	[IBP] = 0.02 mM; [TiO ₂] = 240 mg/L; T = 25°C; pH = (-); LP Hg lamp (UV-A); P _{UV} = 27 W; λ _{UV} = 200 – 280 nm; dark light lamp; P _{UV} = 27 W, λ _{UV} = 315 – 400 nm	X _{IBP} = 13% (UV-A), 99% (UV-C), 93% (UV-A/TiO ₂), 100% (UV-C/TiO ₂) in 120 min; X _{TOC} ≤ 40% in 120 min. Direct photolysis by UV-C light was an effective process for IBP removal but not for mineralization process.
Homogeneous Fenton [24]	Photo-	[IBP] = 0.87 mM; T = 30°C; pH = 3; [H ₂ O ₂] = 0.32 mM; [Fe(II)] = 1.2 mM; Xenon lamp ; P _{UV} = 1000 W; λ _{UV} = 290-400 nm	X _{IBP} = 100% in 60 min, X _{TOC} = 40% in 120 min. Application of UV light to Fenton process increased IBP and TOC removal by up to 2 and 4 times, respectively.
Photocatalytic oxidation [45]		[IBP] = 0.05 mM; [TiO ₂] = 10 mg/L; room temperature; pH = 7; MP Hg lamp ; P _{UV} = 60 W; λ _{UV} = 320-400 nm	X _{IBP} = 90% in 180 min. IBP was rapidly degraded in the first 20 min of photocatalytic treatment, then the degradation rate decreased probably due to the deactivation of catalyst active sites by degradation by-products.
Photocatalytic oxidation [46]		[IBP] = 100 mg/L; T = 30 °C ; pH = 6 ; [TiO ₂] = 1 g/L; [O ₂] = 40 mg/L. Xenon lamp 1000 W	X _{IBP} = 90%, X _{TOC} = 50% in 240 min. Removal yield increased with increase of catalyst concentration.
Electro-Fenton [47]		[IBP] = 0.2 mM (in 20% ACN); T = 23±2°C; pH = 3; Electrolytes: [Na ₂ SO ₄] = 50 mM; [Fe(II)] = 0.2 mM; Electrodes: BDD / Pt-Graphite; I = 500 mA	X _{IBP} = 100% in 50 min. The oxidation rate increased with applied current and BDD anode showed higher removal rate than Pt anode.
O ₃ /H ₂ O ₂ [48]		[IBP] = 2 μM; T = 10°C; pH = 7; [O ₃] = 0.1 mM; [H ₂ O ₂] = 0.05 mM	X _{IBP} = 99% in 10 min. Simple ozonation was found to be ineffective to remove ibuprofen (X _{IBP} =12%), while the application of O ₃ /H ₂ O ₂ was very effective.
O ₃ /ZVI/US [49]		[IBP] = 0.05 mM; T = 25°C; pH = 3; [O ₃] = 12 mg/min; D _{US} = 230 W/L ; [ZVI] = 5 mg/L	X _{IBP} = 100%, X _{TOC} = 58% in 40 min. Ultrasound facilitates the diffusion of solutes from the bulk solution to the bubble-liquid and solid-liquid interfaces, thus improving the O ₃ /ZVI process.

Despite it is difficult to compare these studies performed in rather different conditions, coupling ozone and hydrogen peroxide seems to be the most effective AOP, with complete removal of IBP in 10 min [48]. However, the high energy consumption for generating ozone by silent electrical discharges makes its use expensive [50]. Some other efficient treatments (photolysis, UV/H₂O₂) use UV-C irradiation ($\lambda = 200\text{-}280$ nm). However, its application to large wastewater treatment plants may be a challenge considering the cost of mercury vapor lamps [51]. In order to reduce energy consumption, development of water treatment processes tends more towards a better utilization of sunlight (with major fraction in the visible domain, $\lambda = 400\text{-}800$ nm). On the other hand, for all the proposed AOPs, complete mineralization of ibuprofen is still a challenging issue. In any case, it should be mentioned that ibuprofen removal by heterogeneous Fenton coupled with ultrasound and light irradiations hasn't been investigated yet.

1.2.3. Transformation products of ibuprofen

Transformation products (TPs), also called degradation products or reaction intermediates, are related to the molecules formed during the oxidation process of the targeted compound. Degradation pathway of ibuprofen generally consists in decarboxylation, demethylation, hydroxylation and cleavage moiety reactions [52]. These reactions form 4-isobutylacetophenone and 4-ethylbenzaldehyde, that were found to be toxic, causing adverse effects to the central nervous system and presenting high dermal absorption [52–54].

Hydroxylated ibuprofen molecules are usually detected as first degradation products by mass spectrometry. Hydroxylation is assumed to take place on the side chains in the secondary or tertiary positions or by attachment to the aromatic benzene ring [24,43,45,55], with H extractions kinetically favored over ring additions [51].

An example of ibuprofen degradation pathways during TiO₂ photocatalytic oxidation is given in [figure 1.4](#) [52]. The first transformation product **TP1** (mono-hydroxylated IBP; m/z: 221) is formed via the addition of a hydroxyl group (⁻OH) onto ibuprofen molecule (**hydroxylation**), which was found here to take place rather on the aromatic ring. Together with hydroxylation, **direct demethylation** can occur in parallel to form **TP2** (4-(1-carboxyethyl) benzoic acid; m/z: 191), which can be further hydroxylated into **TP3** (C₁₂H₁₅O₃; m/z: 207). **TP4** (1-ethyl-4-(2-hydroxy)isobutylbenzene; m/z: 177) is formed by removal of carboxylic acid from the isobutyl moiety (**decarboxylation**) of TP1. Then, **TP5**

keto-derivative (4-isobutylacetophenone; m/z: 175) is formed, as well as **TP6** (4-ethylbenzaldehyde; m/z: 133) resulting for instance from **TP4** by **hydroxylation** and **loss of 2-propanol**. Another molecule, **TP7**, with molecular formula $C_9H_9O_2$ (m/z: 149) is specifically formed during sono-photocatalytic oxidation on TiO_2 because of the **cleavage of isobutyl moiety**.

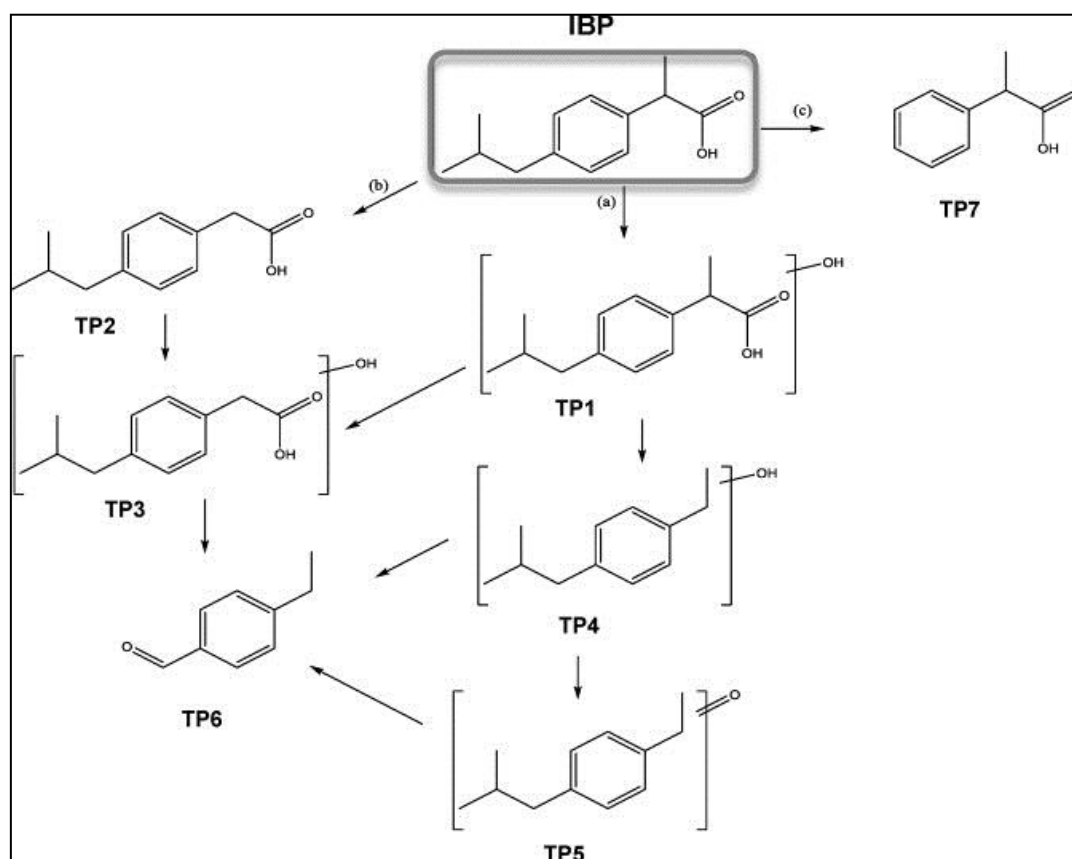


Figure 1.4. Possible transformation pathways of IBP during TiO_2 photocatalysis under UV-A and simulated solar irradiation, and sono-photocatalysis (adapted from reference [52])

IBP transformation products reported by several researchers working on different Advanced Oxidation Processes (AOPs) are summarized in [table 1.4](#). We can note that similar intermediates are found which indicates that hydroxyl radical plays important role in all these degradation processes.

Table 1.4. Transformation products of ibuprofen observed in different AOPs

Treatment	Transformation products	References
Electro-Fenton	p-Benzoquinone (m/z 107.98) 4-Isobutylphenol (m/z 150.03) 1-(1-Hydroxyethyl)-4-isobutylbenzene (m/z 178.86) 4-Isobutylacetophenone (m/z 175.97) Isomer molecule 1 (m/z 249.08) Isomer molecule 2 (m/z 249.12)	[47]
Photo-Fenton	1 or 2-Hydroxy-IBP (m/z 221) (2RS)-2-(4-Methylphenyl)propanoic acid (m/z 163) 1-ethyl-4-(2-hydroxy)isobutylbenzene (m/z 177) 1-ethyl-4-(1-Hydroxy)isobutylbenzene (m/z 175) 1-[4-(2-Methylpropyl)phenyl]ethanone (m/z 175) 4-(1-hydroxy-2-methylpropyl)acetophenone (m/z 191) 2-Methyl-1-phenylpropane (m/z 133) 2-hydroxy-2-[4-(2methylpropyl)phenyl]peroxic acid (m/z 238)	[24]
Sono-photo-catalysis using TiO ₂	1 or 2-Hydroxy-IBP (m/z 221) (2RS)-2-(4-Methylphenyl)propanoic acid (m/z 163) 1-ethyl-4-(2-hydroxy)isobutylbenzene (m/z 177) 1-ethyl-4-(1-Hydroxy)isobutylbenzene (m/z 175) 1-[4-(2-Methylpropyl)phenyl]ethanone (m/z 175) 4-(1-hydroxy-2-methylpropyl)acetophenone (m/z 191) 2-Methyl-1-phenylpropane (m/z 133) 2-hydroxy-2-[4-(2methylpropyl)phenyl]peroxic acid (m/z 238)	[43]
Sono-photo-catalysis using TiO ₂	1 or 2-Hydroxy-IBP (m/z 221) 4-(1-carboxyethyl) benzoic acid (m/z 191) C ₁₂ H ₁₅ O ₃ (m/z 207) C ₁₂ H ₁₇ O (m/z 177) 4-isobutylacetophenone (m/z 175) 4-ethylbenzaldehyde (m/z 133) C ₉ H ₉ O ₂ (m/z 149)	[52]

1.3. FENTON REACTION

1.3.1. Principle and mechanism

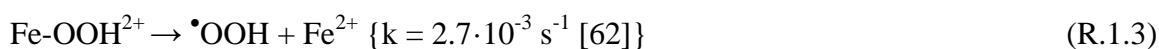
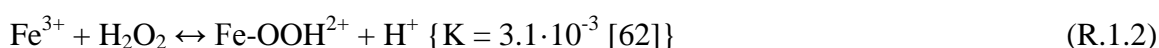
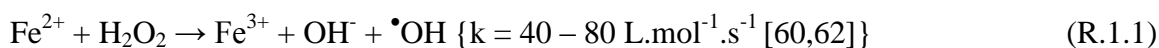
1.3.1.1. Homogeneous system

Among the Advances Oxidation Processes, Fenton oxidation is one of the most promising one owing to (i) the use of easy-to-handle and environmental-friendly reagents (Fe²⁺ or Fe³⁺ and H₂O₂), (ii) the low energy consumption compared to other oxidation technologies, (iii) the ability to destroy a large number of organic compounds along with a reduction of toxicity, odor and color and an improvement of biodegradability, and (iv) the

simplicity of the required equipment allowing an easy scale-up from laboratory to large scale [56–58].

The Fenton reaction was discovered in 1894 by H.J.H. Fenton, who reported that H_2O_2 could be activated by ferrous (Fe^{2+}) salts to oxidize tartaric acid [59]. Recently, Fenton reaction has been proved to be very effective in the removal of many hazardous organic pollutants from water. The Fenton reaction causes the dissociation of the oxidant and the formation of highly reactive hydroxyl radicals that attack and destroy the organic pollutants [56,60].

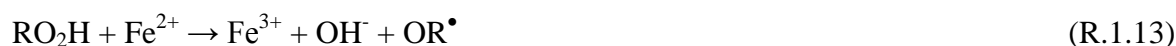
It is usually accepted that Fenton reaction follows a free radical mechanism [56,60,61]: hydroxyl radicals ($\bullet\text{OH}$) are generated by the reaction between ferrous ions (Fe^{2+}) and hydrogen peroxide (H_2O_2) in acid condition (pH between 2 – 4):



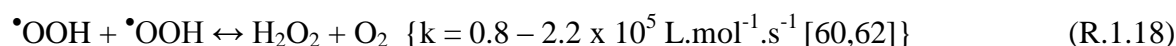
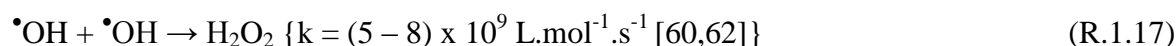
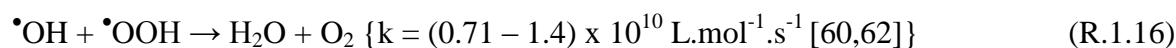
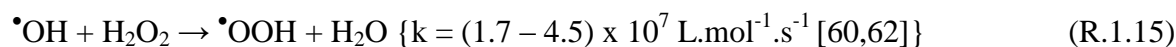
As abovementioned, generated hydroxyl radicals ($\bullet\text{OH}$) can oxidize organic compounds (RH) by different mechanism [34], *i.e.* electron transfer reaction (as oxidizing agent), abstraction of protons producing organic radicals ($\text{R}\bullet$) and electrophilic addition on a double bond or aromatic ring:



The organic radicals ($\text{R}\bullet$) are highly reactive and can further react with hydrogen peroxide, ferrous or ferric ions, dissolved oxygen, hydroperoxyl radicals ($\bullet\text{OOH}$) or form a dimer, leading to reactions (R.1.7) to (R.1.14):

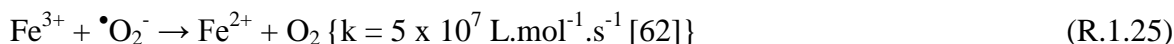
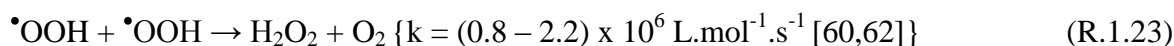
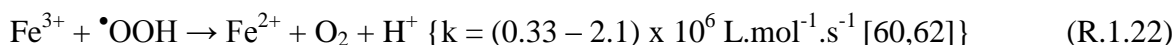
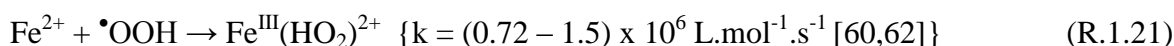


Besides the reactions that generate free radicals, several detrimental reactions occur during the Fenton oxidation process, such as radical scavenging reactions (reactions between hydroxyl radicals with non-organic substances - (R.1.15) to (R.1.21), or decomposition of H_2O_2 into water and oxygen (R.1.22):





The hydroperoxyl radicals ($\bullet\text{OOH}$) produced in reaction (R.1.3) and (R.1.11) exhibit lower oxidation potential compared to $\bullet\text{OH}$ ($E^0 = 1.65 \text{ V vs. } 2.8 \text{ V}$) and also unstable in water [35]. These molecules react with ferrous or ferric ions, combine each other or undergo disproportionation to superoxide ($\bullet\text{O}_2^-$) and hydrogen ion (H^+) rather than reacting with the contaminants:



In addition, some studies proposed non-radical pathway producing high-valent iron species (Fe(IV)), especially under circumneutral pH condition [63–66]:



1.3.1.2. Heterogeneous system

There are several major drawbacks associated with homogeneous Fenton oxidation especially when applied at large scale, among which [37,57,67]:

- i. the need of operating in an acid pH range to avoid the precipitation of iron oxyhydroxides, requiring subsequent neutralization of the effluent;
- ii. the difficulty to separate and recover dissolved iron ions from the treated solution, thus requiring an additional treatment stage;
- iii. the possibility of iron sludge formation which creates disposal problems;

- iv. the limitations in oxidant utilization efficiency due to radical scavenging and H_2O_2 self-decomposition;
- v. the slow regeneration of ferrous ion (rate limiting step), thus increasing the catalyst demands.

Utilization of heterogeneous catalysts (containing surface ferrous and/or ferric species) is expected to overcome some of the drawbacks associated with Fenton oxidation: the uneasy recovery of dissolved catalyst and the necessity of iron sludge management.

There are numerous types of iron containing solids that can be used as Fenton oxidation catalysts: iron oxide minerals (*e.g.* ferrihydrite, ferrite, goethite, magnetite, hematite, pyrite, schorl), iron oxide immobilized on high specific area materials (*e.g.* activated carbon, alumina, biosorbent, polymer fiber, silica, zeolite), iron containing clays (*e.g.* laterite, bentonite, kaolinite, laponite, vermiculite, sepiolite, saponite, montmorillonite), waste materials (*e.g.* fly ash, pyrite ash, steel industry waste, iron sludge), and zero valent iron (ZVI) [35,60,68,69]. Among these catalysts, iron containing zeolites are very promising due to their high activity and stability [68].

Compared with the homogeneous reaction, the mechanism of pollutant degradation via heterogeneous reaction has been less investigated and is still subject of discussion. In general there are two possible mechanisms for heterogeneous Fenton reaction (figure 1.5) [65]: first, a heterogeneous Fenton reaction mechanism induced by iron surface species on the catalyst [70,71] and second, a homogeneous Fenton reaction mechanism induced by leached iron in solution [72,73]. A surface radical mechanism similar to that of the homogeneous reaction has been proposed by several researchers [70,71,74,75].

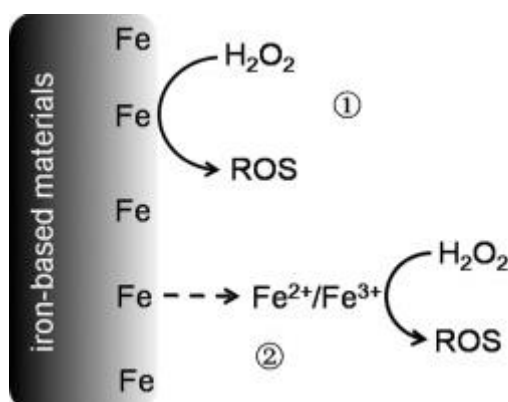


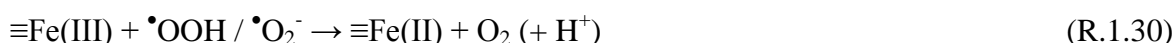
Figure 1.5. Schematic diagram of Fenton reaction using iron containing solids: (1) heterogeneous mechanism induced by iron surface species and (2) homogeneous mechanism induced by leached iron (adapted from reference [65])

If ferrous active sites are already available on catalyst surface, they can react directly with hydrogen peroxide (R.1.27). If not, hydrogen peroxide first forms a complex with ferric sites located on catalyst surface, that are subsequently converted to ferrous species ((R.1.28) and (R.1.29)) [70,71,75];

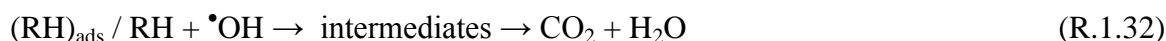


Where \equiv indicates species on catalyst surface

Hydroperoxyl radical ($\bullet\text{OOH}$) can be dissociated into superoxyde ($\bullet\text{O}_2^-$) and hydrogen ion (H^+), as shown previously in equation (R.1.24). Similarly to what reported for the homogeneous system (see equations (R.1.22) and (R.1.25)), $\bullet\text{OOH}$ and $\bullet\text{O}_2^-$ radicals play an important role in the redox cycle of iron, because they can react with ferric sites to form ferrous active sites (R.1.30), which subsequently react with H_2O_2 and generate hydroxyl radicals ($\bullet\text{OH}$) [71,75]:



The hydroxyl radical may attack species adsorbed on active sites, as well as aqueous species:



In heterogeneous Fenton oxidation, some studies also reported a non-radical pathway producing high-valent iron species [50,65,76]:



Both mechanisms are illustrated on figure 1.6 for the case of an iron containing zeolite [50].

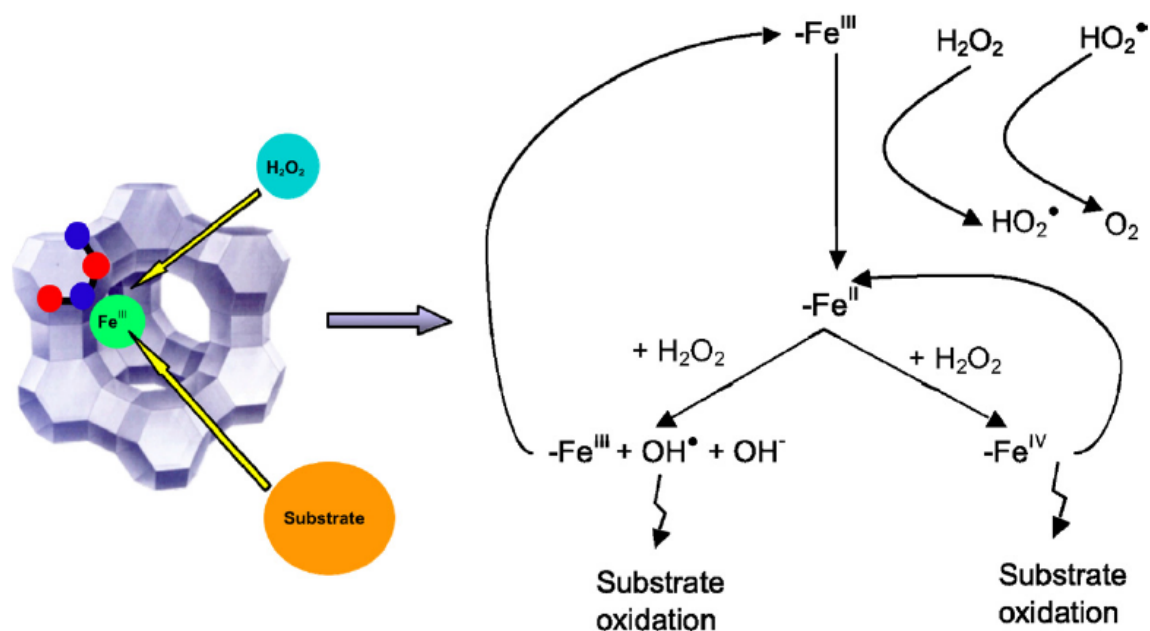


Figure 1.6. Representation of possible mechanisms involved in heterogeneous Fenton-like reactions catalyzed by Fe-zeolites (adapted from reference [50])

1.3.2. Review of recent studies on Fenton oxidation

Examples of recent studies (≥ 2013) about homogeneous Fenton oxidation of organic compounds are given in table 1.5. Homogeneous Fenton reaction was found to be effective for the removal of pharmaceuticals [77,78]; however, the conversion and mineralization yield depended on the target pollutant [79].

Some recent studies (≥ 2000) on heterogeneous Fenton oxidation are summarized in table 1.6: on the whole they exhibited slower degradation rates than the homogeneous system (see table 1.5), as shown by longer reaction times to yield significant X_{pol} and X_{TOC} . For instance, Kusić et al [80] reported that the removal rate of phenol was much slower in heterogeneous Fenton oxidation using Fe-ZSM5 than in homogeneous Fenton process performed under similar theoretical total iron concentration, as complete pollutant conversion required 30 and 2 min, respectively. Despite of its advantages described above, the application of the heterogeneous process thus requires activation techniques to improve its performance.

Table 1.5. Recent studies on homogeneous Fenton process

References	Typical experimental conditions	Remarks
Siddique et al. (2014) [81]	Pollutant: Reactive Blue 19 (25 mg/L); catalyst: FeSO₄ 3 mg/L Fe(II); [H ₂ O ₂] = 0.5 mM; T = 25°C; pH = 3.5	X _{pol} = 10% in 30 min. No significant removal of dyes was observed under investigated operating conditions.
Cavalcante et al. (2013) [79]	Pollutant: mitoxantrone 0.07 mM; catalyst: FeSO₄ 0.54 mM Fe(II); [H ₂ O ₂] = 18.8 mM; T = 25°C; pH = 3	X _{pol} = 10% in 140 min. Voltammetric and spectrophotometric experiments indicated that Fenton reactions were hindered by the complexation of Fe(III) with mitoxantrone.
Wang et al. (2015) [82]	Pollutant: diazinon 50 mg/L; catalyst: FeSO₄ 10 mg/L Fe(II); [H ₂ O ₂] = 100 mg/L; T = 25°C; pH = 3	X _{pol} = 62%, X _{TOC} = 6% in 60 min. The ratio of TOC removal/diazinon removal was very low indicating that diazinon was only transformed to other organic by-products.
Velásquez et al. (2014) [83]	Pollutant: sulfathiazole 47 μM; catalyst: FeSO₄ 0.2 mM Fe(II); [H ₂ O ₂] = 1.9 mM; T = 25°C; pH = 3	X _{pol} = 84% in 8 min, X _{TOC} = 30% in 60 min. Oxamic acid formed as a by-product remained stable during Fenton oxidation.
de Luna et al. (2013) [78]	Pollutant: paracetamol 5 mM; catalyst: FeSO₄ 0.5 mM Fe(II); [H ₂ O ₂] = 25 mM; T = 25°C; pH = 3	X _{pol} > 90%, X _{TOC} = (-) in 40 min. k = 1.68 mM/min. Fenton oxidation was effective for paracetamol removal. Paracetamol removal increased with increase of Fenton reagent concentration.

X_{pol} refers to the conversion of pollutant, X_{TOC} to the conversion of total organic carbon (mineralization yield)

Table 1.6. Recent studies on heterogeneous Fenton processes

Processes	Typical experimental conditions	Remarks
Centi et al. (2000) [84]	Pollutant: propionic acid (TOC = 30 mg/L); catalyst: Fe-ZSM5 0.7 g/L; [H ₂ O ₂] = 1.5× stoichiometric amount; T = 70°C; pH = 4	X _{TOC} = 60% in 240 min. Compared to the homogeneous Fenton process, heterogeneous process exhibited slower degradation rate, but higher TOC removal efficiency.
Kusić et al. (2006) [80]	Pollutant: phenol (TOC = 80 mg/L); catalyst: Fe-ZSM5 1.5 g/L; [H ₂ O ₂] = 40 mM; T = 25°C; pH = 3	X _{pol} = 100% in 30 min, X _{TOC} = 45% in 60 min. Longer reaction time (30 min vs. 2 min) was needed by Fe-ZSM5 catalyst to obtained similar conversion of phenol as homogeneous system.
Zhou et al. (2008) [85]	Pollutant: 4-chlorophenol 100 mg/L (0.8 mM); catalyst: ZVI 1 g/L (18 mM of Fe); [H ₂ O ₂] = 1.7 g/L (50 mM); T = 20°C; pH = 4	X _{pol} = 100%, X _{TOC} = (-) in 30 min. The authors conclude on a two-stage mechanism: a slow then much faster degradation. The latter was attributed to iron leaching inducing homogeneous reaction.
Velichkova et al. (2013) [58]	Pollutant: paracetamol 0.66 mM; catalyst: Fe₃O₄ 1 g/L; [H ₂ O ₂] = 28 mM; T = 60°C; pH = 2.6	X _{pol} = 100% in 150 min, X _{TOC} = 45% in 300 min. A small excess of oxidant should be preferred because of the occurrence of scavenging effect.
Zha et al. (2014) [73] 1.1.1.	Pollutant: amoxicillin 50 mg/L (0.14 mM); catalyst: ZVI 500 mg/L (9 mM of Fe); [H ₂ O ₂] = 224 mg/L (6.6 mM); T = 30°C; pH = 3	X _{pol} = 87%, X _{COD} = 71% in 25 min. Initial pH was the most significant operating parameter since it affected the extent of Fe ²⁺ leaching from ZVI.
Cihanoğlu et al. (2015) [86]	Pollutant: Acetic acid (100 mg/L (1.7 mM); catalyst: Fe-ZSM5 1.33 g/L; [H ₂ O ₂] = 8.35 mM; T = 60°C; pH = 4	X _{TOC} = 50% in 120 min. Acetic acid degradation was accelerated in acidic medium with the increase in temperature, H ₂ O ₂ and catalyst amount.

X_{pol} refers to the conversion of pollutant, X_{TOC} to the conversion of total organic carbon (mineralization yield)

1.4. SONOLYSIS AND SONO-FENTON PROCESSES

1.4.1. Principle and mechanisms

1.4.1.1. Ultrasound process

The development of ultrasound-based technology in water treatment originated from the discovery that ultrasonic waves (at 20 kHz) were able to cause a thinning of cell walls of microbes, attributed to the freeing of the cytoplasm membrane from the cell wall [87]. In recent years, ultrasound has been used for water disinfection, anti-scaling treatment and algae control [88].

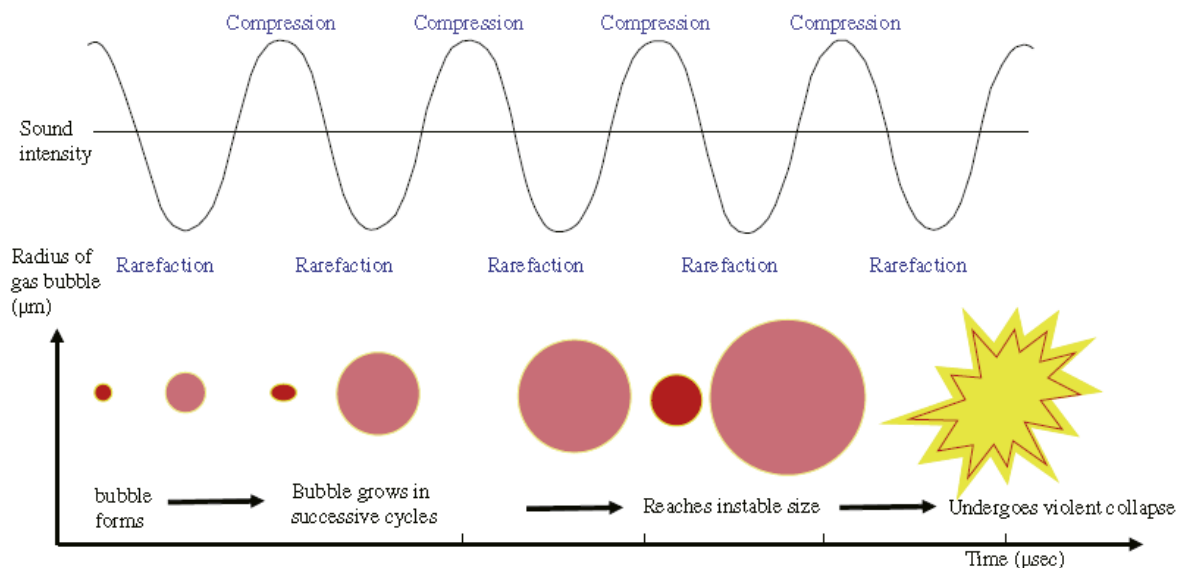


Figure 1.7. Typical scheme of acoustic cavitation
(adapted from reference [89])

Theoretically, ultrasound irradiation (or ultrasonication) alone is capable to generate hydroxyl radicals through water pyrolysis. When water is irradiated with sound waves, it generates compressions and rarefactions, thus micro-bubbles (cavitation bubbles) are formed in the rarefaction regions (figure 1.7). These micro-bubbles grow in successive cycles until they reach their resonant diameter and finally collapse violently producing shock waves (temperature of around 5000°C and pressure of 500 atmospheres during a few microseconds). The process of rapid growth and implosive collapse of bubbles is known as cavitation and creates three regions for sonochemical reactions to take place (figure 1.8) [90,89,91]:

- i. The region inside the bubble cavity (gaseous region) where volatile and hydrophobic molecules are degraded via pyrolysis and hydroxyl radicals attacks

- ii. The region at the bubble-liquid interface where hydrophobic molecules are degraded via hydroxyl radical attacks
- iii. The liquid bulk region where free radicals formed at the bubble-liquid interface generate secondary sonochemical reactions

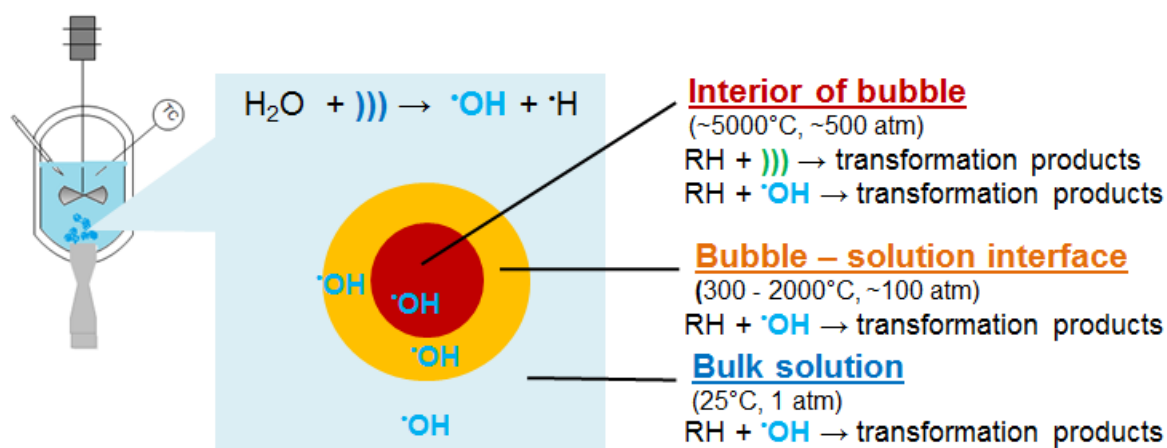
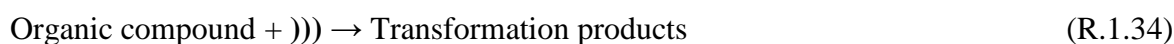


Figure 1.8. General mechanism of sonochemical reactions
 (adapted from reference [92])

In bubble cavity, both thermal cleavage (direct sonolysis) of organic compounds (R.1.34) and generation of reactive radical species (R.1.36) occur [91–93]:



Where))) refers to the ultrasound irradiation

$\cdot\text{OH}$ radicals formed by water sonolysis can further react with pollutants or recombine to form H_2O_2 . It is well known that the resonance radius and duration of the collapse of a bubble are lower at high frequencies (> 100 kHz) because the finite time of the rarefaction cycle is too short to allow a bubble to grow and collapse [94]. For instance, the resonance radius of acoustic bubble ranges from 3.3 μm at 1 MHz, 7 μm at 515 kHz and 170 μm at 20 kHz according to linear acoustic theory [92,95]. Note, however, that in practice the size of cavitation bubbles is usually smaller than this radius, due to the nonlinear nature of the

bubble pulsation [96]. Since the resonance radius and duration of the bubble are lower at high frequency, $\bullet\text{OH}$ could be ejected more efficiently from bubble cavity into liquid phase before they have time to recombine in the cavitation bubble. In liquid bulk solution, $\bullet\text{OH}$ can either react with target pollutant or recombine to form H_2O_2 . At low US frequency (especially in the typical 20-40 kHz range), bigger and long-lived bubbles are formed and $\bullet\text{OH}$ are preferentially recombined or even scavenged by other radicals in bubble cavity and bubble-liquid interface causing smaller portion of $\bullet\text{OH}$ ejected into bulk solution. Under this condition, only volatile and hydrophobic compounds which easily diffuse into bubble cavity or interface can be degraded (figure 1.8) [92]. Apart from that, low frequency ultrasound bubble has sufficient rarefaction time to grow, thus results a in more violent collapse, generating shockwave and favoring mechanical effects [89].

Numerous works have been devoted to the sonolysis of organic compounds. Various ultrasound frequencies (f_{US}) ranging from 20 kHz to 1200 kHz have been used [40,41,97–106]. However, most studies used a single frequency, and only a few investigated different frequencies [41,99,100,103–107]. Based on their conclusions, the optimum frequency range in sonochemical processes seems to be molecule- and transducer-dependent. Degradation of volatile compounds are favored at low frequencies [103], while removal of non-volatile compounds usually increased with increasing frequencies [41,99,100,104–106]. However, there exists an optimum frequency beyond which negative effects of frequency on degradation rates are observed [99,100,104,108,109]. In addition, even some ultrasound transducer are multi-frequency, the effective power may be very low at working limits (at low and high frequency limit) [100,108] that may explain why the optimum frequency for sonochemical process is normally around 580 – 860 kHz. In any cases, the comparison of low and high frequency ultrasound is still rarely studied [110,111].

Regarding the effect of ultrasound power, some researchers reported the existence of optimum value, beyond which sonochemical effect is reduced because of the scattering effect and/or coalescence of cavitation bubbles resulting into lower collapse pressure [92,112]. Similar to ultrasound frequency, the optimum ultrasound power in sonochemical processes seems to be transducer-dependent.

1.4.1.2. Activation of Fenton reaction by ultrasound

However, due to the low mineralization yield and high energy consumption of ultrasound, it is usually not recommended as single treatment [92,97,100,111]. On the other

hand, there is a strong interest in combining it with other AOPs such as Fenton reaction and taking advantage of possible beneficial synergistic effects for reducing treatment time and chemical costs [82,113–115].

Indeed, in situ hydrogen peroxide generated from ultrasound can react with Fe^{2+} , producing $\bullet\text{OH}$ in the solution bulk that can more easily react with the contaminants (R.1.1). Ultrasound also enhances the decomposition of Fe-OOH^{2+} into Fe^{2+} and hydroperoxyl radicals [93] (R.1.37):



Moreover, hydrogen radicals ($\bullet\text{H}$) formed by water sonolysis can react either with hydrogen peroxide, ferric ion, hydroperoxyl radicals or hydroxyl radical to produce hydroxyl radical, ferrous iron, hydrogen peroxide, or water respectively [116]:



Ferrous ion produced from (R.1.37) and (R.1.39) can react subsequently with hydrogen peroxide, as per Fenton oxidation mechanism.

With heterogeneous catalysts, the sono-Fenton reactions are similar to those reported for the homogenous system, but they occur on the catalyst surface [117]. A coupling of heterogeneous catalyst with low frequency ultrasound can also be interesting since the ultrasonic irradiation may (i) improve mixing and decrease mass transfer limitation, (ii) reduce the particle size of heterogeneous catalysts leading to a higher amount of available catalyst active sites, and (iii) promotes a continuous cleaning of the solid catalyst surface. In addition, the presence of solid particles provides additional nuclei enhancing cavitation phenomena [118–122]. However it can also result into ultrasound attenuation by scattering

effect or viscous loss, depending on the particle size with respect to the sound wavelength [123]. Similar mechanism to the homogeneous one is usually postulated for heterogeneous systems in which reaction (R.1.37) is assumed to occur on the solid catalyst surface [121,124].

1.4.2. Review of recent studies

Previous works have showed that low and high frequency ultrasound was able to yield partial or complete degradation of pharmaceuticals [40,41,97–100,102,111,108,125,109]. However, complete mineralization is usually difficult to achieve under single ultrasound process [40,41,92,97,99,100,111,125].

Furthermore, several studies also have been devoted to evaluate the performance of sono-Fenton oxidation with homogeneous and heterogeneous systems. In homogeneous system, coupling ultrasound with Fenton reaction slightly improved the degradation rate of methyl tert-butyl ether, bisphenol A and dye RB19 compared with that observed for ultrasound or Fenton alone [81,113,126]. On the other hand, the advantage of coupling ultrasound process with heterogeneous Fenton reaction is still a matter of discussion. It can be seen from table 1.7 that either a synergistic interaction [64,105,119] or minor effects (less than additive effects) [127–129] were reported. In some studies, the possibility of catalyst surface activation by ultrasound was unclear as no comparison was made with the sole Fenton reaction or the activity of leached iron was not evaluated [117,121,124,130–132].

Table 1.7. Examples of studies on sonolysis and sono-Fenton oxidation processes

Processes	Typical experimental conditions	Remarks
Sonolysis [125]	Pollutant: paracetamol 83 μM ; T = 20 ± 1 $^{\circ}\text{C}$; pH = 5,6; $f_{\text{US}} = 600$ kHz; $P_{\text{US}} = 60$ W*, $D_{\text{US}} = 200$ W/L	$X_{\text{pol}} = 46\%$ in 60 min. Sonolysis of paracetamol was improved in acidic condition for which paracetamol was in molecular form.
Sonolysis [99]	Pollutant: diclofenac 30 μM ; T = 25 $^{\circ}\text{C}$; pH = 5.7; $f_{\text{US}} = 861$ kHz; $D_{\text{US}} = 230$ W/L*	$X_{\text{pol}} = 100\%$ in 60 min. $k = 0.005$ min^{-1} . Sonolysis of diclofenac was improved at low pollutant concentration and acidic condition.
Homogeneous sono-Fenton [113]	Pollutant: methyl tert-butyl ether 0.1 mM; catalyst: FeSO₄ 1 mM Fe(II); $[\text{H}_2\text{O}_2] = 500$ mM; T = 20 $^{\circ}\text{C}$; pH = 3; $f_{\text{US}} = 20$ kHz; $P_{\text{US}} = 11.7$ W; $D_{\text{US}} = 80$ W/L	$X_{\text{pol}} = 100\%$ in 300 min. Addition of Fe(II) significantly improved (7 times) oxidation process efficiency (compared to silent-Fenton).

Homogeneous sono-Fenton [81]	Pollutant: RB 19 0.04 mM; Catalyst: FeSO₄ 3 mg/L Fe(II); [H ₂ O ₂] = 0.5 mM; pH = 3.5; f _{US} = 20 kHz ; P _{US} = 45.6 W; I _{US} = 8 W/cm ² ; D _{US} = 50 W/L	X _{pol} = 78% in 30 min. Synergistic interaction between ultrasound and Fenton was observed. The decoloration of dye solution increased with the increase of hydrogen peroxide concentration, ultrasonic power and iron sulfate concentration, but decreased by increasing the initial dye concentration.
Heterogeneous sono-Fenton [105]	Pollutant: 4-chlorophenol 100 mg/L; catalyst: iron powders (slag) 1 g/L; [H ₂ O ₂] = 3 mM; T = 30°C; f _{US} = 200 kHz; P _{US} = 50 W*; D _{US} = 50 W/L	X _{pol} = 40% in 60 min. The addition of iron powder and H ₂ O ₂ significantly enhanced the degradation rate compared to ultrasound only.
Heterogeneous sono-Fenton [127]	Pollutant: 2,4-dichlorophenoxyacetic acid 1.1 mM; catalyst: ZVI 0.6 g/L; [H ₂ O ₂] = 85.5 mM; T = 22°C; pH = 3; f _{US} = 20 kHz; P _{US} = 45 W*; I _{US} = 57.3 W/cm ² ; D _{US} = 150 W/L	X _{TOC} = 64% in 60 min. Low frequency ultrasound slightly improved Fenton oxidation process efficiency (7% improvement with respect to sole Fenton process).
Heterogeneous sono-Fenton [121]	Pollutant: C.I. Acid Orange 7 0.23 mM; catalyst: goethite 0.2 g/L; [H ₂ O ₂] = 7.8 mM; T = 20°C; pH = 3; f _{US} = 20 kHz; P _{US} = 20 W*; I _{US} = 25.5 W/cm ² ; D _{US} = 80 W/L	X _{pol} = 100% in 30 min; X _{TOC} = 42% in 90 min. Hydrogen peroxide concentration and pH played an important role in the degradation process
Heterogeneous sono-Fenton [117]	Pollutant: phenol 2.5 mM; catalyst: Fe₂O₃/SBA-15 0.6 g/L; [H ₂ O ₂] = 70 mM; T = 25°C; pH = 3; f _{US} = 584 kHz; D _{US} = 29 W/L*	X _{TOC} = 30% in 240 min; Heterogeneous sono-Fenton was more effective than heterogeneous Fenton and US/H ₂ O ₂ processes. Ultrasound frequency of 584 kHz was better than 20 kHz and 1142 kHz.
Heterogeneous sono-Fenton [119]	Pollutant: bisphenol A 0.09 mM; catalyst: Fe₃O₄ 0.6 g/L; [H ₂ O ₂] = 160 mM; T = 35±1°C; pH = 3; f _{US} = 40 kHz; P _{US} = 100 W	X _{pol} = 95%, X _{TOC} = 45% in 480 min. Coupling of heterogeneous Fenton reaction and ultrasound was very synergic (increase of the removal efficiency by up to 4 times compared to the separate processes).
Heterogeneous sono-Fenton [129]	Pollutant: C.I. Acid Orange 7 0.14 mM; Catalyst: Fe-ZSM5 ([Fe equivalent] = 0.1 mM); [H ₂ O ₂] = 5 mM; f _{US} = 850 kHz; P _{US} = 22.3 W*; D _{US} = 112 W/L	X _{pol} = 47% in 120 min. Degradation of C.I. Acid Orange 7 under sono-Fenton was dominated by US/H ₂ O ₂ process

*Ultrasound (US) power measured by calorimetry

X_{pol} refers to the conversion of pollutant, X_{TOC} to the conversion of total organic carbon (mineralization yield)

1.5. PHOTOLYSIS AND PHOTO-FENTON PROCESSES

1.5.1. Principle and mechanisms

1.5.1.1. Photo-degradation

Initially restrained to water disinfection, ultraviolet (UV) photochemical processes continue to expand in water treatment due to the following features: (i) simple and chemical free process; (ii) inactivation of a broad range of microorganisms; (iii) formation of a minimum of side products; (iv) formation of innocuous and biodegradable low molecular weight products; (v) diminution of effluent toxicity [133]. The rate of photochemical transformation of a compound A is related to quantum yield (Φ) of the reaction at given wavelength (λ) and the local volumetric rate of photon absorption of the species A at given λ (amount of photons absorbed by the species per unit of time and per unit of reactor volume). The second parameter depends upon the concentration of the species A, its Napierian molar absorption coefficient and the irradiance field (both function of λ). The irradiance field is a function of light source (power and wavelength), transparency of the medium and reactor geometry (shape, path length) [133,134]. Several types of UV-Vis lamps are available for water treatment (especially AOPs), which are described in [table 1.8](#).

Table 1.8. Characteristics of UV-Visible lamps used for AOPs

Lamp	Wavelength	Description
Lower pressure mercury (LP Hg) lamp	185 – 265 nm (max around 254 nm) or 254 nm, depending on bulb type	A gas-discharge lamp that uses mercury vapor as electric initiation gas and works at a low vapor pressure promoting the production of monochromatic light (254 nm). Type of quartz bulb material may affect emission spectrum.
Medium pressure mercury (MP Hg) lamp	200 – 600 nm (high around 250 – 365 nm with some peaks in visible region)	A gas-discharge lamp that uses mercury vapor as electric initiation gas and works at a high vapor pressure promoting the production polychromatic light
Black light blue lamp	315 – 400 nm (max at 365 nm)	A modification of MP Hg lamp that emits long wave (UV-A) ultraviolet light due to a utilization of a blue/violet filter material
Halogen lamp	400 – 1000 nm (high around 700 – 900 nm)	A classic incandescent lamp that emits visible light
Xenon lamp	300 – 800 nm (high around 400 – 550 nm)	A gas-discharge lamp that uses xenon vapor as electric initiation gas and works at a high vapor pressure producing white light mimicking natural sunlight

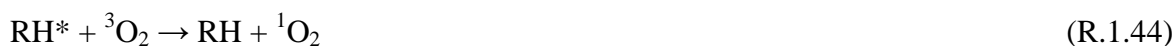
Excimer lamp	108 – 351 nm	Quasi monochromatic light sources that can operate over a wide range of wavelengths in the ultraviolet (UV) and vacuum ultraviolet (VUV) spectral regions
--------------	--------------	---

The first mechanism implied in UV-Vis activated oxidation processes is the direct photolysis of the pollutant. Under light irradiation, organic compounds are transform into their excited singlet states then undergo degradation process through homolysis, heterolysis or photoionization [133,135,136] :



Where $h\nu$ refers to the light irradiation and $()^*$ refers to excited state

Furthermore, the excited state of the pollutant can undergo photo-sensitization reactions generating a high energy form of oxygen (called singlet molecular oxygen (1O_2)) [133,135] or producing active radicals [137,138] according to following reactions :

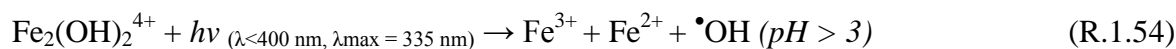
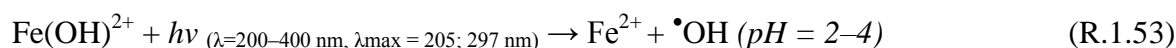
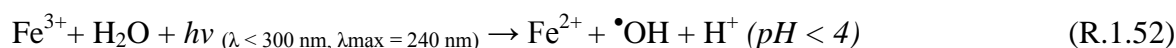


In addition, if the light irradiation emits light near vacuum UV spectrum, $\bullet OH$ can be formed [42,44,139–141] according to reactions:



1.5.1.2. Activation of Fenton reaction by (UV/Vis) light

In previous studies, UV photolysis has been used in combination with H₂O₂, ozone and Fenton reaction [18,142,143] in order to improve pollutant removal and mineralization rate. In the presence of Fenton reagent, not only photo-decomposition of H₂O₂ occurs (R.1.48), but also other reactions including photo-reduction of ferric ions (R.1.52), photo-reduction of iron(III)-hydroxo complexes (R.1.53-R.1.54) and photo-reduction of ferric-H₂O₂ complex (R.1.55) [63,144–148]:



In addition, photo-decarboxylation of the ferric carboxylates formed by complexation of ferric ions with organic ligands is also possible under UV-A and visible light [149–152]:



Reactions (R.1.52) to (R.1.55) are promoted in different wavelength ranges, and tables 1.9 and 1.10 report their quantum yields Φ .

Table 1.9. Quantum yield of $\cdot\text{OH}$ generation by photolysis of iron(III)-hydroxo complexes

Hydroxo complexes of iron (III)	λ (nm)	Φ ($\cdot\text{OH}$)	Φ (Fe^{2+})	References
$\text{Fe}^{3+}(\text{H}_2\text{O})_6$	254	0.046-	0.13	[146,153]
	< 300	0.065 0.05		
$\text{Fe}(\text{OH})^{2+}(\text{H}_2\text{O})_5$	240	0.83	0.14–0.19	[146]
	254	0.69		[146]
	280	0.31		[152]
	313	0.1–0.2		[63,146]
	370	0.07		[145]
	380	0.05		[146]
$\text{Fe}_2(\text{OH})_2^{4+}(\text{H}_2\text{O})_8$	350	0.007		[153]

Table 1.10. Quantum yield of Fe(II) formation by photolysis of ferricarboxylate complex

Carboxylic acids	Φ at 365 nm
Formic acid	0.5 – 0.55
Tartaric acid	1.1
Oxalic acid	1.0 – 1.2
Citric acid	0.589
Malic acid	0.510
Maleic acid	0.2 – 0.29
Malonic acid	0.026

(adapted from reference [148])

Reports about mechanisms of heterogeneous photo-Fenton oxidation are scarce, and the authors usually assumed that they are similar to the ones of homogeneous system, but implying iron surface species [132,154]. On the other hand, Wang et al. [155] proposed the mechanism illustrated in [figure 1.9](#) for the case of goethite. It suggests that light irradiation promotes dissolution of iron complex formed on the solid surface, inducing photochemical reactions in the liquid phase. Likewise, some works using ZVI reported a higher iron leaching under UV light irradiation [140,156].

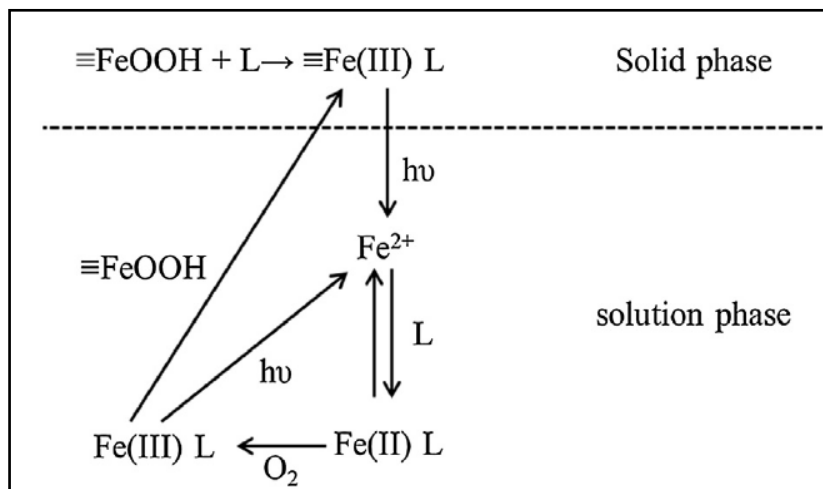


Figure 1.9. Mechanism of photo-reductive dissolution of Fe(III) complex on goethite (adapted from reference [151,155])

1.5.2. Review of recent studies

Recent studies on photolysis, UV/H₂O₂ and photo-Fenton are summarized in [table 1.11](#). Some researchers reported that UV irradiation is effective for removal of pharmaceuticals due to their high absorption in the UV-C spectrum region ($\lambda=200 - 280$ nm). Addition of H₂O₂ on UV photolysis was also found beneficial, but the enhancement is dependent on the molecule sensitivity to direct photolysis [18,42,142,157]. Regarding photo-Fenton process, coupling light irradiation and homogeneous Fenton reaction was usually beneficial [67,158,159].

Conversely, real synergistic interaction in heterogeneous photo-Fenton is still subject of debate. Numerous studies observed that heterogeneous photo-Fenton was more efficient than heterogeneous Fenton oxidation [80,132,154,160–166]. However, some of them concluded that the enhancement was due to the UV/H₂O₂ reaction [161–163], or reported a significant contribution of iron leaching [164–166]. The latter is rather difficult to assess considering the evolution of iron concentration and speciation during the reaction [161]. Therefore, more studies are needed to evaluate the possible synergistic effect and get better understanding in the involved mechanisms.

Table 1.11. Examples of studies on photolysis and photo-Fenton oxidation processes

Process	Typical experimental conditions	Remarks
Photolysis [18]	Pollutant: naproxen (NPX) 10 mg/L and carbamazepine (CBP) 7 mg/L; T = 25°C; pH = 7; MP Hg lamp; P _{UV} = 1000 W	k = 0.29 min ⁻¹ (NPX), k = 0.004 min ⁻¹ (CBP). Photolysis degradation of naproxen was faster than carbamazepine due to higher UV absorbance in UV-C region.
Photolysis [142]	Pollutant: 5-methyl-1,3,4-thiadiazole-2-methylthio (MMTD) 1 - 100 mg/L; T = 25°C; LP Hg lamp; P _{UV} = 17 W; λ = 254 nm (2.8x10 ⁻⁶ Einstein/s)	X _{Pol} > 90% (for C ₀ =1 mg/L), X _{Pol} = 40% (for C ₀ =100 mg/L). MMTD degradation rate and yield increased with decrease in initial concentration of pollutant.
UV/H ₂ O ₂ [18]	Pollutant: naproxen (NPX) 10 mg/L and carbamazepine (CBP) 7 mg/L; [H ₂ O ₂] = 50 mg/L; T = 25°C; pH = 7; MP Hg lamp; P _{UV} = 1000 W	k = 0.69 min ⁻¹ (NPX), k = 0.70 min ⁻¹ (CBP). Effect of H ₂ O ₂ addition on photolysis process was more remarkable for less photo-degradable compound such as carbamazepine.
Homogeneous photo-Fenton [159]	Pollutant: sulfamonomethoxine 4.5 mg/L; catalyst: Fe²⁺ 0.02 mM; [H ₂ O ₂] = 0.49 mM; T = 25°C; pH = 4; P _{UV} = 12 W; λ = 365 nm	X _{Pol} = 98%, X _{TOC} = 99% in 120 min. Degradation of SMMS in photo-Fenton process was described by first-order kinetics, and the apparent activation energy was 23.95 kJ/mol.
Homogeneous photo-Fenton [158]	Pollutant: valproate 0.35 mM; [Fe²⁺] = 0.18 mM; [H ₂ O ₂] = 4.4 mM; pH = 3; T = 25°C; UV-C lamp; λ = 254 nm; P _{UV} = 24W (1.85 x 10 ⁻⁵ E/s)	X _{Pol} = 100%, X _{TOC} = 76.3% in 120 min. Photo-Fenton reaction was more effective under UV-A than visible light
Heterogeneous photo-Fenton [160]	Pollutant: phenol 1 mM; catalyst: Fe-laponite 1 g/L; [H ₂ O ₂] = 50 mM; T = 30°C; pH = 3; UV-C and UV-A lamps; P _{UVC} = 15 W; λ _{UVC} = 254 nm; P _{UVC} = 40 W; λ _{UVC} = 365 nm	X _{Pol} = 100% in 5 min (UV-C) and X _{Pol} = 100% in 25 min (UV-A). Fast degradation of phenol was observed under UV-C irradiation due to the contribution of UV/H ₂ O ₂ reaction. On the other hand, synergistic effect was clearly observed under UV-A light. Contribution of iron leaching was also negligible.
Heterogeneous photo-Fenton [161]	Pollutant: reactive red HE-38 100 mg/L; Catalyst: Fe-laponite 1 g/L; [H ₂ O ₂] = 500 mg/L; T = 30°C; pH = 3; UV-C lamp; P _{UVC} = 16 W; λ _{UVC} = 254 nm	X _{TOC} = 76% in 120 min. Additive interaction between Fenton and UV/H ₂ O ₂ reactions was observed in terms of TOC mineralization.
Heterogeneous photo-Fenton [80]	Pollutant: phenol 1 mM; catalyst: Fe-ZSM5 1.5 g/L (1 mM of Fe); [H ₂ O ₂] = 40 mM; T = 25°C; pH = 3; LP Hg lam; P _{UV} = 125 W; λ = 254 nm (0.34x10 ⁻⁵ E/s)	X _{Pol} = 100%, X _{TOC} = 86% in 60 min. UV irradiation enhanced TOC removal of heterogeneous Fenton oxidation by up to 43%. However, no comparison with UV or UV/H ₂ O ₂ alone.

Heterogeneous photo-Fenton [162]	Pollutant: C.I. Acid Blue 74 0.086 mM; catalyst: Fe-ZSM5 0.5 g/L (1 mM of Fe); [H ₂ O ₂] = 21.4 mM; T = 25°C; pH = 5.2; P _{UV} = 15 W; λ = 254 nm (1.09x10 ⁻⁵ E/s)	X _{Pol} = 100%, X _{TOC} = 85% in 120 min. Additive effect between heterogeneous Fenton and UV/H ₂ O ₂ was observed in terms of TOC removal. Fe-ZSM5 showed a good stability upon multi-run experiments.
Heterogeneous photo-Fenton [167]	Pollutant: RB 137 dye 20 mg/L; catalyst: Fe-ZSM5 1.5 g/L (1 mM of Fe); [H ₂ O ₂] = 10 mM; T = 25°C; pH = 6; LP Hg lamp (4.4 mW/cm ² , 0.37x10 ⁻⁵ E/s)	X _{Pol} = 100%, X _{TOC} = 80% in 60 min. UV/H ₂ O ₂ process was more effective than heterogeneous photo-Fenton due to light filtering effect by the catalyst.
Heterogeneous photo-Fenton [163]	Pollutant: azo-dye Orange II 0.1 mM; catalyst: Fe-ZSM5 0.2 g/L; [H ₂ O ₂] = 6 mM; T = 53°C; pH = 3; MP Hg lamp; P _{UV} = 150 W; λ = 200 – 600 nm	X _{Pol} = 100%, X _{TOC} = 60% in 120 min. Degradation by UV/H ₂ O ₂ process was found to be significant and even more effective than heterogeneous Fenton. An additive effect between UV/H ₂ O ₂ and Fenton reactions was observed.
Heterogeneous photo-Fenton [164]	Pollutant: phenol 0.52 mM; catalyst: Fe-ZSM5 2 g/L ; [H ₂ O ₂] = 22.7 mM; T = 35°C; pH = 7; Xenon arc lamp (765 W/m ²); λ = 290 – 800 nm	X _{Pol} = 100%, X _{TOC} = 50% in 180 min. In the presence of light (photo-Fenton), phenol removal was about 1.6 times faster than in dark Fenton. Leaching test revealed that the contribution of homogeneous photo-Fenton reaction was significant.
Heterogeneous photo-Fenton [165]	Pollutant: paracetamol 0.66 mM; catalyst: Fe-ZSM5 1 g/L; [H ₂ O ₂] = 28 mM; T = 30°C; pH = 5; MP Hg lamp covered with glass cooling tube; P _{UV} = 450 W; λ = 280 – 355 nm	X _{Pol} = 100%; X _{TOC} = 58% in 300 min. Faster paracetamol conversion and higher mineralization yield were obtained under photo-Fenton process. Leaching test revealed that the contribution of homogeneous photo-Fenton reaction was significant.

X_{pol} refers to the conversion of pollutant, X_{TOC} to the conversion of total organic carbon (mineralization yield)

1.6. SONO-PHOTO-FENTON PROCESSES

1.6.1. Principle and mechanisms

Combining different advanced oxidation processes can be more efficient for wastewater treatment as compared to individual processes, due to higher energy efficiency, chemical savings and/or enhanced generation of free radicals. In coupling ultrasound and ultraviolet irradiation process, hydroxyl radicals can be produced by UV decomposition of hydrogen peroxide generated by (high frequency) ultrasound. Apart from that, coupling of ultrasound, light irradiation and Fenton reaction should lead to faster pollutant conversion and higher mineralization yield due to higher generation of hydroxyl radicals and regeneration of ferrous ions according to reactions (R.1.36) and (R.152-R.1.56), respectively.

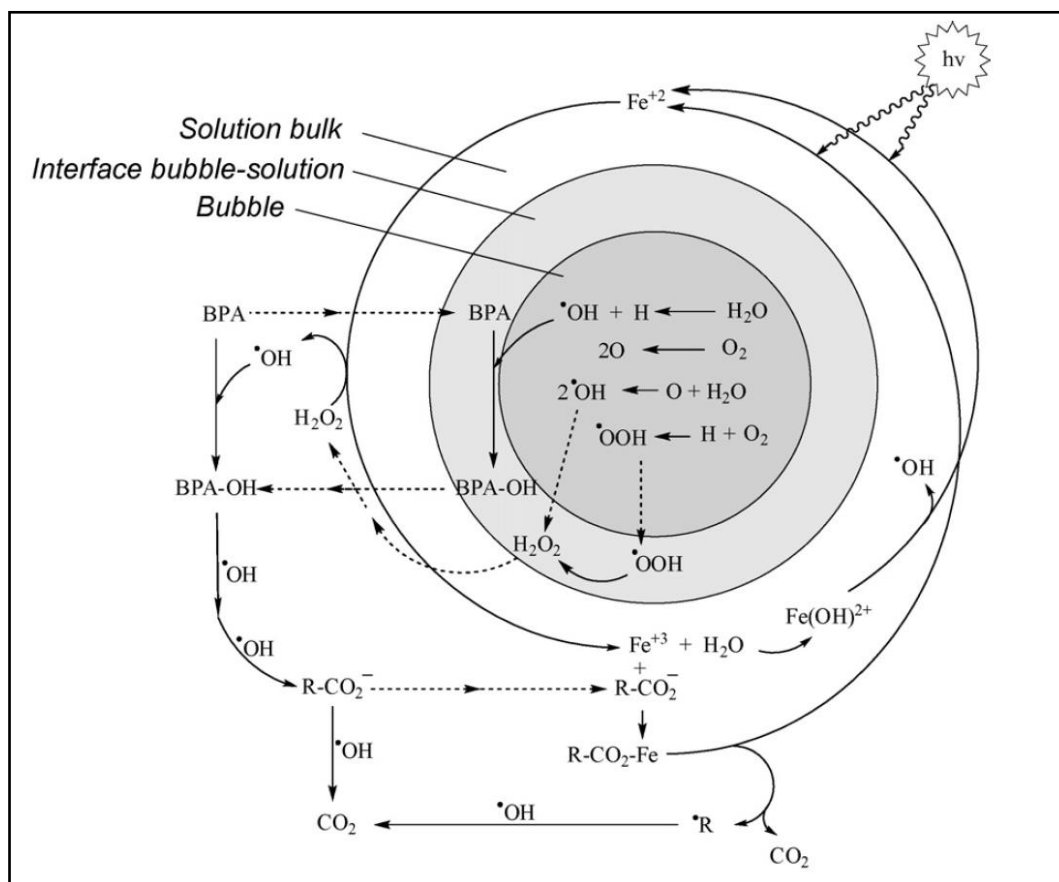


Figure 1.10. Schematic illustration of bisphenol A (BPA) mineralization under ultrasound/solar light/Fe(II) process (adapted from reference [126])

Possible mechanisms involved in the homogeneous sono-photo-Fenton oxidation are illustrated in [figure 1.10](#) for bisphenol A (BPA) [126]. The proposed pathways mainly combine those reported for the separate processes. In this scheme, •OH radicals generated from sonolysis of water oxidize BPA into more hydrophilic products at the bubble surface. These intermediates are degraded mainly in the solution bulk by •OH radicals coming from the photo-Fenton reaction ($h\nu/H_2O_2/Fe^{2+}$). This reaction is possible thanks to *in-situ* generation of H₂O₂ by ultrasound (no external H₂O₂ addition in this case). On the other hand, Fe³⁺ can form complex with aliphatic acids, but they are rapidly decomposed in the presence of light. Fe²⁺ regeneration is improved by light irradiation and possibly ultrasound, generating additional •OH radicals.

1.6.2. Review of recent studies

Some contradictory findings are actually present in the literature. Only seven of the eleven studies (table 1.12) observed a net synergistic effect [126,168–172], while in others the effect of ultrasound was found to be marginal. This indicates a possible predominant effect of photo-Fenton over sono-Fenton process in some cases [33,43,173,174]. In addition, it worth noting that only two studies applied external H₂O₂ addition, because most of the studies were performed under high frequency ultrasound (200-300 kHz).

Table 1.12. Works related to homogeneous sono-photo-Fenton oxidation

References	Typical experimental conditions	Remarks
Torres and coworkers (2007) [168]	Pollutant: bisphenol A 0.118 mM; catalyst: FeSO₄ 0.1 mM Fe(II); T = 20°C; pH = 3; f _{US} = 300 kHz; P _{US} = 80 W*; I _{US} = 4.1 W/cm ² ; D _{US} = 267 W/L; P _{UV} = 25 W; λ = 254 nm (1.5·10 ⁻⁶ E/s); O ₂ saturated solutions	X _{pol} = 95% in 75 min, X _{TOC} = 100% in 240 min. Sono-photo-Fenton is presented as the most cost-effective treatment for mineralization of bisphenol A.
Torres and coworkers (2008) [126]	Pollutant: bisphenol A 0.118 mM; catalyst: FeSO₄ 0.1 mM Fe(II); [H ₂ O ₂] = 1.6 μM/min**; T = 20°C; pH = 5; f _{US} = 300 kHz; P _{US} = 80 W*; I _{US} = 4.1 W/cm ² ; D _{US} = 133 W/L; P _{UV} = 200 W; λ = 400 – 800 nm; O ₂ saturated solutions	X _{pol} = 92% in 75 min, X _{TOC} = 70% in 240 min. Sono-Fenton was more effective in removing the initial substrate (bisphenol), while photo-Fenton was more effective in degrading reaction intermediates (TOC reduction).
Méndez-Arriaga and coworkers (2009) [33]	Pollutant: ibuprofen 0.039 mM; catalyst: FeSO₄ 0.1 g/L Fe(II); [H ₂ O ₂] = 2.5 μmol/(L.min) (in-situ); T = 25°C; pH = 3; f _{US} = 300 kHz; P _{US} = 47* W; I _{US} = 3.7 W/cm ² ; D _{US} = 78 W/L; Xenon arc lamp	X _{pol} > 90% in 60 min, X _{COD} = 55% in 240 min. The addition of ultrasound to photo-Fenton process did not improve ibuprofen degradation because Fenton-like reaction is probably favored.
Madhavan and coworkers (2010) [43]	Pollutant: ibuprofen 0.09 mM; catalyst: Fe(NO₃)₃ 0.05 mM Fe(III); T = 20°C ; pH = 2,7; f _{US} = 213 kHz; P _{US} = 13.75 W*; I _{US} = 0.6 W/cm ² ; D _{US} = 55 W/L; P _(UV) = 450 W; Xenon arc lamp	X _{pol} = 100% in 60 min, X _{TOC} = 70% in 240 min. Combination of photo-Fenton-like oxidation and US showed a slight improvement for ibuprofen conversion.
Madhavan and coworkers (2010) [173]	Pollutant: monocrotophos 0.12 mM; catalyst: Fe(NO₃)₃ 0.025 mM Fe(III); T = 25°C ; pH = 2,7; f _{US} = 213 kHz; P _{US} = 13.75 W*; I _{US} = 0.6 W/cm ² ; D _{US} = 55 W/L; P _(UV) = 450 W; Xenon arc lamp	X _{pol} = 100% in 40 min, X _{TOC} = 51% in 180 min. Performance of photo-Fenton-like oxidation was not improved by sonication.

Madhavan and coworkers (2010) [169]	Pollutant: Acid red 88 0.09 mM; catalyst: Fe(NO₃)₃ 0.05 mM Fe(III); T = 25°C ; pH = 2,7; f _{US} = 213 kHz; P _{US} = 13.75 W*; I _{US} = 0.6 W/cm ² ; D _{US} = 55 W/L; P _(UV) = 450 W; Xenon arc lamp	X _{TOC} = 40% in 240 min. Synergistic interaction between sono-Fenton and visible light irradiation was observed in the degradation and mineralization of AR88.
Katsumata and coworkers (2011) [170]	Pollutant: linuron 0.04 mM; catalyst: FeSO₄ 0.12 mM Fe(II); T = 25°C ; pH = 3; f _{US} = 200 kHz; P _{US} = 100 W; Light intensity = 2 mW/cm ² ; λ _{UV} = 320 – 410 nm	X _{pol} = 100% in 20 min, X _{TOC} = 100% in 120 min. Sono-photo-Fenton process exhibited higher degradation and mineralization rates than photolysis and sono-Fenton oxidation, but the degradation efficiency was strongly affected by pH and catalyst concentration.
Xu and coworkers (2013) [171]	Pollutant: n-butyl phthalate 0.01 mM; catalyst: FeSO₄ 0.1 mM Fe(II); T = 24°C pH = 2; f _{US} = 400 kHz; P _{US} = 7.5 W*; D _{US} = 30 W/L, λ _{UV} = 254 nm (1.72 x 10 ⁻⁶ E/(L.s))	X _{pol} = 100% in 120 min. Synergistic effects were observed in sono-photo-Fenton process, due to the enhanced generation of hydroxyl radicals.
Madhavan and coworkers (2013) [172]	Pollutant: paracetamol (P) 0.07 mM; catalyst: Fe(NO₃)₃ 0.05 mM Fe(III); T = 25°C; pH = 2,7; f _{US} = 213 kHz; P _{US} = 13.75 W*; D _{US} = 55 W/L; P _{UV} = 450 W; Xenon arc lamp	k = 18.6 x 10 ⁻⁷ M/min (P), X _{TOC} > 80% in 180 min. Synergistic interaction was observed in sono-photocatalytic oxidation using Fe ³⁺ . Sonication of paracetamol led to the formation of hydroxylated derivatives.
Dükkancı and coworkers (2014) [129]	Pollutant: C.I. Acid Orange 7 0.14 mM; catalyst: FeSO₄ 0.1 mM Fe(II); [H ₂ O ₂] = 5 mM; f _{US} = 850 kHz; P _{US} = 22.3 W*; D _{US} = 112 W/L; λ _{UV} = 254 nm	X _{pol} = 81% in 120 min. Synergistic interaction between processes was observed and decomposition of H ₂ O ₂ by UV played an important role.
Chakma and Moholkar (2014) [174]	Pollutant: bisphenol A 10 mg/L; catalyst: FeSO₄ 0.36 mM Fe(II); [H ₂ O ₂] = 7.85 mM; f _{US} = 40 kHz; D _{US} = 8.71 W/L; P _{UV} = 160 W; λ _{UV} = 365 nm	X _{pol} = 86.5% in 60 min. No synergy was observed, probably due to the predominance of UV/H ₂ O ₂ reaction.
Papoutsakis and coworkers (2015) [115]	Pollutant: phenol 80 mg/L, diuron 100 mg/L, bisphenol A 80 mg/L; catalyst: FeSO₄ 0.018 mM Fe(II); [H ₂ O ₂] = 6 mM; f _{US} = 400 kHz; P _{US} = 450 W; Solar light	X _{phenol} = 100% in 60 min, X _{bisphenol A} = 100% in 60 min. Combined effect between ultrasound and photo(solar)-Fenton oxidation was pollutant dependent: synergistic for phenol, only additive for diuron and detrimental for bisphenol A (photo-Fenton predominant)

*US power measured by calorimetric, ** No external H₂O₂ addition if ultrasound applied

X_{pol} refers to the conversion of pollutant, X_{TOC} to the conversion of total organic carbon (mineralization yield)

Table 1.13. Works related to heterogeneous sono-photo-Fenton oxidation

References	Typical experimental conditions	Remarks
Segura et al. (2009) [120]	Pollutant: phenol 2.5 mM; catalyst: Fe₂O₃/SBA-15 0.6 g/L; [H ₂ O ₂] = 35 mM; T = 22°C (and not controlled in photo-Fenton); pH = 3; f _{US} = 20 kHz; P _{US} = 52 W*; I _{US} = 39.2 W/cm ² ; D _{US} = 130 W/L; P _{UV} = 150 W; λ = 313 nm	X _{pol} = 100% in 120 min; X _{TOC} = 90% in 360 min. Synergistic effect was observed only in sequential sono-photo-Fenton process. However, it was probably due to elevated temperature during sonication and/or contribution of iron leaching (4 mg/L).
Zhong et al. (2011) [175]	Pollutant: C.I. Acid Orange 7 100 mg/L; catalyst: Fe₂O₃/SBA-15 0.3 g/L; [H ₂ O ₂] = 8 mM; T = 20°C; pH = 2; f _{US} = 20 kHz; P _{US} = 80 W**; P _{UV} = 4 W; λ _{UV} = 254 nm	X _{pol} = 80% in 60 min. Sono-photo-Fenton oxidation corresponded to the sum of sono-Fenton and photo-Fenton contributions.

*US power measured by calorimetric, ** Specific information not available

X_{pol} refers to the conversion of pollutant, X_{TOC} to the conversion of total organic carbon (mineralization yield)

On the other hand, the combined heterogeneous process has been scarcely studied (table 1.13). Segura et al. [120] compared sono-photo-Fenton with sono- and photo-Fenton oxidation and reported that it was superior to these processes, only if it was applied as sequential process (sono-Fenton followed by photo-Fenton). When both processes were performed simultaneously, photo-Fenton mechanism was dominant. However, a firm conclusion cannot be drawn due to the increase of temperature during photo-Fenton process (temperature not controlled) and higher iron leaching concentration (up to 4 mg/L). Likewise, Zhong et al [175] also observed an additive effect for removal of acid orange 7 by sono-photo-Fenton oxidation (sum of sono-Fenton and photo-Fenton contributions).

1.7. EFFECT OF OPERATING PARAMETERS IN (SONO-)(PHOTO-)FENTON PROCESSES

1.7.1. Hydrogen peroxide concentration

A higher H₂O₂ dosage than the theoretical stoichiometric amount (1.5 to 5 times) is usually required to achieve high mineralization yields due to the presence of inorganic ions that react with hydroxyl radicals [58,86,120,176]. Generally, the degradation rate of organic compounds increases with an increase in initial H₂O₂ concentration until an optimum value is reached, after which it decreases mainly due to scavenging of •OH by excess H₂O₂ [86,119,177,178]. Indeed, at high H₂O₂ concentration, hydroxyl radicals preferentially react

with H₂O₂ than with organic compounds, generating less reactive species such as $\cdot\text{OOH}$ and $\cdot\text{O}_2^-$ (see R.1.15 and R.1.24). Moreover, stepwise or continuous addition of H₂O₂ has been therefore proposed to overcome these detrimental effects [33,179,180]. In all cases, low H₂O₂ dosage should be preferred because an excessive H₂O₂ dosage would increase the treatment cost and be harmful for the microorganisms [155,181].

1.7.2. Effect of iron catalyst concentration

Degradation rate of organic compounds first increases with an increase in (homogeneous or heterogeneous) iron catalyst. However, beyond an optimum value, the degradation efficiency reaches a plateau [60,155].

In the homogeneous Fenton oxidation, the optimum iron concentration corresponds to a [H₂O₂] / [Fe] molar ratio between 10 to 50 [80,129,182–185] and this ratio can be much higher up to 400 if dealing with real and concentrated wastewater [186]. According to Koprivana and Kusic [187], the minimal concentration of Fe²⁺ or Fe³⁺ required for Fenton reaction is in the range 3 – 15 mg/L (0.05 – 0.3 mM). On the other hand, excessive iron concentration would increase the process cost due to the subsequent iron precipitation required to lower its concentration below the discharge limit (2 mg/L in EU [188]), the management of generated iron sludge and the uneasy catalyst recovery [155].

The same criteria ([H₂O₂] / [Fe] ratio or minimal iron concentration) are not easily applied to the heterogeneous process, as only a fraction of immobilized iron is in fact accessible. Solid catalyst concentrations ranging from 0.2 to 5 g/L have been used in previous studies using Fe-ZSM5 catalyst [50,80,84,86,162,189], but values up to 25 – 70 g/L have been also reported [190,191]. Indeed, the associated operating cost is now only related to catalyst separation/retention (by membrane filtration for instance) and catalyst stability.

Note that, in heterogeneous (sono-)(photo-)Fenton process, low concentration of solid catalyst should be preferred (≤ 2 g/L) to limit light and sound wave scattering/attenuation [103,160,161,165,192].

1.7.3. Effect of temperature

Based on Arrhenius law, it is expected that an increase in temperature leads to a faster generation of hydroxyl radicals by the Fenton reaction. However several studies reported an optimal value (about 40°C), due to the concomitant accelerated decomposition of H₂O₂ into oxygen and water [60,193].

Compared to Fenton, effect of temperature was found to be marginal in homogeneous photo-Fenton oxidation [183]. Regarding ultrasound mediated processes, too high temperature could be detrimental because it increases the amount of vapor in cavitation bubbles cushioning their implosion, and it also results into a higher number of bubbles attenuating ultrasound propagation [194,195]. Therefore, the effect of temperature in combined (sono-)(photo-)Fenton processes has been rarely studied and the set temperature is typically around 20 – 25°C (see tables 1.8 - 1.11).

It should be finally noted that high temperature may affect the stability of heterogeneous iron catalyst by increasing metal leaching [177].

1.7.4. Effect of pH

Besides catalyst recovery, heterogeneous Fenton reaction was also developed to overcome the classical problem of narrow pH range (pH=2-4) in homogeneous Fenton reaction. However, most of the studies using solid catalyst – in Fenton [58,85,86,177,191], sono-Fenton [121,127], photo-Fenton [80,162,163] and sono-photo-Fenton [120,175] oxidation – still work at low pH values (2 to 5). Only a few works report good results at circumneutral pH (6 – 7) [74,167,191,196]. In heterogeneous Fenton, acidic pH may be important if the main mechanism of degradation is through leached iron (homogeneous Fenton process), like observed for instance with ZVI catalyst [73].

Basically, the efficacy of Fenton reaction is reduced at both high and low pH [60]. At high pH, the oxidation potential of hydroxyl radicals decreases and H₂O₂ is decomposed into HO₂⁻ or H₂O and O₂ [162,197,198]. Low degradation rate at high pH (> 4) can also be explained by the formation of selective oxidants, such as ferryl ions (FeO²⁺) [65,198]. On the other hand, at low pH (below 3), iron active species may be converted into iron complexes which react more slowly with hydrogen peroxide [199]. Moreover, at pH ≤ 2, •OH can be scavenged by H⁺ and H₂O₂ can be stabilized through the formation of oxonium ion (H₃O₂⁺), reducing its reactivity with ferrous species, and thus decreasing the process efficiency [155,200]. Therefore, the optimum pH of homogeneous Fenton reaction is usually around 3. It is also worth noting that iron leaching from heterogeneous catalyst is favored at low pH. In addition, pH may evolve during the reaction due to H₂O₂ depletion [178] and formation of acidic intermediates [57,115].

Several researchers investigated the effect of initial pH in heterogeneous Fenton reaction and observed contrasted trends. Cihanoğlu et al. (2015) found that a pH increase

from 4 to 7 in Fe-ZSM5 catalyzed Fenton oxidation of acetic acid reduced COD conversion after 120 min from 50% to 20% [86]. Queirós et al. (2015) also reported a decrease of azo dye removal (from 70% to 20%) when the initial pH was increased from 2 to 4 [177]. On the contrary, Aleksić et al. (2010) and Centi et al. (2000) reported that Fe-ZSM5 activity was not sensitive to pH and could work well in mildly acidic conditions (pH=4-6) [84,167]. A plausible explanation lies in the acidic property of Fe-ZSM5 [165,201] and/or the existence of an interaction between the positively charged iron ions and negatively charged zeolite framework that prevents or postpones the formation of stable iron hydro-complexes as pH approaches neutral value [167].

Regarding sonochemical process, degradation of organic compounds is improved if $\text{pH} < \text{pK}_a$ because in its molecular form the molecule can be vaporized into the cavitation bubbles and both thermal cleavage and oxidation with $\bullet\text{OH}$ radicals can occur [40,195,202]. On the other hand, the effect of direct photolysis is more pronounced at alkali pH since deprotonated species are less stable under light irradiation [136,139].

Regarding heterogeneous sono-photo-Fenton process, we can cite the work of Zhong et al. (2011) which investigated pH effect on the degradation of acid orange 7 using mesoporous iron-containing silica ($\text{Fe}_2\text{O}_3/\text{SBA-15}$): the increase of initial pH from 3 to 5 led to the reduction of removal efficiency from 65% to 40% [175].

1.7.5. Effect of initial concentration of pollutant

The degradation rate usually decreases when increasing the initial concentration of the pollutant (other conditions remaining the same) due to an insufficient number of hydroxyl radicals [86,198,203]. At high concentration, the pollutant may also occupy iron active sites on the catalyst surface to the detriment of H_2O_2 , resulting in less $\bullet\text{OH}$ generation [198].

Furthermore, along with temperature, pH and H_2O_2 concentration, initial pollutant concentration can influence the complex mechanism of iron leaching [204].

1.7.6. Effect of dissolved gas

Dissolved oxygen in solution can react with organic radicals ($\text{R}\bullet$) to form organic peroxy radicals ($\text{ROO}\bullet$) and organic peroxides (ROOH). These radicals can participate to the degradation process as secondary oxidants. Segura et al. (2015) showed that air injection (5 L/min) can improve TOC removal in heterogeneous Fenton process by up to 17% [178].

Furthermore, dissolved oxygen reacts with H^\bullet and $\bullet\text{OH}$, and thereby prevents their loss by termination reactions. Likewise, high O_2 concentration disfavors $\bullet\text{OOH}$ recombination [174,205]:



Gases affect differently sonochemical reactions depending on their thermodynamic properties. For instance, Gültekin and Ince observed that sonolysis of biphenol A under argon was slightly faster than under oxygen, which could be ascribed to its higher polytropic ratio and low conductivity, favoring higher collapse temperatures [206]. Regarding photolysis, injection of nitrogen could be detrimental by inhibiting the formation of reactive oxygenated species ($^1\text{O}_2$, O_2^\bullet , $\bullet\text{OH}$) by photo-sensitization reactions (R.1.44 – R.1.48), as observed for the photodegradation of ibuprofen [42].

1.7.7. Effect of ultrasound power and frequency

The effect of ultrasound power in homogeneous sono-Fenton process has been scarcely investigated. Siddique et al [81] reported that dye sono-oxidation (at 20 kHz) increased from 60% to 75% by increasing ultrasonic intensity from 4 W/cm^2 (40 W/L) to 8 W/cm^2 (80 W/L). The authors attributed this enhancement to better mixing and improved hydroxyl radical generation by ultrasound.

In heterogeneous system, similar results have been reported: degradation yield increased by increasing ultrasound power [122,124,130] and optimum value was rarely observed [130]. This trend was explained by more hydroxyl radicals generated from water sonolysis [124] and more intense mixing [122]. Note, however, that these explanations were not supported by study of sole sonolysis and activity of iron leached was not investigated.

Effect of US frequency on sono-Fenton reaction, particularly on decomposition of Fe-OOH^{2+} iron complex into Fe^{2+} and $\bullet\text{OOH}$ (R.1.37), is not well-known. Bremner et al [117] varied US frequency between 20 and 1142 kHz and found that 584 kHz should be preferred for heterogeneous sono-Fenton oxidation of phenol over $\text{Fe}_2\text{O}_3/\text{SBA}$ catalyst.

1.7.8. Effect of lamp type (wavelength) and power

Various lamp types have been used by researchers to study photo-Fenton and sono-photo-Fenton oxidation processes: low pressure mercury vapor (LP Hg) lamp [168,207], medium pressure mercury vapor (MP Hg) lamp [80,152,163], halogen lamp [208], black light blue (BLB) lamp [209] and xenon Arc (Xe) lamp [24,33,43,164,172,183]. Among them, LP Hg, MP Hg and xenon arc lamp are the most utilized. Various possible photo-chemical reactions induced by these lamps are given in figure 1.11.

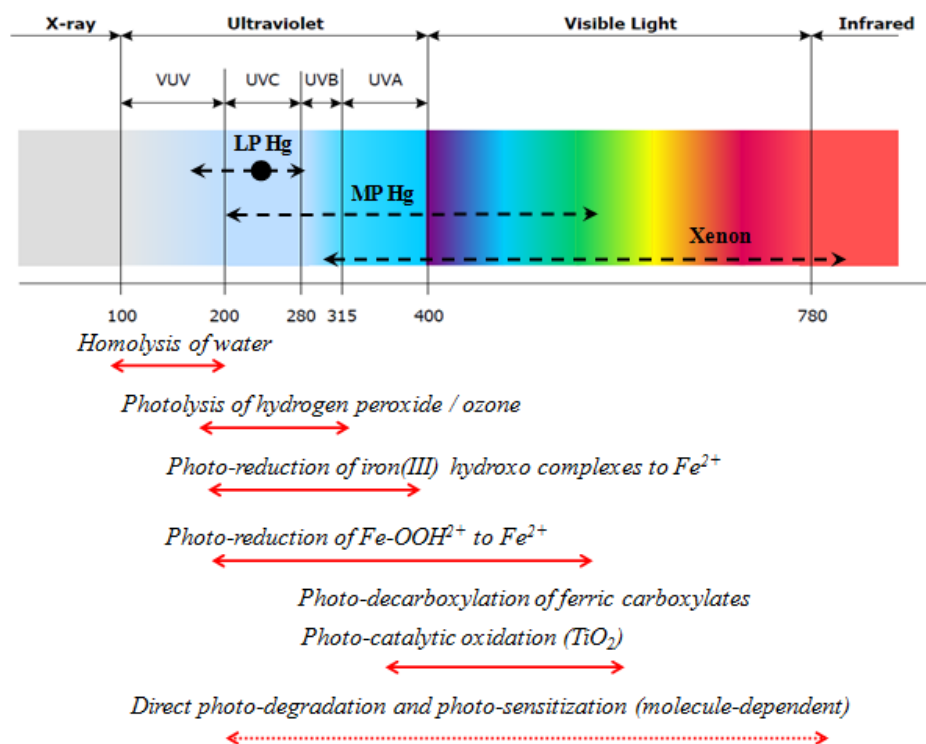


Figure 1.11. Classification of photo-based AOPs according to lamp type and wavelength

Among them, MP Hg lamp is the most effective since it covers a wide range of wavelengths ($\lambda=200-600$ nm), but it is more expensive compared to the other lamps. LP Hg lamp ($\lambda=254$ nm) is also interesting due to its low cost, efficiency for H₂O₂ decomposition and ability to initiate photo-reduction of ferric to ferrous iron. Xenon arc lamp ($\lambda=300-800$ nm) may be not as effective as MP and LP Hg lamps, but it can be used to assess the efficiency of a solar process since it mimics sunlight irradiation.

Increase of irradiation power is generally followed by an increase in the catalytic activity, due to faster photo-reduction of Fe (III) to Fe(II) [161].

1.8. CONCLUSION

Complete removal and mineralization of pharmaceuticals are still a major challenge in conventional water treatment processes. On the other hand, this literature review showed that advanced oxidation (AOPs) processes are very promising techniques for the remediation of refractory organic compounds in water, such as pharmaceuticals. Among them, ibuprofen was chosen as model molecule due to its regular presence in aquatic environment and potential environmental risks. To eliminate ibuprofen, both homogeneous and heterogeneous Fenton processes were evaluated. However, drawbacks associated to each process, such as uneasy regeneration of ferrous ion and use of dissolved iron concentrations well above the discharge limit for homogeneous system or lower reaction rates for heterogeneous system, encourage more developments by coupling processes. Indeed, despite of the limited oxidation capacity of sole ultraviolet/visible and ultrasound irradiation, it was demonstrated that these processes can be used to (re)activate Fenton reaction, mainly by improving the regeneration of ferric to ferrous iron species.

Notwithstanding, more information is actually needed, especially concerning mechanisms of ibuprofen degradation by ultrasound and ultraviolet irradiation, effects of ultrasound power and frequency on sono-Fenton oxidation, effect of light wavelength on photo-Fenton oxidation and possible synergistic effect by coupling these process (in the so-called sono-photo-Fenton oxidation).

The originality of the present work relies in the activation of homogeneous Fenton reaction carried out at relatively low iron concentration (1.8 – 7.5 mg/L of Fe) and the combination of low frequency ultrasound and visible irradiation with heterogeneous Fenton reaction.

Prior to result report and discussion, next chapter details analytical methods and equipment, as well as experimental set-up and procedures.

CHAPTER 2 METHODS AND MATERIALS

This chapter presents the methods and materials involved in this study. The first part of this chapter is dedicated to the analytical methods used for the characterization of liquid samples and heterogeneous catalysts. Then properties of chemicals and catalysts are provided. Finally, the experimental apparatus and procedures applied for investigating AOPs are described.

This page is intentionally left blank

2.1. ANALYTICAL METHODS

2.1.1. Analysis of liquid phase

2.1.1.1. Quantification of ibuprofen by HPLC/UV

High-Performance Liquid Chromatography coupled with UV detection (HPLC/UV) was used as a routine method to monitor the degradation of ibuprofen during the oxidation experiments. HPLC uses a liquid mobile phase (solvent mixture) to transport the molecules (analytes) in a sample through a stationary phase (sorbent particles packed inside a column) and separates them according to their affinity for mobile and stationary phases. At the end of the system ([figure 2.1](#)), a UV/Vis spectrophotometer monitors the absorbance of analytes in the eluent and shows the output in the form of a chromatogram. Thus, a calibration is needed in order to transform the peak area on the chromatogram into analyte concentration.

The HPLC system used in this work (ACCELA PDA, Thermo scientific Inc.) consists in a dual-piston quaternary mixing pump, an auto-sampler, and a photodiode array detector capable to scan the analyte absorbance on a range of wavelengths. Acquisition and treatment of chromatograms were performed by Chromeleon software (version 6.8, Thermo scientific Inc.).

IBP stock solution was prepared by dissolving 40 mg of IBP powder in 2 L of distilled water and stirred for 14 hours using a magnetic stirrer (600 rpm) at 25°C to ensure complete powder dissolution. Complete dissolution was confirmed by comparison to the peak area obtained when IBP solution was prepared in acetonitrile. Before each analysis, five standard solutions were prepared to calibrate the machine, with concentration ranging from 2 to 20 mg/L ([example of calibration curve can be found in appendix: figure II](#)). Analysis of standard solution was duplicated, showing a coefficient of variation lower than 2%.

Detail of HPLC separation method is given in table 2.1. Acetonitrile (Scharlau, Ref. AC03334000) and ultrapure water acidified with phosphoric acid (Sigma-Aldrich, Ref. 79606) were chosen as eluents due to their low absorption in UVC region. Acidification of water eluent (pH = 2.3) prevented ionization of ibuprofen (pKa = 4.9) during the analysis so as to improve reproducibility and resolution of the method. According to the absorption spectrum of ibuprofen (see [figure 2.8](#)) exhibiting a maximum at 222 nm, this wavelength was chosen for pollutant monitoring. A temperature of 40°C was set to improve the separation between the pollutant and its degradation intermediates, especially to prevent co-elution

between ibuprofen and 4-isobutylacetophenone (see appendix: figure I). Limits of detection and quantification of ibuprofen with this method were 10 µg/L and 30 µg/L, respectively.

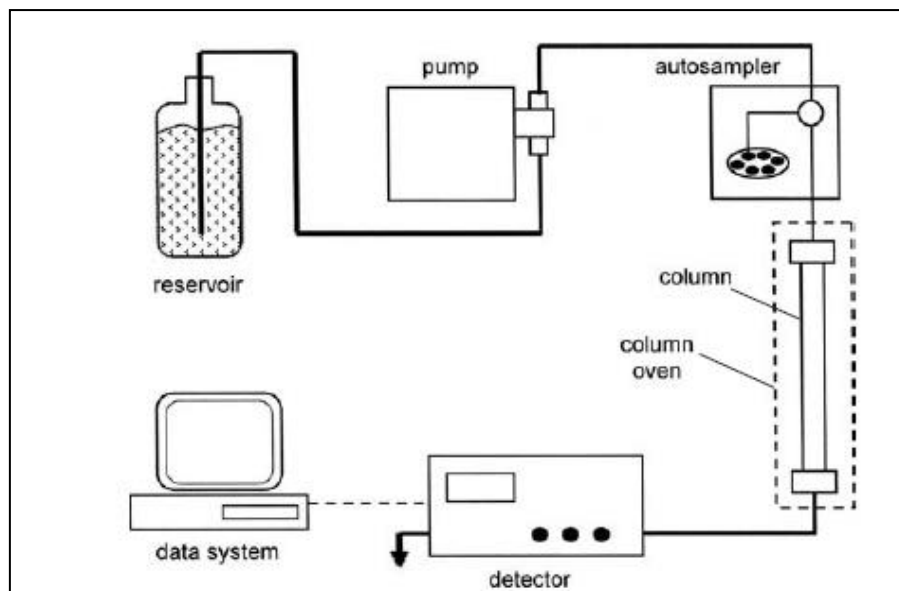


Figure 2.1. Schematic diagram of HPLC system
(adapted from reference [210])

Table 2.1. HPLC method for ibuprofen analysis

Parameters	
Column	C18 250x4 mm, 5 µm (ProntoSIL C18 AQ, Bischoff chromatography)
Elution method	Isocratic
Aqueous solvent (A)	Ultrapure water with H ₃ PO ₄ 0,1% (v/v)
Organic solvent (B)	Acetonitrile
Volumetric A/B ratio	40/60
Elution flow rate (mL/min)	1
Temperature (°C)	40
Injection volume (µL)	20
Retention time (min)	8.8 ± 0.3
Principal wavelengths (nm)	222
Diode array detector wavelengths (nm)	200 – 800

2.1.1.2. Analysis of reaction intermediates by HPLC/MS

High Performance Liquid Chromatography coupled with high resolution Mass Spectrometry (HPLC/MS) was used as complementary analysis in order to identify the reaction intermediates (degradation products) formed during the different oxidation processes. In the MS detector, the injected compounds are vaporized, ionized and undergo

fragmentation. The fragmented ions are separated according to their mass-to-charge ratio (m/z).

These analyses were carried out using a liquid chromatograph (ACCELA LC, Thermo scientific Inc.) working in tandem with a mass spectrometer (Exactive™ Plus Orbitrap Mass Spectrometer, Thermo scientific Inc.) in positive and negative ion modes. This HPLC machine was also equipped with diode array detector in order to detect non-ionizable compounds. The applied method and schematic diagram of MS system are depicted in [table 2.2](#) and [figure 2.2](#), respectively. Prediction of compound formula and noise reduction was performed by Xcalibur software (version 2, Thermo scientific Inc.) and MetAlign software (version 041011, Arjen Lommen). HPLC/MS characterizations were performed by David Riboul at Laboratoire de Génie Chimique, Toulouse.

Table 2.2. LC/MS method for analysis of reaction intermediates

Parameters	
Column	PFP 150x2 mm, 3µm (Luna PFP 2, Phenomenex)
Elution method	Gradient
Aqueous solvent (A)	Ultrapure water acidified with formic acid 0.1% (v/v)
Organic solvent (B)	Acetonitrile
Volumetric A/B ratio	0-5 min, 3% de B ; 5-25 min, 3-95% de B, 25-30min, 95% de B; 30-31min, 95-3% de B, 31-37min, 3% de B
Elution flow rate (mL/min)	0.2
Temperature (°C)	40
Injection volume (µL)	5
Diode array detector wavelengths (nm)	200 – 600
Sheath gas flow rate (arbitrary unit)	50
Auxiliary gas (arbitrary unit)	20
Capillary temperature (°C)	350
Spray voltage (V)	± 3000
Capillary voltage (V)	± 25
Tube lens voltage (V)	± 30
Skimmer voltage (V)	± 16
Mass range (m/z)	50 – 1000
Mass resolution	100000
Acquisition rate (Hz)	1

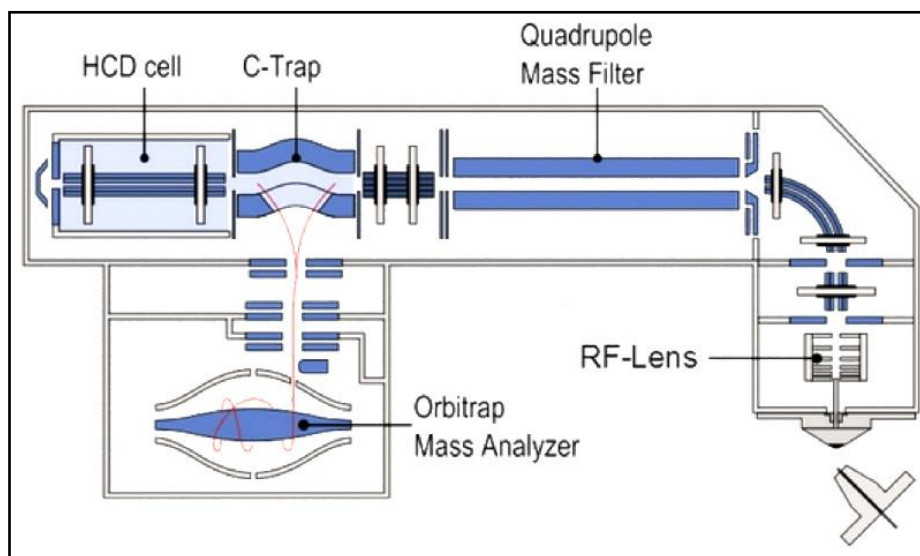


Figure 2.2. Schematic diagram of MS system
(adapted from reference [211])

2.1.1.3. Analysis of Total Organic Carbon (TOC)

Analysis of total organic carbon (TOC) was performed in order to determine the whole concentration of contaminant and transformation products during the oxidation. This analysis was carried out using TOC analyzer (TOC-L, Shimadzu Co.).

TOC is the Total Organic Carbon present in an aqueous sample as dissolved compounds and suspended material. The quantification of TOC is based on the difference between Total Carbon (TC) and Inorganic Carbon (IC) (analyzed separately as it can be seen on figure 2.3). TC is measured by oxygen combustion of the sample at 680°C using a platinum catalyst that converts all carbon present into carbon dioxide (CO₂), while IC is measured by transformation of carbonate (CO₃²⁻) and bicarbonate (HCO₃⁻) ions into CO₂ after acidification (by adding HCl 2N) and degassing by nitrogen sparging. The evolved gases are transferred to a dehumidifier, then CO₂ is quantified using a non-dispersive infrared sensor (NDIR).

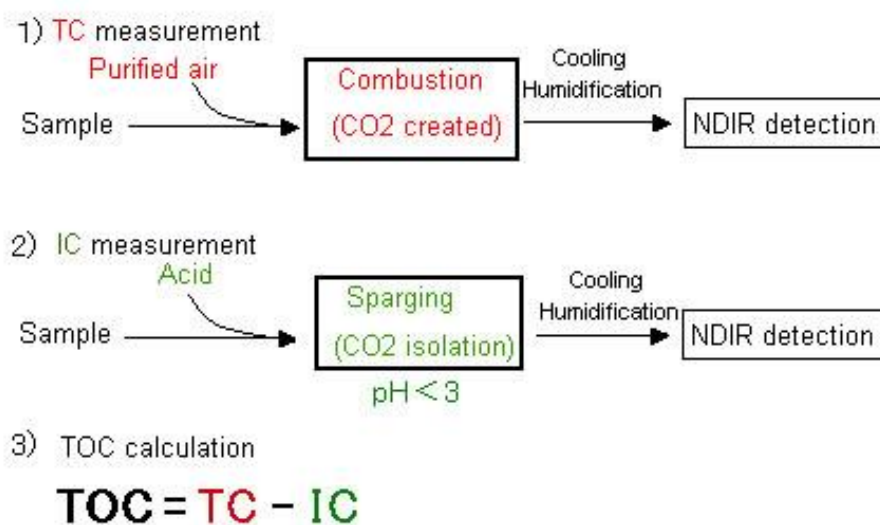


Figure 2.3. Principle of TOC measurement
(adapted from reference [212])

Calibration of TC analysis was conducted with the target contaminant: eight calibration points ranging from 0.66 mg/L to 20 mg/L of ibuprofen (0.5 mg/L to 15 mg/L of TC) were used. In addition, calibration of IC analysis was conducted between 0.2 and 2 mg/L, using standards prepared from a 100 mg/L IC solution, corresponding to a mixture of 0.35 g sodium bicarbonate NaHCO₃ (Sigma Aldrich, Ref. S6014) and 0.441 g sodium carbonate Na₂CO₃ (Sigma Aldrich, Ref. S7795) in 1 L ultrapure water. The injection volume was 50 µL and 400 µL for TC and IC, respectively ([example of calibration curve of TC and IC can be found in appendix: figure III and IV](#)).

Theoretical TOC concentration of prepared solutions ($[TOC]_{theo}$ in mg/L) was calculated by the following equation:

$$[TOC]_{theo} = \frac{n_C \times M_C \times [Molecule]}{M_{Molecule}} \quad (E.2.1)$$

With

n_C : number of carbons in the molecule

M_C : molecular weight of carbon (g/mol)

$[Molecule]$: concentration of the molecule (mg/L)

$M_{Molecule}$: molecular weight of the molecule (g/mol)

In case of ibuprofen (molecular weight 206.29 g/mol), this leads to:

$$[\text{TOC}]_{\text{theo}} = \frac{13.12 \cdot [\text{IBP}]}{206.29} = 0.756 [\text{IBP}] \quad (\text{E.2.2})$$

According to the supplier, detection limits were 50 µg/L and 4 µg/L for TC and IC, respectively. By default, the measurement was duplicated; extra measurements were performed only if the coefficient of variation of the first ones was higher than 2%.

2.1.1.4. Analysis of (residual) hydrogen peroxide by spectrophotometry

(Residual) hydrogen peroxide after oxidation/sonication was determined by the titanium tetrachloride method [213,214]. This method has also been used in literature both to determine sono-generation of H₂O₂ [174] and conversion of H₂O₂ in sono-photo-Fenton process [171] due to its large application range. It is based on the reaction between H₂O₂ and Ti⁴⁺ in acidic condition to form a yellow complex, pertitanic acid (TiO₂.H₂O₂) (R.2.1).



At the end of the experiment, a 25 mL aliquot was withdrawn and filtered. Then, 1 mL of TiCl₄ solution at 0.09 M (Sigma-Aldrich, Ref. 404985) and 1 mL of 1 M H₂SO₄ (Sigma-Aldrich, Ref. 35276) were added, yielding an orange-yellow coloration. This colored complex is stable during several hours and exhibits a molar extinction coefficient ε=742 L/(mol.cm) at 410 nm [213]. Its concentration was measured on a Genesys 2 (Thermo Electron Corporation) or UV-1800 (Shimadzu Corporation) spectrophotometer. For quantification, a calibration plot using different H₂O₂ solutions was performed (for example see appendix figure V). Examples of coloration formed at different complex concentrations can be seen in figure 2.4. This method allows the measurement of hydrogen peroxide concentration between 0.01 and 3 mM (0.34 – 102 mg/L), the detection limit being 0.003 mM (0.1 mg/L). For higher concentration ranges, a smaller sample volume was taken and diluted with distilled water before treatment and analysis.

The result of H₂O₂ analysis was expressed in either residual (remaining) concentration (in mM) or in percentage consumption.(%).

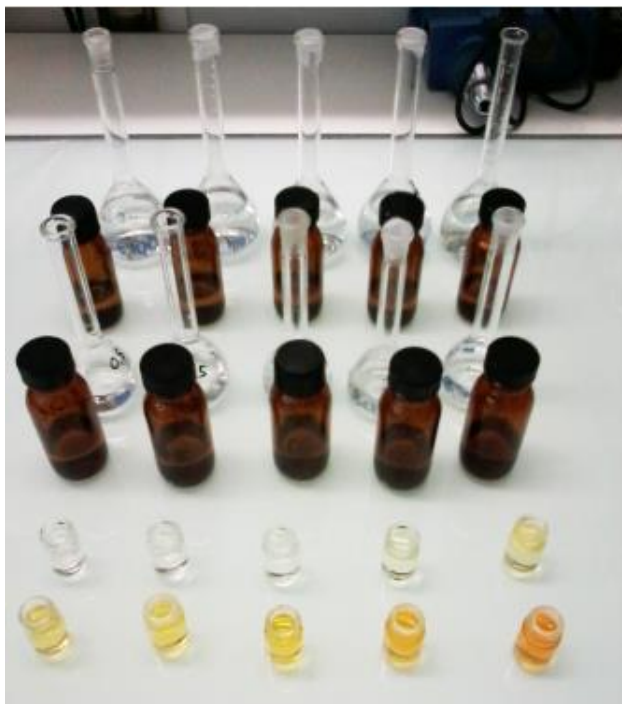


Figure 2.4. Standard solutions of titanium (IV)-hydrogen peroxide complex at different concentrations

2.1.1.5. Analysis of total dissolved iron by ICP-AES

Inductively Coupled Plasma Atomic Emission Spectroscopy (ICP-AES) was used to measure the total iron concentration leached from the heterogeneous catalyst during the reaction after filtering the final solution. In the ICP-AES apparatus (figure. 2.5), the sample is sprayed as a mist of droplets in a nebulizer and introduced in a high temperature plasma (6000 to 10000 K) resulting in excitation and ionization of the atoms. Once the atoms or ions are in their excited state, they can decay to lower states through thermal or radiative (emission) energy transitions. The intensity of the light emitted at specific wavelengths is measured and used to determine the concentration of the elements of interest [215].

This analysis was also used to measure the iron content of Fe-MFI. In this case, extraction of iron from the zeolite matrix was carried out by mixing 0.15 g of Fe-MFI with 5 mL of 15 M HNO₃ at high temperature (120°C) until complete discoloration of the solid residue (96 hours).

Analysis of total dissolved iron was carried out by Marie-Line De Solan Bethmale using Ultima 2 ICP-AES spectrometer (HORIBA Jobin Yvon) at Service Analyse et Procédés (SAP) of LGC Toulouse. Limits of detection and quantification were 1 µg/L and 10 µg/L, respectively.

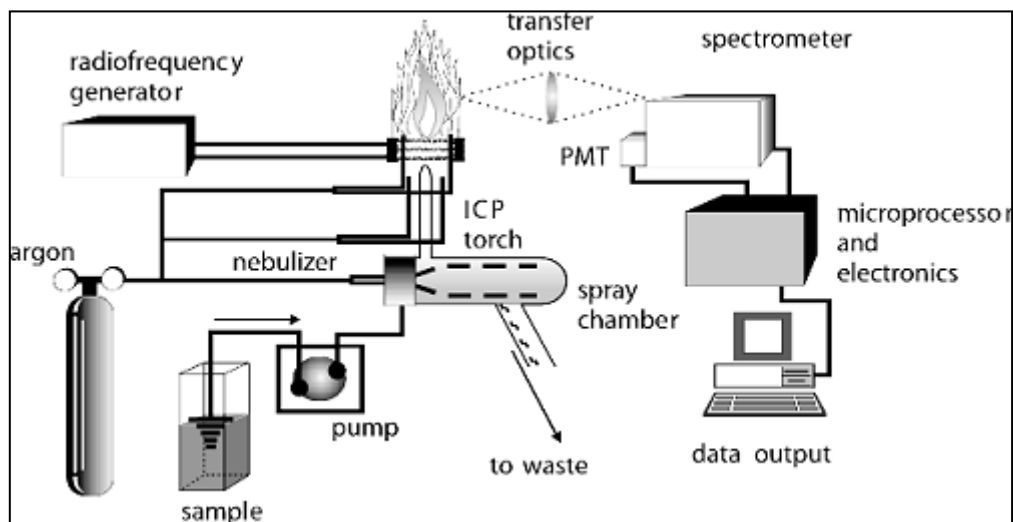


Figure 2.5. Schematic diagram of ICP-AES apparatus
(adapted from reference [215])

2.1.2. Analysis of solid phase (heterogeneous catalyst)

2.1.2.1. Laser diffraction

Laser diffraction was used to measure the particle size distribution of the heterogeneous catalysts (Fe-ZSM5 [Fe-MFI] and zero valent iron [ZVI]). When a sample containing suspended particles is irradiated with a laser beam (infrared and blue light), light is scattered, diffracted, refracted, absorbed and transmitted. The intensity of diffracted/scattered light is analyzed using Mie theory to calculate the size distribution of the particles, in the range 0.02-2000 μm . This presupposes knowledge of the light refractive index of the particles and the dispersion media and the imaginary part of the refractive index of the particles (see [table 2.3](#)).

Measurement of Fe-MFI particle size distribution was carried out in wet dispersion (using a Malvern Mastersizer 2000 equipped with Hydro 2000S accessory) in order to approach the experimental conditions. On the other hand, ZVI was analyzed as dry powder (Malvern Mastersizer 3000 equipped with Aero 3000 accessory) because these magnetic particles easily agglomerate in liquid causing poor repeatability of the measurement. Details of analytical methods are given in [table 2.3](#).

Particle size analyses were carried out by Christine Rey Rouch at SAP, LGC Toulouse.

Table 2.3. Methods for particle size analyses

Parameters	Solid catalyst	
	Fe-MFI	ZVI
Dispersion media (unit)	water (Hydro 2000S)	air (Aero 3000)
Stirrer-pump speed (rpm)	1750	N/A
Air pressure (bar)	N/A	2
Refractive index	1.503	1.520
Absorption index	0.1	0.1
Obscuration level (%)	3	9

2.1.2.2. Scanning Electron Microscopy and Energy Dispersive X-ray Spectroscopy

Scanning Electron Microscopy (SEM) – coupled to elemental analysis – was performed to evaluate the morphology of the solid catalysts and the (surface) distribution of iron. The measurement is based on the interaction of the primary electron beam with the sample causing the emission of secondary electrons (related to the surface topography), backscattered electrons and X-rays (figure 2.6). The latter can be used to obtain elemental information by coupling with Energy-Dispersive X-Ray Spectroscopy (EDX) detector. When the sample is bombarded by the SEM electron beam, electrons are ejected from the atoms on the sample surface. The resulting electron vacancies are filled by electrons from a higher state, and X-rays are emitted to balance the energy difference between the two electron states. The resulting X-ray spectrum exhibits specific energy lines which depend on the atomic number of the atoms.

This analysis was carried out by Marie-Line De Solan Bethmale using a LEO 435VP microscope (SEMTECH Solutions, Inc.) equipped with EDS detector (INCA System, Oxford Instrument) at SAP, LGC Toulouse.

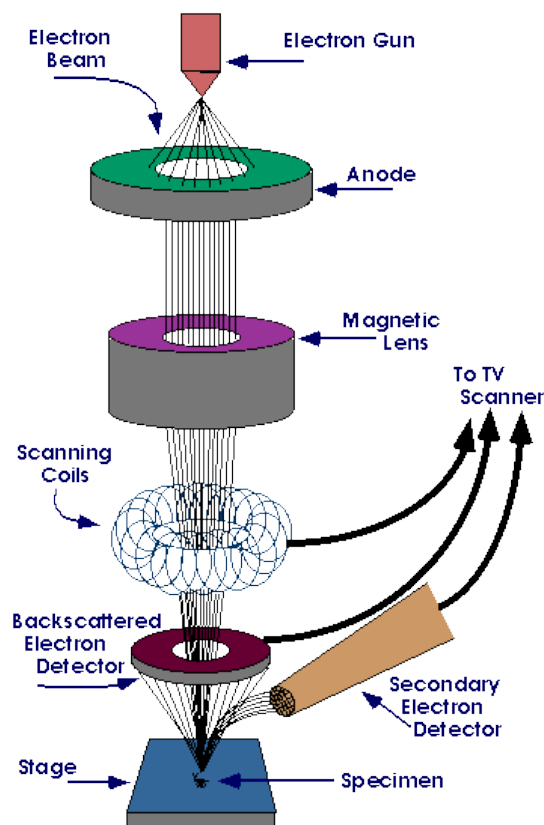


Figure 2.6. Schematic diagram of SEM
 (adapted from reference [216])

2.1.2.3. X-ray diffraction

X-ray diffraction (XRD) was used to characterize the crystalline phases of the catalysts (*e.g.* for identification of crystalline phases, evaluation of crystallite size, etc ...). This analytical technique is based on the diffraction pattern formed by the interaction between incident beam of monochromatic X-rays and target material (described by Bragg's law). X-rays refracted and captured by the detector are depicted as diffraction peaks. Each peak appearing on the diffractogram pattern representing a crystal plane is then compared with a database from Joint Committee on Powder Diffraction Standards – International Centre for Diffraction Data (JCPDS–ICDD). The size of the crystallites can be estimated by Scherrer's equation using the width of the diffraction peaks:

$$d_c = k\lambda / (\beta \cdot \cos\theta) \quad (\text{E.2.3})$$

With

d_c : average diameter of crystallites (nm)

k	: shape factor of the crystallite (typically around 0.9)
λ	: X-ray wavelength (nm)
β	: peak broadening at half the maximum intensity
θ	: half diffraction angle

This analysis was carried out by Cédric Charvillat at Centre Inter-universitaire de Recherche et d'Ingénierie des Matériaux (CIRIMAT), Toulouse.

2.1.2.4. Gas porosimetry

Gas porosimetry was used to determine the specific surface area of the solid catalyst. The measurement is based on the physical adsorption of a gas (nitrogen, argon or helium) on the surface of a solid material, which depends upon temperature and pressure.

Prior to the analysis, the solid samples were degassed at 200°C during 2 h. The adsorption isotherm (or quantity of gas adsorbed as a function of pressure) was then measured at the temperature of liquid nitrogen (77 K), and the specific surface area was determined by calculating the amount of adsorbed gas corresponding to a monomolecular layer (Brunauer, Emmet and Teller, or BET equation). Furthermore, gas porosimetry also gave access to mesoporous and microporous volumes by application of Barrett-Joyner-Halenda (BJH) and Horvath-Kawazoe (HK) models, respectively.

This analysis was carried out by Gwenaëlle Raimbeaux using an ASAP 2010 M porosimeter (Micromeritics Instrument Corporation) at SAP, LGC Toulouse.

2.1.2.5. CO chemisorption

Chemisorption of carbon monoxide was used to determine the dispersion of iron on the surface of Fe-MFI (Fe-ZSM5) and the size of crystallites. During chemisorption process, the adsorbing gas forms a chemical bond with the adsorption site. A wide range of metals react with CO forming single or multiple bonds. Knowing the stoichiometry of the reaction, the number of molecules of CO chemisorbed per gram of catalyst provides the metal dispersion, defined as the percentage of accessible metal atoms with respect to the total metal content.

0.5 g of Fe-MFI catalyst was degassed at 200°C and 400°C during 30 min and 1 h, respectively, then reduced under flowing H₂ at 450°C for 12 h (ramp of 5°C/min), and placed under vacuum for 1 hour at 400°C before cooling to 35°C for CO adsorption [189,217]. A first isotherm was measured, then the sample was evacuated at 35°C to remove physisorbed

CO and a second isotherm was recorded. The difference between the two isotherms gave chemisorbed gas amount. Afterwards, the sample was degassed and re-oxidized at 450°C by using 10% of O₂ in helium to determine the extent of reduction. Assuming a CO uptake per Fe atom of ½, as well as crystallites of uniform size and spherical shape, iron dispersion D (%) and crystallite diameter (d_c) was calculated according to following equations [217]:

$$D = 1.117 X / (W \cdot f) \quad (\text{E.2.4})$$

$$d_c = 96/D \quad (\text{E.2.5})$$

With

- D : iron dispersion (%)
- X : chemisorbed CO amount (μmol/g)
- W : total weight percentage of iron in the catalyst (%)
- f : fraction of reduced iron determined by O₂ titration
- d_c : average diameter of crystallites (nm)

Note that caution must be taken on the interpretation of such measurement for Fe/zeolite, as Fe²⁺ ions (resulting from the preliminary reduction of ionic iron species) also chemisorb CO [218]. Therefore room temperature (RT) ⁵⁷Fe Mössbauer spectroscopy of Fe/MFI was performed on a WissEl spectrometer to investigate iron oxidation state and quantify the amount of isolated ionic species. It showed mainly hematite and a very low amount of Fe³⁺ ions in octahedral coordination (7%) [165], whose contribution to CO chemisorption was neglected.

CO chemisorption was carried out by Pascale Mascunan at Institut de Recherches sur la Catalyse et l'Environnement de Lyon (IRCELyon), Villeurbanne.

2.1.2.6. Identification of the pH at the point of zero charge

The pH at the point of zero charge (pH_{pzc}) is the pH at which a solid surface immersed in an electrolyte solution has a net neutral charge. When the pH of the solution is below pH_{pzc}, the solid surface is positively charged, thus promoting the adsorption of organic

compounds in ionic form. Conversely, at a pH value above pH_{pzc} , the catalyst surface is negatively charged and repels anions.

pH_{pzc} value was measured by mass titration method [219]. Several suspensions with concentrations of solid catalyst ranging from 2 and 14 g/L were prepared in distilled water and bubbled with nitrogen. Then the suspensions were agitated during 24 h and filtered before measuring the pH (Model C861 pH-meter, Consort). Beyond a certain concentration of solid, the contact pH reached a plateau corresponding to the pH at the point of zero charge.

2.1.2.7. Carbon trace analysis

Carbon traces analysis was performed to determine the (residual) organic amount adsorbed on Fe-ZSM5 catalyst, so that to calculate the global mineralization yield (TOC removal in both solid and liquid phases). At the end of heterogeneous reaction, the suspension was filtered through a nitrocellulose membrane filter with 0.22 μm pore size (GSWP, Merck Millipore) and the collected solid was dried at 70°C during 24 h. About 400 mg of dried sample was subjected to combustion at 1350°C, in the presence of oxygen. The formed carbon dioxide was detected using an infrared detector (SC144, LECO, dosing range from 50 ppm to 10% of C).

This analysis was carried out by Patrick Jame at Institut des Sciences Analytiques (ISA), Villeurbanne.

2.2. CHEMICALS AND CATALYSTS

Considering that our objective was to develop and evaluate the efficiency of a hybrid wastewater treatment process, synthetic wastewater (ibuprofen solution) has been used in almost all experiments (unless otherwise stated) in order to avoid delicate sample analysis and interferences that may arise from real pharmaceutical wastewaters. All reagents and catalysts used in this study were analytically grade and used as received unless otherwise specified.

2.2.1. Ibuprofen

Classed in the World Health Organization's (WHO) model list of essential medicines for pain and palliative care, ibuprofen ((2-(4-isobutylphenyl)propionic acid) -marketed as Advil, Brufen, Motrin, Nurofen, etc- is a non-steroidal anti-inflammatory drug (NSAID) used for relieving pain, alleviating fever, reducing inflammation and osteoarthritis. The recommended dosage of ibuprofen as a pain reliever is 200 to 400 mg and as an anti-rheumatic for adults from 1.2 to 3.2 g/day in separate doses [220].

Ibuprofen was purchased from BASF Corporation (Ref. 30076128, purity 99.9%). Physicochemical properties and UV absorption spectrum of ibuprofen are given in [table 2.4](#) [figure 2.7](#) and [2.8](#), respectively.

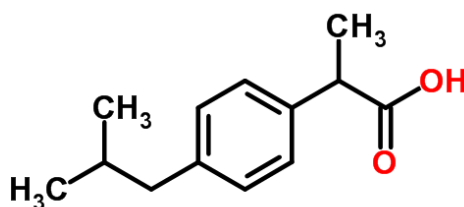


Figure 2.7. Chemical structure of ibuprofen

As mentioned previously in chapter 1, concentration of ibuprofen (IBP) in the water bodies of the environment is usually of tens ng/L to tens µg/L. However considering that application of AOPs is more economical for high contaminant loadings (and small volumes) [221,222], as well as to facilitate the analytical aspects, 20 mg/L (0.097 mM) of IBP was used as initial concentration.

Table 2.4. Physicochemical properties of ibuprofen

Properties		Ref.
IUPAC name	2-(4-Isobutylphenyl)propionic acid	[220]
CAS number	15687-27-1	[220]
Formula	C ₁₃ H ₁₈ O ₂	[220]
Molecular weight	206.29 g/mol	[220]
Molecular size	1.3 nm x 0.6 nm	[223]
Log Kow*	3.8 – 3.97	[220,224]
pKa	4.3 – 4.9 (carboxylic group)	[225,226]
Solubility in water	21 mg/L (0.1 mM) at 25°C	[227]
Henry's law constant	1.5 x 10 ⁻⁷ atm.m ³ /mol	[40]
Vapor pressure	1.18 x 10 ⁻⁸ atm at 25°C	[228]
Rate constant with [•] OH	6.5 x 10 ⁹ M ⁻¹ .s ⁻¹	[229]
Rate constant with ¹ O ₂	6 x 10 ⁴ M ⁻¹ .s ⁻¹	[54]

*Kow: octanol-water partition coefficient

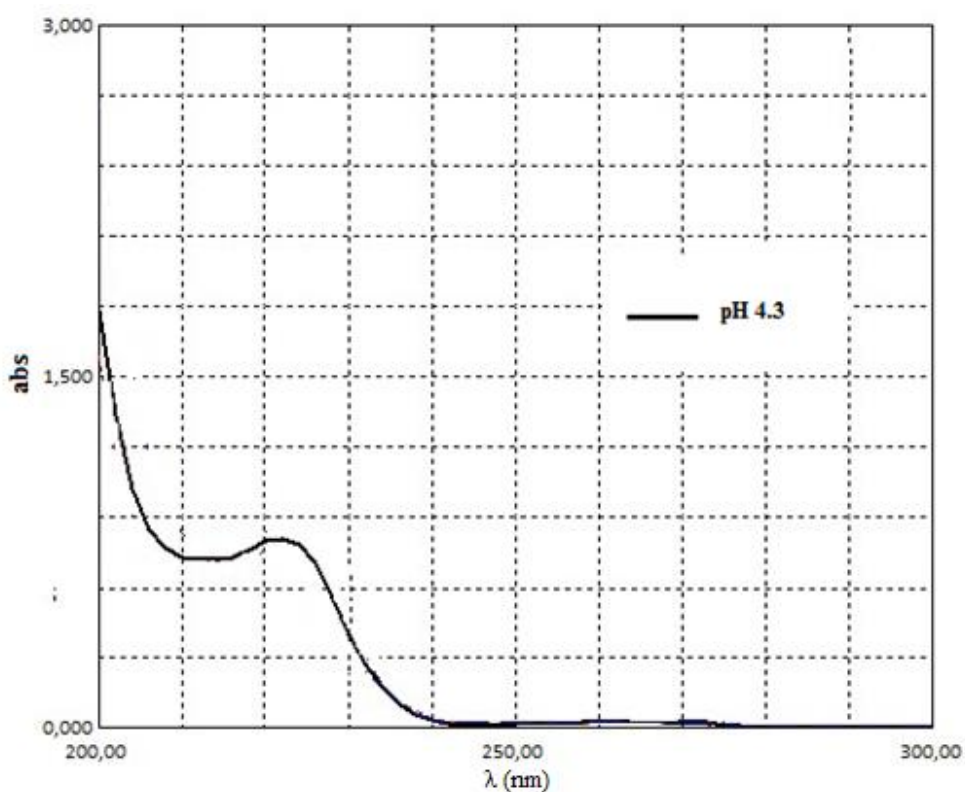


Figure 2.8. UV absorption spectrum of ibuprofen solution ([IBP] = 20 mg/L; pH₀ = 4.3)

2.2.2. Hydrogen peroxide

Hydrogen peroxide (H₂O₂) is known as "green" oxidant because it releases only water as by-product. Since addition of sole H₂O₂ for oxidation of organic compounds has limited efficiency due to its relatively low oxidation potential (1.77 V), H₂O₂ is rather used as source of stronger oxidants in advanced oxidation processes (AOPs), such as hydroxyl radical •OH that exhibits higher oxidation potential (2.80 V). Physicochemical properties and UV absorption spectrum of H₂O₂ are depicted in [table 2.5](#) and [figure 2.9](#), respectively.

The stoichiometric amount of H₂O₂ required for the total oxidation of 20 mg/L ibuprofen was 3.2 mM and it was calculated based on the following equation:



Hydrogen peroxide (H₂O₂) was purchased from Sigma-Aldrich as a 30% wt. solution (ref. 95294) with density of 1.14 g/cm³

Table 2.5. Physicochemical properties of hydrogen peroxide

Properties		Ref.
IUPAC name	Hydrogen peroxide	[230]
CAS number	7722-84-1	[230]
Formula	H ₂ O ₂	[230]
Molecular weight	34 g/mol	[230]
Density	1.1 g/cm ³ at conc. 30%	[231]
Log Kow	-1.5	[230]
pKa	11.62	[230]
Koc	0.2 L/kg	[230]
Solubility in water	miscible	[230]
Henry's law constant	7.4 x 10 ⁻⁹ atm.m ³ /mol at 20 °C	[230]
Vapor pressure	0.003 atm at 25°C	[230]

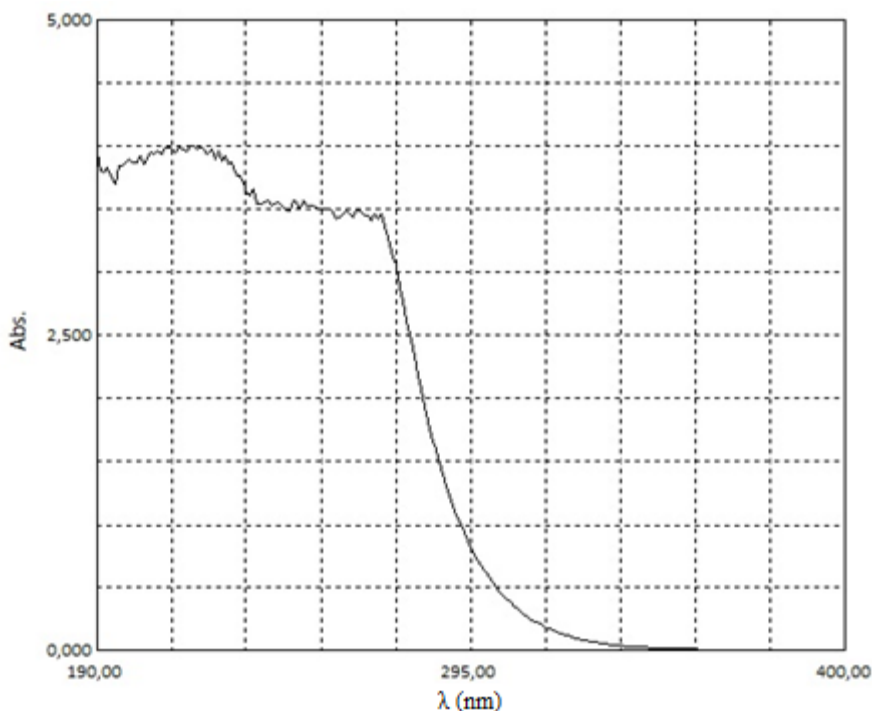


Figure 2.9. UV absorption spectrum of H₂O₂

2.2.3. Soluble catalysts

Homogeneous Fenton oxidation experiments were performed as reference using the classical Fe²⁺/H₂O₂ system. FeSO₄·7H₂O (Sigma, purity ≥ 99%) was used as ferrous ion source.

Table 2.6. Physicochemical properties of ferrous sulfate

Properties		Ref.
IUPAC name	Iron(II) sulfate heptahydrate	[232]
CAS number	7782-63-0	[232]
Formula	FeSO ₄ ·7H ₂ O	[232]
Molecular weight	278 g/mol	[232]
Solubility in water	25.6 g/100 mL at 20°C	[233]
Vapor pressure	0.019 atm at 25°C	[233]

2.2.4. Heterogeneous catalysts

2.2.4.1. Iron containing zeolite (Fe-MFI)

Iron containing zeolite catalyst (Fe-MFI) was obtained from Süd-Chemie AG (ref. Fe-MFI-27). This catalyst has a ZSM5 structure (pentasil zeolite). ZSM5 framework exhibits a 10-ring channel structure, with minor and major axis dimensions of $5.1 \text{ \AA} \times 5.5 \text{ \AA}$ and $5.4 \text{ \AA} \times 5.6 \text{ \AA}$ for sinusoidal and straight channels, respectively [234] (figure 2.10).

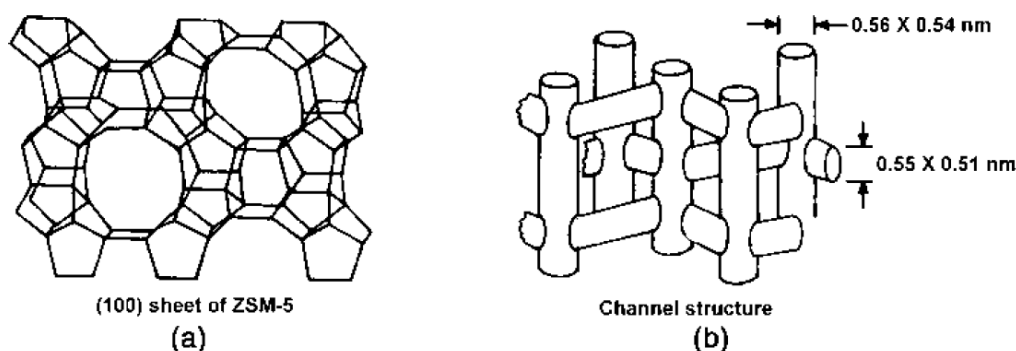


Figure 2.10. (a) Skeletal diagram of the (100) face of ZSM5, (b) Channel structure of ZSM5 (adapted from reference [234])

According to SEM analysis, Fe-MFI particles consisted in agglomerates of micronic grains (figures 2.11A and 2.11B). Laser diffraction analysis showed a narrow size distribution of the suspended particles (mainly between 1 - 20 μm), with volume mean diameter (d_{43}) of 7.9 μm (figure 2.12). EDX analysis (figure 2.11C) shows a “surface” iron content of $3.1 \pm 0.9 \text{ wt\%}$, almost same as the bulk content, and confirms a homogeneous distribution of the metal within the particles. Iron can be located either in the framework of the zeolite or in the form of cations at the exchange sites in the channels, or in the form of oxide nanoparticles [77]. As abovementioned (cf. § 2.1.2.5), iron is mainly present as hematite phase and to a much lesser extent as Fe^{3+} ions according to Mössbauer spectroscopy [165]. X-ray diffractograms of Fe-MFI and MFI (without iron, ref. H-MFI-27) are very similar (figure 2.13), indicating that incorporation of iron has not resulted into any significant structural change of the zeolite.

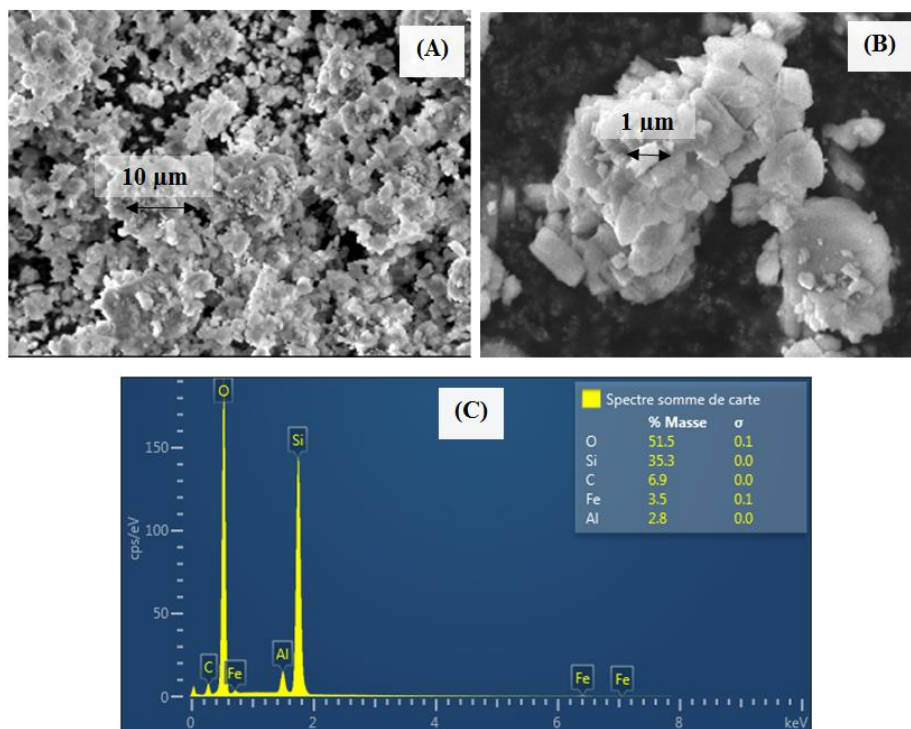


Figure 2.11. SEM images (A and B) and EDX analysis (C) of fresh Fe-MFI catalyst

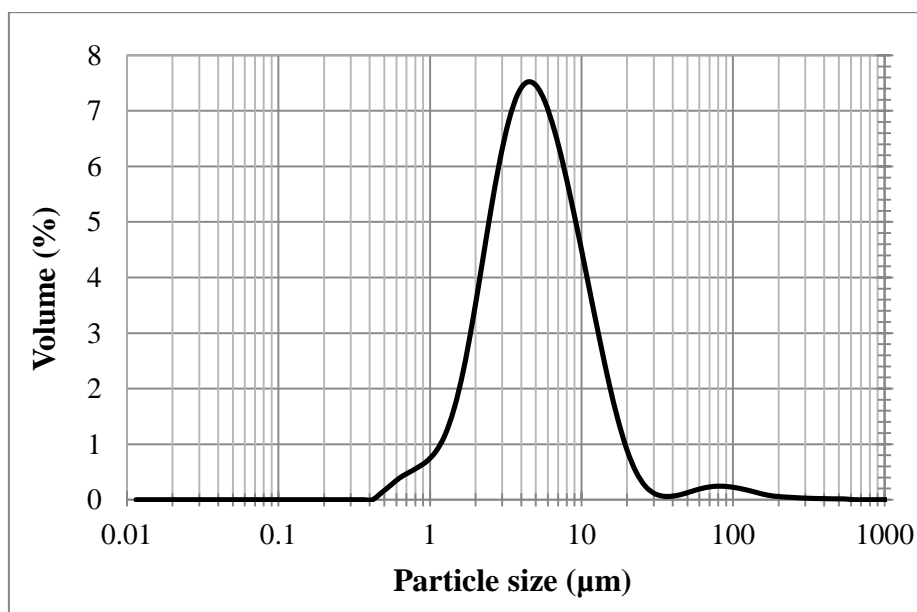


Figure 2.12. Particles size distribution of Fe-MFI (in suspension)

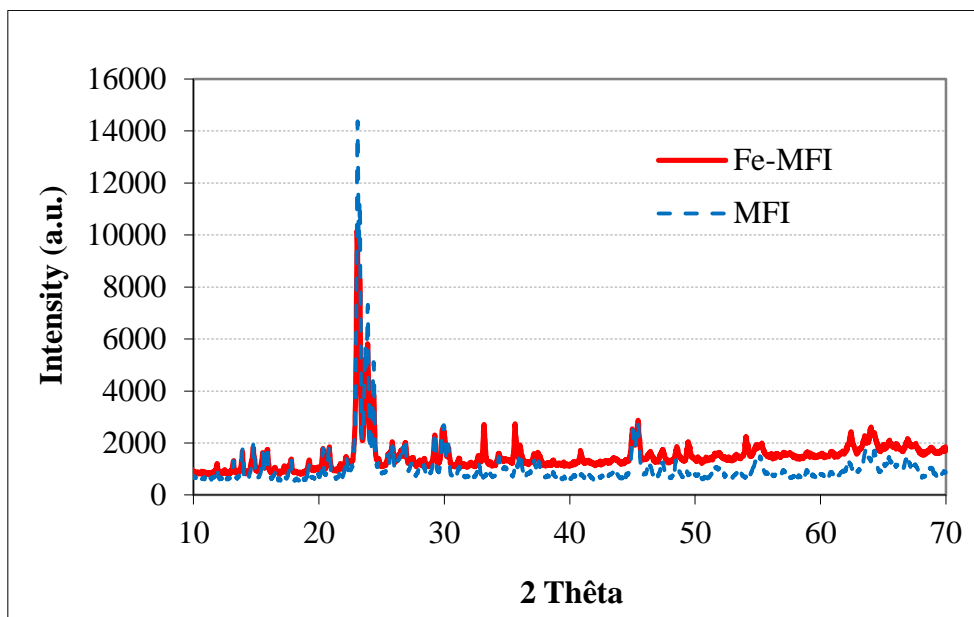


Figure 2.13. XRD patterns of fresh Fe-MFI and MFI

Moreover, iron oxide phase corresponding to hematite (Fe_2O_3 , reference pattern 01-086-2368) can be hardly distinguished for Fe-MFI, which can be the result of high metal dispersion. CO chemisorption indeed gives a mean size of iron crystallite of about 4 nm. On the other hand, TEM/EDX indicates the presence of iron-rich clusters, but of a few tens of nanometers (figure 2.14). Detailed properties of Fe-MFI catalyst are summarized in table 2.7.

Table 2.7. Properties of Fe-MFI

Properties	
Label	Fe-MFI
Support	ZSM5 ($\text{SiO}_2/\text{Al}_2\text{O}_3=27$)
%Fe	$3.4^a / 3.1 \pm 0.9^b / 3.6^c$
Iron dispersion (%)	22^d
$d_{c,\text{CO}}$ (nm)	4^d
$d_{c,\text{XRD}}$ (nm)	Non visible ^e
S_{BET} (m^2/g)	329^f
$V_{\text{Mesopores}}$ (cm^3/g)	0.05^f
$V_{\text{Micropores}}$ (cm^3/g)	0.13^f
V_{Porous} (cm^3/g)	0.18^f
d_{43} (μm)	7.9^g
pH_{pzc}	2.9^h

Iron content according to: ^aICP-AES analysis of acid leachate, ^bSEM-EDX analysis of Fe-MFI, ^cSüd-Chemie supplier; ^dMetal dispersion and mean diameter of crystallites calculated from CO chemisorption; ^eMean diameter of crystallites calculated from XRD ^fSpecific surface area, mesoporous, microporous and total porous volumes measured by N_2 porosimetry; ^gVolume mean diameter of agglomerates in suspension (laser diffraction method); ^hpH at the point of zero charge measured by mass titration.

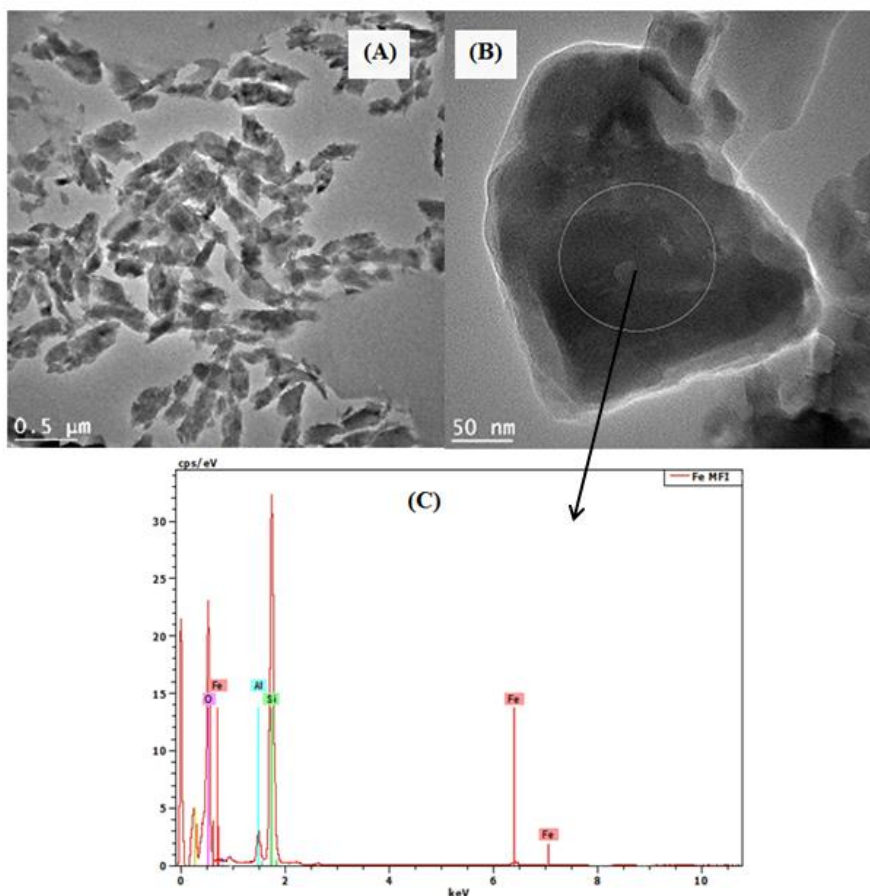


Figure 2.14. TEM images (A and B) and EDX analysis (C) of fresh Fe-MFI catalyst

2.2.4.2. Zero-valent iron (ZVI)

Zero-valent iron catalyst (ZVI) was purchased from Strem Chemicals Inc. (Ref. 93-2601). It consists into a grey to black powder with magnetic properties. SEM images (figure 2.15) and laser diffraction measurements (figure 2.16) show that ZVI powder is composed of polydisperse aggregates, between 2 and 100 μm. The elemental particle diameter calculated from BET surface area (table 2.8) indicates that ZVI contains micronic polycrystalline grains, resulting in a very low dispersion of iron (< 0.1%).

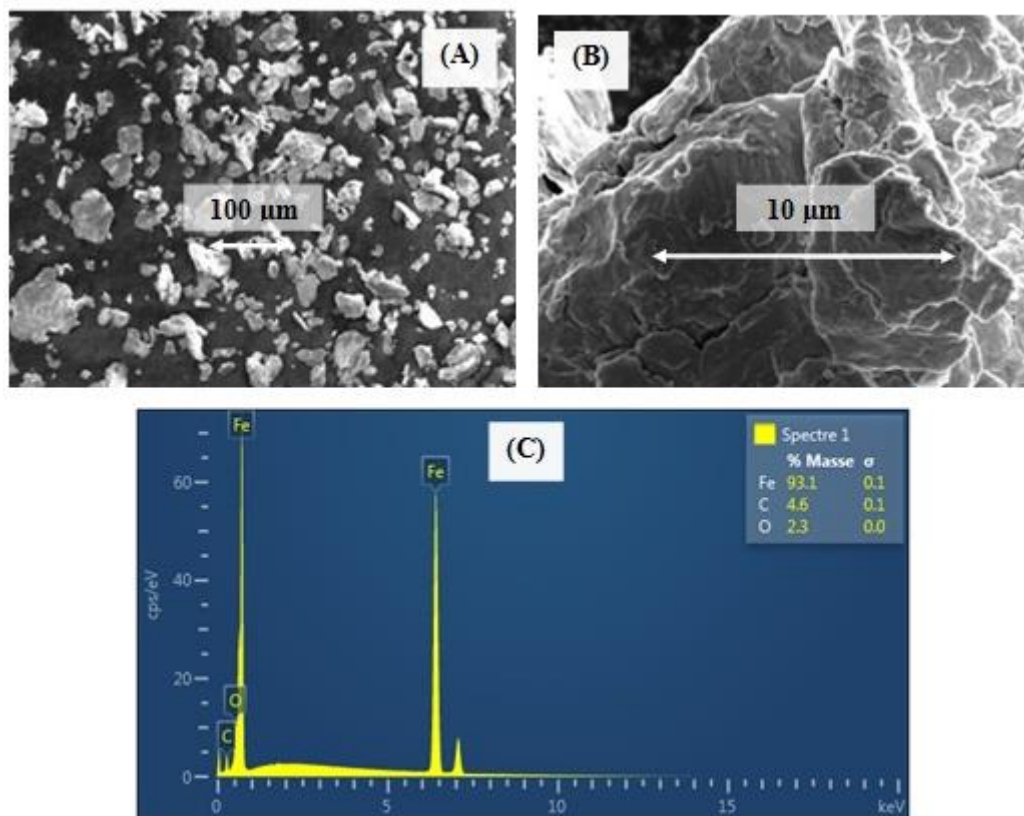


Figure 2.15. SEM images (A and B) and EDX analysis (C) of fresh ZVI catalyst

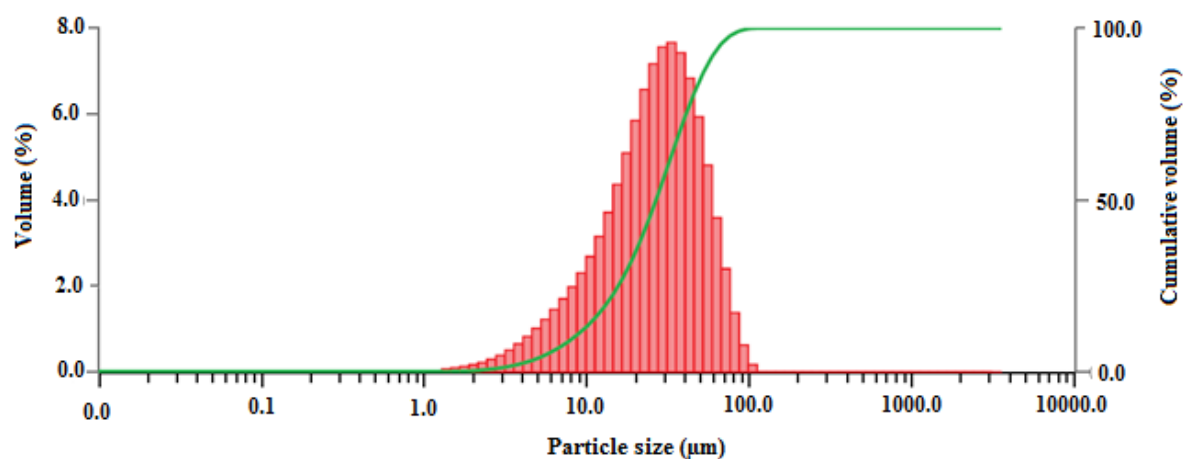


Figure 2.16. Particle size distribution of ZVI powder

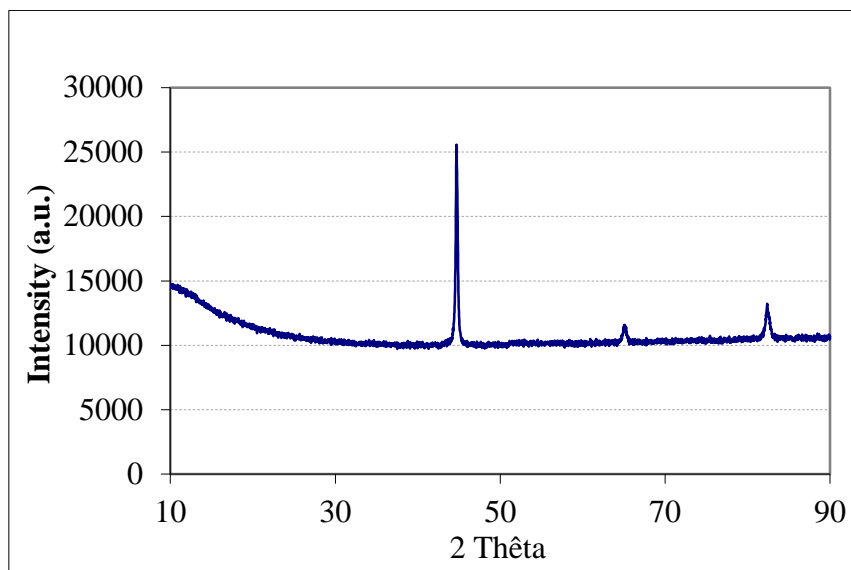


Figure 2.17. XRD pattern of fresh ZVI

Table 2.8. Properties of ZVI

Properties	
Label	Iron powder
Fe content (%)	99.9 ^a (88±5) ^b
S_{BET} (m ² /g)	0.47 ^c
$d_{\text{c,XRD}}$ (nm)	45 ^d
d_{ep} (nm)	1620 ^e
Iron dispersion (%)	< 0.1 ^f
d_{43} (μm)	30 ^g
pH_{pzc}	5.8 ^h

Iron content according to ^asupplier (^bSEM-EDX analysis); ^cSpecific surface area measured by N₂ porosimetry; ^dMean diameter of crystallites calculated from XRD; ^eMean diameter of elemental particles calculated from S_{BET} assuming spherical shape ($d_{\text{ep}} = 6/(S_{\text{BET}} \cdot \rho)$); ^fIron dispersion (%) = 96/ d_{ep} (nm); ^gVolume mean diameter of agglomerates in dry powder (laser diffraction method); ^hpH at the point of zero charge measured by mass titration

According to the supplier, ZVI is a pure iron powder (purity 99.9%), but evaluation of elemental composition by SEM-EDX shows that surface iron content is only of 88±5%. Detected oxygen and carbon might be due either to the adhesive carbon tape used to stick the particles for observation or to the presence of a surfactant on the surface. Indeed, the intense characteristic peaks at $2\theta = 44.70, 65.06$ and 82.38 confirm that fresh catalyst is mainly in its reduced state Fe⁰ (in agreement with JCPDS 65-4899). Main properties of ZVI are given in [table 2.8](#).

2.3. EXPERIMENTAL SETUP

Three types of sono-photochemical reactors have been used in the previous works, *i.e.* combined sono-photo-reactor with immersed lamp [175], combined sono-photo-reactor with external lamp [120,129,170,171] and separate sono- and photo-reactors [33,126,235]. To the author's knowledge, there is no report on the advantages and disadvantages of each system. However, Segura et al. (2009) pointed out that the presence of an ultrasonic field results in light scattering (due to cavitation bubbles) and thus a lower efficiency for the combined reactors. Therefore, a system comprising separate sono- and photo-reactors was chosen for this study.

Experiments were thus performed using two batch glass reactors (sono- and photo-reactors), either individually or in a loop system. Each was equipped with a jacket connected to a thermostated bath (F18, Julabo). The suspension was circulated in between the two reactors by a dual-head peristaltic pump (Masterflex, model 7554-95, Teflon tubing) at a high flow rate (150 mL/min) to ensure a uniform concentration.

2.3.1. Sono-reactor

The sono-reactor (1000 mL) was of Cup-Horn type and equipped with a pitch blade impeller (400 rpm), temperature probe, several injection/sampling points. The sonication probe was placed at the bottom of the reactor and the fitting between glass reactor and sonication probe was accommodated by Teflon joint braced with a clamp ring (figure 2.18A).

Three sonication devices emitting different frequencies were used in this study (figure 2.18). Note that almost all experiments performed at 20 kHz were carried out in equipment 1. In addition, it should be mentioned here that experiments with high frequency ultrasound (ultrasonic equipment 3, figure 2.18D) were conducted in Instituto Superior de Tecnologías y Ciencias Aplicadas (InSTEC), at University of Habana, Cuba. Properties of the sonication devices used in this study are given in table 2.9.



Figure 2.18. Ultrasonic equipment 1 mounted in sono-reactor (A), ultrasonic probe of equipment 1 (B), ultrasonic equipment 2 (C), and sono-reactor with ultrasonic equipment 3 (D)

Table 2.9. Characteristics of sonication systems

Properties	Equipment		
	1	2	3
Supplier	Sonics & Materials, Inc.	SinapTec	Meinhardt Ultraschalltechnik
Model	VCX750	NexTgen Inside 500	E/805/T/M
Frequency (kHz)	20	12 / 20	580 – 862
Max nominal power (W) ^a	180	200	250
Max calorimetric power (W) ^b	131	156	32
Efficiency (%)	73	78	13
Applied power (W) ^c	25, 50, 75 ^f , 100	50	12.5
Liquid volume (mL)	1000 (+500 ^f)	1000	250
Applied D _{US} (W/L) ^d	25, 50, 100	50	50
Probe diameter (mm)	51	35	40
Applied I _{US} (W/cm ²) ^e	1.25, 2.45, 4.9	5.2	1

^a Nominal power displayed on generator

^b Dissipated power measured by calorimetry [236]

^c Power used in experiments

^d Sonication density : applied power / liquid volume [91]

^e Sonication intensity : applied power / probe surface area [91]

^f If coupled with photo-reactor

The actual sonication power was determined by calorimetric method [236]. A vertical mechanical stirrer was used to ensure the homogeneity of temperature throughout the reactor and cooling jacket is emptied during the test. Calorimetric sonication power delivered into the solution (P_{cal}) can be determined using following equation:

$$P_{cal} = (dT/dt) \times (C_{pw} + C_{pg}) \times (M_w + M_g) \quad (E.2.6)$$

Where P_{cal} is the calorimetric power (W), dT/dt is the rate of temperature increase (K/s), C_{pw} is the specific heat of water = 4181 J/kg.K and M_w is the mass of solution (kg). It should be noted that the accumulation of heat in the glass reactor wall (in contact with water) was not taken into account since the corresponding mass ($M_g \sim 0.2$ kg) and heat ($C_{pg} = 720$ J/kg.K for glass) are much smaller than those of water, thus giving an imprecision of less than 3%. Calorimetric evaluation of ultrasound equipment 1 is illustrated in figure 2.19, for three different amplitudes (Amp).

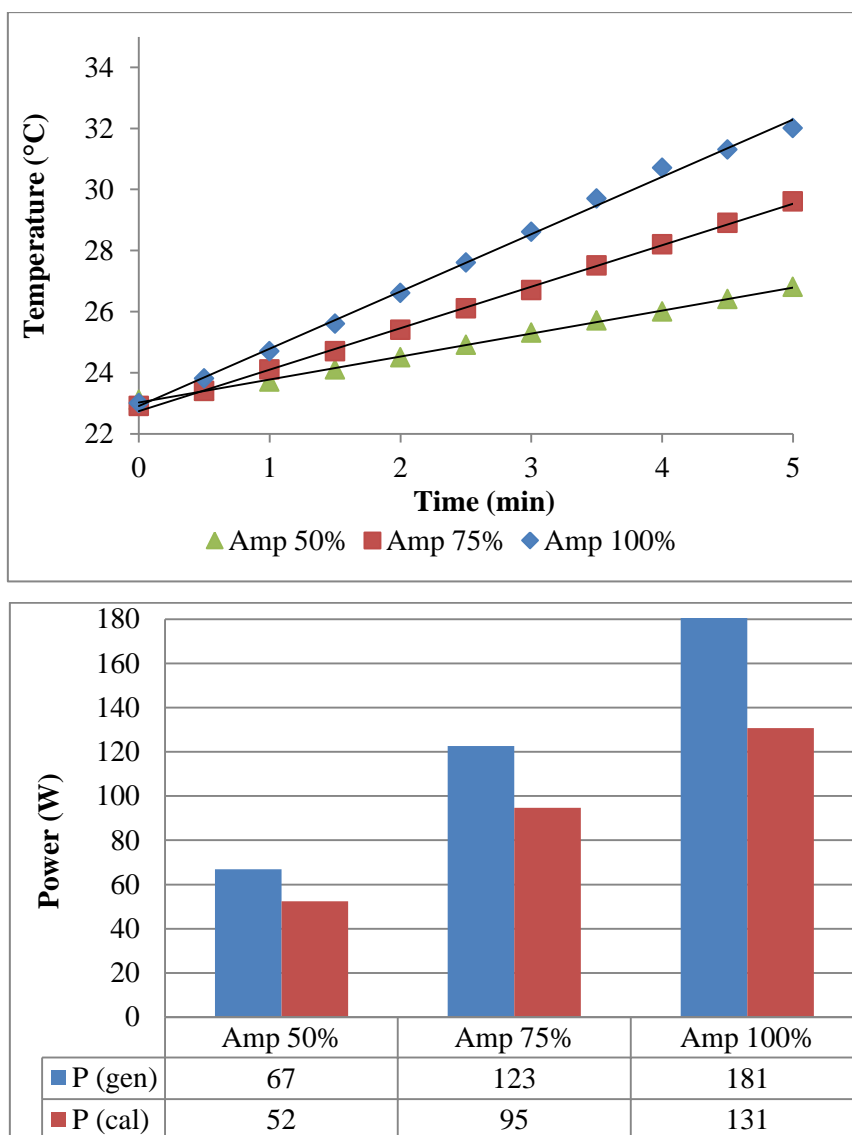


Figure 2.19. Calorimetric evaluation of ultrasonic equipment 1
 Amp: Amplitude, P_{gen} : Electrical power consumed by US generator (W), P_{cal} : calorimetric power (W)

Furthermore, several parameters can be defined to characterize the ultrasound power delivered into the solution (suspension) [91]:

$$I_{US} = P_{cal} / A_P \quad (E.2.7)$$

$$D_{US} = P_{cal} / V \quad (E.2.8)$$

$$E_{US} = (P_{cal} \times t) / M \quad (E.2.9)$$

Referred to as I_{US} : sonication intensity (W/cm^2), D_{US} : sonication density (W/L) and E_{US} : specific energy input (kJ/kg), with P_{cal} : actual power determined by calorimetry (W), A_P : probe area (cm^2), V : volume of treated solution or suspension (L), M : weight of treated solution or suspension (kg), and t : sonication time (s).

2.3.2. Photo-reactor

The photo-reactor (500 mL) consisted in a cylindrical glass reactor with an immersion lamp contained in a thermostated quartz sleeve. Quartz lamp holder was chosen to ensure that almost all ultraviolet (UV) and visible irradiation emitted by the tested lamps was transmitted to the treated solution (>90% light transmittance between 200-1000 nm). A magnetic stirrer was used to prevent particle settling. For safety reasons, this photochemical reactor was installed inside a closed cabinet and equipped with an automatic shutdown system if the temperature of the solution exceeds $60^\circ C$ and/or the box door was opened (figure 2.20A).

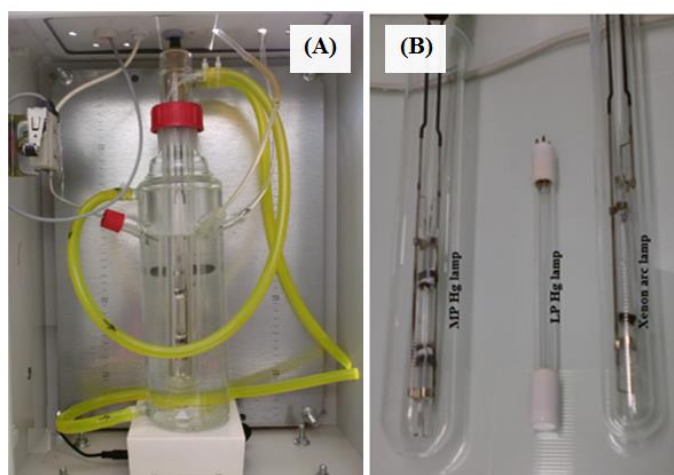


Figure 2.20. Photo-reactor (A) and investigated lamps (B)

Three UV-vis lamps (medium and low pressure mercury lamps and xenon arc lamp (figure 2.20B), differing by their irradiation spectrum (figures 2.21 and 2.22) and intensity,

were used in this study. The MP Hg lamp was selected due to its wide range of irradiation spectrum covering UV and visible irradiation. The LP Hg lamp (monochromatic) was chosen considering its low energy consumption. The Xenon-Arc lamp was selected as a model of sunlight irradiation. The main characteristics of the lamps are given in [table 2.10](#) and [figure 2.23](#).

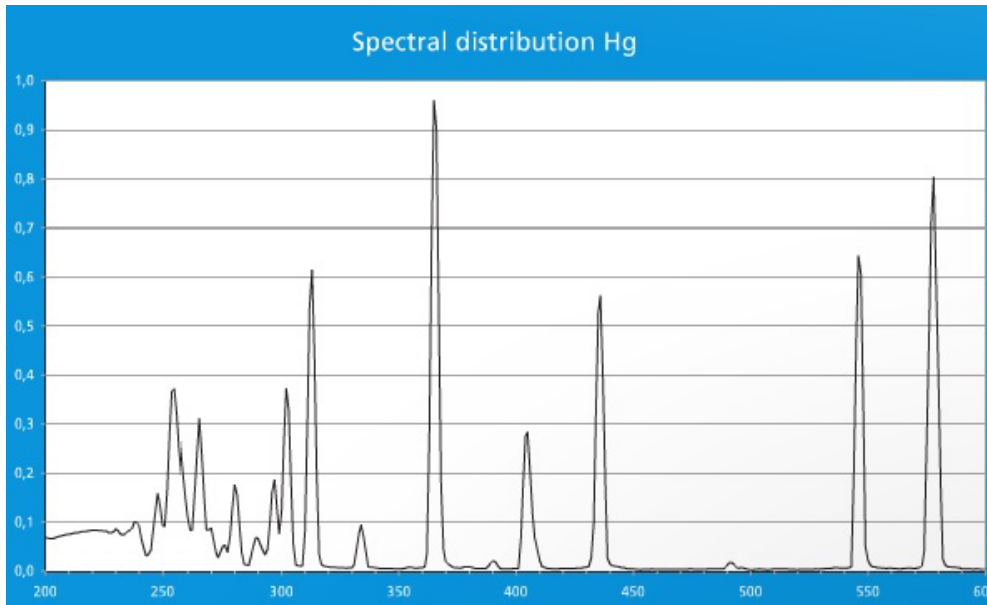


Figure 2.21. Spectral distribution of TQ150 lamp (medium pressure Hg vapor lamp)
(Data provided by supplier)

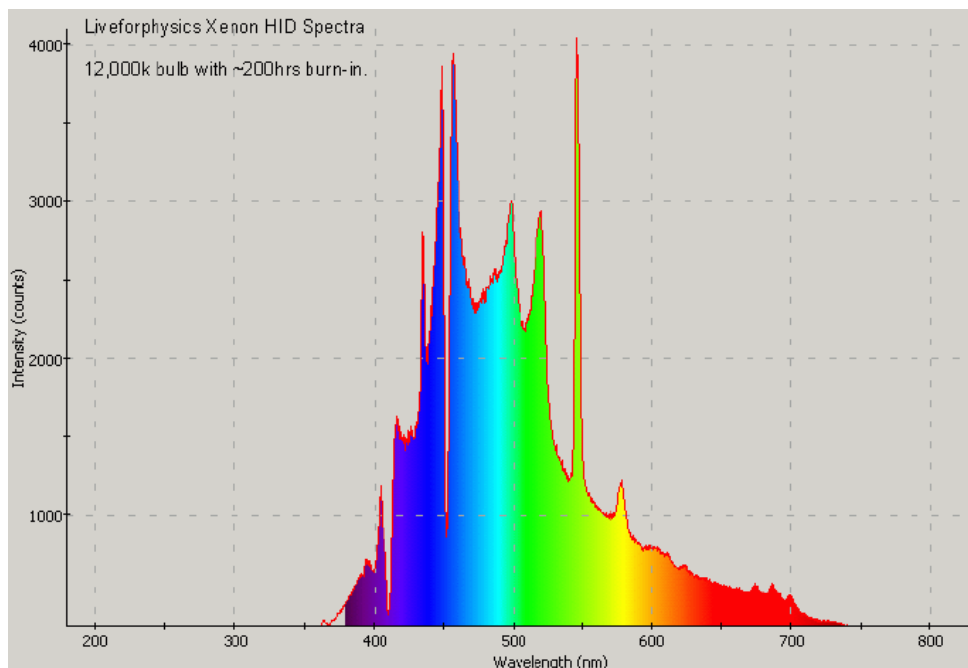


Figure 2.22. Spectral distribution of lamp TXE150 lamp (xenon arc lamp)
(Data provided by supplier)

Table 2.10. Characteristics of UV-Vis lamps

Characteristics	Lamp 1	Lamp 2	Lamp 3
Supplier	Peschl Ultraviolet	Heraeus	Peschl Ultraviolet
Model	TQ150	GPH150T5L	TXE150
Type	MP Hg	LP Hg	Xenon-Arc
λ (nm)	200 – 577	254	360 – 740
Electric power (W)	150	6	150

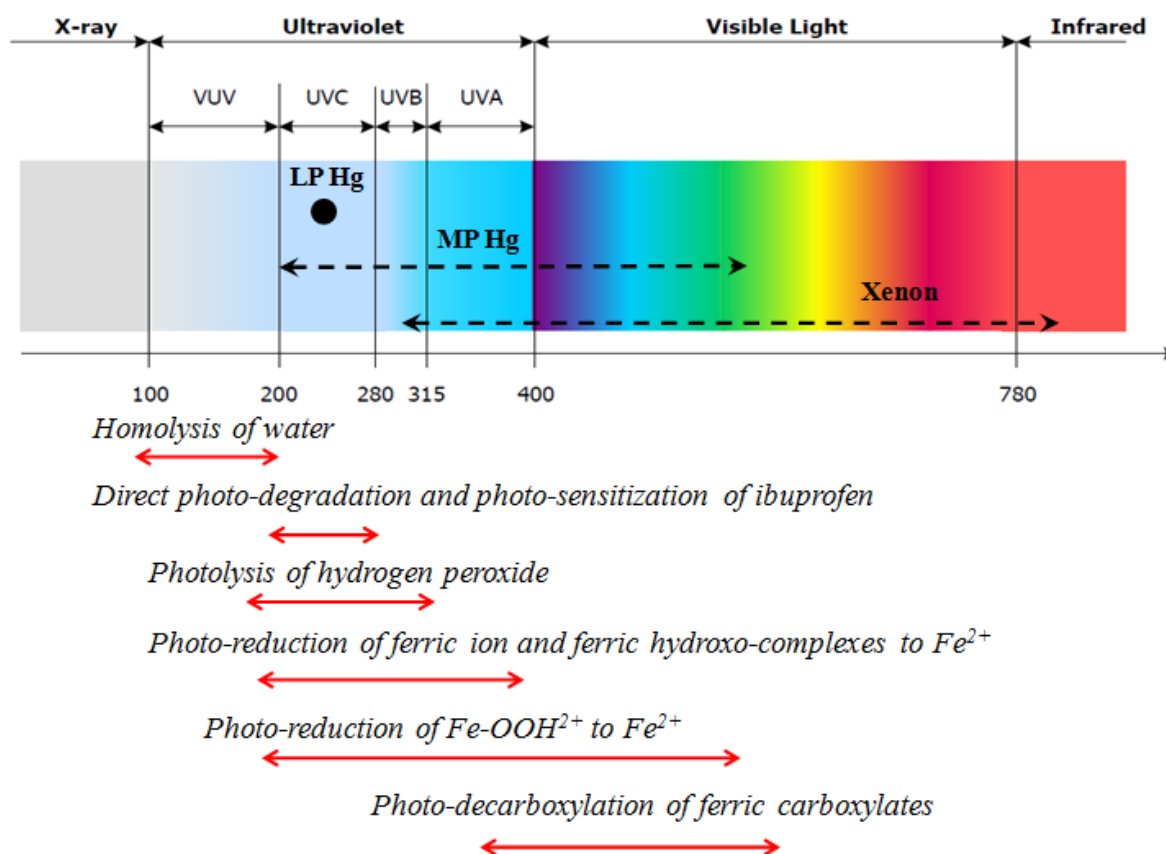


Figure 2.23. Irradiation spectrum of the lamps vs. useful ranges for the different photochemical reactions

Finally, figure 2.24 shows the complete sono-photochemical reactor system.

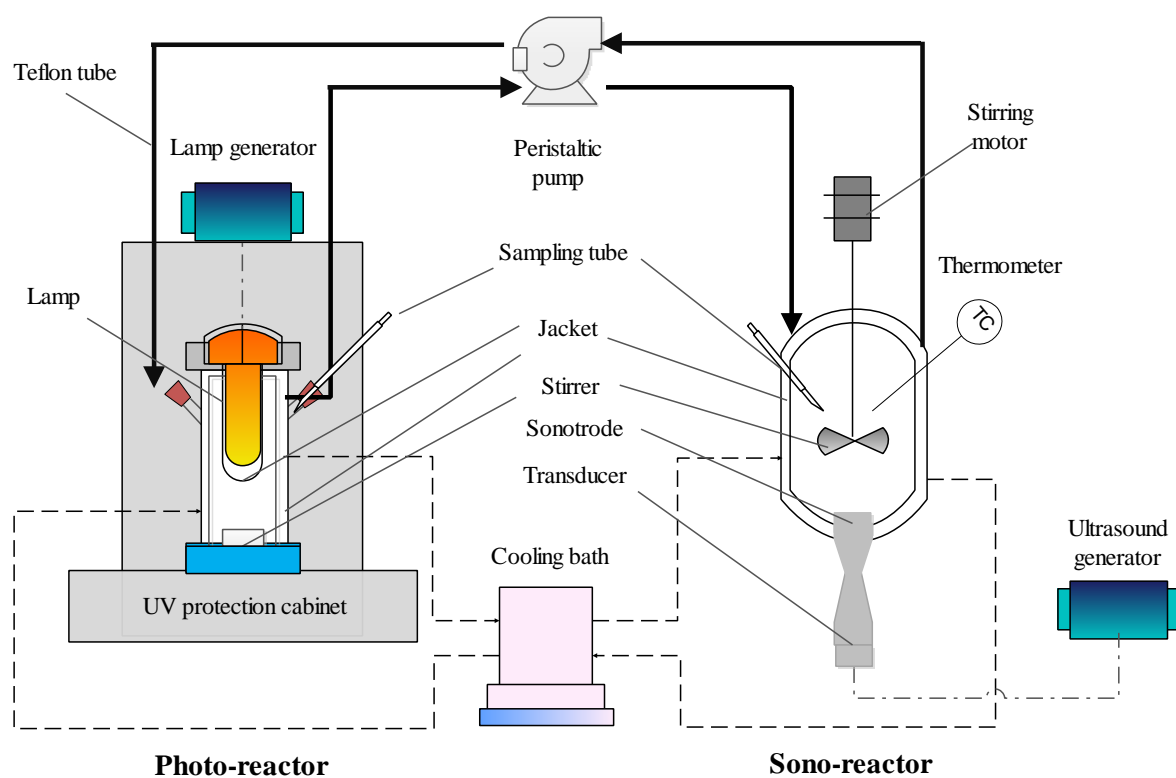


Figure 2.24. Schematic drawing and photograph of the sono-photochemical reactor system

2.4. EXPERIMENTAL PROCEDURE

As abovementioned, 20 mg/L ibuprofen solution was treated in this work. After introduction of the solution in the sono-reactor and/or photo-reactor, stirring, thermostat and pump circulation were turned on. The zero time of the reaction depended on the type of experiment (homogeneous or heterogeneous, with or without ultrasound/light irradiation).

2.4.1. Homogeneous processes

In homogeneous processes (*e.g.* Fenton, ultrasound and/or light irradiation, sono-Fenton, photo-Fenton, etc), a first sample (9 mL) was taken once the desired temperature was reached (referred to as zero time of the reaction) and oxidation was started by the addition of H₂O₂ and/or application of ultrasound. In case of experiment using light irradiation, lamp was turned on 2 min before in order to attain a constant irradiation prior to the oxidation. In case of Fenton reaction, ibuprofen solution was previously mixed with iron salt (FeSO₄·7H₂O) and the pH was adjusted with 1 M H₂SO₄ and 1 M NaOH. Aliquots samples (9 mL) were withdrawn throughout the reaction (*t* = 5, 10, 30, 60, 120, 180 min).

2.4.2. Heterogeneous processes

When heterogeneous reaction was performed, the solution was first contacted with the solid catalysts (Fe-MFI or ZVI) under stirring in order to approach the adsorption equilibrium (adsorption step). After 120 min, 15 mL of solution was withdrawn and this first sampling corresponded to zero time of the reaction. Oxidation step was starting by addition of H₂O₂ and/or US application. As for homogeneous process, lamp was turned on 2 min before. Aliquots samples (9 mL) were withdrawn throughout the reaction (*t* = 5, 10, 30, 60, 120, 180 min). At the end of experiment with solid catalyst, the suspension was filtered on a nitrocellulose membrane filter with 0.22 μm pore size (GSWP, Merck Millipore). Final pH, as well as concentrations of residual H₂O₂ and leached iron were measured according to the methods described in section 2.1.1. The recovered Fe-MFI was also analyzed for carbon content (see § 2.1.2.7).

In order to examine the repeatability, some experiments were duplicated and the coefficients of variation of the principal parameters such as IBP, TOC and residual H₂O₂

concentrations did not exceed 5% of the averaged values (example of experiment with error bars can be found in appendix: figure VI).

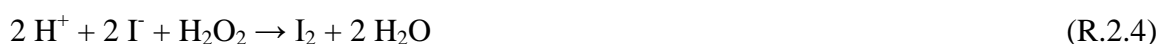
2.4.3. Sample preparation for HPLC/UV and TOC analysis

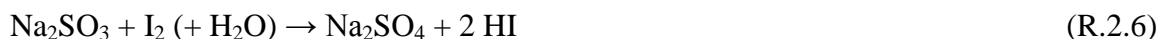
All withdrawn samples containing heterogeneous catalyst were filtered with 0.45 μm regenerated cellulose (RC) syringe filter (Thermo Scientific National; ref. F2513-7). A preliminary study showed that retention of ibuprofen on this filter was negligible, contrarily to 5% retention observed with nylon filter syringe (Fisherbrand; ref. 11812743). The 1 mL filtered samples were mixed with 1 mL of phosphate buffer before HPLC/UV analysis to precipitate leached (or dissolved) iron, and filtered again through RC membrane. Phosphate buffer solution consisted in a mixture of monopotassium phosphate (KH_2PO_4) 0.05 M and $\text{Na}_2\text{HPO}_4 \cdot 2\text{H}_2\text{O}$ 0.05 M [58]. All phosphate reagents were purchased from Sigma-Aldrich (ref. 60220 and 30412).

Table 2.11. Composition of phosphate buffer and quenching solution

Solutions	Composition	C (mM)
Phosphate buffer	KH_2PO_4	0.05
	$\text{Na}_2\text{HPO}_4 \cdot 2\text{H}_2\text{O}$	0.05
Quenching	KH_2PO_4	0.05
	$\text{Na}_2\text{HPO}_4 \cdot 2\text{H}_2\text{O}$	0.05
	KI	0.1
	Na_2SO_3	0.1

Likewise, the rest of sample filtrate (8 mL) was mixed with a quenching solution (3 mL), filtered again through RC membrane then diluted with ultrapure water up to 20 mL before TOC analysis. The quenching solution was added to withdrawn samples in order to stop the reaction immediately after sampling. Quenching solution consisted in a mixture of potassium iodide 0.1 M (KI), sodium sulfite (Na_2SO_3) 0.1 M and the phosphate buffer. While the phosphate buffer precipitates solubilized iron, iodide ion (I^-) and sodium sulphite (Na_2SO_3) reduces residual hydrogen peroxide (H_2O_2) and radicals according to the following equations [58,237–239]:





Recently, it was found that potassium iodide can pass through the halogen filter and accumulate in the NDIR cell detector of TOC analyzer reducing the lifetime of the NDIR cell. Therefore, the utilization of potassium iodide should be avoided in further studies before the installation of specific iodide filter in TOC analyzer.

2.4.4. Experimental data analysis

In chapter 3 and chapter 4, IBP degradation and TOC elimination during the reaction were presented in terms of normalized concentration (C/C_0). In addition, a first-order kinetic constant (k) for IBP degradation was also estimated from linear regression of the logarithm of ibuprofen concentration against time:

$$\ln ([\text{IBP}]_0 / [\text{IBP}]_t) = kt \rightarrow y = ax + b \quad (\text{R.2.7})$$

k values in each experiment were based on data corresponding to IBP removal level of less than 60%.

2.5. CONCLUSION

This chapter has given details about the analytical methods used to characterize liquid samples, as well as solid catalysts studied in this work. The experimental tools have been also presented. Two batch reactors connected in a loop system have been implemented: a sono-reactor and a photo-reactor whose main characteristics have been described. Finally, the operating protocols, including the treatment of the liquid samples before analysis, have been explained. The following chapters investigate the removal of ibuprofen by homogeneous and heterogeneous advanced oxidation processes.

This page is intentionally left blank

CHAPTER 3 HOMOGENEOUS PROCESSES

As mentioned in the literature section, main limitation of the conventional Fenton reaction lies in the uneasy regeneration of ferrous iron that may cause wastage of expensive H_2O_2 reagent by limiting the pollutant mineralization. Furthermore, high iron salt concentrations - well above European discharge limit (2 mg/L) - are normally needed to gain appreciable reactions rates, leading to techno-economic issues related to the formation of excessive ferric hydroxide sludge and continuous loss of iron especially in large scale operation. Therefore, activation methods would be of special interest if they can significantly reduce the required amounts of Fenton's reagent.

Beyond their ability for direct pollutant lysis or radical generation, ultrasound and UV/Vis light irradiation have shown to be promising methods for the (re)activation of iron catalyst, but the underlying mechanisms are complex and their contribution is not easily appreciable, due to the large number of concomitant processes involved.

In this first chapter dedicated to the degradation of ibuprofen (IBP) by homogeneous advanced oxidation treatments, the study will progress stepwise, from the separate processes – sonolysis, photolysis, and Fenton oxidation – then their two-by-two combinations, to conclude about the benefit(s) of the global hybrid process. At each stage the effect of several operating parameters on the pollutant conversion and mineralization (Total Organic Carbon removal) will be investigated, such as pH of the solution, amount of reagents, applied power, sound frequency or irradiation spectrum etc., in order to get some insight of the implied phenomena.

This page is intentionally left blank

3.1. IBUPROFEN REMOVAL BY SINGLE PROCESSES

3.1.1. Preliminary considerations: reference conditions of the study

It should be first recalled that a 20 mg/L solution of IBP (just below the molecule solubility, 21 mg/L at 25°C) was used for all the experiments. This concentration is much higher than encountered in usual wastewaters, but according to recent reviews on hybrid processes [240,241], advanced oxidation processes would be better used downstream a pre-concentration step so as to treat smaller streams, limit radical scavenging and save chemicals. This concentration also allowed both the liquid and the solid phases to be analyzed with enough precision to determine the fate of the pollutant during the batch oxidation tests.

The synthetic solution was first prepared in distilled water, leading to a “natural” pH of 4.3. However, other values were also considered, namely 2.6 and 8.0, in order to mimic pH condition of the Fenton reaction on the one hand, and pH of wastewater effluent on the other hand (cf. § 3.4).

Regarding chemical oxidation, the stoichiometric amount of H₂O₂ required for IBP mineralization was calculated according to reaction R.3.1 (cf. § 2.2.2 for more detail information):



As shown in figure 3.1, it was checked that simple addition of H₂O₂ at two times (2x) or seven times (7x) the stoichiometric amount did not result in any measurable IBP and H₂O₂ conversion within 3 hours corresponding to the standard reaction time. The same observation could be made at the two other pH values and confirmed that a catalyst and/or physical activation process(es) were required to decompose H₂O₂ into more active species able to degrade the molecule. On the other hand, addition of ferrous iron catalyst in the absence of H₂O₂ did not result in any pollutant conversion.

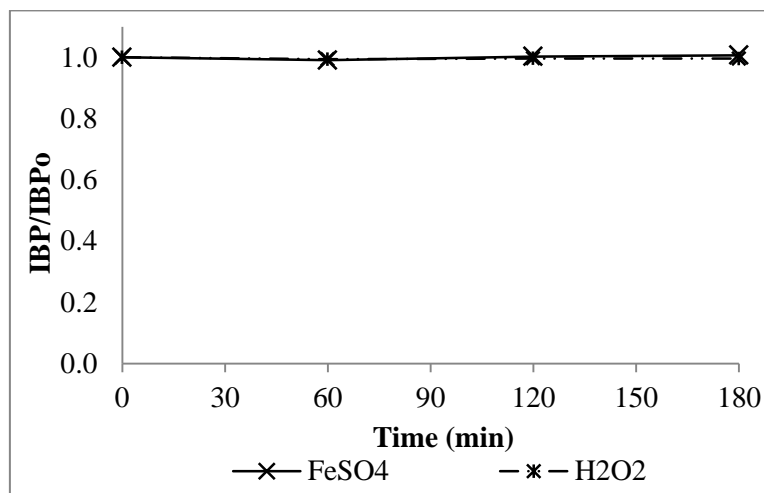


Figure 3.1. Effect of addition of H₂O₂ (alone) or iron salt (without H₂O₂)
 ([IBP]₀ = 20 mg/L, pH₀ = 2 – 8, T = 25°C, [FeSO₄·7H₂O]₀ = 0.13 mM, [H₂O₂]₀ = 6.4 – 22.4 mM)

With regard to iron catalyst, [H₂O₂] / [Fe] ratio was set to 48 - corresponding to the upper bound of the recommended range (between 10 to 50 [62,129,184,242]) - in order to limit metal concentration in the treated water.

As mentioned previously in chapter 2 (§ 2.3), 20 kHz was chosen as reference ultrasound frequency considering its practical application in water treatment [60,243]. Likewise, low pressure mercury vapor lamp irradiating around 254 nm was used as reference equipment for photochemical processes, due to its moderate cost and successful application in photo-degradation of pharmaceutical compounds [13,18,19,42,44,139,143,157].

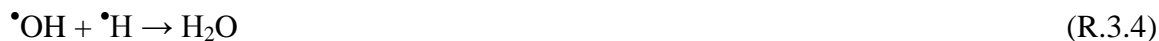
3.1.2. Ultrasound irradiation

Tests described in this section were performed in the sono-reactor only (V = 1000 mL).

3.1.2.1. IBP degradation by ultrasound and its mechanisms

Before applying ultrasound for IBP oxidation, a preliminary sonication test at 20 kHz was performed in water. It is well known that sonication of water can generate hydroxyl radicals that should be recombined to form H₂O₂ (R.3.2 – R.3.7) [95,244,245]. Indeed, it was found that a small quantity of H₂O₂ (0.41 μM/min) was formed during sonication, confirming the occurrence of transient cavitation in the investigated conditions (D_{US} = 50 W/L, corresponding to the calorimetric ultrasound power per unit volume).





Degradation of IBP by low frequency ultrasound (20 kHz) or sonolysis process is depicted in [figure 3.2](#). As final conversion was below 50%, time evolution of IBP can be fitted using both zero ($k = 0.0002 \text{ mM/min}$, $R^2 = 0.992$) and first order (0.0035 min^{-1} , $R^2 = 0.996$) kinetics, but the latter was chosen in accordance with the literature (and to facilitate comparison with other processes). After 180 min of sonication, 48% of IBP was degraded and mainly converted to oxidation intermediates, as mineralization yield was only 7%. For comparison, Xiao and coworkers [41] reported that 60% of IBP was degraded after 60 min of 20 kHz sonication, but they used much higher ultrasound density ($D_{\text{US}} = 400 \text{ W/L}$) and different pH (8.5). Based on the result of HRMS analysis, low TOC conversion in sonolysis process can be ascribed to the formation of more hydrophilic degradation products such as 1-hydroxyibuprofen and 2-hydroxyibuprofen ($\log K_{\text{ow}} = 2.25$ [246]).

As mentioned in the literature section, organic compounds can be degraded under ultrasound (US) irradiation in three different zones: inside cavitation bubble ([R.3.8](#)) and/or at the bubble-liquid interface and/or in the solution bulk ([R.3.2](#) and [R.3.9](#)), depending on the volatility and hydrophobicity of the molecule [40,41,98,103].



According to its low volatility (Henry's law constant = 1.5×10^{-7} atm.m³/mol [40], vapor pressure = 1.18×10^{-8} atm [228] at 25°C) and low water solubility (Log K_{ow} = 3.97 [247]), IBP degradation mechanism may correspond to a radical attack at the bubble surface [40,41].

In order to confirm this hypothesis, two types of radical scavengers, namely n-butanol and acetic acid, were added to the IBP solution before 20 kHz sonolysis: n-butanol is a short chain alcohol with only partial solubility in water (log K_{ow} = 0.88) and known to be an effective •OH scavenger for the gaseous region and/or the interfacial region of the collapsing bubble [100,109], while fully miscible acetic acid (log K_{ow} = -0.17) reacts with •OH in the solution bulk [248]. As shown in figure 3.2, addition of n-butanol and acetic acid (at 50 mM, *i.e.* 500 times the molar concentration of IBP) reduced the pollutant conversion from 48% after 3 h to 8% and 40%, respectively. Therefore, sono-degradation of IBP is mainly due to •OH attack at the liquid-bubble interface.

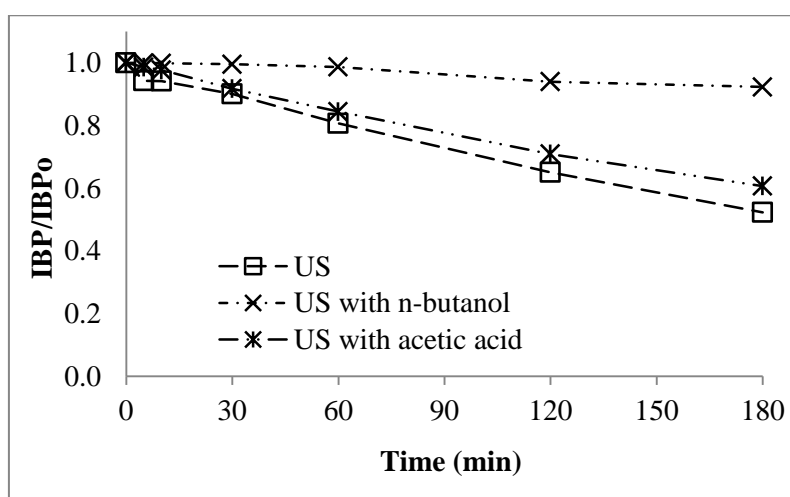


Figure 3.2. Sonolysis of IBP and effect of radical scavenger
([IBP]₀ = 20 mg/L, pH₀ = 4.3, T = 25°C, f_{US} = 20 kHz, D_{US} = 50 W/L, [Scavengers]₀ = 50 mM)

3.1.2.2. pH effect

In order to separate possible effects in the combined process and with the wastewater matrix, the pH of IBP solution was also adjusted before sonolysis to 2.6 and 8.0 with H₂SO₄ and NaOH (1 M solution), respectively.

Lowering the pH did not modify IBP degradation rate, but a significant reduction was observed at the alkaline value (figure 3.3A): the identified first-order rate constant shifted

from 0.0035 to 0.0020 min⁻¹. It can be explained by the different forms of IBP at a given pH. As the pKa of its carboxyl group is 4.9, IBP is in molecular form at pH 2.6 and 4.3 (natural pH), but fully deprotonated at pH 8.0. In ionic form, IBP should be less accumulated at the surface of the cavitation bubbles, where radical attacks mainly occurred. This result is also in agreement with previous studies on the sonolysis of ibuprofen [40], diclofenac [99], dicloxacilin [249] and paracetamol [125], that showed a reduction of the degradation rate at a pH value higher than the pKa of the molecule.

In all cases, removal of total organic carbon (TOC) remained below 8% (figure 3.3B).

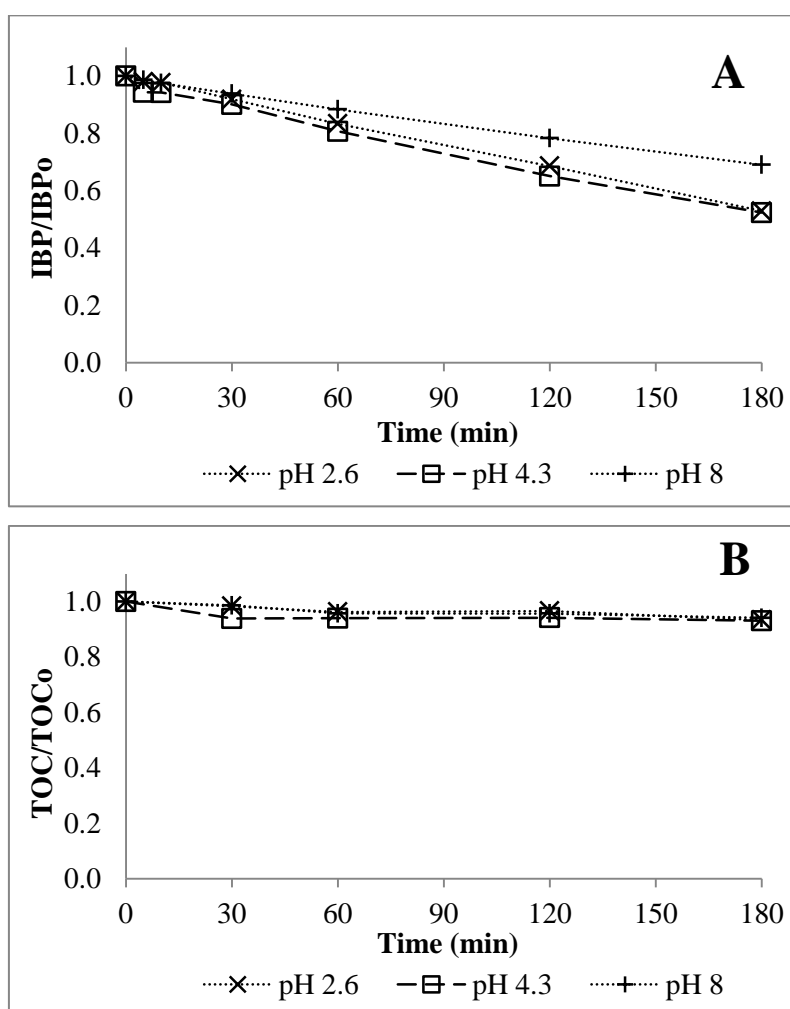


Figure 3.3. Effect of the solution pH on: (A) IBP and (B) TOC removal by sonolysis ([IBP]₀ = 20 mg/L, pH₀ = 2.6 – 8, T = 25°C, f_{US} = 20 kHz, D_{US} = 50 W/L)

3.1.2.3. Effect of ultrasound density

Three levels of ultrasound density (D_{US}) - 25, 50 and 100 W/L - were tested during 180 min, corresponding to a specific energy input (E_{US}) of 270, 540 and 1080 kJ/kg, respectively.

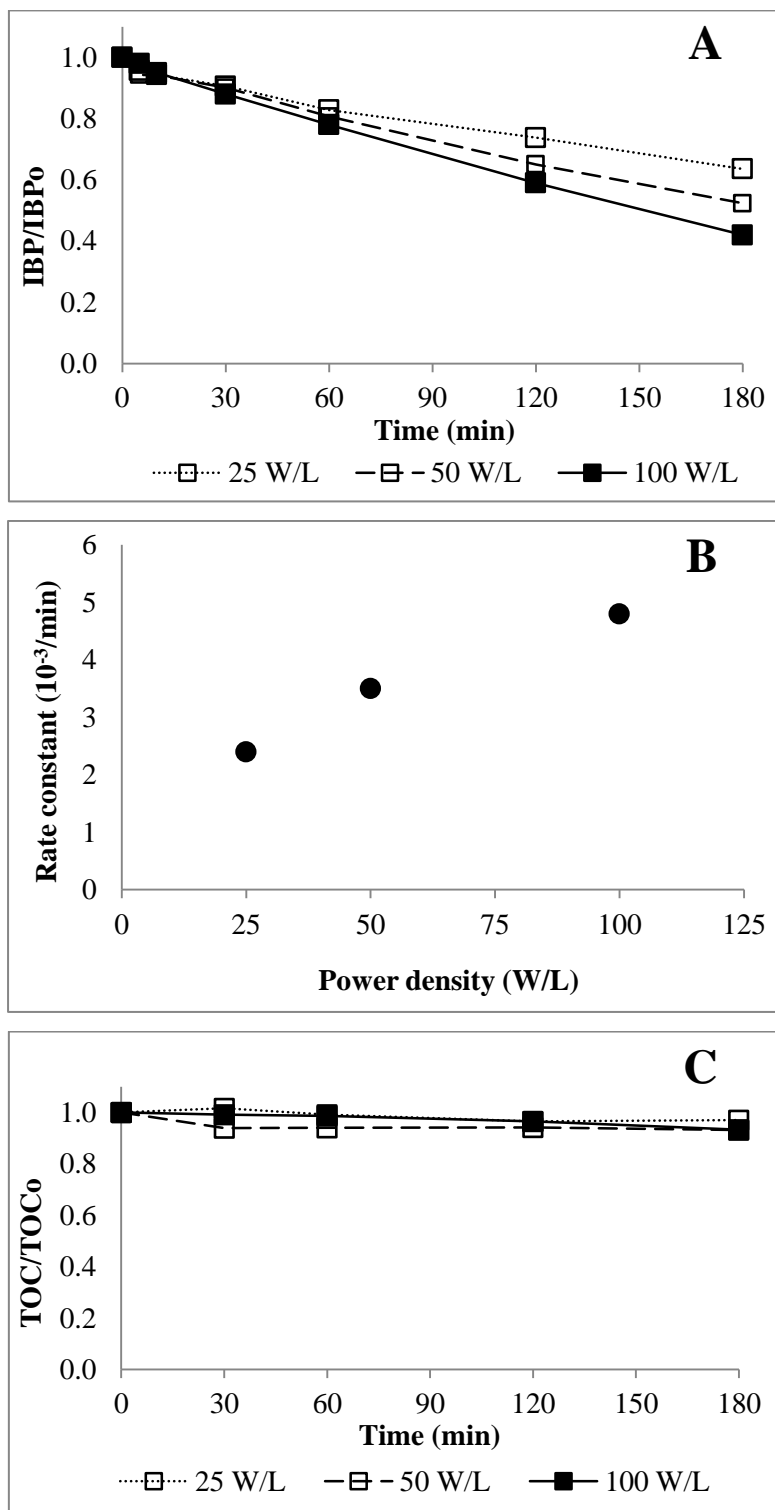


Figure 3.4. Effect of ultrasound density on IBP sonolysis: (A) IBP concentration-time profile, (B) first-order rate constant and (C) TOC concentration-time profile ($[IBP]_0 = 20$ mg/L, $pH_0 = 4.3$, $T = 25^\circ\text{C}$, $f_{US} = 20$ kHz, $D_{US} = 25 - 100$ W/L)

As shown in [figure 3.4A](#), the degradation rate of IBP increased with increasing D_{US} in the investigated range. This could be explained by a higher number of collapsing bubbles that

enhanced the formation of hydroxyl radicals. An optimum value of D_{US} should be expected, due to bubble cloud formation on the emitter surface absorbing or scattering the sound waves above a critical value [250], but due to the limitation of our ultrasonic equipment it could not be attained. Calculated first-order rate constants were as follows: $k_{25W/L} = 0.0024 \text{ min}^{-1}$ ($R^2 = 0.992$), $k_{50W/L} = 0.0035 \text{ min}^{-1}$ ($R^2 = 0.996$), $k_{100W/L} = 0.0048 \text{ min}^{-1}$ ($R^2 = 0.994$), showing however that the positive effect of D_{US} already leveled off (figure 3.4B). Moreover, the enhancement of TOC removal by increasing D_{US} was also negligible (figure 3.4C). Therefore, ultrasound density of 50 W/L was chosen as reference.

3.1.2.4. Effect of sonication frequency

The influence of frequency on sonochemistry is complex. Despite cavitation threshold increases and less energy is released upon collapse at high frequency (>100 kHz), fewer acoustic cycles are required for the bubbles to reach their resonant size [251]. Moreover, more radicals can escape before being recombined due to faster collapse and smaller bubbles [252]. Therefore, high frequency is usually preferred for “pure” sonochemistry applications.

As part of a collaborative work with Instec Cuba, two high US frequencies (580 and 862 kHz) were thus investigated for the sonolysis of IBP (details on the corresponding equipment is also provided in chapter 2). In addition, an audible frequency (12 kHz) was also applied to further evaluate the impact of this parameter in the low value range.

According to figure 3.5A, IBP removal after 180 min was increased from 48% to 87% when increasing f_{US} in the 20 - 862 kHz range. Degradation rates followed a first-order kinetic trend with: $k_{20kHz} = 0.0035 \text{ min}^{-1}$ ($R^2=0.996$), $k_{580kHz} = 0.0084 \text{ min}^{-1}$ ($R^2=0.984$) and $k_{862kHz} = 0.0102 \text{ min}^{-1}$ ($R^2=0.959$) (figure 3.5B). Close values obtained at 580 and 862 kHz could be explained by similar $\bullet\text{OH}$ effective production rate, as reported by Güyer and Ince on an analogous high f_{US} equipment by monitoring H_2O_2 concentration [99]. An optimal frequency for radical-mediated sonolysis was also observed by these authors at 861 kHz as the consequence of abovementioned antagonist effects at high frequency.

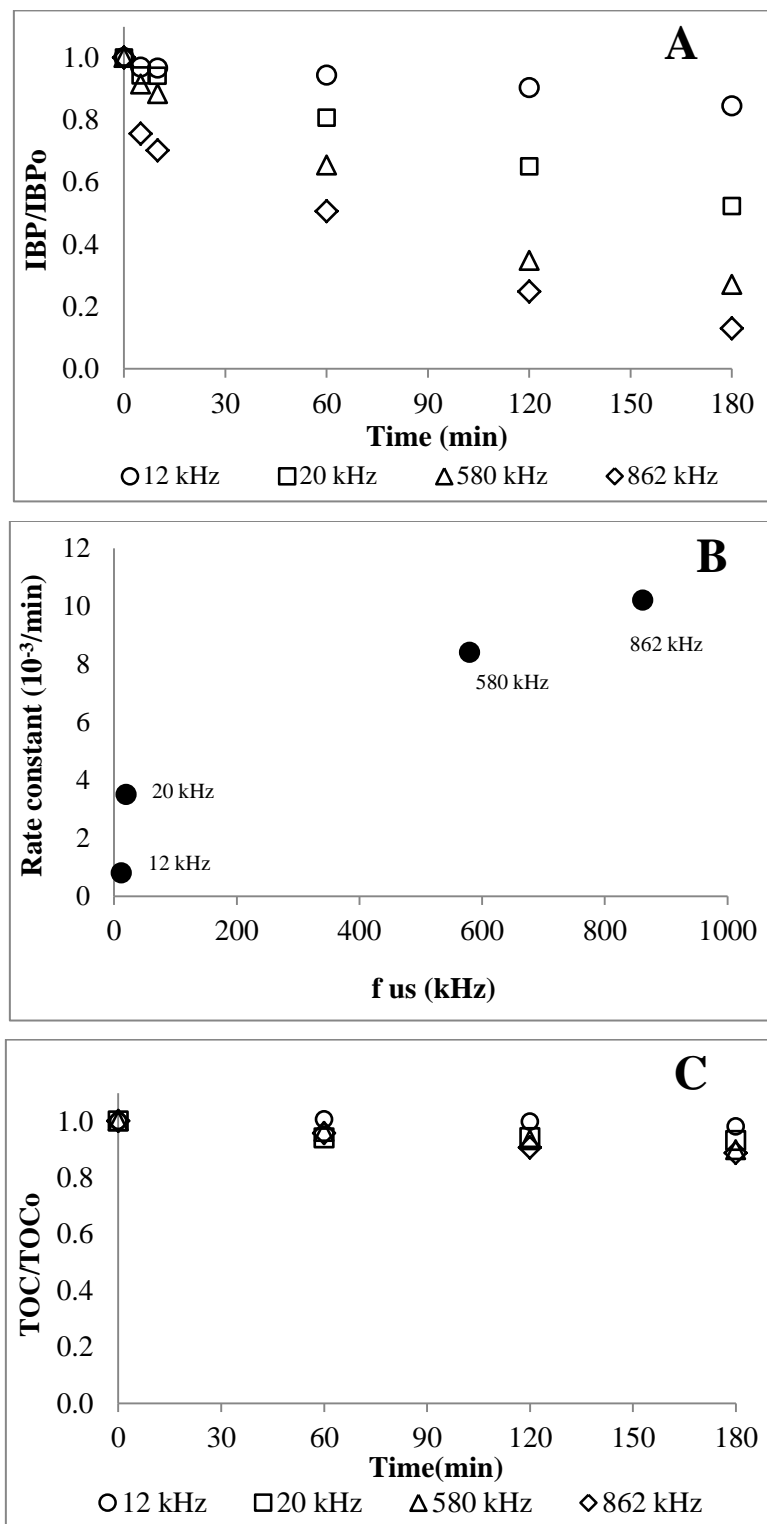


Figure 3.5. Effect of sonication frequency on IBP sonolysis: (A) IBP concentration-time profile, (B) first-order rate constant, (C) TOC concentration-time profile ([IBP]₀ = 20 mg/L, pH₀ = 4.3, T = 25°C, f_{US} = 12-862 kHz, D_{US} = 50 W/L)

Interestingly, audible frequency (12 kHz) was able to only slightly degrade IBP (16% after 3 h, $k_{12\text{kHz}} = 0.0008 \text{ min}^{-1}$). Corresponding H₂O₂ generation rate was 0.18 μM/min vs.

0.41 $\mu\text{M}/\text{min}$ for 20 kHz irradiation, which confirmed the similar evolution of H_2O_2 generation and IBP degradation rates. This significant loss of efficiency from 20 to 12 kHz is in complete contrast with the gain observed in sludge treatment where radical formation is not involved [89,253].

In all cases, total organic carbon (TOC) removal was low: 2%, 7%, 10% and 11% under 12, 20, 580 and 862 kHz irradiation, respectively (figure 3.5C).

3.1.2.5. Effect of H_2O_2 addition on 20 kHz sonolysis

Several previous studies mentioned that addition of H_2O_2 could significantly enhance the efficacy of US-based water treatment process [129,192]. Indeed, even if it had only a negligible effect on IBP degradation in its molecular form (cf. § 3.1.1), it is expected to be decomposed by US and/or to react with $\cdot\text{H}$ generated by water sonolysis (R.3.2) thus generating additional $\cdot\text{OH}$ (R.3.10 and R.3.11) [95,192].



On the other hand, a too large excess of H_2O_2 can be deleterious, as hydroxyl radicals can also react with H_2O_2 to the detriment of organic molecules, generating less active hydroperoxyl radicals [109,174,192] (R.3.12).



This complex interaction usually leads to an optimum value for H_2O_2 dosage. This optimum H_2O_2 /pollutant molar ratio was found to vary in between 19 and 280, depending on solution pH, ultrasound parameters and nature of the pollutant [95,192]. The latter was found to be an important factor, as volatile and hydrophobic compounds are normally not affected by addition of H_2O_2 [95].

In this study, two and seven times the stoichiometric amount of H_2O_2 (calculated according to R.3.1) were added, which corresponded to 6.4 mM and 22.4 mM, respectively (for 0.1 mM of IBP). They matched the doses applied for the Fenton oxidation of the molecule (cf. § 3.1.3), and were thus much higher than that generated by the sole sonolysis

(0.41 $\mu\text{M}/\text{min}$). Alkaline conditions were also investigated, as the sono-degradation of IBP was previously found to be reduced for $\text{pH} > \text{pK}_a$ of the molecule. The corresponding concentration-time profiles of the pollutant are exhibited on [figure 3.6A](#) and [figure 3.6B](#) for the two pH levels (4.3 and 8.0), respectively. The oxidation results under silent conditions are also recalled for comparison purpose.

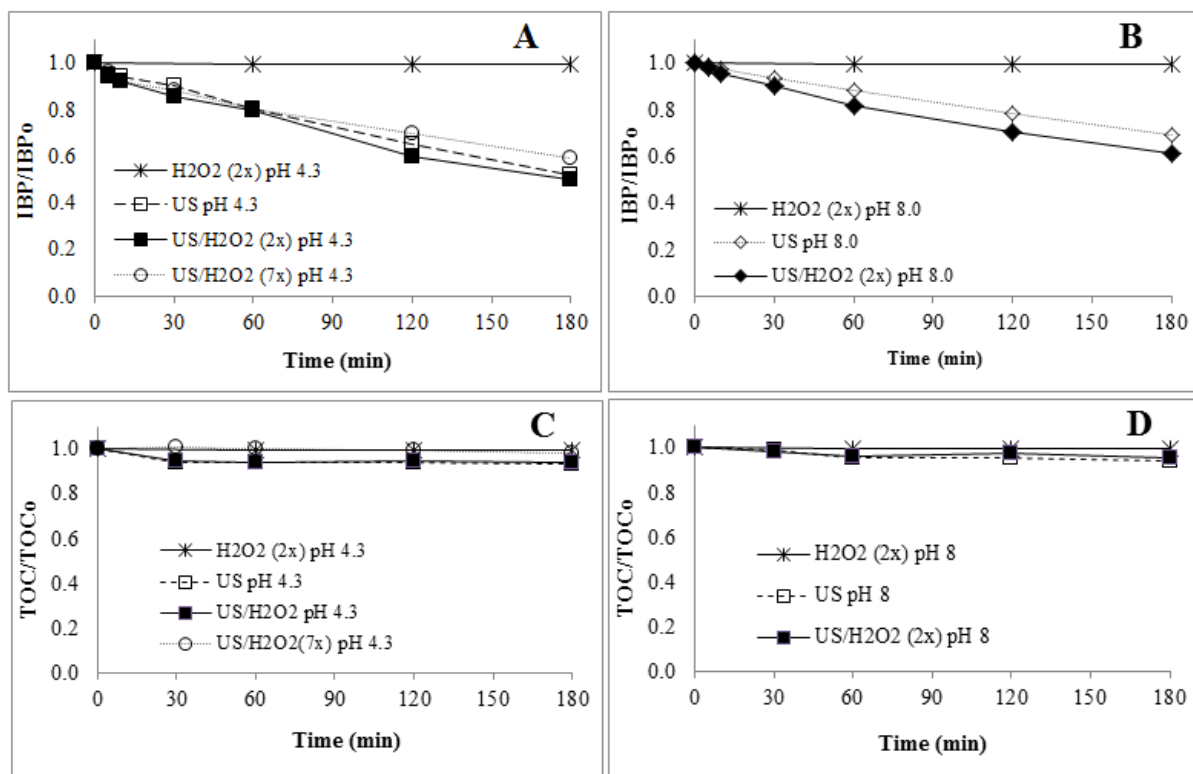


Figure 3.6. Effect of H₂O₂ addition on IBP and TOC removal under sonolysis: IBP removal at $\text{pH}_0 = 4.3$ (A) and 8.0 (B); TOC removal at $\text{pH}_0 = 4.3$ (C) and 8.0 (D) ($[\text{IBP}]_0 = 20 \text{ mg/L}$, $T = 25^\circ\text{C}$, $f_{\text{US}} = 20 \text{ kHz}$ with $D_{\text{US}} = 50 \text{ W/L}$, $[\text{H}_2\text{O}_2]_0 = 0 - 22.4 \text{ mM}$)

First, at natural pH, addition of two times (2x) the stoichiometric amount of H₂O₂ did not modify IBP sono-oxidation rate, while a slight decrease was observed for the highest amount of oxidant. These results are thus in agreement with studies reporting negligible [174] or detrimental effect of H₂O₂ [97] for hydrophobic compounds and low frequency US. The existence of different reaction zones for IBP (bubble surface) and H₂O₂ (bulk solution) could be hypothesized to explain why H₂O₂ did not help the pollutant degradation under US irradiation [97], while its scavenging effect at high concentration (R.3.12) could explain the results observed at 22.4 mM. In the first hypothesis, part of the ultrasound energy should be spent for H₂O₂ decomposition which in turn would be partly wasted into H₂O or O₂ by radical recombination (R.3.4 and R.3.5). However, no decomposition of H₂O₂ was measured at the

lowest concentration, excluding this mechanism. The oxidation of IBP by $\bullet\text{OH}$ (R.3.9) exhibits a rate constant of $6.5 \cdot 10^9$ L/(mol.s) at ambient temperature [229], which is much higher than that reported for the reaction in between H_2O_2 and $\bullet\text{OH}$ (R.3.12): $2.7 \cdot 10^7$ L/(mol.s) [254]. However, at the largest excess of H_2O_2 (22.4 mM vs. 0.1 mM of IBP), the rates of the two reactions become comparable, confirming a possible competition effect.

On the other hand, at alkaline pH, a slight H_2O_2 sonolysis was observed (5% conversion after 3 h) and accelerated the pollutant oxidation at 6.4 mM (figure 3.6B), although not reaching the degradation yield observed at pH 4.3. Note that H_2O_2 is a weak acid with a pKa value of 11.8 [255], therefore it is only marginally decomposed at pH = 8.0 as seen under silent conditions.

Finally, it should be mentioned that TOC conversion was marginally modified by the addition of H_2O_2 (figures 3.6C and 3.6D).

3.1.3. Light irradiation (UV, Vis and UV-Vis)

3.1.3.1. IBP degradation under monochromatic UV light (254 nm) irradiation and its mechanisms

Photolysis experiments were first performed using a 6W low pressure mercury vapor lamp (LP Hg) with main light emission at 254 nm, under the following operating conditions: irradiated volume = 500 mL (only photo-reactor was used here), $\text{pH}_0 = 4.3$ (natural pH), $T = 25^\circ\text{C}$. After 3 hours of irradiation, 69% of IBP was converted (figure 3.7) and a mineralization yield of 12% was achieved. Assuming first-order kinetics with respect to IBP as proposed in literature [42,135,139], the following rate constant was obtained: $k = 0.0063$ min^{-1} ($R^2 = 0.9805$).

According to previous studies, ibuprofen (IBP) degradation by ultraviolet (UV) irradiation can occur through several possible mechanisms:

(i) *direct photo-degradation of the molecule*: IBP is transformed by photon absorption into excited IBP (IBP*), which then undergoes bond scission (R.3.13 – R.3.14) [133,135],

(ii) *photo-sensitization*: IBP* transfers its energy to dissolved oxygen and generates a high energy form of oxygen (called singlet molecular oxygen ($^1\text{O}_2$)) which subsequently attacks IBP (R.3.15 – R.3.16) [133,135], or produces active radicals according to reactions R.3.17 – R.3.20 [137,138],

(iii) *UV-driven homolysis of water* which produces $\bullet\text{OH}$ [44,140,141]. However, considering the emission spectrum of LP Hg lamp, this mechanism should thus be excluded here, as water photolysis occurs only below 200 nm.



UV absorption spectrum of IBP (figure 3.8) exhibits a maximum at 222 nm and a weak peak around 255 – 265 nm which might be sufficient to induce molecule degradation by direct photolysis or through photo-sensitization reactions involving IBP*.

As some of the reported mechanisms involve radical pathways, methanol was added as radical scavenger to evaluate their contribution. Since methanol absorbs light at wavelength lower than 240 nm, its addition should not lower the photon absorption by IBP under 254 nm irradiation, nor quenched the possible contribution of ${}^1\text{O}_2$ [135]. In the presence of 50 mM methanol, IBP degradation yield and rate constant were reduced to 47% (figure 3.7) and 0.0035 min^{-1} , respectively. A plausible explanation for this observation may be related to the possibility that photo-sensitization reactions produced active radicals (R.3.17 – R.3.20) [133,256]. Furthermore, an additional experiment carried out under anoxic condition (solution was bubbled with N_2) showed similar result as the addition of methanol (IBP removal 50%, rate constant 0.0038 min^{-1}) indicating negligible contribution of ${}^1\text{O}_2$.

Therefore, it can be concluded that degradation of IBP under UV light irradiation ($\lambda = 254$ nm, pH = 4.3) is mainly due to direct photolysis (R.3.13 – R.3.14) and to a lesser extent to radical mechanism (R.3.17 – R.3.20).

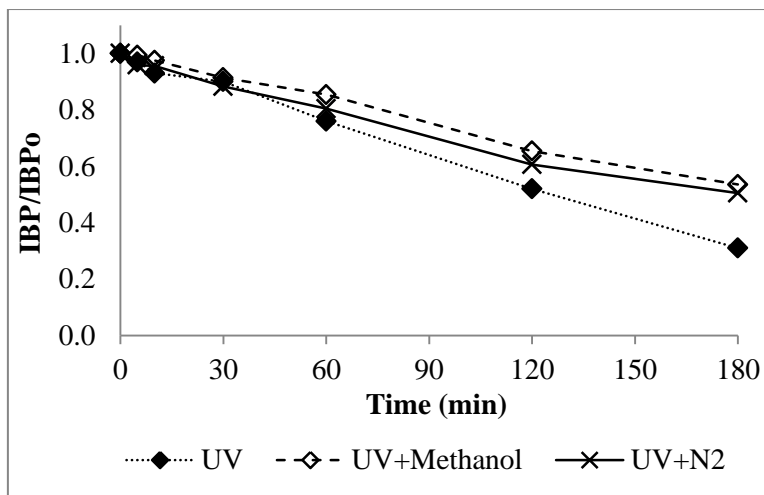


Figure 3.7. IBP photolysis and effect of radical scavenger or oxygen depletion ([IBP]₀ = 20 mg/L, pH₀ = 4.3, T = 25°C, irradiated volume = 500 mL, lamp = 6W LP Hg)

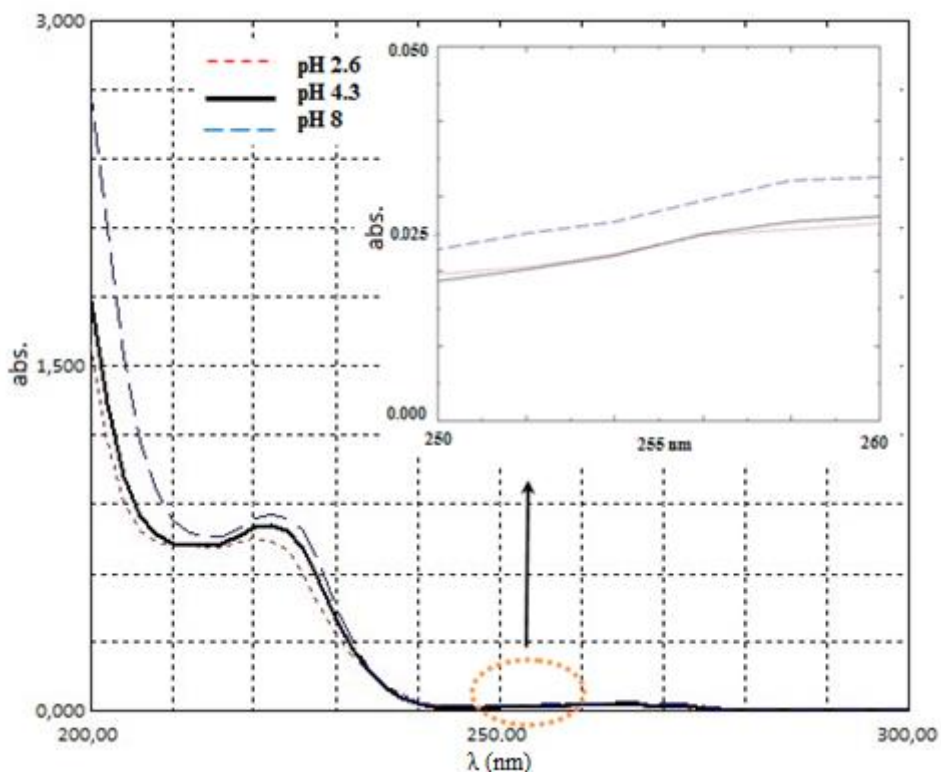


Figure 3.8. Effect of pH on UV absorption spectrum of IBP ([IBP] = 20 mg/L)

3.1.3.2. pH effect

As for sonolysis, the effect of pH on IBP photolysis was investigated using three levels (2.6, 4.3 and 8.0).

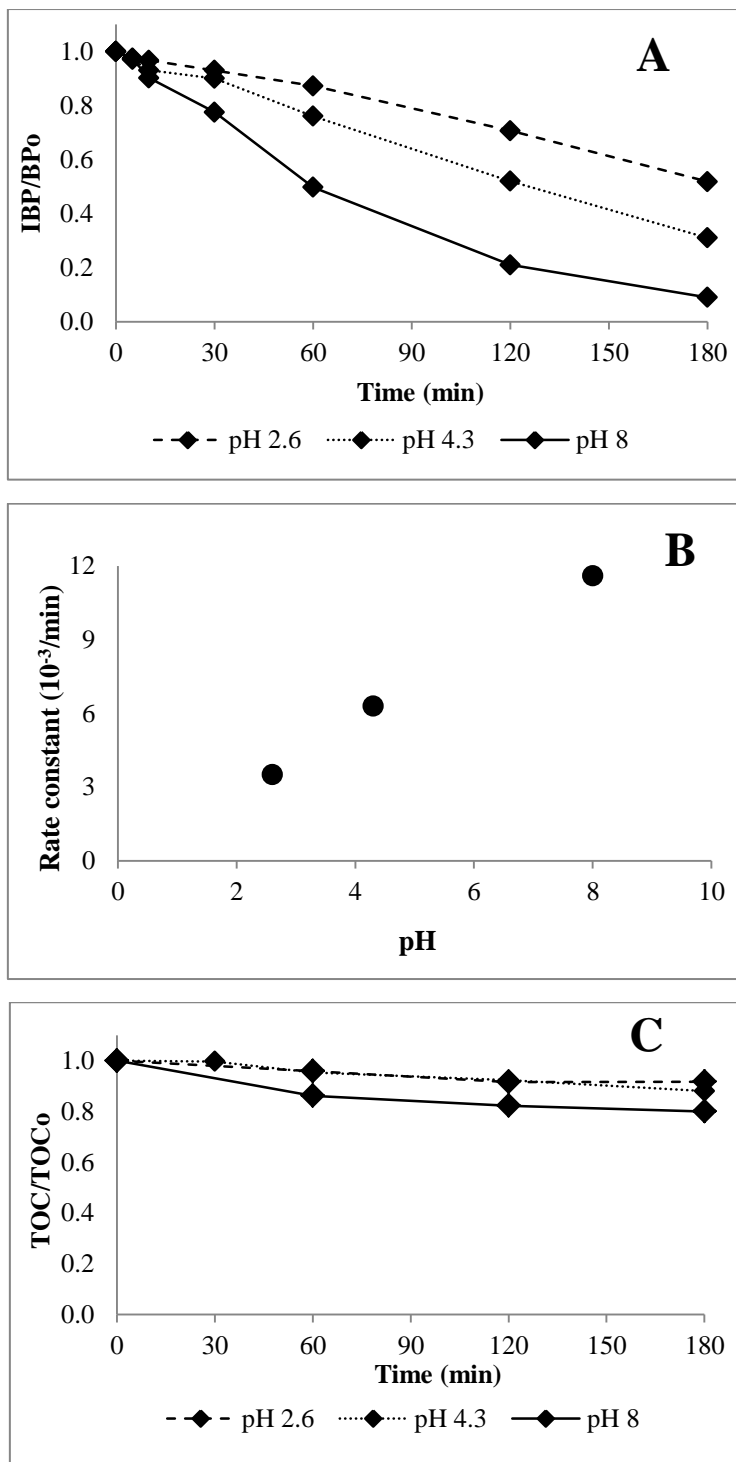


Figure 3.9. Effect of the solution pH on IBP photolysis: (A) IBP concentration-time profile, (B) first-order rate constant, (C) TOC concentration-time profile ([IBP]₀ = 20 mg/L, pH₀ = 2.6 – 8.0, T = 25°C, irradiated volume = 500 mL, lamp = 6W LP Hg)

Figure 3.9A shows that the degradation of IBP was enhanced when increasing the pH of the solution and followed a first-order kinetic trend with: $k_{\text{pH}2.6} = 0.0035 \text{ min}^{-1}$ ($R^2 = 0.9663$), $k_{\text{pH}4.3} = 0.0063 \text{ min}^{-1}$ ($R^2 = 0.9805$) and $k_{\text{pH}8.0} = 0.0116 \text{ min}^{-1}$ ($R^2 = 0.9813$). The plot of these rate constants on figure 3.9B revealed an almost linear increase with respect to pH value. Regarding TOC removal (figure 3.9C), main improvement seemed to occur at the alkaline pH value for which up to 19% mineralization was observed.

At pH 8.0, IBP molecule is mainly in anionic form and it seems to be more photo-active [139]. To evaluate this effect, the absorbance of ibuprofen at the different pH values was measured in the 200-300 nm range: the corresponding spectra indicate that IBP absorbs more light at higher pH (figure 3.8). However, it did not explain the gap between photolysis under pH 2.6 and 4.3.

3.1.3.3. Effect of irradiated volume fraction

As described in chapter 2, two distinct reactors were used to investigate sono- and photo-based processes and the solution was circulated in between the two by means of a peristaltic pump for coupling tests (loop reactor system). Thus for a proper comparison of the corresponding effects, photolysis experiments were also performed for the same configuration of partly irradiated volume (500 mL vs. 1.5 L of total volume) with ultrasound OFF.

As seen in figure 3.10A, this new configuration led to a decrease of final IBP conversion from 69% to 40%, which is expected considering the larger volume to be treated and its partial irradiation. On the other hand, TOC removal was slightly higher in the loop reactor system (figure 3.10B). In this case, less degradation products were formed (lower IBP conversion), that could absorb light and limit photo-sensitization reactions if less photo-active than IBP. Note that higher mineralization in loop reactor system vs. unique photo-reactor has already been reported in literature [133].

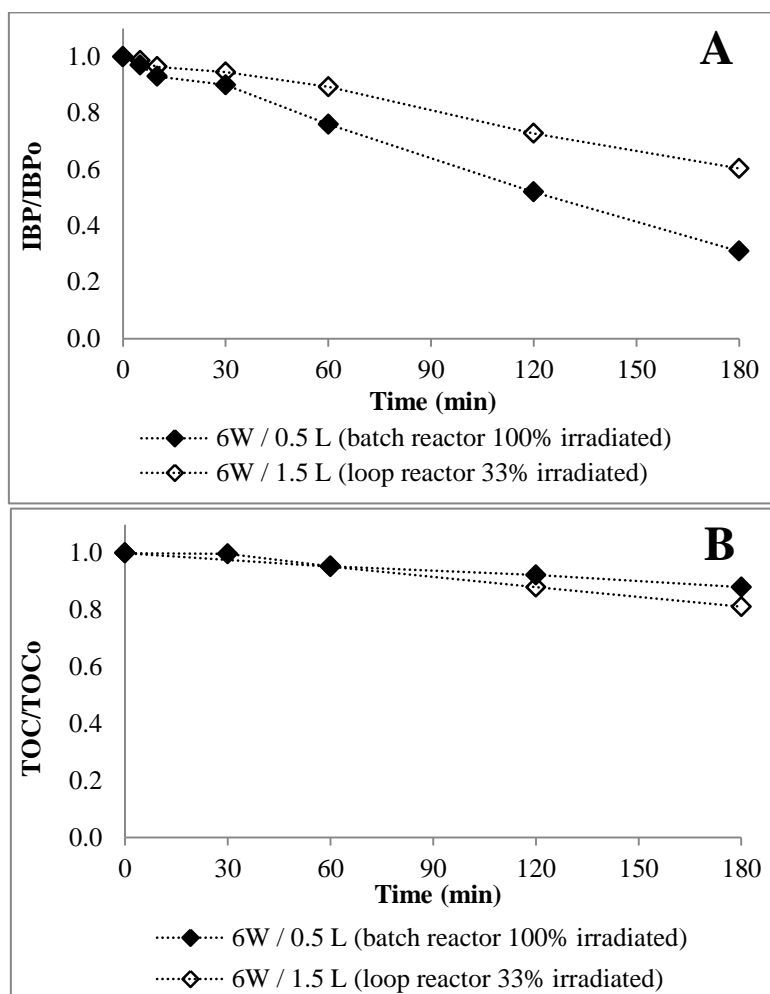


Figure 3.10. Effect of irradiated volume fraction on IBP photolysis: (A) IBP and (B) TOC concentration-time profiles ([IBP]₀ = 20 mg/L, pH₀ = 4.3, T = 25°C, irradiated volume = 500 mL, total volume = 500 and 1500 mL, lamp = 6W LP Hg)

3.1.3.4. Effect of lamp type (irradiation spectrum)

Three different lamps varying from their emission spectrum, namely LP Hg (6W, $\lambda = 254$ nm), Xe (150W, $\lambda = 360 - 740$ nm) and UV-Vis (150W, $\lambda = 200 - 577$ nm), were evaluated for IBP photolysis in the loop reactor configuration.

As expected, IBP was very stable under visible irradiation (Xe lamp) due to a negligible absorption in the visible region (figure 3.11A). This observation also suggests that photo-degradation of IBP by sunlight should be very limited in the natural environment.

On the other hand, fast degradation until complete removal of IBP was observed under UV-Vis irradiation ($k = 0.0567 \text{ min}^{-1}$, $R^2 = 0.9969$). This result is in agreement with Shu and coworkers [18] who found that MP Hg lamp can effectively degrade IBP ($k = 0.097 \text{ min}^{-1}$, $R^2 = 0.998$). The superior performance of MP Hg lamp compared to LP Hg lamp could be

ascribed to both higher power and larger emission band in the UVC region. As abovementioned (§ 3.1.3.1), UVC wavelength (200 – 280 nm) can promote both direct and indirect photo-degradation of IBP. In terms of mineralization efficiency (figure 3.11B), 45% of TOC was removed after 3 h of irradiation with MP Hg lamp vs. 19% for LP Hg. These findings are in agreement with previous studies reporting that degradation products formed during photolysis were less photoactive, resulting in TOC conversion less than 50% [42,44].

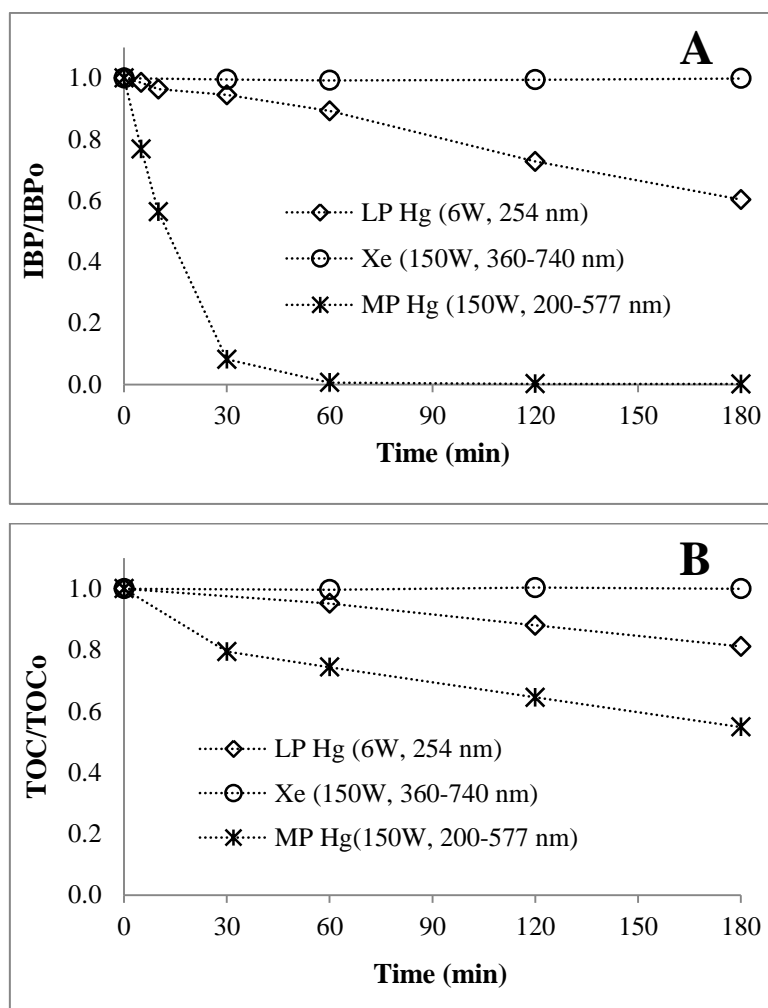


Figure 3.11. Effect of lamp type on IBP photolysis: (A) IBP and (B) TOC concentration-time profiles ([IBP]₀ = 20 mg/L, pH₀ = 4.3, T = 25°C, irradiated volume = 500 mL, total volume = 1500 mL, lamp = 6W LP Hg, 150W Xe, or 150W MP Hg)

3.1.3.5. Effect of H₂O₂ addition

Hydrogen peroxide (H₂O₂) was proven to be an effective promoter in photo-initiated oxidation reactions [37,257]: under UV irradiation, H₂O₂ can be excited and undergo O-O bond scission, producing highly reactive hydroxyl radicals (R.3.19) [60,133].

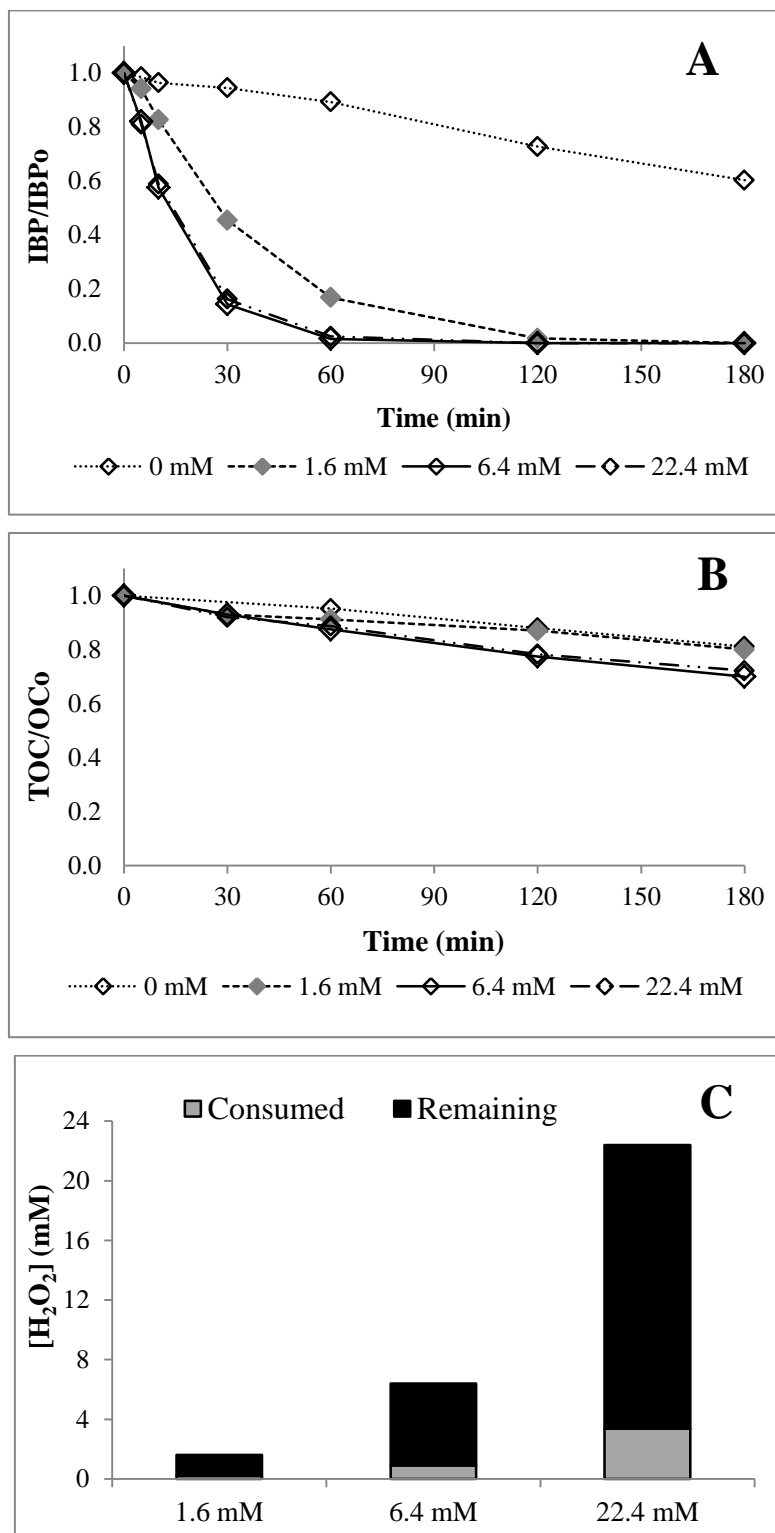


Figure 3.12. Effect of H₂O₂ concentration on photo-oxidation of IBP: (A) IBP and (B) TOC concentration-time profiles, and (C) H₂O₂ consumption ([IBP]₀ = 20 mg/L, pH₀ = 4.3, T = 25°C, irradiated volume = 500 mL, total volume = 1500 mL, lamp = 6W LP Hg, [H₂O₂]₀ = 0 – 22.4 mM)

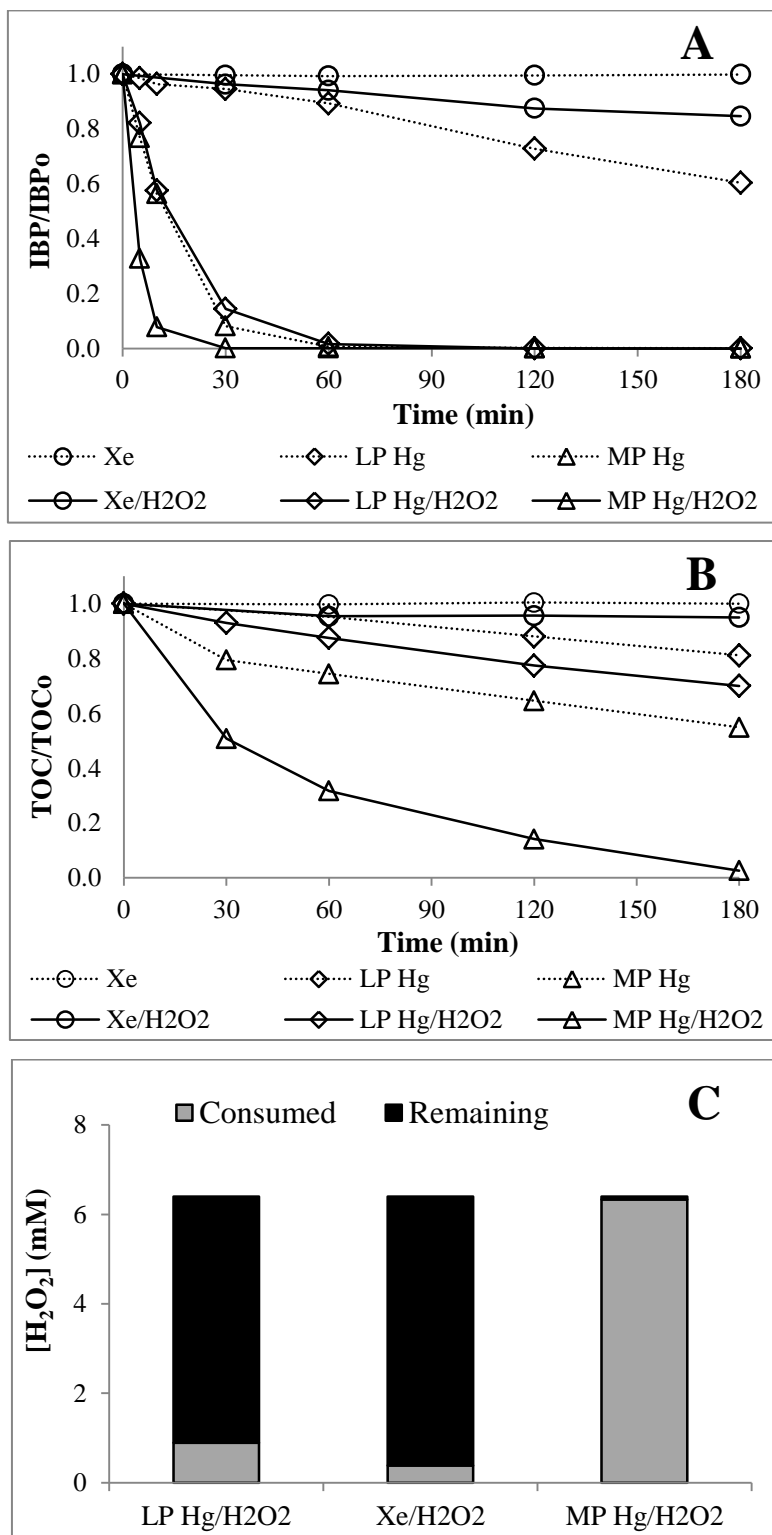


Figure 3.13. Effect of lamp type on photo-oxidation of IBP: (A) IBP and (B) TOC concentration-time profiles, and (C) H₂O₂ consumption ([IBP]₀ = 20 mg/L, pH₀ = 4.3, T = 25°C, irradiated volume = 500 mL, total volume = 1500 mL, lamp = 6W LP Hg (UV), 150W Xe (Vis), or 150W MP Hg (UV-Vis), [H₂O₂]₀ = 6.4 mM). Photolysis results are recalled for comparison purpose

The effect of H₂O₂ addition was first studied with 6W LP Hg lamp (in loop reactor configuration). A set of experiments varying H₂O₂ concentration from 1.6 to 22.4 mM (0.5 to 7 times the stoichiometric amount) was performed, whose results are depicted on [figure 3.12](#). IBP degradation rate increased with increasing H₂O₂ concentration up to 6.4 mM (k varying from 0.0028 min⁻¹ without H₂O₂ to 0.0664 min⁻¹ at 6.4 mM). However, further increase to 22.4 mM did not show additional benefit. As previously seen under ultrasound, the existence of an optimum H₂O₂ concentration could be explained by the scavenging of •OH at high H₂O₂ concentration ([R.3.12](#)).

On the other hand, addition of H₂O₂ only modestly improved TOC conversion with similar optimum dose found at 6.4 mM. Moreover, it was observed that LP Hg lamp was only able to partly convert H₂O₂ ([figure 3.12C](#)). This was not expected considering the overlapping of H₂O₂ adsorption spectrum ($\lambda_{\text{max}} = 200 - 280 \text{ nm}$) with the maximum emission of LP Hg lamp ($\lambda_{\text{max}} = 254 \text{ nm}$). However, comparison with existing literature is rather difficult due to the lack of information in terms of H₂O₂ consumption in other studies. Then, the effect of 6.4 mM H₂O₂ was assessed for the two other lamps (MP Hg and Xe), [figure 3.13](#).

Degradation of IBP under Vis/H₂O₂ was not expected due to the negligible absorbance of IBP and H₂O₂ above 280 and 300 nm, respectively. However, according to the manufacturer of the xenon lamp, if 97% of its emission is in the 400-740 nm range, it also exhibits a small portion (3%) at lower wavelength range. In addition, it should be mentioned that several studies reported that xenon lamp has emission at wavelengths as low as 300 nm [13,20,136,158,164]. This might be responsible for a weak H₂O₂ decomposition ([figure 3.13B](#)), resulting into 15% of IBP conversion after 3 h. Measurement of H₂O₂ absorption spectrum also indicates a small absorbance in UVA region (cf. chapter 2, [figure 2.9](#)).

Conversely, significant enhancement due to H₂O₂ addition was observed with MP Hg lamp, resulting in a 5-fold increase of the rate constant (from 0.0567 to 0.261 min⁻¹). However this improvement was less remarkable than with LP Hg lamp (24-fold increase), because photolysis of IBP was already very effective with MP Hg lamp, and thus H₂O₂ decomposition contributed to a lesser extent to IBP degradation.

On the other hand, the combination of H₂O₂ and MP Hg lamp was more effective for TOC removal as complete mineralization was achieved after 3 h vs. only 30% by LP Hg/H₂O₂. Analysis of H₂O₂ concentration at the end of reaction showed 14%, 5% and 99% consumption for LP Hg, Xe and MP Hg lamp, respectively. Therefore, the remarkable performance of MP Hg/H₂O₂ process in mineralization of IBP could be ascribed to both high

power and wide UV-C spectral emission inducing an effective direct photolysis and photo-decomposition of H₂O₂ reactions.

3.1.4. Fenton oxidation

Classical Fenton oxidation (without activation technique) generally uses relatively high iron concentration (>10 mg/L *i.e.* 0.18 mM) and the few works which investigated ibuprofen removal by homogeneous Fenton reaction used iron concentration as high as 1 mM [38,258]. Conversely, in this study, much lower concentrations, in the 0.033-0.134 mM range (1.8-7.5 mg/L) were investigated, interestingly close to the iron discharge limit (2 mg/L or 0.035 mM).

A H₂O₂ dosage corresponding to either half the stoichiometric amount required for mineralization (see R.3.1) or to a limited excess (2x) was applied to avoid extensive hydroxyl radical scavenging [58,86,120], while the [H₂O₂] / [Fe] molar ratio was always set to 48. Reactions were performed in the same reactor as used for sono-mediated processes (but under silent conditions).

Thereby, three levels of Fenton's reagent concentration were applied: (i) [Fe²⁺]₀ = 0.033 mM and [H₂O₂]₀ = 1.6 mM (referred to as "F(-)"), (ii) [Fe²⁺]₀ = 0.067 mM and [H₂O₂]₀ = 3.2 mM ("F(med)") and (iii) [Fe²⁺]₀ = 0.134 mM and [H₂O₂]₀ = 6.4 mM ("F(+)").

In the presence of Fenton's reagent, a fast oxidation of IBP was observed in the first 5 minutes followed by a much slower degradation (figure 3.14A), which cannot be fitted either with first or second order kinetics. This behavior is consistent with that reported in previous studies [38,63,258,259] where it was explained by radical pathway at acidic pH. A supplementary experiment in the presence of methanol as radical scavenger confirmed that the degradation of ibuprofen in homogeneous-Fenton reaction was indeed due to radical mechanism (figure 3.15).

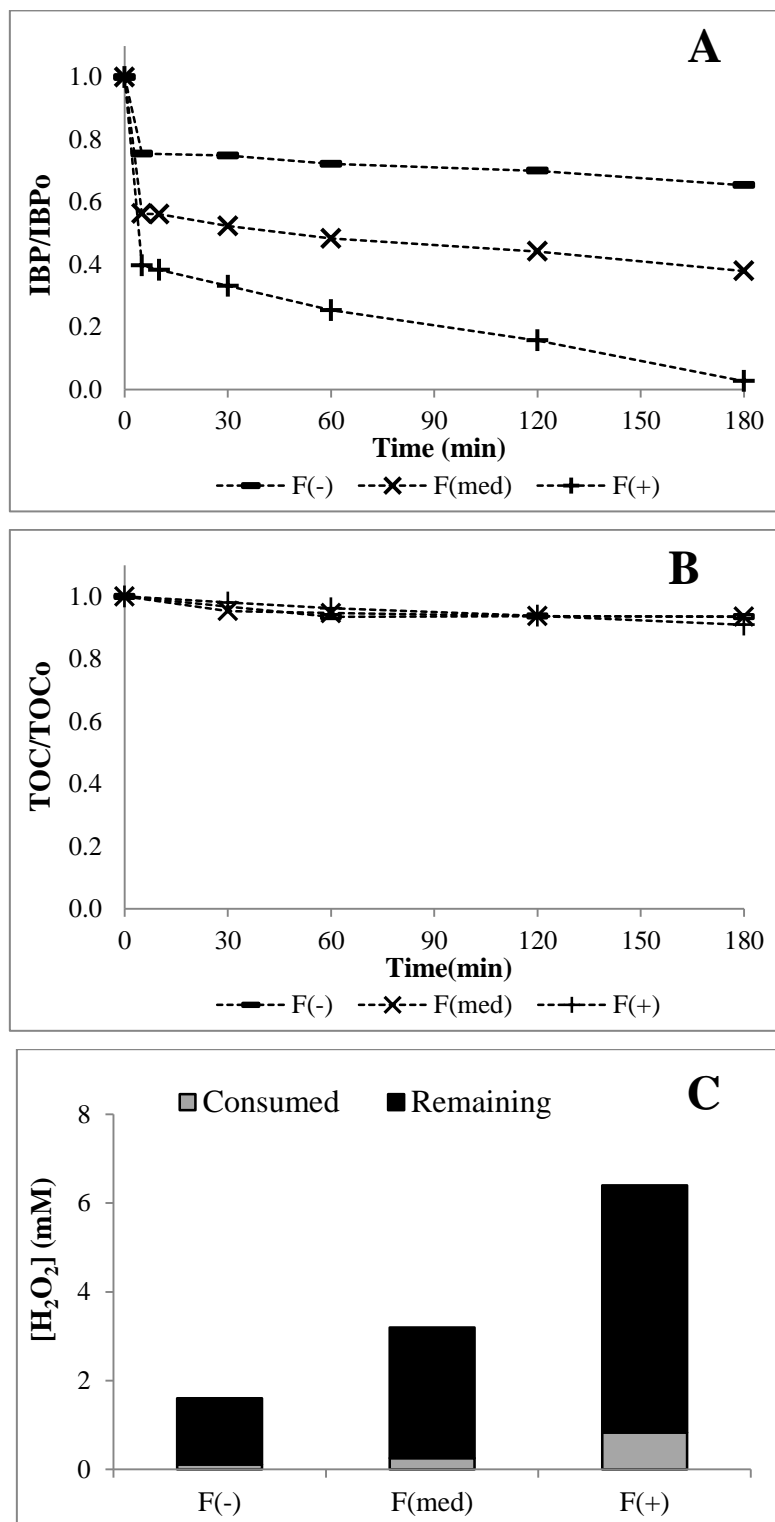


Figure 3.14. Effect of Fenton's reagent concentration on IBP oxidation: (A) IBP and (B) TOC concentration-time profiles, and (C) H₂O₂ consumption ([IBP]₀ = 20 mg/L, pH₀ = 2.6, T = 25°C, F(-): [Fe²⁺]₀ = 0.033 mM and [H₂O₂]₀ = 1.6 mM, F(med): [Fe²⁺]₀ = 0.067 mM and [H₂O₂]₀ = 3.2 mM, F(+): [Fe²⁺]₀ = 0.134 mM and [H₂O₂]₀ = 6.4 mM)

According to this mechanism, the initial reaction stage corresponded to the fast hydroxyl radical generation from reaction between ferrous ions and hydrogen peroxide (R.3.21). Then, formation of stable ferric complexes, such as Fe-OOH²⁺ (R.3.22 and R.3.23), hindered Fe²⁺ regeneration and further radical generation.

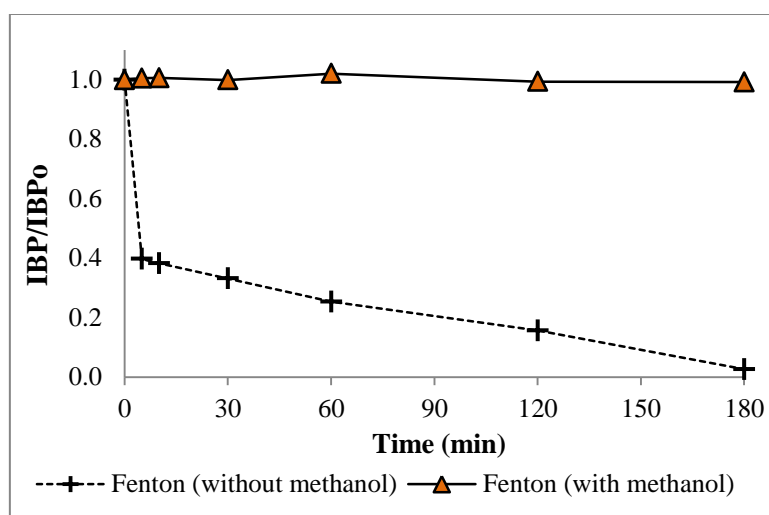
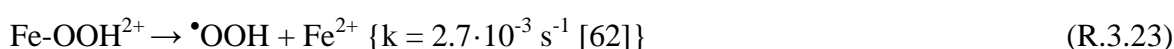
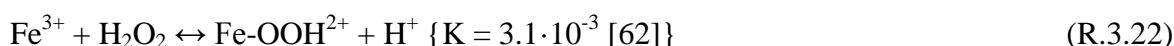
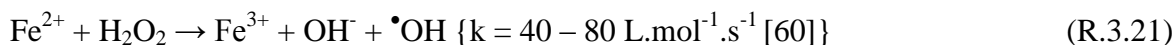


Figure 3.15. Effect of methanol on Fenton oxidation of IBP
 ([IBP]₀ = 20 mg/L, pH₀ = 2.6, T = 25°C, [Fe²⁺]₀ = 0.134 mM, [H₂O₂]₀ = 6.4 mM, [MeOH]₀ = 50 mM)

Furthermore, IBP and/or reaction intermediates could form a complex with Fe³⁺, which renders iron less reactive towards H₂O₂, thus hindering the cycle of Fenton reactions [260,261]. A blank experiment in F(+) conditions indeed showed higher H₂O₂ consumption without IBP (38% vs. 13% with IBP, figure 3.14C), confirming this possible binding effect. This effect is dependent upon IBP/Fe³⁺ ratio and higher ratio promotes stronger binding effect [261]. Therefore, at given [H₂O₂] / [Fe] molar ratio, increasing Fenton's reagent was found beneficial (no scavenging effect from H₂O₂ or Fe²⁺), and F(+) yielded 97% conversion of IBP after 3 hours. However TOC removal remained almost unchanged for all investigated conditions, to less than 10% at the end of reaction (figure 3.14B).

Highlights: *homogeneous single processes*

- ✓ *Partial degradation of ibuprofen was observed after 3 hours of ultrasound and light (ultraviolet and visible) irradiation.*
- ✓ *Degradation mechanism of ibuprofen under ultrasound corresponded to radical attack, mainly at the bubble-solution interface.*
- ✓ *Sono-degradation of ibuprofen was favoured by high power and high frequency.*
- ✓ *Degradation mechanism of ibuprofen under ultraviolet light corresponded mainly to direct photolysis and in a lower extent to radical attack.*
- ✓ *Photo-degradation of ibuprofen was improved in the ultraviolet wavelength range and oxic condition.*
- ✓ *Effect of H₂O₂ as radical promoter was found to be significantly beneficial for ultraviolet irradiation process only.*
- ✓ *Fenton reaction was mainly effective during the first 5 minutes, then hindered by the formation of ferric complexes.*

3.2. IBUPROFEN REMOVAL BY COMBINED PROCESSES

3.2.1. Sonophotolysis and sonophoto-oxidation with H₂O₂

Actually, study on the combination of ultrasound and light irradiation without catalyst or oxidant promoter (called sonophotolysis process) is scarce [262–264]. Moreover sonophotolysis using low frequency ultrasound has not been studied yet. Basically, this combined process is based on the photo-decomposition of hydrogen peroxide produced by ultrasound [263,264], and thus it has the main advantage of being chemical-free.

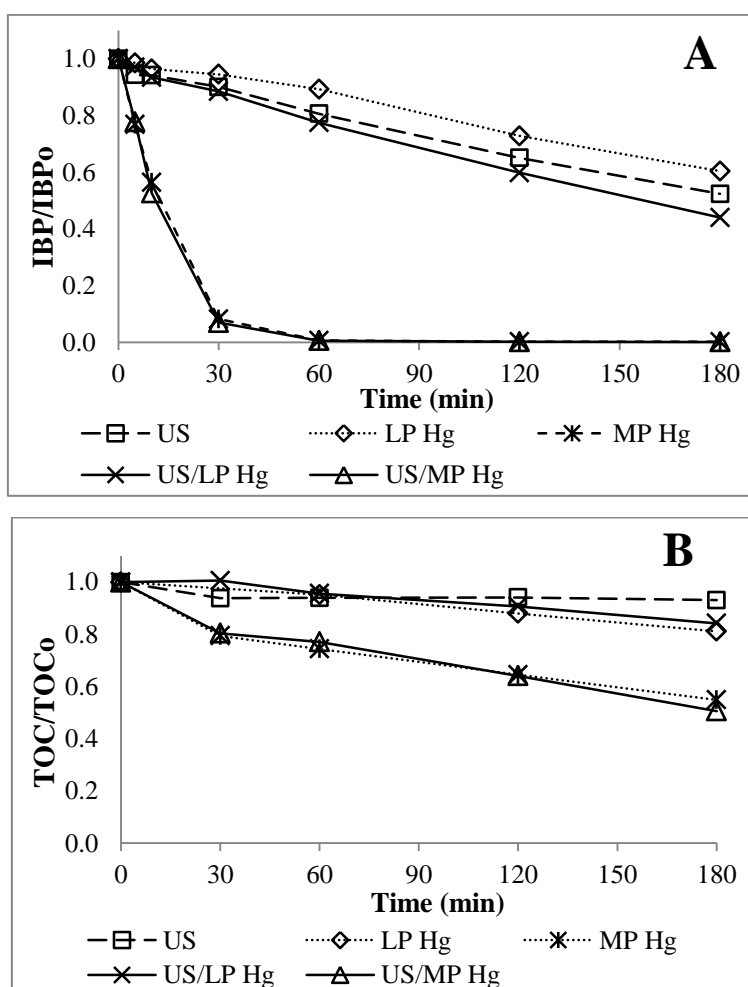


Figure 3.16. Sonophotolysis of IBP: (A) IBP and (B) TOC concentration-time profiles ([IBP]₀ = 20 mg/L, pH₀ = 4.3, T = 25°C, irradiated volume = 500 mL, total volume = 1500 mL, lamp = 6W LP Hg (UV) or 150W MP Hg (UV-Vis), f_{US} = 20 kHz, D_{US} = 50W/L)

In this work, combined US/light irradiation process was evaluated using 20 kHz US, LP Hg and MP Hg lamps. Note that the value of D_{US} (50 W/L) was based here on the whole treated volume (in both sono-reactor and photo-reactor, containing 1 L and 0.5 L,

respectively) or in other words $P_{US} = 75 \text{ W}$ was applied in this configuration. It was checked that sonolysis of IBP remained identical as that performed at same D_{US} in the sono-reactor only (cf. § 3.1.2).

In fact, [figure 3.16A](#) reveals no significant beneficial interaction between the processes with both the lamps. Indeed, IBP removal rate constant for US/ LP Hg was 0.0045 min^{-1} ($R^2 = 0.9971$), which is lower than the sum of those corresponding to the separate processes: $k = 0.0035 \text{ min}^{-1}$ for single US and $k = 0.0028 \text{ min}^{-1}$ for 254 nm photolysis. It should be noted that, since US and UV were applied in separate reactors, light scattering effect by cavitation bubbles was not possible. Competition in between IBP and reaction intermediates might be then suspected, either for photons (« inner filter effect ») or radicals formed by both the processes, limiting a possible additive effect.

Interestingly, even though US was slightly more effective than LP Hg lamp in IBP removal (48% vs. 40%), US process was found less effective for TOC removal (7% vs. 19%, [figure 3.16B](#)). This could be explained by the formation of degradation products being less hydrophobic than IBP, but still exhibiting similar absorption properties, such as 1-hydroxyibuprofen and 2-hydroxyibuprofen ($\log K_{ow} = 2.25$ [246], $\lambda_{max} = 222 \text{ nm}$). These oxidation intermediates would be less sensitive to radicals formed by US, mainly located at the bubble interface, while they could be decomposed by light through direct photolysis or radical attack in the bulk.

With MP Hg lamp, a simple additive effect was observed in the combined process: $k = 0.0647 \text{ min}^{-1}$ ($R^2 = 0.9872$) vs. $k = 0.0567 \text{ min}^{-1}$ without US. In this case, competition effect was not observed because MP Hg lamp was very effective for both IBP and TOC degradation ([figure 3.16A](#)).

Thus synergistic effect was not observed under any circumstances for 20 kHz sonophotolysis that should be mainly due to the too low sono-generation of H_2O_2 at this low frequency ($0.41 \text{ }\mu\text{M}/\text{min}$). Nonetheless, ultrasonic frequency should not be the only explaining factor, since a previous study about US/UV process using $f_{US} = 800 \text{ kHz}$ only reported an additive effect [264]. Conversely, it could depend upon model pollutant or reactor configuration.

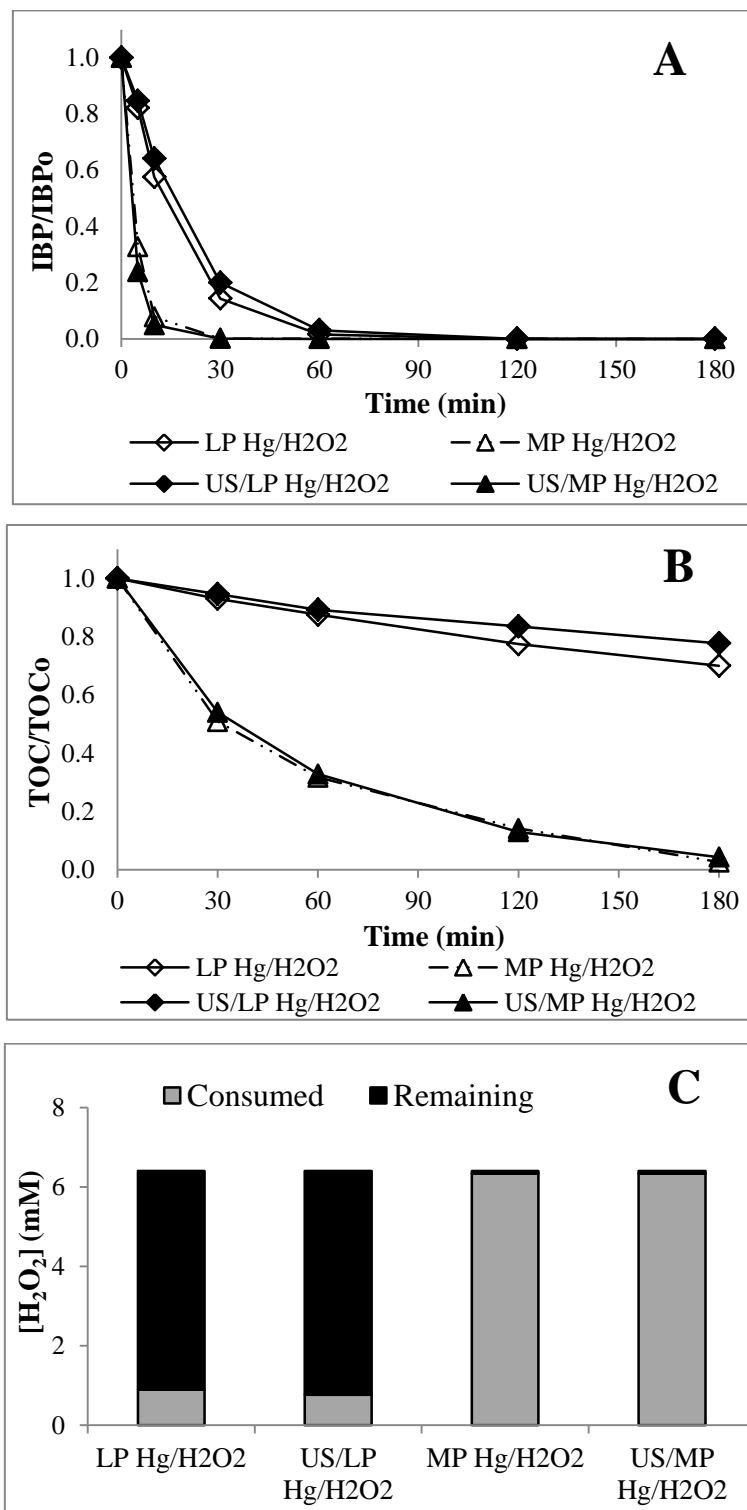


Figure 3.17. Sonophoto-oxidation of IBP: (A) IBP and (B) TOC concentration-time profiles, and (C) H₂O₂ consumption.

([IBP]₀ = 20 mg/L, pH₀ = 4.3, T = 25°C, irradiated volume = 500 mL, total volume = 1500 mL, lamp = 6W LP Hg (UV) or 150W MP Hg (UV-Vis), f_{US} = 20 kHz, D_{US} = 50W/L, [H₂O₂]₀ = 6.4 mM). Photo-oxidation results are recalled for comparison purpose

The effect of 6.4 mM H₂O₂ dosage on US/UV(-Vis) combined process was also evaluated, and the results compared to those of the corresponding photo-oxidation (figure 3.17). Following the trend observed for the photo-mediated process, H₂O₂ addition enhanced the removal rate of both IBP and TOC (cf. figure 3.13). For both the lamps, photolysis of H₂O₂ producing hydroxyl radicals was clearly the dominating process and the role of ultrasound appeared to be insignificant.

3.2.2. Sono-Fenton oxidation

In order to evaluate sonication as an activation technique for Fenton oxidation, some of the oxidation tests described in section 3.1.4 were repeated under ultrasound irradiation, starting with the reference frequency of 20 kHz and a power density of 50 W/L. The effects of several parameters were successively investigated: concentration of Fenton's reagent, ultrasound density and sonication frequency.

3.2.2.1. Effect of Fenton's reagent concentration on sonolysis (20 kHz)

For this study, low and high concentration levels of Fenton's reagent were applied, corresponding to half the stoichiometric amount of H₂O₂ (1.6 mM) and twofold excess (6.4 mM), respectively, keeping [H₂O₂] / [Fe] = 48.

As depicted in figure 3.18, 20 kHz irradiation clearly improved the performance of Fenton oxidation. For instance, at low reagent concentration, IBP conversion increased from 35% to 89% after 3 hours (figure 3.18A). However, accounting for 48% of IBP removal by US alone, the interaction between US and Fenton oxidation seemed to be additive rather than synergistic. Likewise, similar additive effect was also observed in TOC removal, as mineralization yields in US, Fenton and US/Fenton at low reagent concentration were 7%, 6% and 12% respectively (figure 3.18B). In other words, Fenton oxidation was found mainly efficient during the first 5 minutes, after which sonolysis prevailed without significantly activating the catalytic process (nor the decomposition of H₂O₂ as shown previously).

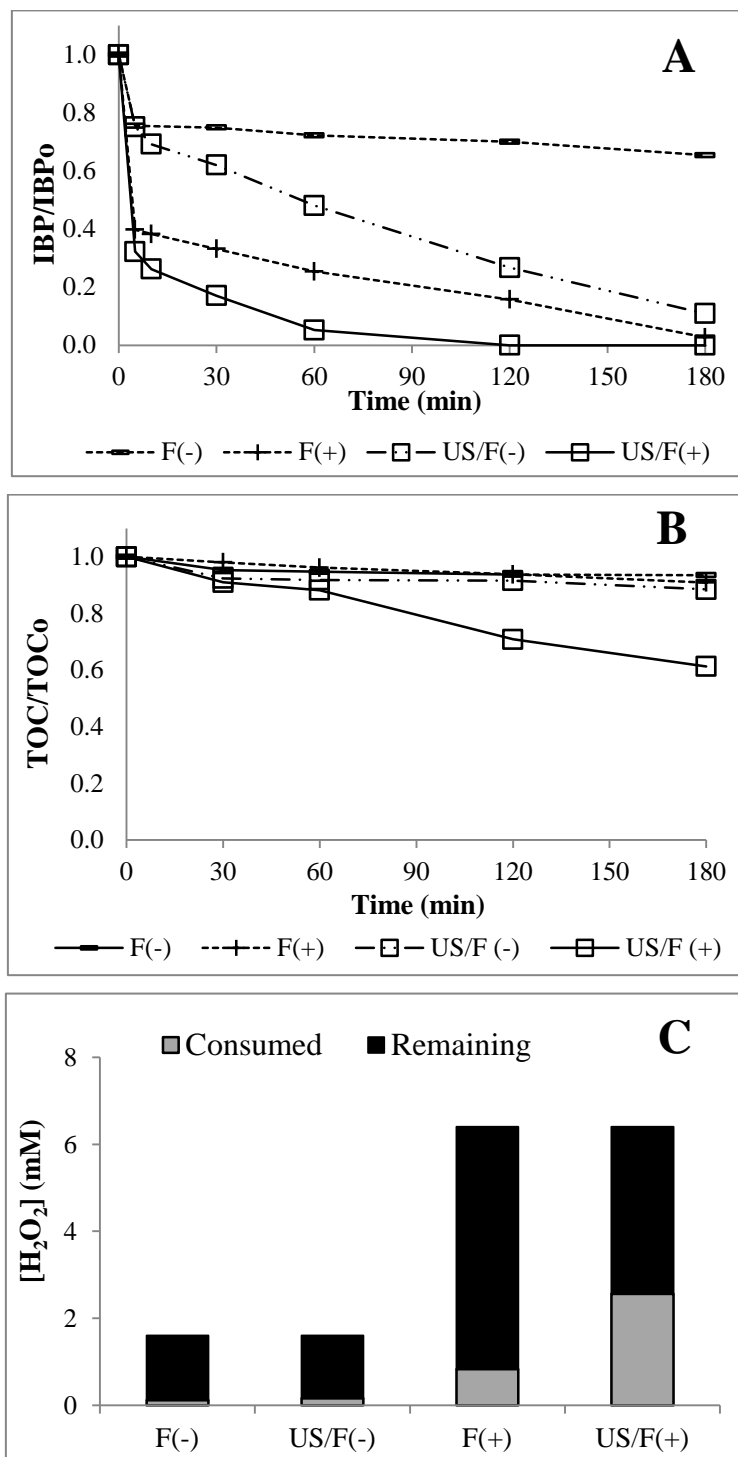


Figure 3.18. Fenton (F) and sono-Fenton oxidation (US/F) of IBP: (A) IBP and (B) TOC concentration-time profiles, and (C) H₂O₂ consumption ([IBP]₀ = 20 mg/L, pH₀ = 2.6, T = 25°C, f_{US} = 20 kHz, D_{US} = 50W/L, F(-): [Fe²⁺]₀ = 0.033 mM and [H₂O₂]₀ = 1.6 mM, (+): [Fe²⁺]₀ = 0.134 mM and [H₂O₂]₀ = 6.4 mM)

On the contrary, synergistic interaction was observed at high reagent concentration, especially in terms of mineralization yield. With high concentration of reagent, sono-Fenton oxidation achieved 40% TOC removal within 180 min, vs. 10% or less for each of the

separate process. In addition, in this condition, H₂O₂ consumption at the end of Fenton and sono-Fenton oxidation tests were 13% and 44%, respectively. Higher amount of residual oxidant confirmed a lower overall activity of the Fenton catalytic system under silent conditions.

Beyond additional radicals generated from water sonolysis (R.3.2), synergistic effect observed in the combined process could be ascribed to the sono-regeneration of ferrous ions, as illustrated by equation R.3.24 [114]. Furthermore, the existence of a minimum Fenton's reagent concentration for synergistic interaction between Fenton oxidation and US is also suggested, that could be due to formation of variety of ferric complexes (for instance, with IBP itself or oxidation intermediates), which are more or less sensitive to sonication.



In order to confirm the activation effect at high reagent concentration, a complementary experiment was conducted. Same amounts of H₂O₂ and ferrous salt as in F(+) experiment were mixed into 100 mL of acidic distilled water (pH 2.6) during 60 min to pre-form the expected Fe-OOH²⁺ complex. Fenton oxidation was then started by addition of this solution into 900 mL of IBP solution. The system was let under stirring for 180 min (silent Fenton oxidation), then sonication was applied for another 180 min period (sono-Fenton oxidation).

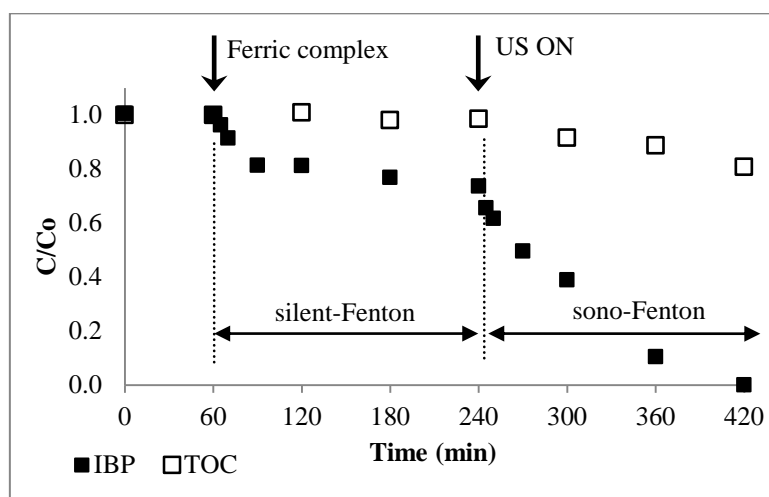


Figure 3.19. Effect of sonication on Fenton catalyst regeneration
 ([IBP]₀ = 20 mg/L, pH₀ = 2.6, T = 25°C, f_{US} = 20 kHz, D_{US} = 50W/L, [H₂O₂]₀ = 6.4 mM, [Fe²⁺]₀ = 0.134 mM)

In this case, only 4% of IBP was converted within 5 min (figure 3.19) vs. 60% for the standard Fenton oxidation procedure (figure 3.14A). The concentration-time profile of the pollutant also exhibited two different stages, with an IBP removal yield almost plateauing at 20-25% after 90 min. Ultrasound application at $t = 240$ min immediately accelerated IBP oxidation, the first-order rate constant ($k = 0.0102 \text{ min}^{-1}$, $R^2 = 0.978$) being three times higher than for the sole sonolysis (cf. § 3.1.2.1, $k = 0.0035 \text{ min}^{-1}$).

3.2.2.2. Effect of ultrasound density

As abovementioned, high ultrasound density (D_{US}) promotes higher formation of hydroxyl radicals and thus improves degradation rate and efficiency of sonolysis process. Nonetheless, the effect of D_{US} on sono-Fenton oxidation process has been scarcely investigated.

Siddique et al. [81] reported that degradation of dye by homogeneous sono-Fenton oxidation increased from 60% to 75% with increasing ultrasonic intensity from 4 W/cm^2 (40 W/L) to 8 W/cm^2 (80 W/L). In our study, the effect of ultrasound density on sono-Fenton oxidation process was evaluated at 25 W/L, 50 W/L and 100 W/L (figure 3.20). Concentration-time profiles of IBP were found similar on the whole D_{US} range, with even a slight decrease of initial degradation rate at 100 W/L. Similarly, varying D_{US} from 25 to 50 W/L improved TOC removal from 29% to 39%, but further increase to 100 W/L also did not show additional benefit. These observations suggest the existence of optimum D_{US} for sono-Fenton process. This trend might be due to a balance in between sono-reduction (R.3.24) and sono-oxidation (due to $\bullet\text{OH}$) mechanisms affecting the iron cycle.

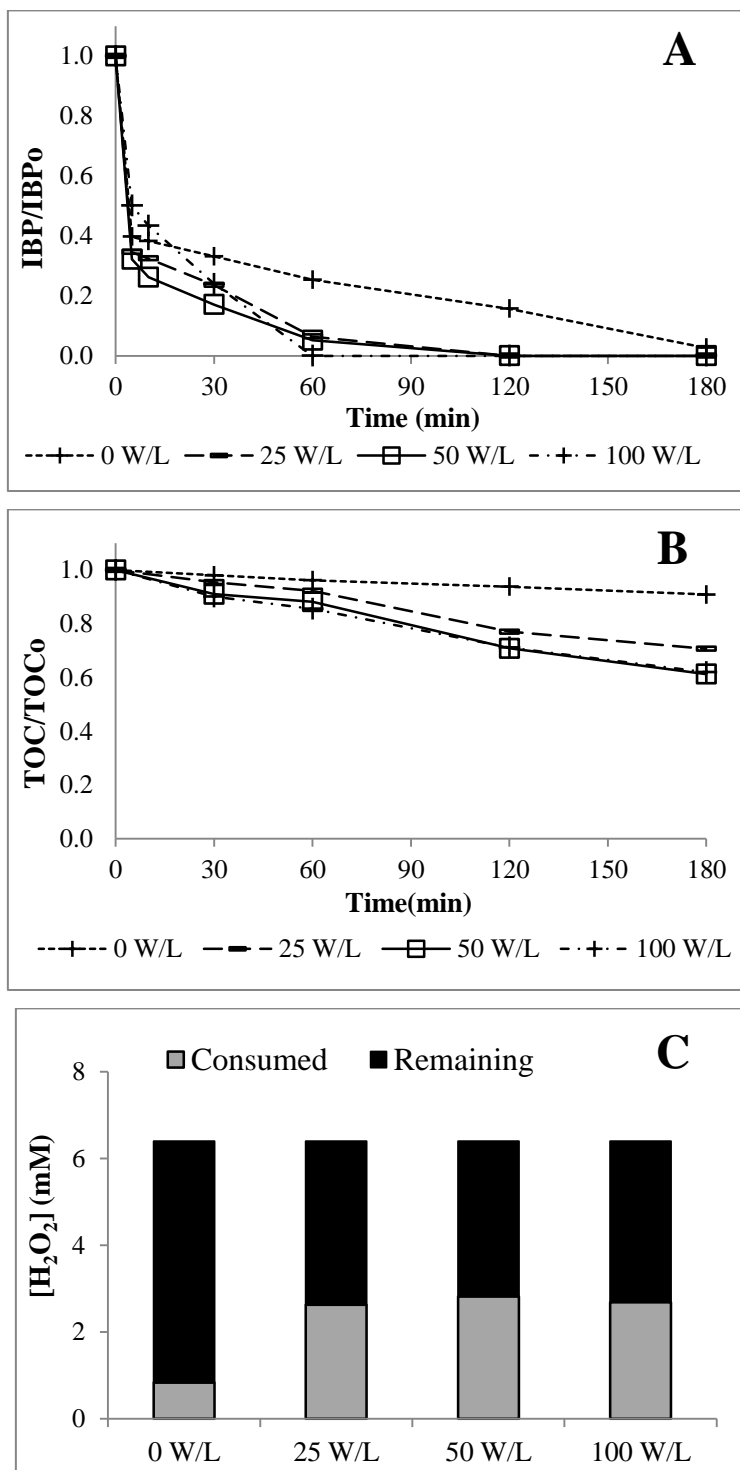


Figure 3.20. Effect of D_{US} on sono-Fenton oxidation of IBP: (A) IBP and (B) TOC concentration-time profiles

($[IBP]_0 = 20$ mg/L, $pH_0 = 2.6$, $T = 25^\circ C$, $f_{US} = 20$ kHz, $D_{US} = 25-100$ W/L, $[H_2O_2]_0 = 6.4$ mM, $[Fe^{2+}]_0 = 0.134$ mM). Fenton oxidation result is recalled for comparison purpose

3.2.2.3. Effect of sonication frequency

Despite growing interest for sono-Fenton process in the literature, information about optimum US frequency is still limited, because previous studies usually operated at a single value (in the 20-40 kHz range) [60,243,265].

Sonochemical effects being suspected in the enhanced ferrous iron regeneration, two high US frequencies (580 and 862 kHz) were investigated. Audible frequency (12 kHz) was also applied since this frequency was never used in sono-Fenton process. As previously, concentration of the Fenton's reagent was set at "high" level. Note that H₂O₂ consumption under high frequencies was not available due to limited equipment at Instec Cuba.

Figure 3.21 revealed that degradation rate of both IBP and TOC, as well as H₂O₂ consumption, increased with increasing sonication frequency, but the differences were mostly marked between 12 and 20 kHz as observed already for sonolysis (cf. § 3.1.2.4). Best TOC abatement was about 50%, which lay within the values reported by previous studies on Fe catalyzed sonodegradation (10% abatement) [43] and sono-Fenton oxidation (55%) [33] of IBP under high frequency US (213-300 kHz).

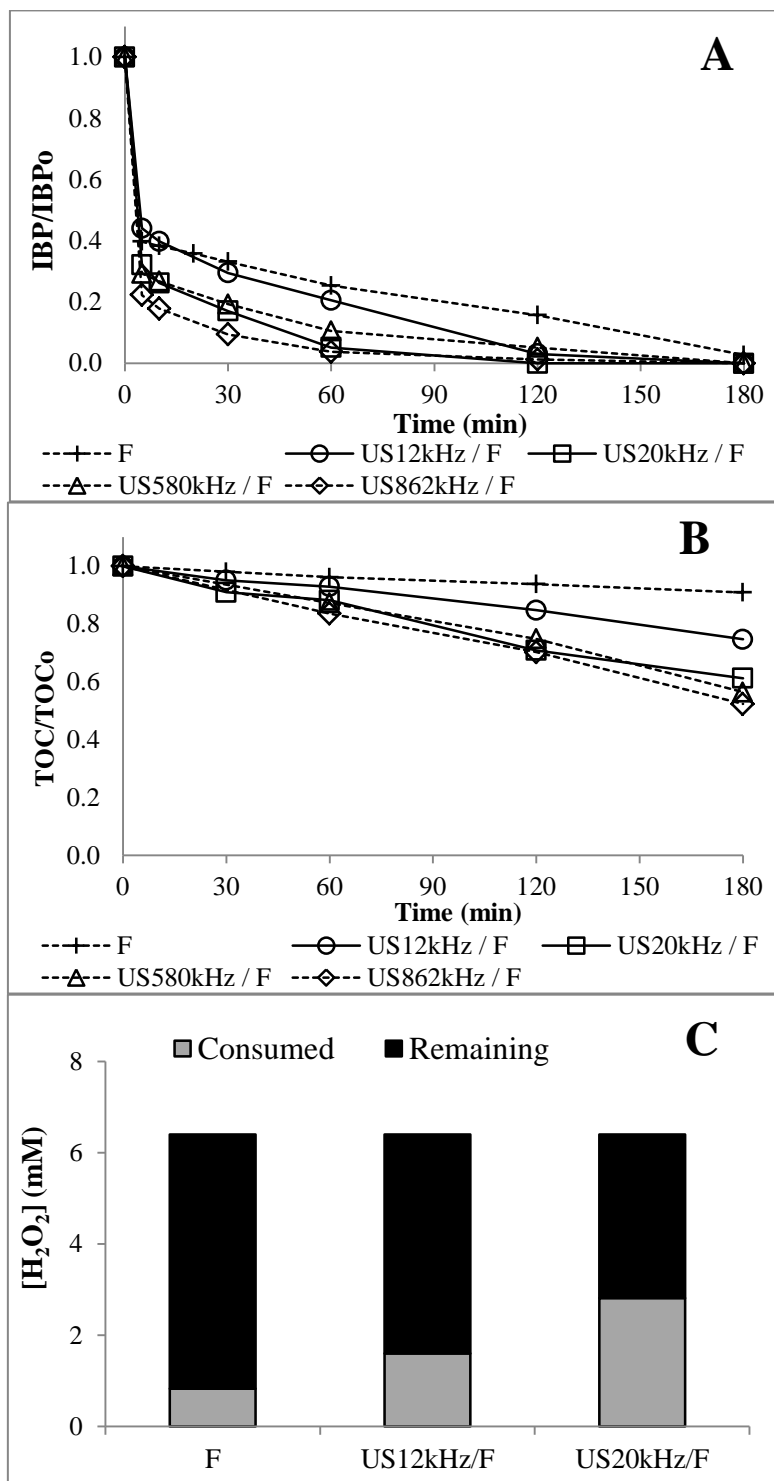
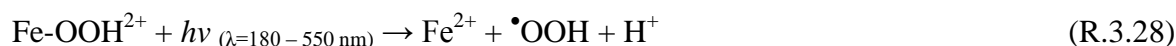
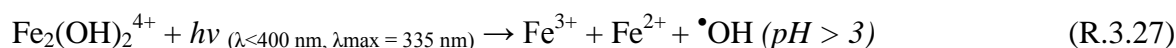
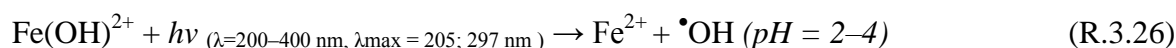
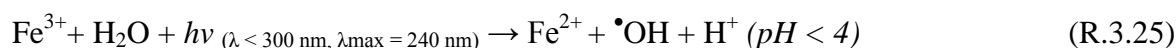


Figure 3.21. Effect of sonication frequency on sono-Fenton oxidation of IBP: (A) IBP and (B) TOC concentration-time profiles, and (C) H₂O₂ consumption ([IBP]₀ = 20 mg/L, pH₀ = 2.6, T = 25°C, f_{US} = 12-862 kHz, D_{US} = 50W/L, [H₂O₂]₀ = 6.4 mM, [Fe²⁺]₀ = 0.134 mM). Fenton oxidation result is recalled for comparison purpose

3.2.3. Photo-Fenton oxidation

Photo-activation of Fenton process has been more largely investigated than sono-activation for the abatement of pharmaceutical compounds [60,67]. Several processes were reported to contribute to the remarkable performance of photo-Fenton oxidation:

- (i) *photolysis* of the organic pollutant and/or its oxidation intermediates, but mainly in the UVC range (see § 3.1.3),
- (ii) *photo-decomposition of H₂O₂* producing $\bullet\text{OH}$ in the 185-300 nm range (R.3.19),
- (iii) *photo-regeneration of ferrous iron catalyst* providing also additional (hydroxyl) radicals, according to the following equations (R.3.25 – R.3.28) [63,144–148]:



- (iv) *photo-decarboxylation of the ferric carboxylates* formed by complexation of ferric ions with organic ligands (R.3.29) [149–152]



Note that in the last two mechanisms, UVA and even visible irradiation can be beneficial. In this study, the effect of two parameters was investigated: concentration of Fenton's reagent, and emission spectrum of the lamp, including the xenon lamp which irradiates mainly in the visible range (97%). As previously seen in § 3.1.3.4 and § 3.1.3.5, IBP photolysis and photo-decomposition of H₂O₂ were confirmed to be marginal with Xe lamp.

3.2.3.1. Effect of lamp type on photo-Fenton oxidation

For the comparison between visible light (xenon lamp) and reference lamp (LP Hg lamp), photo-Fenton oxidation experiments were performed with high concentration of Fenton's reagent (0.134 mM of Fe and 6.4 mM of H₂O₂) in order to gain appreciable mineralization yield. The corresponding results are depicted in [figure 3.22](#), where they are compared to those of Fenton and UV/H₂O₂ oxidation (performed with LP Hg lamp).

First, it can be concluded that photo-Fenton oxidation at 254 nm yielded much higher IBP and TOC oxidation rates than the previous processes, and the expected synergistic interaction was clearly visible.

What is more, the xenon lamp was also found very efficient for photo-Fenton process, albeit not outperforming LP Hg lamp. With these two lamps, H₂O₂ consumption was 80% (Xe lamp) and 99% (LP Hg lamp), as compared to 13% only in Fenton oxidation ([figure 3.22C](#)).

Accounting for the much lower nominal power of the LP Hg lamp (6 W vs 150 W), its remarkable effect - especially on mineralization rate - could be attributed to additional •OH formed by H₂O₂ photolysis ([R.3.19](#)), but also to higher photo-reduction yields of ferric ions and/or iron(III) complexes ([R.3.25](#) - [R.3.28](#)), favored rather under UVC than UVA [145] or visible irradiation [183]. It is also worth mentioning that TOC removal by Xe/Fenton (59%) and LP Hg/Fenton (82%) was comparable to that obtained by previous studies on photo-Fenton oxidation of IBP (40-96% mineralization) [24,266].

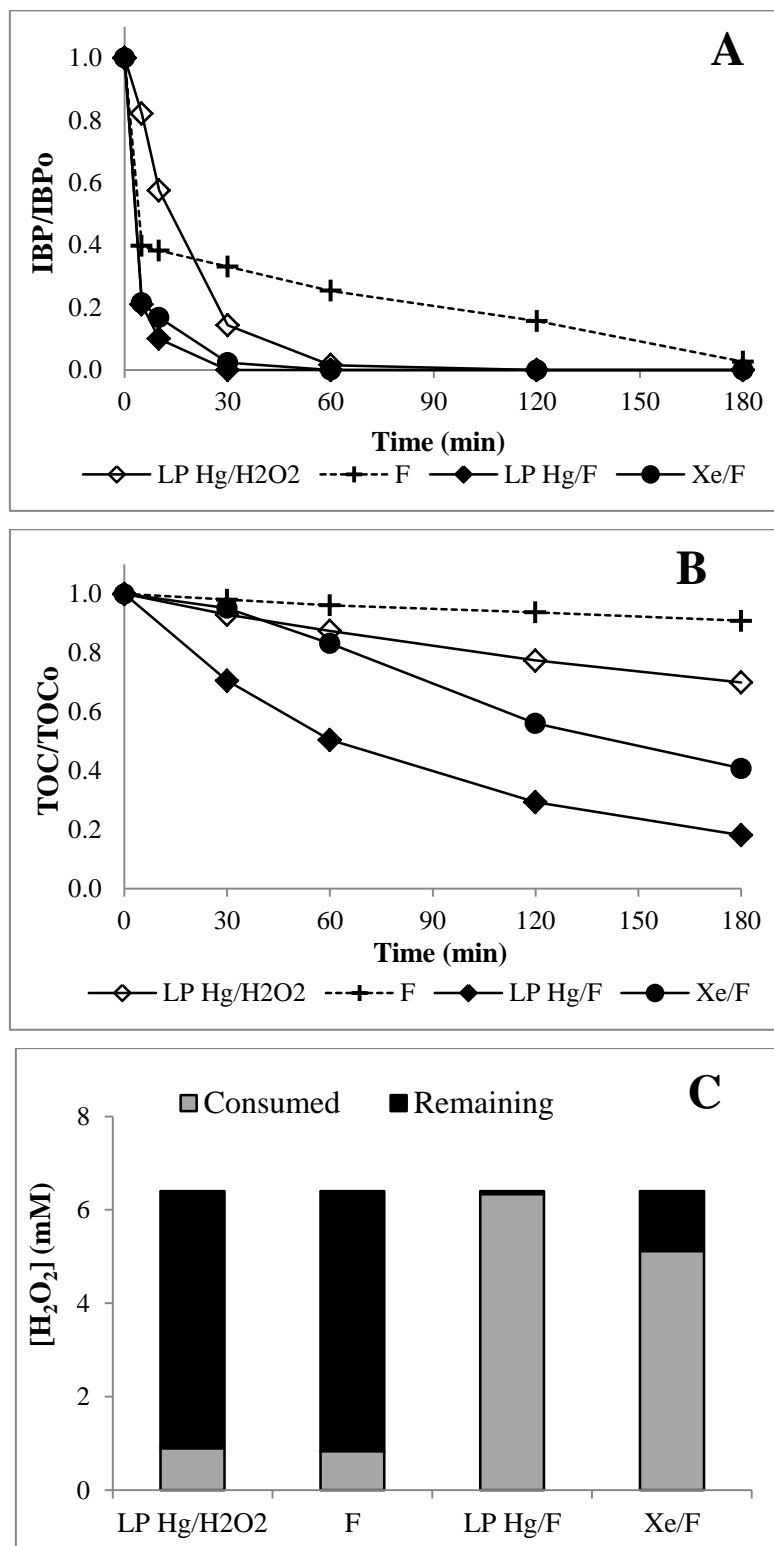


Figure 3.22. Effect of irradiation spectrum on photo-Fenton oxidation of IBP: (A) IBP and (B) TOC concentration-time profiles, and (C) H₂O₂ consumption ([IBP]₀ = 20 mg/L, pH₀ = 2.6 (photo-Fenton) and 4.3 (LP Hg/H₂O₂), T = 25°C, irradiated volume fraction = 1/3, lamp = 6W LP Hg or 150W Xe, [H₂O₂]₀ = 6.4 mM and [Fe²⁺]₀ = 0.134 mM). Fenton and LP Hg/H₂O₂ oxidation results are recalled for comparison purpose

3.2.3.2. Effect of Fenton's reagent concentration (Xe lamp)

This effect was investigated with the xenon lamp, which interestingly was able to significantly enhance Fenton oxidation (figure 3.23).

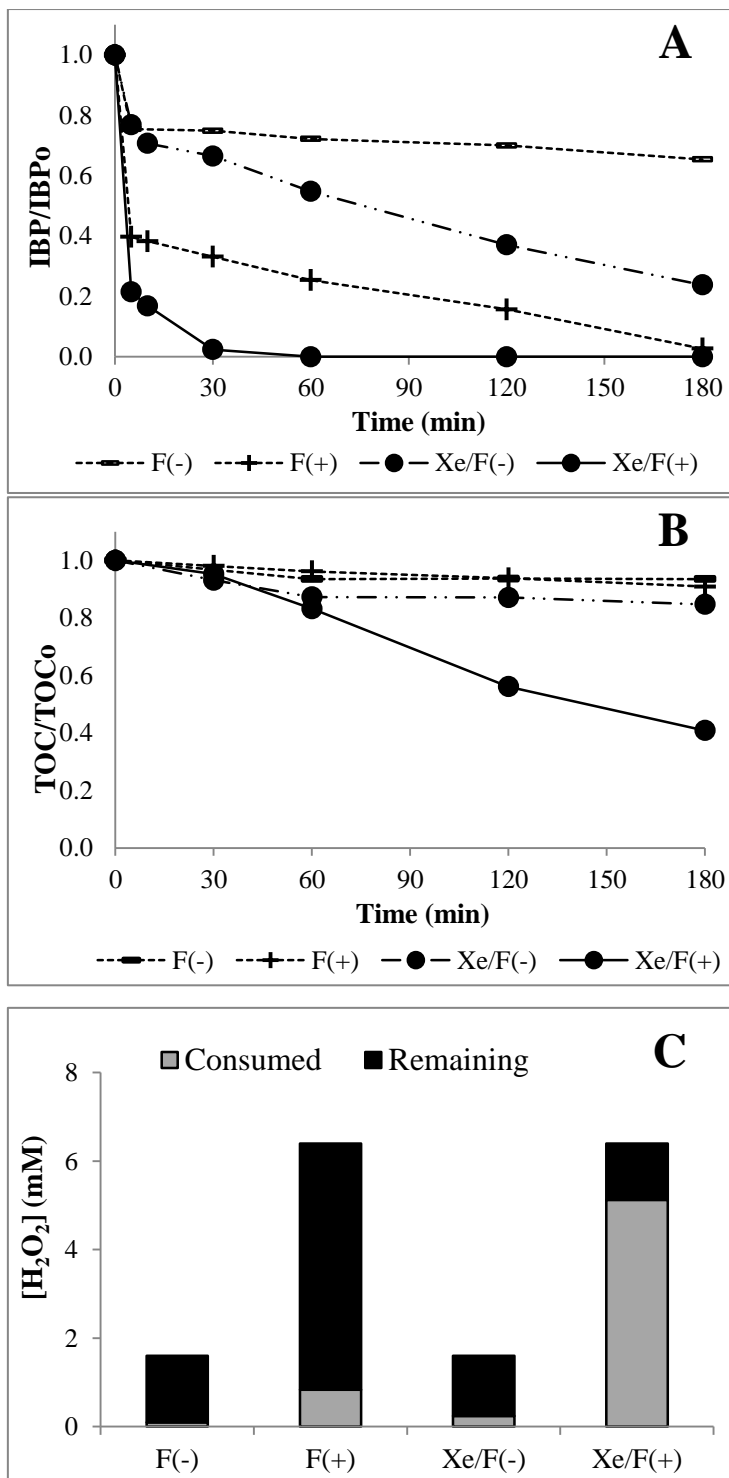


Figure 3.23. Effect of the concentration of Fenton's reagent on Fenton oxidation and photo-Fenton oxidation of IBP under visible irradiation: (A) IBP and (B) TOC concentration-time profiles ([IBP]₀ = 20 mg/L, pH = 2.6, T = 25°C, irradiated volume fraction = 1/3, lamp = 150W Xe (Vis), F(-): [Fe²⁺]₀ = 0.033 mM and [H₂O₂]₀ = 1.6 mM, F(+): [Fe²⁺]₀ = 0.134 mM and [H₂O₂]₀ = 6.4 mM)

It should be indeed recalled that it mimics sunlight irradiation. As for sono-Fenton oxidation, activation of the reaction was also assessed at the low concentration level of Fenton's reagent. At this concentration, 76% IBP was converted in photo-Fenton oxidation vs. 35% in Fenton oxidation. Contrarily to the ultrasound irradiation (cf. § 3.2.2.1), it is worth noting that visible light irradiation was able to activate Fenton reaction performed at very low concentration of Fenton's reagent. On the other hand, higher iron catalyst concentration was necessary to gain appreciable TOC removal (figure 3.23B) and minimize possible complexation effect (significant amount of residual H₂O₂ being measured for Xe/Fe(-) (figure 3.23C).

3.2.4. Sono-Photo-Fenton oxidation (20 kHz US / Xe lamp)

Combining homogeneous Fenton oxidation, ultrasound and light irradiation may be expected to reduce reaction time and/or minimize the utilization of chemical reagents, due to higher generation of hydroxyl radicals coming from various concomitant processes (*i.e.* Fenton reaction, sono- and photo-regeneration of ferrous ions). However, as mentioned in chapter 1, contradictory findings are actually present in literature. For instance, the coupling of UV irradiation and high frequency sono-Fenton oxidation was found synergistic for the decolorization of azo dye Orange II solution [129], but detrimental interaction between UV and sono(40 kHz)-Fenton was observed by Chakma and coworkers [174] for degradation of bisphenol A. On the other hand, Méndez-Arriaga et al. [33] reported that ibuprofen oxidation by photo(visible)-Fenton and sono(300 kHz)-photo(visible)-Fenton process was similar. In addition, Papoutsakis et al. [115] observed that the combined effect between ultrasound (400 kHz) and photo(sunlight)-Fenton oxidation was pollutant-dependent: it was synergistic for phenol, only additive for diuron, while photo-Fenton process dominated in the case of bisphenol A.

Therefore, further investigation is required to conclude about the possible benefits of sono-photo-Fenton oxidation.

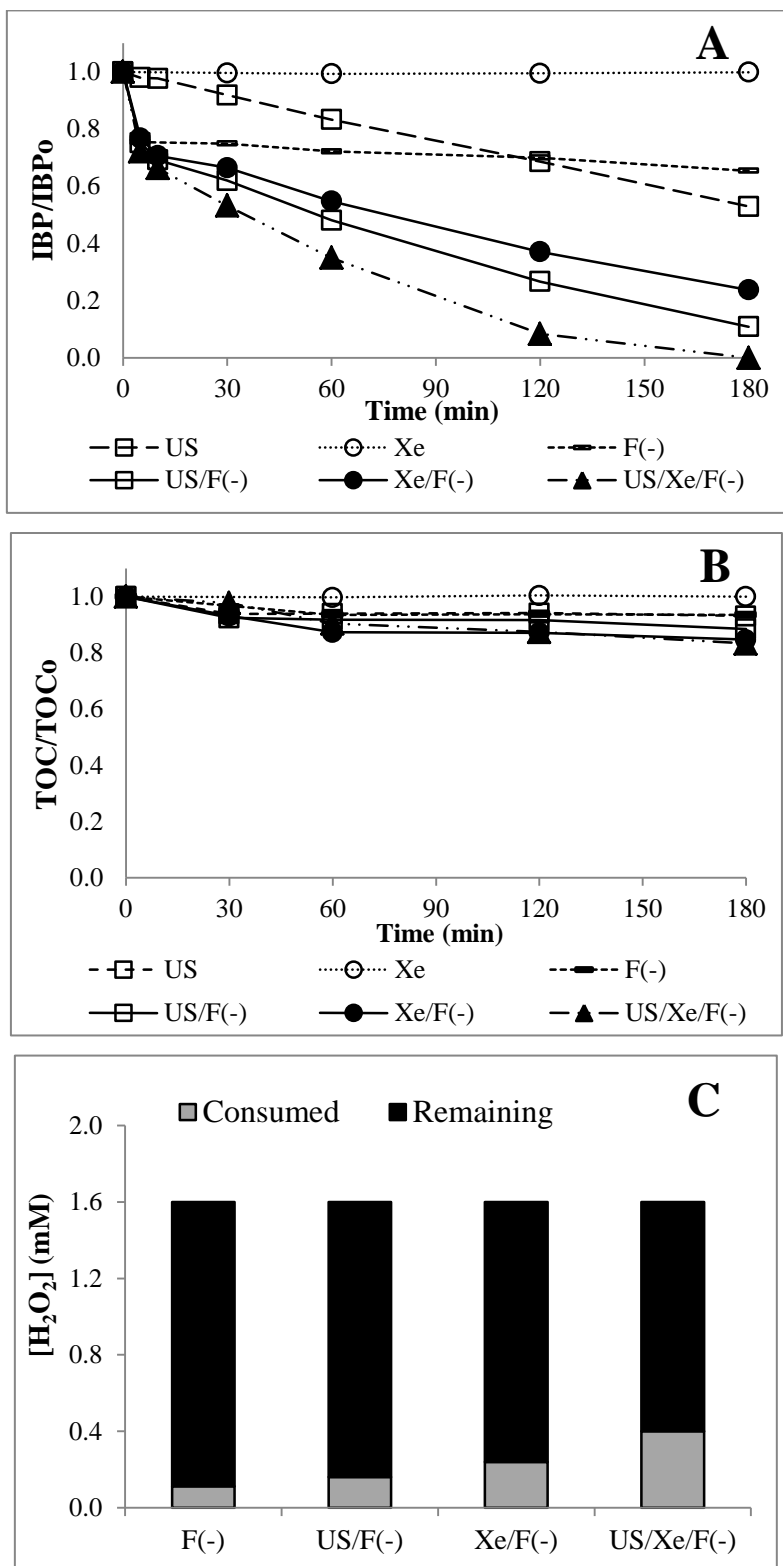


Figure 3.24. Comparison of sono-photo-Fenton and other Fenton-related processes, for low reagent concentration: (A) IBP and (B) TOC concentration-time profiles, and (C) H₂O₂ consumption. ([IBP]₀ = 20 mg/L, pH₀ = 2.6, T = 25°C, f_{US} = 20 kHz, D_{US} = 50W/L, irradiated volume fraction = 1/3, lamp = 150W Xenon, [H₂O₂]₀ = 1.6 mM and [Fe²⁺]₀ = 0.033 mM)

In our case, low frequency ultrasound and visible irradiation were applied: 20 Hz ultrasound was chosen as most usual equipment and already very good efficiency in sono-oxidation with respect to higher frequencies (cf. § 3.2.2.3), and xenon lamp to examine the potential of sunlight irradiation.

In order to estimate quantitatively the interaction coming from different individual processes, some researchers proposed to calculate a synergy factor (SF) according to the following equation [129,267]:

$$SF = k_{\text{coupling process}} / (k_{\text{process 1}} + k_{\text{process 2}} + k_{\text{process ...}}) \quad (\text{E.3.1})$$

in which k is the corresponding first-order degradation rate constant.

The coupling process can be thus considered as synergistic if $SF > 1$.

Sono-photo-Fenton oxidation of IBP was first performed at low reagent concentration (0.033 mM of Fe, 1.6 mM of H₂O₂) and the results, as well as those of corresponding Fenton (F), sono-Fenton (US/F) and photo(visible)-Fenton (Xe/F) oxidation, are shown on [figure 3.24](#). This combined process allowed full conversion of IBP after 180 min oxidation ([figure 3.24A](#)), with respect to 89% and 76% by US/F and Vis/F, respectively. Since the degradation of IBP by Fenton-related processes was very rapid in the first 5 minutes, calculation of rate constant was done afterwards. Values corresponding to the separate and combined processes are listed in [table 3.1](#).

Table 3.1. Final conversion and first-order degradation rate constant of IBP for the separate and combined processes (20 kHz US, Vis irradiation, low concentration of Fenton's reagent)

Process	Final conversion (%)	Degradation rate constant ^a (min ⁻¹)	R ²
US	47	0.0035	0.9787
Xe	0	negligible	N/A
F(-)	35	0.0008	0.9940
US/F(-)	89	0.0088	0.9940
Xe/F(-)	76	0.0065	0.9955
US/Xe/F(-)	100	0.0130	0.9975

^a based on IBP concentration-time profile after 5 minutes of reaction

It shows that the rate constant for sono-photo-Fenton oxidation was higher than the sum of k values for the separate processes (namely US, Xe and F), and also than the sum of k values for sonolysis and photo-Fenton or photolysis and sono-Fenton (table 3.2), resulting in synergy factors of 3.0, 1.5 and 1.3, respectively.

Table 3.2. Synergistic factor of sono-Fenton, photo-Fenton and sono-photo-Fenton processes for low concentration of Fenton's reagent

Process	Equation	SF
US/F(-)	$k_{US/F} / (k_{US} + k_F)$	2.0
Xe/F(-)	$k_{Xe/F} / (k_{Xe} + k_F)$	8.1
US/Xe/F(-)	$k_{US/Xe/F} / (k_{US} + k_{Xe} + k_F)$	3.0
	$k_{US/Xe/F} / (k_{US/F} + k_{Xe})$	1.5
	$k_{US/Xe/F} / (k_{US} + k_{Xe/F})$	1.3

Therefore, it is clear that combination of these three processes was synergistic and combination of Fenton process with visible light (photo-Fenton) exhibited higher synergistic effect with ultrasound (sono-Fenton). Superiority of visible light over ultrasound as activation technique can be ascribed to its negligible effect for pollutant photolysis (or photo-peroxide oxidation), but very high efficiency in ferrous iron regeneration (R.3.25 - R.3.28). However, this beneficial effect was hardly observed for TOC removal: the highest mineralization yield was only 17% under sono-photo-Fenton process, very similar to that of photo-Fenton oxidation (15%) (figure 3.24B).

IBP and TOC concentration-time profiles observed during the different Fenton-related processes at high reagent concentration (0.134 mM of Fe, 6.4 mM of H₂O₂) are then compared on figure 3.25. Contrarily to the results at low reagent concentration, sono-photo-Fenton and photo-Fenton oxidation exhibited essentially the same performance in terms of both IBP and TOC removal, therefore indicating no synergistic interaction between Vis/F and US at high reagent concentration. This suggests the existence of a threshold Fe/IBP concentration ratio for interaction between photons and ferric ions/complexes to be high enough so that photo-regeneration of iron (R.3.25 - R.3.28) became predominant over sono-regeneration. At low reagent concentration (molar ratio of Fe/IBP = 0.3) IBP and its intermediates acted as inner filter, while at high reagent concentration (ratio = 1.4) this competition for photons was strongly reduced. Indeed, IBP degradation by US/F was better than Vis/F at low reagent concentration, but Vis/F was more efficient at high dosage. On the

other hand, the moderate differences between the two processes in the latter case would not allow to presume of their combined effect.

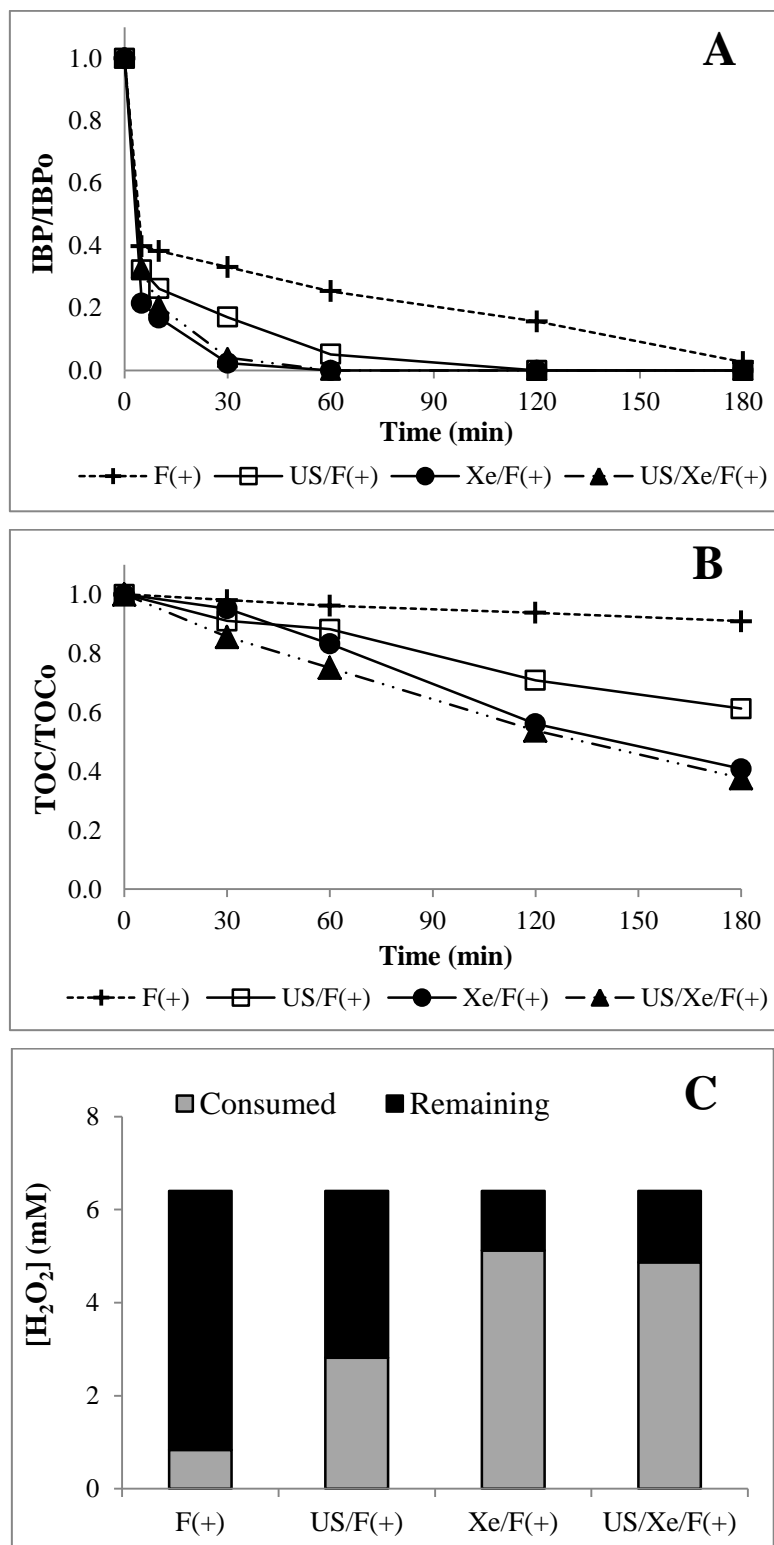


Figure 3.25. Comparison of sono-photo-Fenton and other Fenton-related processes, for high reagent concentration: (A) IBP and (B) TOC concentration-time profiles, and (C) H₂O₂ consumption ([IBP]₀ = 20 mg/L, pH₀ = 2.6, T = 25°C, f_{US} = 20 kHz, D_{US} = 50W/L, irradiated volume fraction = 1/3, lamp = 150W Xe (Vis), [H₂O₂]₀ = 6.4 mM and [Fe²⁺]₀ = 0.134 mM)

Highlights: homogeneous combined processes

- ✓ *Both (ultra)sound and light irradiation were able to activate Fenton reaction conducted under relatively low Fenton reagent concentration.*
- ✓ *The interaction effect seemed to be dependent on the Fenton reagent concentration.*
- ✓ *In all cases, sufficient Fenton reagent concentration was necessary to gain appreciable mineralization yield.*

3.3. EVALUATION OF TRANSFORMATION PRODUCTS

Ultrasound (US), UV (LP Hg) irradiation, UV/H₂O₂ (LP Hg/H), homogeneous Fenton (F), sono-Fenton (US/F) and photo(Vis)-Fenton (Xe/F) were chosen as model treatments for intermediate monitoring due to possibly different mechanisms occurring in each process. Samples collected at various time intervals from corresponding experiments were analyzed on a liquid chromatograph coupled to a HR mass spectrometer working in positive and negative ionization modes and scanning mass range from 50 to 1000 m/z. However, due to the limited availability of analytical standards (and use of gradient method), these intermediates were not quantified.

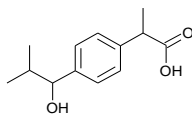
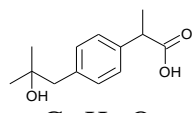
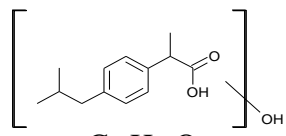
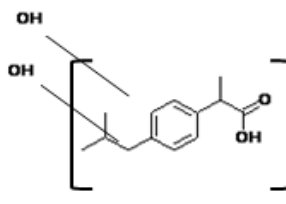
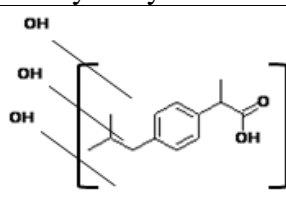
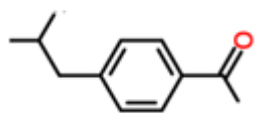
3.3.1. Identified intermediates and general IBP degradation scheme

Up to 16 transformation products of ibuprofen (IBP) were found during the reactions, including several isomers. Among them, three could be unequivocally identified thanks to available standards: **1-hydroxy-IBP** (referred to as **TP1A**), **2-hydroxy-IBP** (**TP1B**) and **4-isobutylacetophenone** (**TP4**). 4-ethylbenzaldehyde (C₉H₁₀O) which was reported in some previous studies [52,268,269] was not detected in any of the samples. [Table 3.3](#) indicates all the compounds identified from HPLC-HRMS, at least by their molecular formula. Note that the developed technique was not suited for either low molecular weight molecules or nonpolar compounds.

Based on these results and on the available information in literature, a general degradation scheme of IBP was presumed which is depicted in [figure 3.26](#). Occurrence of the intermediates in the different AOPs is also reported in this figure.

It can be seen that the principal reactions involved in IBP degradation by AOPs are *hydroxylation*, *decarboxylation* and *cleavage of C-C bond*. The latter mechanism was assumed, as **TP7** formula (C₉H₁₀O₂) matched that of 2-phenyl-propionic acid, observed in preceding works [52,55].

Table 3.3. Identified compounds from LC-HRMS

Name	Molecule	t _R (min)	Ion mode	m/z	Remark
TP1A	 C ₁₃ H ₁₈ O ₃ 1-hydroxy-IBP (std)	19.75	Neg	221.118	
TP1B	 C ₁₃ H ₁₈ O ₃ 2-hydroxy-IBP (std)	18.7	Neg	221.118	
TP1C TP1D	 C ₁₃ H ₁₈ O ₃ Mono-hydroxylated IBP	21.15 22.15	Neg	221.118	2 identified isomers of TP1A & TP1B
TP2 (A-C)	 C ₁₃ H ₁₈ O ₄ Di-hydroxylated IBP	19.8 20.05 20.5	Neg	237.113	3 identified isomers
TP3 (A-C)	 C ₁₃ H ₁₈ O ₅ Tri-hydroxylated IBP	18.35 18.65 19.15	Neg	253.108	3 identified isomers
TP4	 C ₁₂ H ₁₆ O 4-isobutylacetophenone (std)	25.1	Pos	177.127	
TP5	C ₁₂ H ₁₆ O	20.95	Neg	175.111	Isomer of TP4
TP6	C ₉ H ₈ O ₃	16.75	Neg	163.040	
TP7	C ₉ H ₁₀ O ₂	16.8	Neg	149.061	
TP8	C ₉ H ₁₀ O	17.7	Neg	133.066	Isomer of 4-ethylbenzaldehyde
TP9	C ₅ H ₁₀ O ₃	~4.0	Neg	117.056	

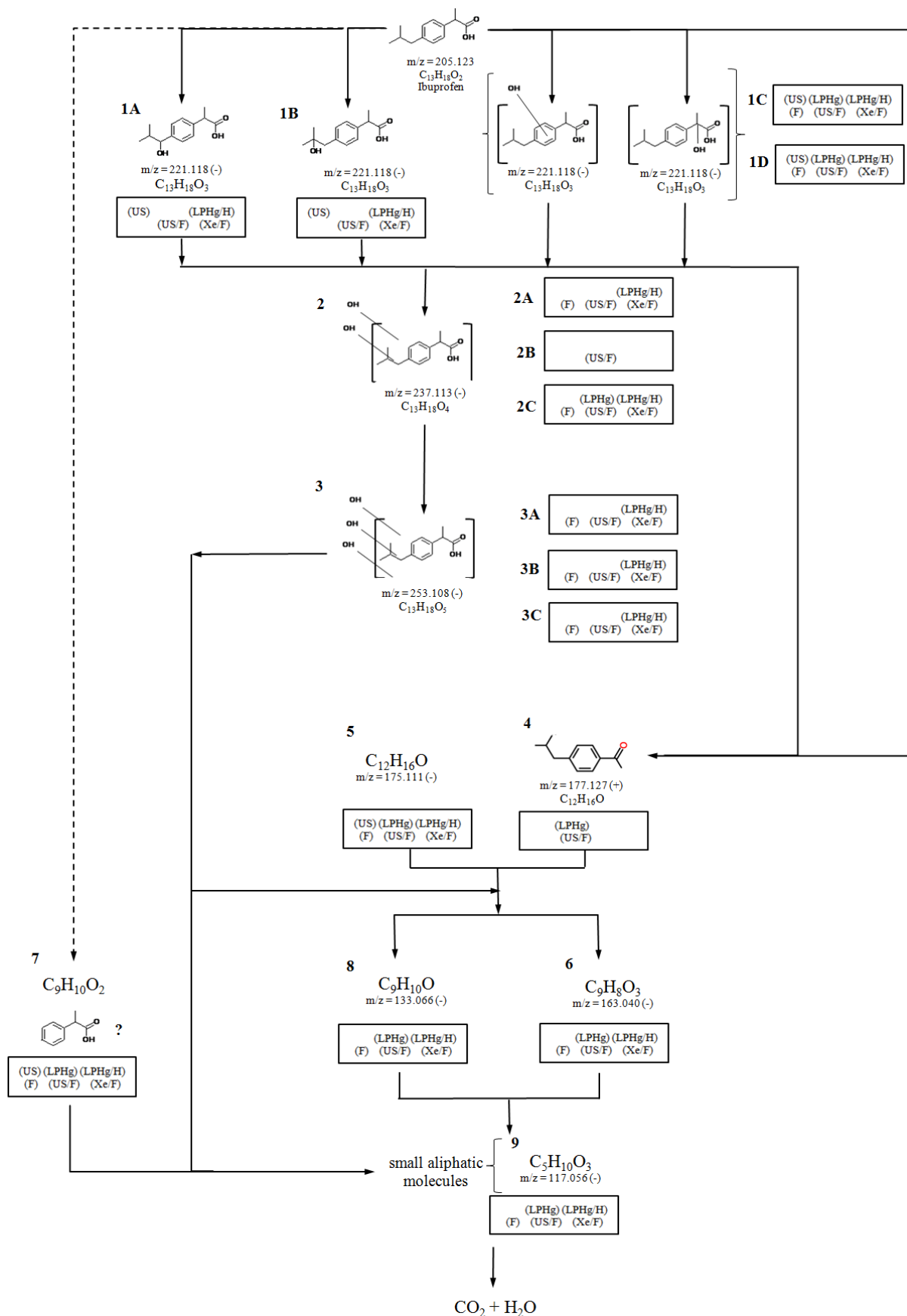


Figure 3.26. Proposed reaction scheme for degradation of ibuprofen by homogeneous AOPs

According to the available sites on IBP molecule, *hydroxylation* can take place either on the side chains (methylpropyl moiety or phenylpropionic moiety) [24,39,43,44] or on the aromatic ring [52,55,258]. In agreement with the literature, **mono-hydroxylated intermediates** (C₁₃H₁₈O₃) were detected, **up to 4** in our case referred to as **TP1(A-D)**, among which those classically mentioned: **1-hydroxy-IBP (TP1A)** and **2-hydroxy-IBP (TP1B)**. These hydroxylated IBP can undergo further hydroxylation forming **TP2** (C₁₃H₁₈O₄) [24,39,44] then **TP3** (C₁₃H₁₈O₅) [39,44]. **3 di-hydroxylated and 3 tri-hydroxylated isomers** were observed, but identification of their detailed structure was not possible.

In parallel to hydroxylation route, *decarboxylation* of hydroxylated IBP may yield **4-isobutylacetophenone (TP4, C₁₂H₁₆O)** [24,39,52]. *Direct photo-decarboxylation of IBP to TP4* was also proposed in literature [54,270]. Isomer of TP4 was observed, referred to as **TP5 (C₁₂H₁₆O)**.

Next, **TP6 (C₉H₈O₃)** could be formed by successive hydroxylation and loss of terminal propyl group from **TP4** [44]. **TP8 (C₉H₁₀O)** was an isomer of 4-ethylbenzaldehyde, but in the absence of structural information its formation pathway could not be clearly derived. It was probably similar to that of TP6. Finally, ring opening could lead to the formation of small aliphatic molecules, such as **TP9 (C₅H₁₀O₃)**. Note that such molecule was rarely mentioned in the literature [44].

In addition, an alternative degradation pathway of IBP might go through the *cleavage of isobutyl moiety from IBP*, forming 2-phenyl-propionic acid (C₉H₁₀O₂, **TP7 ?**) [52,55].

3.3.2. Comparison of different homogeneous processes

Comparison of degradation pathways induced by different AOPs is still rarely reported in literature. As shown in [figure 3.26](#), similar intermediates were formed during ultrasound (US), ultraviolet irradiation (LPHg), UV/H₂O₂ (LPHg/H), homogeneous Fenton (F), sono-Fenton (US/F) and photo(Vis)-Fenton (Xe/F), which is consistent with the involved mechanisms: with the exception of photolysis, for which a direct transformation pathway was put into evidence (cf. § 3.1.3.1), all other processes involved hydroxyl radical attack. However all transformation products were not observed during the different AOPs.

Under *ultrasound irradiation* 20 kHz (US), only six transformation products were identified *i.e.* TP1A, TP1B, TP1C, TP1D, TP5 and TP7 ([figure 3.27](#)). Formation of mono-hydroxylated IBPs (TP1A-D) is consistent with radical attack at cavitation bubble surface

(and to a much smaller extent in the liquid bulk). By comparing the concentration-time profiles of these compounds, it can be seen that all degradation products reached their maximum almost at the end of the reaction time, resulting in rather high residual TOC. As mentioned previously, plausible explanation for this limited mineralization (only 7% after 180 min) could be that several of these intermediates were more hydrophilic, thus less prone to be degraded by the radicals formed at the bubble interface. For instance, subsequent hydroxylation of TP1 ($\text{Log } K_{ow} = 2.25$ [246]) was rather difficult, as confirmed by the absence of TP2 and TP3, and the reaction might mainly progress through decarboxylation of TP1 to TP5 (and/or C-C bond cleavage of IBP forming TP7).

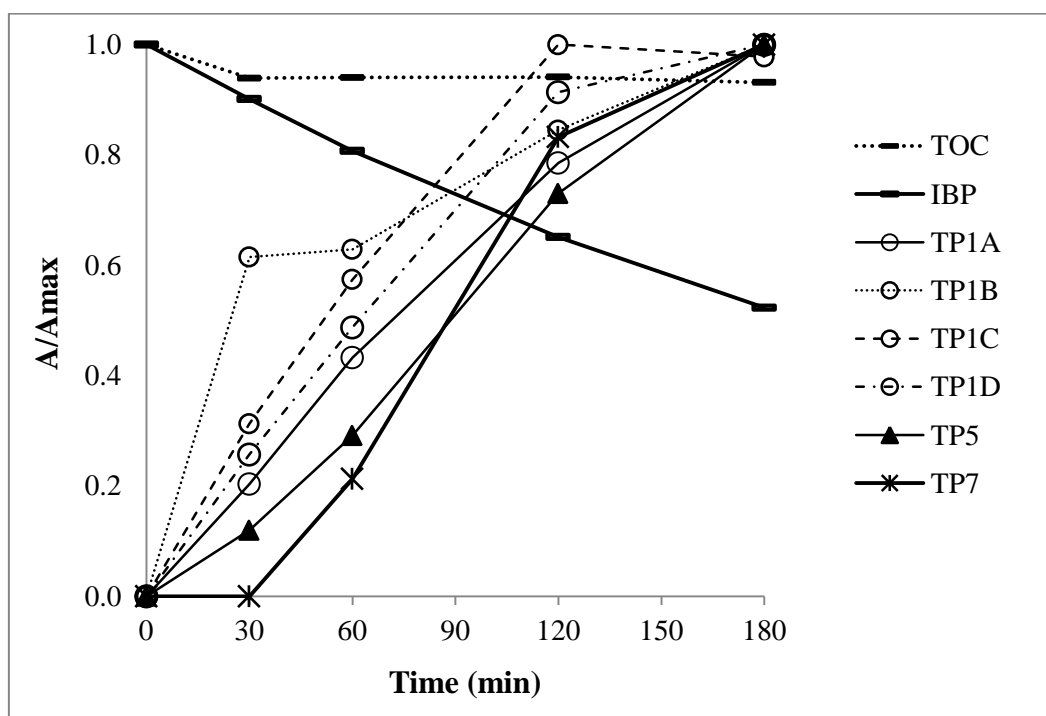


Figure 3.27. Evolution of normalized* concentration of IBP transformation products during UV irradiation (*based on the maximum peak area measured for each compound)

Only three hydroxylated-IBP (TP1C, TP1D, TP2C) were observed during UV irradiation with LP Hg lamp, indicating that hydroxylation of methylpropyl moiety was not favored in this case. According to the measured peak area, TP1 and TP4 were the main intermediates formed during UV irradiation, while TP2 was only in a low amount, as well as TP5, TP7 and TP8 which were detected only at the end of reaction. TP6 also appeared later in the sequence (figure 3.28). This observation indicated that principal degradation pathways of IBP under UV irradiation could from decarboxylation of mono-hydroxylated-IBP ($\text{IBP} >$

TP1D > TP4 > ...) and direct photo-decarboxylation of IBP (IBP > TP4 > ...). As abovementioned, direct pollutant photolysis was indeed observed in addition to radical-mediated route (cf. § 3.1.3.1).

UV irradiation at 254 nm was able to yield higher mineralization (TOC removal = 19%) than US and thus more intermediates were detected. Moreover TP4 exhibits a maximum absorbance ($\lambda_{\max}=255$ nm) closer to the lamp emission wavelength than IBP ($\lambda_{\max}=222$ nm).

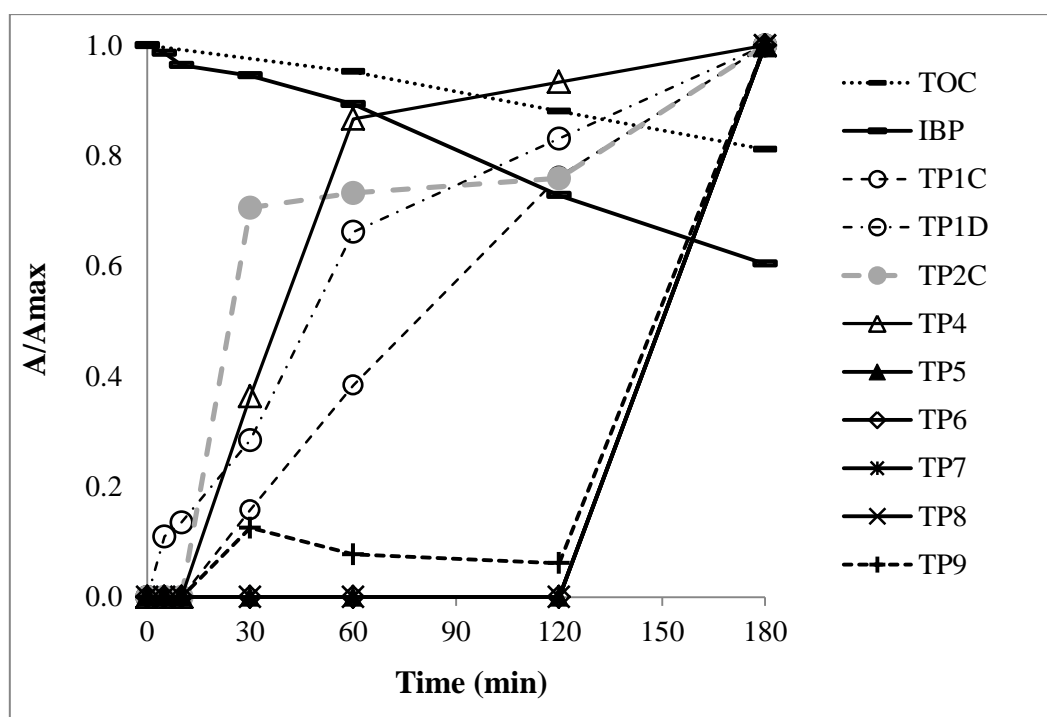


Figure 3.28. Evolution of normalized* concentration of IBP transformation products during UV-photolysis with LP Hg lamp
 (*based on the maximum peak area measured for each compound)

Furthermore, IBP degradation pathways under *UV/H₂O₂ (LPHg/H)*, *homogeneous Fenton (F)*, *sono-Fenton (US/F)* and *photo(Vis)-Fenton (Xe/F)* were similar, wherein almost all the transformation products were detected. These findings could be explained by the dominant contribution of powerful and non-selective free radical attack in these processes. However, it is not clear why TP1A, TP1B, TP1D and TP2B were not detected under Fenton oxidation. Interestingly, even if similar mineralization yield was obtained for ultrasound (7%) and Fenton reaction (9%), Fenton reaction was able to degrade almost all hydroxylated IBP within reaction time (figure 3.29).

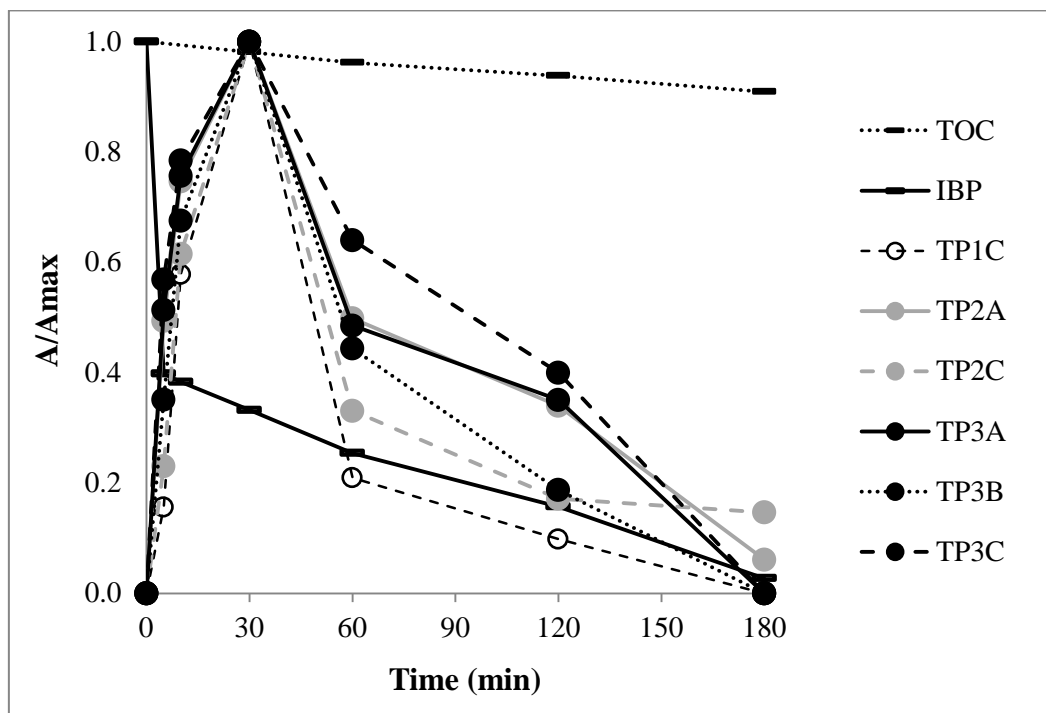


Figure 3.29. Evolution of normalized* concentration of hydroxylated IBP compounds during homogeneous Fenton reaction
 (*based on the maximum peak area measured for each compound)

3.3.3. Evolution of selected intermediates during homogeneous processes

The evolution of four transformation products, TP1A (1-hydroxy-ibuprofen), TP1B (2-hydroxy-ibuprofen), TP4 (4-isobutylacetophenone) and TP5 (TP4 isomer), was more particularly examined. While TP1A and TP1B are the most frequently reported in the literature [24,39,43–46,52,55,258,269], TP4 (and probably TP5) is known for its possible toxicity effects [53,55,271,272].

TP1A and TP1B exhibited very similar profiles for all the homogenous AOPs (figures 3.30 and 3.31, respectively): continuous concentration increase under ultrasound, and maximum observed at 30 minutes or less in LP Hg/H₂O₂, Xe/F and US/F processes.

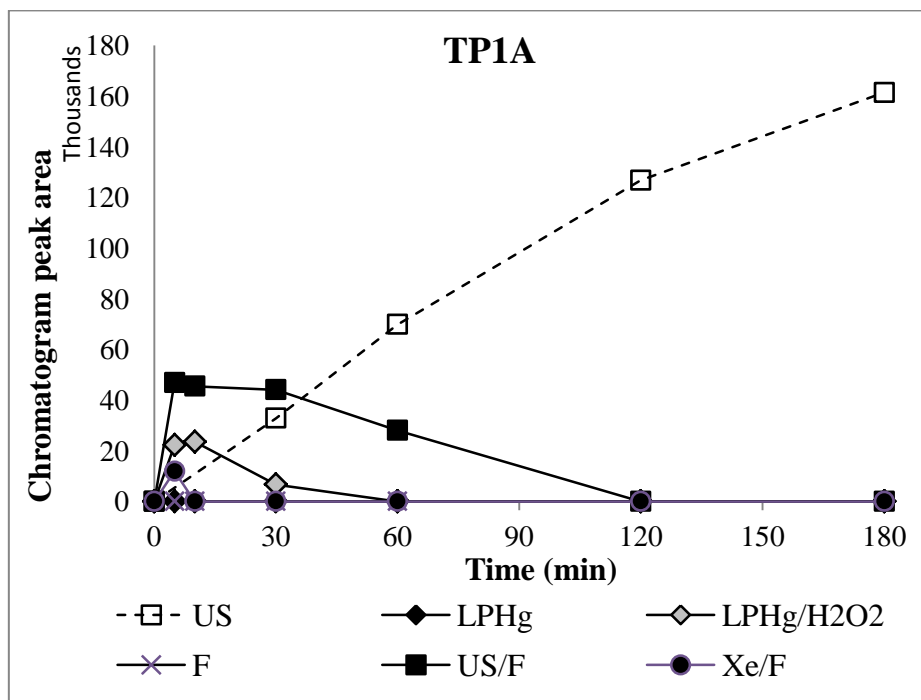


Figure 3.30. Evolution of TP1A concentration during homogeneous AOPs

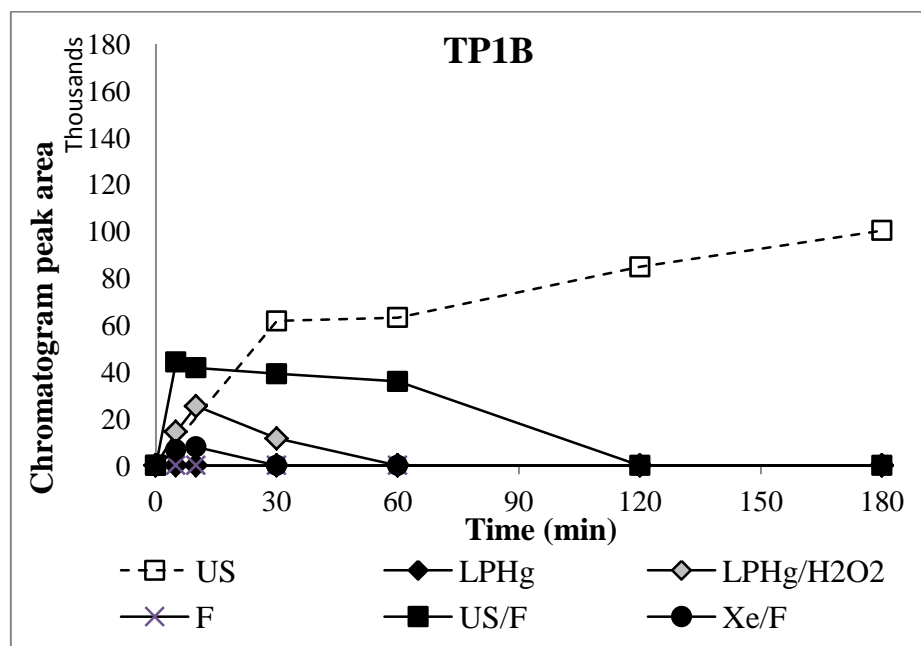


Figure 3.31. Evolution of TP1B concentration during homogeneous AOPs

Moreover, in combined US/F, the presence of Fenton's reagent was able to significantly reduce the amounts of TP1A and TP1B with respect to US. As abovementioned, TP1A was not detected in LP Hg and Fenton process. Hydroxylation of IBP under LP Hg irradiation seemed to occur rather on phenylcarboxylic acid moiety or on the aromatic ring. It is not

clear why these compounds were not found during Fenton oxidation considering its occurrence – however in very low amount – in photo-Fenton process (Xe/F).

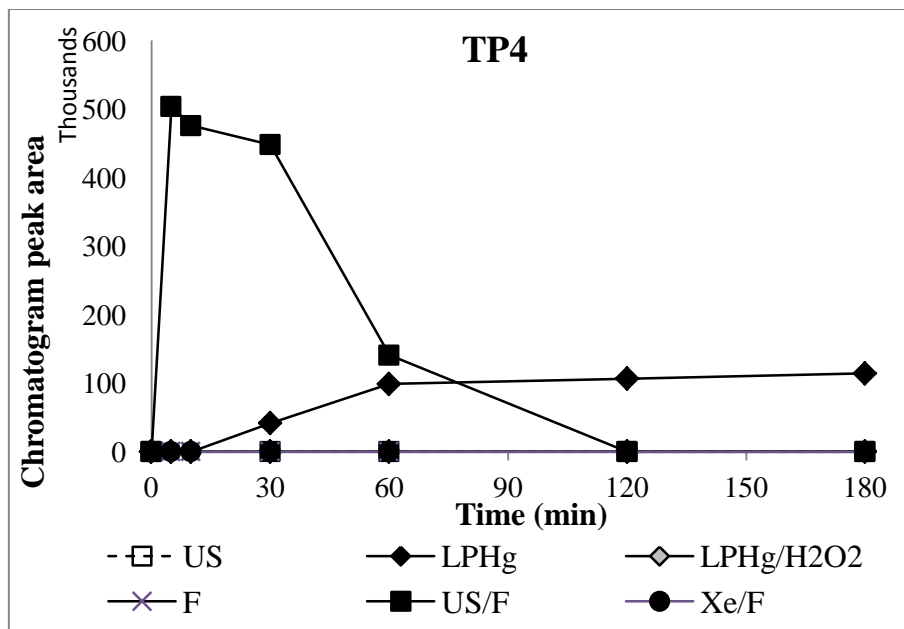


Figure 3.32. Evolution of TP4 concentration during homogeneous AOPs

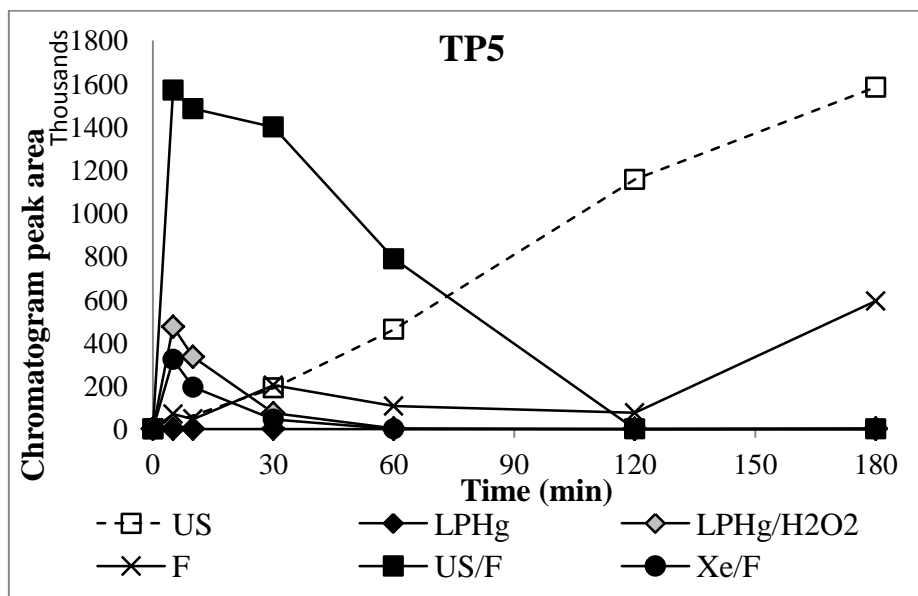


Figure 3.33. Evolution of TP5 concentration during homogeneous AOPs

Differences in process selectivity even more clearly arose in case of TP4 and TP5 (figures 3.32 and 3.33, respectively). TP4 was only observed under UV and US/F processes. High concentration of TP4 was formed in the first 5 minutes of US/F, and then it decreased

until complete removal after 120 minutes. Conversely, less TP4 was formed under UV irradiation, but the concentration was relatively stable during the reaction. TP5 was detected in all processes except photolysis, for which radical mechanism was not dominant. Moreover, in US/F similar trend was observed for this compound as for TP4: rapid concentration increase in 5 minutes and slow decrease afterwards. A complete removal of formed TP5 was also achieved in 60 min for LPHg/H₂O₂ and Xe/F. Therefore, it can be concluded that, even if IBP removal can be achieved rather rapidly by some processes such as US/F, much longer reaction time is needed to gain sufficient mineralization and remove some toxic intermediates formed during the reaction.

3.4. EFFECT OF WATER MATRIX

Sono- and photo-Fenton oxidation processes were shown to be promising methods for the removal of ibuprofen (IBP) in water. However, all the experiments that have been done so far were conducted in distilled water (DW). In order to investigate the efficiency in real application, some experiments with a real wastewater matrix (WW) were performed. Wastewater consists in a complex mixture of organic and inorganic compounds, such as nutrients, salts and many substances that could influence the outcome of advanced oxidation processes [235]. For instance, the presence of organic (humic acid, fulvic acid, ...) and inorganic compounds (chloride, carbonate, bicarbonate, and phosphate ions) in WW may hamper Fenton reaction by scavenging $\cdot\text{OH}$ and/or forming iron complex [41,273]. On the other hand, phenolic compounds that WW may contain could reduce ferric ion to ferrous ion and thus enhance Fenton reaction [273].

According to recent reviews on hybrid processes [240,241], AOPs are recommended in combination with membrane filtration as post-treatment of biological process for destruction of refractory organics in concentrate stream. Such hybridization allows the AOPs to reach appreciable mineralization level in relatively short oxidation time, and to save chemicals and energy.

In this study, water samples taken after biological treatment of a municipal wastewater treatment plant located in Nailloux village (France) were used to prepare the IBP solution (at 20 mg/L). [Table 3.4](#) shows the physicochemical characteristics of this effluent. After addition of IBP, TOC concentration increased to 25 mg/L, IBP being the major organic compound in the resulting solution. The amount of carbonate and bicarbonate was evaluated from inorganic carbon (IC) analysis and the measured concentration level (29.4 mg/L) could be high enough to scavenge hydroxyl radicals at neutral and alkaline pH [121]. On the other hand, the initial iron concentration (< 0.05 mg/L) appeared too low to effectively contribute to Fenton oxidation mechanism.

Table 3.4. Physicochemical properties of the wastewater effluent

Parameter	Value
pH	8
Turbidity (NFU)	1
BOD (mg/L)	< 2
COD (mg/L)	< 30
TC (mg/L)	39.2
IC (mg/L)	29.4
TOC (mg/L)	9.8 (25 ^a)
Total Fe (mg/L)	< 0.05

^a after the addition of IBP

Matrix effect was first evaluated for sonolysis (US), homogeneous Fenton (F) and sono-Fenton (US/F) oxidation in [figure 3.34](#). The treatment efficiency in distilled water (DW) was also recalled for comparison purpose. As usual, the initial pH of DW and WW was set to 2.6 (using H₂SO₄) for the Fenton and sono-Fenton oxidation runs, while the pH of WW was not adjusted for sonolysis.

Degradation of both IBP and TOC by ultrasound was significantly hampered in WW. Lower IBP removal in WW (24% vs. 48% in DW after 180 min) could be mainly explained by a pH effect, the initial pH of the IBP solution varying from 4.3 to 8.0 whether prepared with DW or WW, respectively. As abovementioned (see [§ 3.1.2.2](#)) pH value of 8.0 indeed reduced the sono-degradation of IBP to 31% in DW by increasing the molecule solubility. Competition or scavenging effects from organic and/or inorganic compounds of WW thus seemed to have only a minor effect.

After preliminary acidification to 2.6, concentration-time profiles of IBP during Fenton oxidation were almost superimposed for the two matrixes, while a slight decrease was observed for sono-Fenton process when in WW ([figure 3.34A](#)). Therefore, it seems to confirm that IBP didn't strongly compete for radicals with the organic molecules present in WW, and that iron complexation and free-radical scavenging were not significantly increased in this matrix. In particular, inorganic carbon content was almost totally converted into carbonic acid and CO₂ by initial acidification.

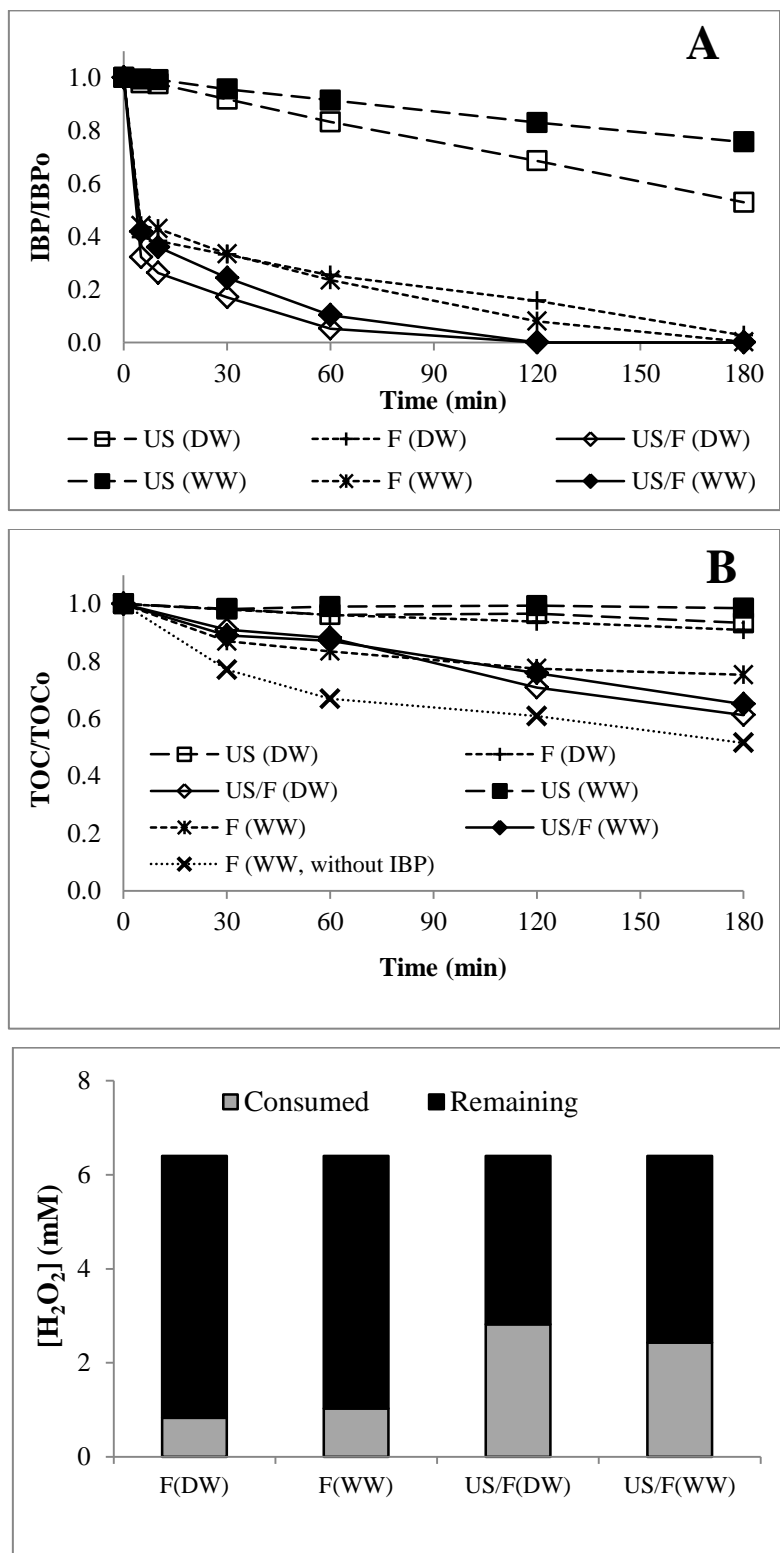


Figure 3.34. Effect of water matrix (DW: distilled water, WW: wastewater effluent) on sonolysis (US), Fenton (F) and sono-Fenton (US/F) oxidation of IBP: (A) IBP and (B) TOC concentration-time profiles, and (C) H₂O₂ consumption.

([IBP]₀ = 20 mg/L, pH₀ = 2.6 except for US in WW (pH₀ = 8.0), T = 25°C, f_{US} = 20 kHz with D_{US} = 50W/L under US, [H₂O₂]₀ = 6.4 mM and [Fe²⁺]₀ = 0.134 mM for F and US/F)

Moreover, overall TOC removal by Fenton oxidation was improved in WW (25% vs. 9%, [figure 3.34B](#)). Fenton oxidation test without IBP proved this result to be mainly the consequence of more readily oxidized organic compounds in WW (50% of TOC removal). However, similar behavior was not observed in sono-Fenton oxidation. This might be due to the selective effect of acoustic cavitation towards specific organic molecules [126] and complex interplay between iron and WW compounds (and/or their oxidation intermediates) somewhat hampering sono-regeneration of Fe^{2+} .

The effect of WW matrix was also evaluated in photo-based advanced oxidation processes, i.e. photolysis under UV light, UV/ H_2O_2 (LP Hg lamp) and photo(Vis)-Fenton (Xe lamp). Despite the possible improvement in IBP removal by UV photolysis under alkaline pH (cf. [§ 3.1.3.2](#)), photolysis of IBP in WW matrix was clearly inhibited ([figure 3.35](#)). IBP removal by UV/ H_2O_2 and photo(Vis)-Fenton was also hampered, but to a lesser extent compared to UV photolysis and complete IBP removal still could be achieved within reaction time. Likewise, mineralization yields were always lower in WW matrix, indicating also that organic compounds present in WW matrix were less photo-active than IBP. Measurement of residual H_2O_2 concentration after reaction also showed smaller H_2O_2 consumption in experiments with WW matrix. Inhibition of UV photolysis and photo-Fenton oxidation by real water matrix has been reported in literature [274,275] and it can be possibly attributed to scattering and filtering of UV and visible light by organic and inorganic compounds present in WW.

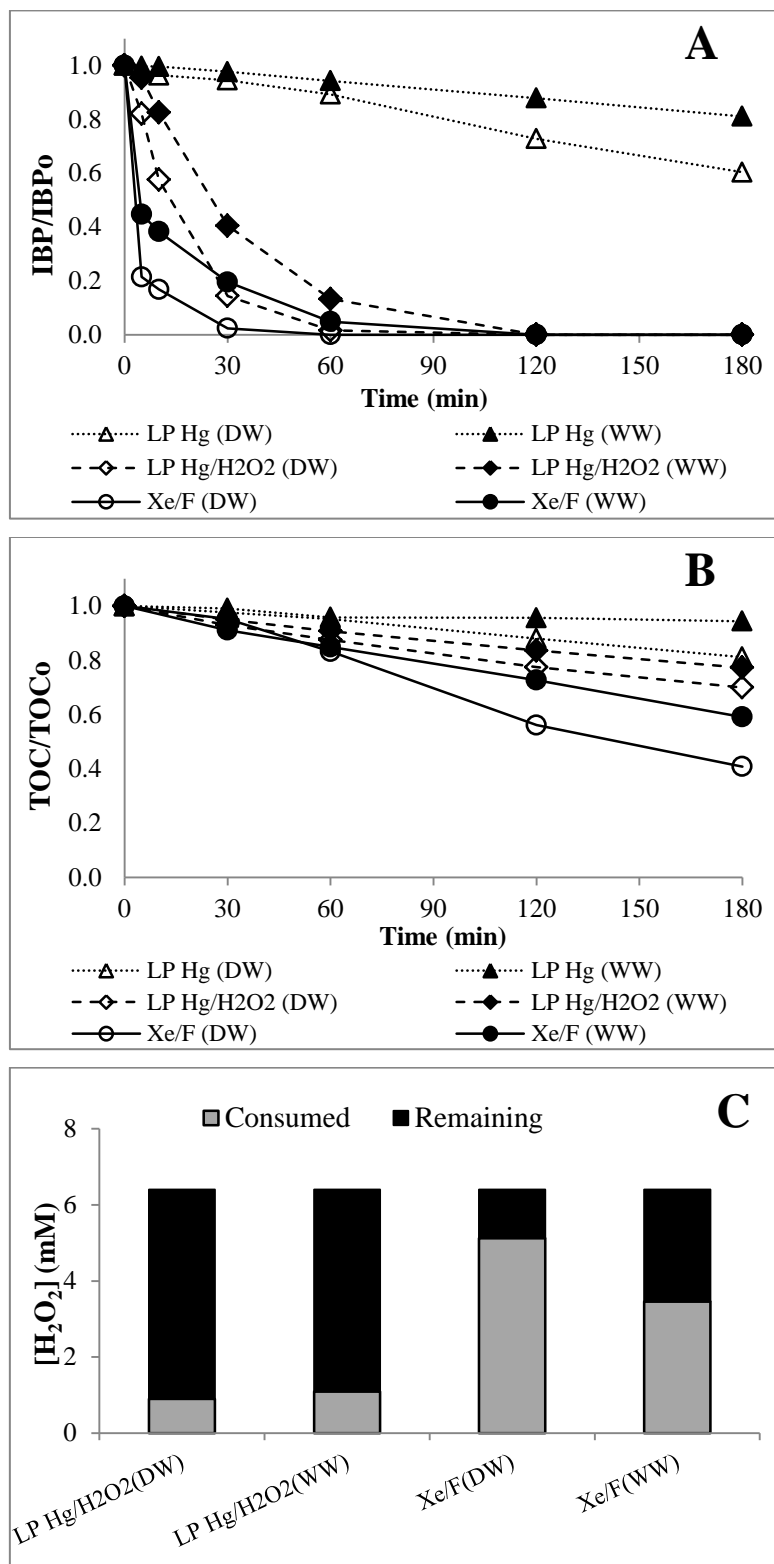


Figure 3.35. Effect of water matrix (DW: distilled water, WW: wastewater effluent) on UV photolysis (LP Hg), UV/H₂O₂ (LP Hg/H₂O₂) and photo(Vis)-Fenton (Xe/F) oxidation of IBP: (A) IBP and (B) TOC concentration-time profiles, and (C) H₂O₂ consumption. ([IBP]₀ = 20 mg/L, pH₀ = 8.0, except for Xe/F in WW (pH₀ = 2.6), T = 25°C, irradiated vol. fraction = 1/3, lamp = 6W LP Hg (UV) or 150W Xe (Vis), [H₂O₂]₀ = 6.4 mM and [Fe²⁺]₀ = 0.134 mM for Xe/F)

3.5. CONCLUSIONS

This chapter was dedicated to the degradation of ibuprofen by homogeneous AOPs. The performance of separated (ultrasound, light irradiation - with or without H₂O₂, Fenton oxidation) and combined processes (sonophotolysis, sono-Fenton, photo-Fenton and sono-photo-Fenton oxidation) was investigated with the aim of identifying synergistic effects, and obtaining “benchmark” for heterogeneous counterparts.

Single processes such as sonolysis, UV photolysis and Fenton oxidation were able to achieve at least partial degradation of ibuprofen in 3 hours, while addition of hydrogen peroxide as promoter was found significantly beneficial under ultraviolet light only (with 5- to 24-fold enhancement of IBP degradation rate). For instance, peroxide oxidation with MP Hg lamp resulted in nearly complete abatement of both IBP and TOC within reaction time. Conversely, Fenton oxidation yielded less than 10% mineralization yield.

Combination of homogeneous Fenton oxidation with ultrasound or light (ultraviolet / visible) irradiation was found to be more effective than the sum of individual processes in most cases, although it seemed to be dependent on the Fenton's reagent concentration. In addition, ultrasound and visible light emitted by xenon lamp was able to activate Fenton oxidation conducted at very low iron concentration (1.8 mg/L). For instance, coupling US/Vis/Hom-F process was found to be synergistic at very low reagent concentration (0.033 mM Fe and 1.6 mM H₂O₂), while Vis/Hom-F becomes predominant at higher reagent concentration (0.134 mM Fe and 6.4 mM H₂O₂). In all cases, sufficient Fenton's reagent concentration was necessary to gain appreciable mineralization yield, which could exceed 60% only under photo-activation.

Up to 16 transformation products (mainly aromatics) were detected during the different AOPs, and the monitoring of their evolution allowed to confirm some specific features of the processes.

In real wastewater effluent, sonolysis and all photo-based advanced oxidation processes were hampered mainly due to alkaline pH and light scattering effect, respectively. On the other hand, preliminary acidification could maintain the efficiency of Fenton and sono-Fenton oxidation.

In the next chapter, degradation of ibuprofen by heterogeneous Fenton oxidation and activation effect by ultrasound and light irradiation are assessed.

CHAPTER 4. HETEROGENEOUS PROCESSES

Degradation of ibuprofen (IBP) by homogeneous Fenton based-processes has been presented in the previous chapter (chapter 3). It was found that an iron concentration in the order of magnitude, but still higher than the discharge limit (7.5 mg/L vs. 2 mg/L), was necessary to achieve within 3 hours almost complete conversion of IBP and appreciable TOC removal (40% or more) under activation by ultrasound, low pressure mercury vapor lamp or xenon lamp. This would thus still require post-treatment to precipitate excess iron. Moreover, the limited pH range (pH = 2 – 4) of the homogeneous Fenton reaction is a major obstacle, especially for real applications since real water matrices are usually buffered around neutral pH [164,178]. In order to overcome these problems, recent studies are moving towards heterogeneous catalyst utilization. This is the purpose of this chapter, where different types of iron-based solid catalysts are first screened for the degradation of IBP. Then a parametric study is conducted with the selected catalyst, before the investigation of heterogeneous reaction coupling with ultrasound and/or light irradiation. The experiments were first performed in sono-reactor, and loop reactor configuration was used for UV/Vis coupling.

This page is intentionally left blank

4.1. PRE-SELECTION OF THE HETEROGENEOUS CATALYST

Extensive comparison of various heterogeneous catalysts for Fenton oxidation including iron oxide particles (hematite, magnetite, maghemite) and iron containing ZSM5 zeolite (Fe-BEA and Fe-MFI) had been conducted in a previous study of our research group on the remediation of paracetamol [189], an analgesic drug with a relatively similar structure to ibuprofen. Among the tested catalysts, Fe-MFI catalyst appeared as the most promising catalyst due to its high catalytic activity and low iron leaching. In addition, zero-valent iron powder (ZVI) was also considered here, based on results from the literature which indicated that ZVI can catalyze H_2O_2 decomposition under circumneutral pH conditions [73,85,198,239]. In this section, efficacies of Fe-MFI and ZVI are compared for the catalytic oxidation of ibuprofen.

4.1.1. Adsorption of ibuprofen over Fe-MFI and ZVI catalysts

Preliminary adsorption tests (without oxidant) were first conducted in order to investigate the possible adsorption of IBP on the solid catalysts. From [figure 4.1](#) it can be seen that negligible adsorption occurred on ZVI (up to 1 g/L). For Fe-MFI, IBP removal increased from 7% to 25% when increasing solid concentration from 0.5 g/L to 4.8 g/L, and adsorption equilibrium was reached within 120 min. These experiments were conducted without any pH adjustment, but the pH of the solution decreased from 4.3 to 3.3-3.7 by simple contact with the Fe-MFI catalyst (depending on its concentration), while no pH change was observed for ZVI. The acidity of Fe-MFI is due to the presence of Brønsted and Lewis acid sites on zeolite framework [201].

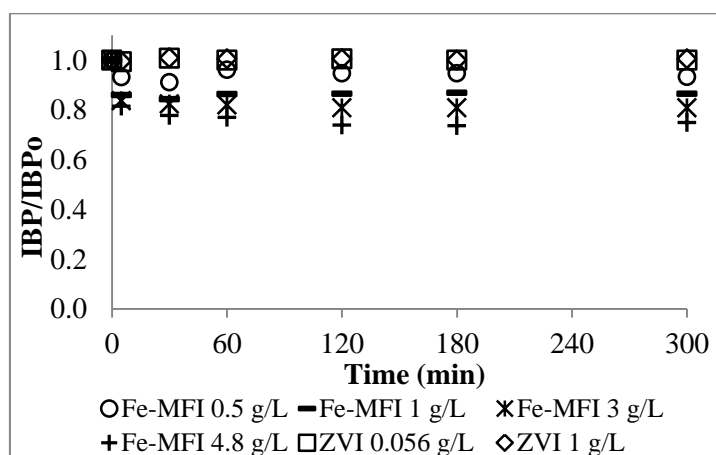


Figure 4.1. Adsorption of ibuprofen over ZVI and Fe-MFI catalysts
 ($[IBP]_0 = 20 \text{ mg/L}$, $[Fe-MFI] = 0.5 - 4.8 \text{ g/L}$, $[ZVI] = 0.056 \text{ and } 1 \text{ g/L}$, $pH_0 = 4.3$, $T = 25^\circ\text{C}$)

Higher adsorption capacity of Fe-MFI compared to ZVI can be attributed to its much larger specific surface area (329 vs 0.5 m²/g). It should be mentioned that since molecular size of IBP (1.3 nm x 0.6 nm) is larger than minor and major axes of the sinusoidal (0.51 nm x 0.55 nm) and straight channels (0.54 nm x 0.56 nm) of Fe-MFI zeolite, IBP molecules may be only adsorbed at the intersection of the straight and sinusoidal channels, as proposed by Yazaydin et al. [276] in the case of methyl tert-butyl ether (MTBE) (figure 4.2). Moreover, strong interaction between IBP and zeolite could be possible due to the formation of iron- or aluminium-ibuprofenate complexes (ibuprofenate coordinately bonded to iron active sites or extra-framework aluminium species) [223,260,261].

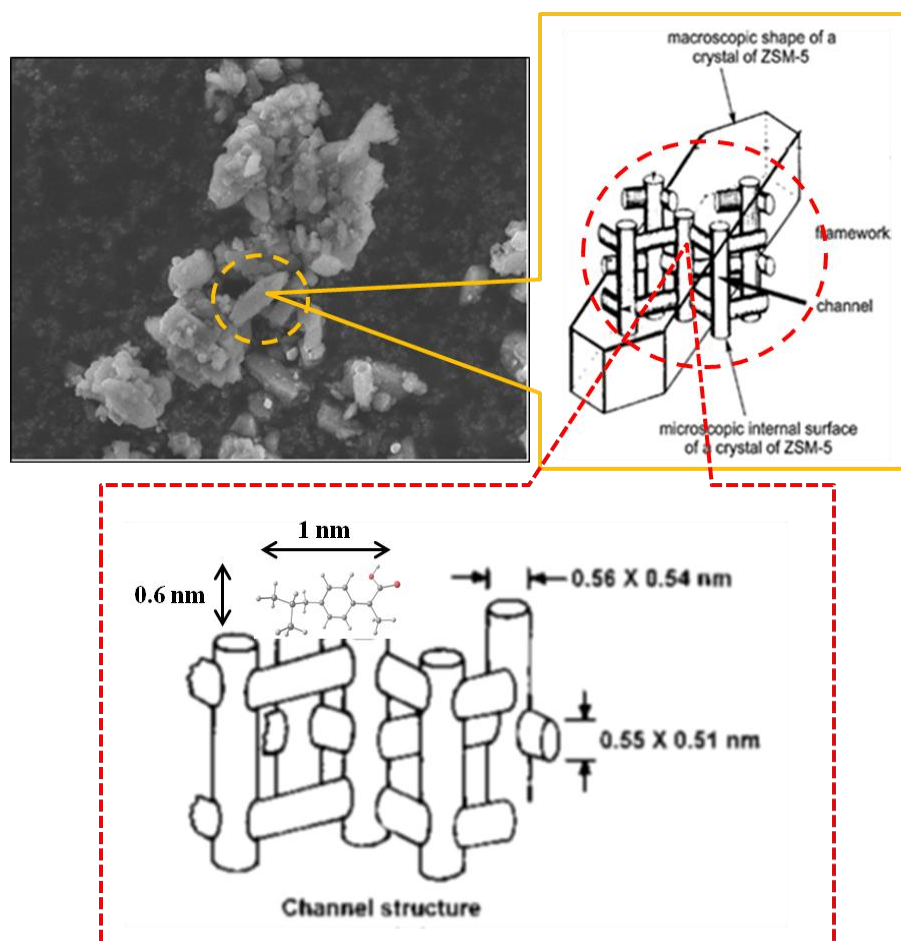


Figure 4.2. Illustration of IBP adsorption on zeolite surface

Since, in the investigated range of catalyst concentration, the majority of IBP molecules were in solution after adsorption, the evolution of liquid phase concentrations allowed to evaluate the oxidation performance. Concentration of IBP (TOC) in the liquid phase after adsorption was then used as reference.

4.1.2. Fenton oxidation of ibuprofen over Fe-MFI and ZVI catalysts

Comparison of the catalytic activity of Fe-MFI and ZVI for Fenton oxidation of IBP was performed under the following operating conditions: [Fe-MFI] = 1 g/L, [ZVI] = 0.056 g/L, [H₂O₂]₀ = 6.4 mM, pH₀ = 3.5 – 4.3 (initial solution pH before contacting with solid), T = 25°C. According to iron dispersion measured by CO chemisorption (see § 2.1.2.5), 1 g/L of Fe-MFI should correspond to 0.13 mM of accessible iron (vs. 0.61 mM of total Fe), same as used for homogeneous Fenton oxidation (“high concentration level”, see chapter 3).

On the other hand, concentration of ZVI (0.056 g/L) was chosen so that the total iron amount (1 mM according to supplier purity data) was of same order of magnitude as with 1 g/L of Fe-MFI. It should be recalled however that, according to S_{BET} value (0.5 m²/g), iron dispersion on ZVI should be lower than 0.1% (cf. chapter 2, table 2.8).

Heterogeneous Fenton experiments started with a preliminary step without oxidant to separate as far as possible the contribution of adsorption and oxidation to the pollutant removal in solution. As abovementioned, 120 min allowed to reach equilibrium for Fe-MFI, and the same duration was fixed for ZVI. The oxidation step was then initiated by injection of hydrogen peroxide (H₂O₂). In the case of Fe-MFI, the test conducted without any pH adjustment led to a partial conversion of IBP and TOC (figures 4.3A and 4.3B), as well as to some consumption of H₂O₂ (figure 4.3C) confirming that Fe-MFI was able to catalyze H₂O₂ decomposition and oxidize IBP. Conversely, no catalytic activity of ZVI was observed (negligible IBP degradation or H₂O₂ consumption), despite some study mentioned H₂O₂ decomposition under circumneutral pH conditions (pH=4-6) over this catalyst [73,85,198,239]. The pH value for optimum ZVI activity being usually around 3 [73,85,198,239], Fenton oxidation with ZVI catalyst was also performed at pH₀ = 3.5 (using 1 M H₂SO₄ for preliminary acidification). Under such acidic condition, a remarkable catalytic activity of ZVI was observed, in which 90% of IBP and 10% of TOC were removed after 30 min of oxidation (figure 4.3).

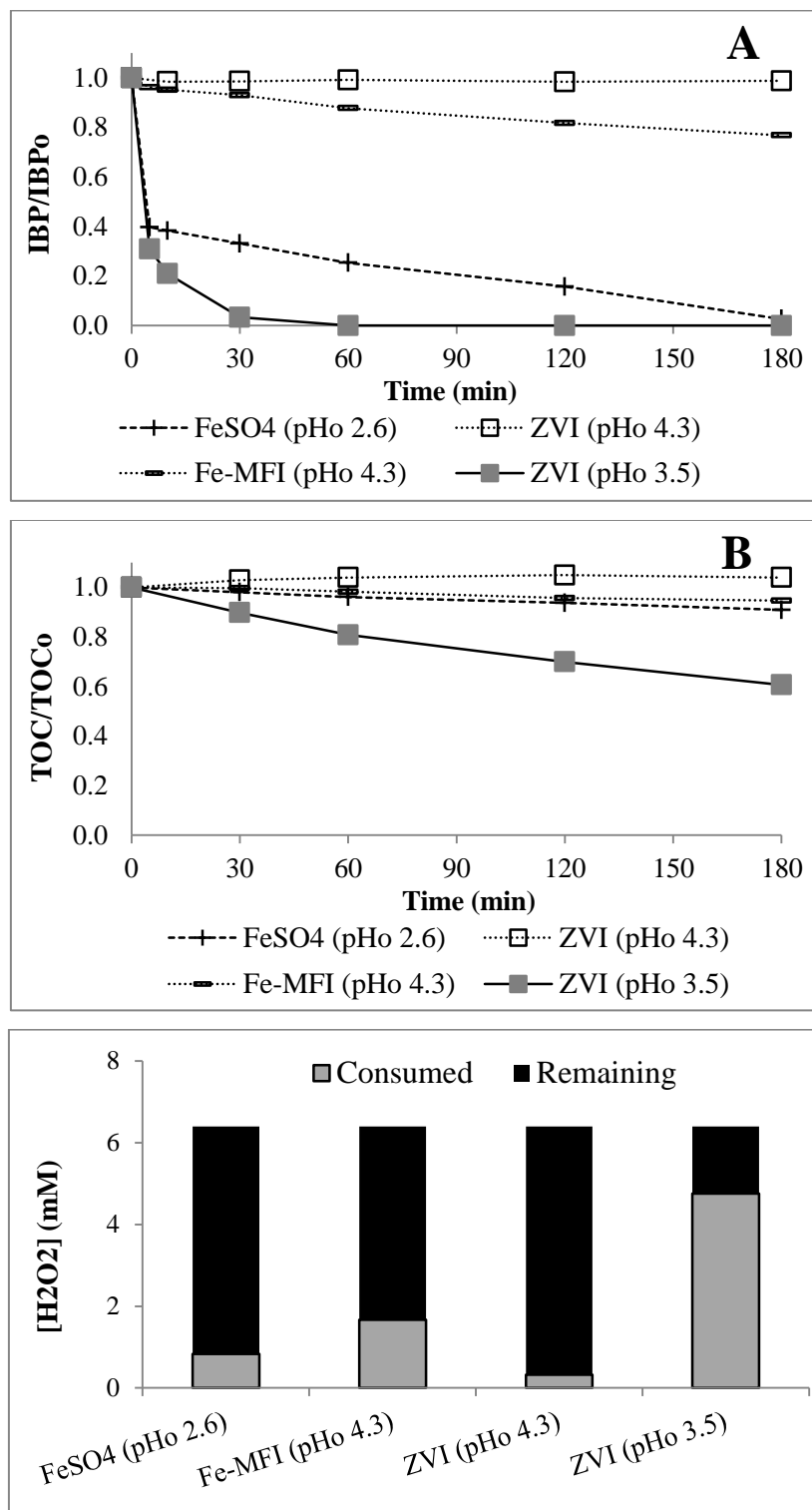


Figure 4.3. Fenton oxidation of ibuprofen over ZVI and Fe-MFI catalysts: evolution of (A) IBP and (B) TOC concentration and (C) H₂O₂ consumption ([IBP]₀ = 20 mg/L, [Fe-MFI] = 1 g/L, [ZVI] = 0.056 g/L, [H₂O₂]₀ = 6.4 mM, T = 25°C). Homogeneous Fenton oxidation using 0.13 mM of FeSO₄·7H₂O was recalled for comparison

Comparison of homogeneous and heterogeneous Fenton reaction has been scarcely investigated, and in almost all cases based on the same total iron amount. For instance, it was

reported that H_2O_2 decomposition (determined as the oxygen release rate measured barometrically) was three times faster using iron salt ($\text{Fe}(\text{NO}_3)_3$) than Fe-ZSM5 [277] as catalyst. Kusić and coworkers [80] also observed that Fenton oxidation of phenol was faster with ferrous or ferric salt than with Fe-ZSM5 (total pollutant conversion being achieved in 2 vs. 30 min, respectively). Conversely, Centi and coworkers [84] reported that Fe-ZSM5 led to a higher removal efficiency (72% in 60 min) of propionic acid than ferric salt (43% in 60 min). Velichkova et al. [30] compared the activity of the same iron containing zeolite as the one used here (Fe-MFI-27) to that of the homogeneous system for the Fenton oxidation of paracetamol. They found a similar mineralization yield of about 30% with 2 g.L^{-1} of Fe-MFI at natural pH (corresponding to *ca.* 0.3 mM of accessible iron) and 0.6 mM of ferrous salt at $\text{pH}_0 = 2.6$ ($T = 45^\circ\text{C}$, $[\text{H}_2\text{O}_2]_0 = 14 \text{ mM}$).

In the present study, based theoretically on the same amount of accessible iron (0.134 mM), IBP oxidation catalyzed by Fe-MFI was clearly slower than the homogeneous reaction catalyzed by $\text{FeSO}_4 \cdot 7\text{H}_2\text{O}$ at the initial stage (figure 4.3A). To check for possible detrimental effect of the adsorbed pollutant (competition with H_2O_2 for iron active sites or porosity blockage), H_2O_2 decomposition by Fe-MFI catalyst was also monitored without IBP. It resulted into 31% of H_2O_2 conversion after 180 min, which was similar to that measured during the oxidation of IBP (26%) indicating the minor role of adsorbed IBP. Interestingly, after the 5 first minutes, the rate of the homogeneous reaction was very similar to that observed with Fe-MFI, suggesting that the initial activity difference could be due to iron speciation (ferrous vs. ferric iron). In accordance with Velichkova et al. [30] both systems yielded similar TOC removal (figure 4.3B).

Furthermore, accounting for the very low iron dispersion on ZVI, it is noticeable that this catalyst outperformed the homogeneous system when the solution was initially acidified, and suggests extensive leaching. These parameters, as well as the aging of the solid catalysts are examined in the following section.

4.1.3. Evaluation of Fe-MFI and ZVI catalysts after reaction

The morphology and iron content of Fe-MFI and ZVI catalysts before and after reaction were investigated by SEM-EDX. Morphology of Fe-MFI catalyst was found unchanged after Fenton oxidation (figures 4.4A and 4.4B), as well as estimated “surface” iron content

($3.3 \pm 1.0\%$ (after Fenton) vs. $3.1 \pm 0.9\%$ (initial)). ICP-AES analysis (table 4.1) confirmed that iron leaching from Fe-MFI catalyst was negligible.

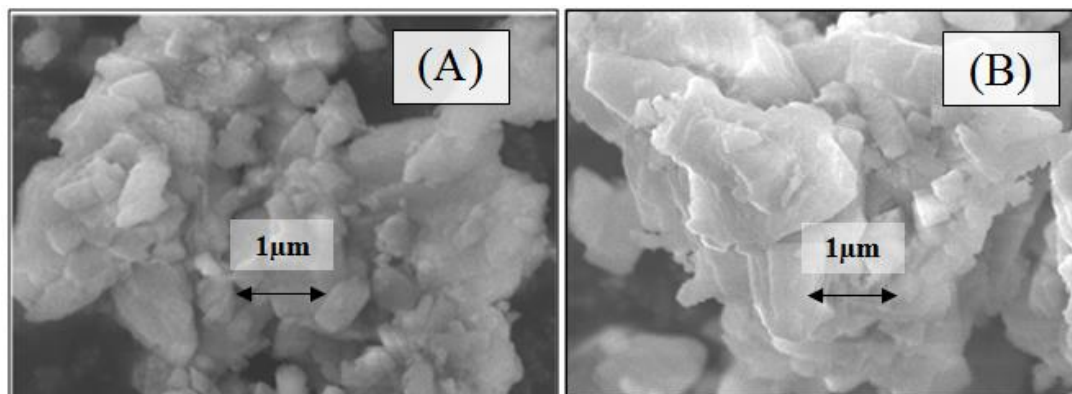


Figure 4.4. SEM images of (A) fresh and (B) used Fe-MFI catalyst after Fenton oxidation

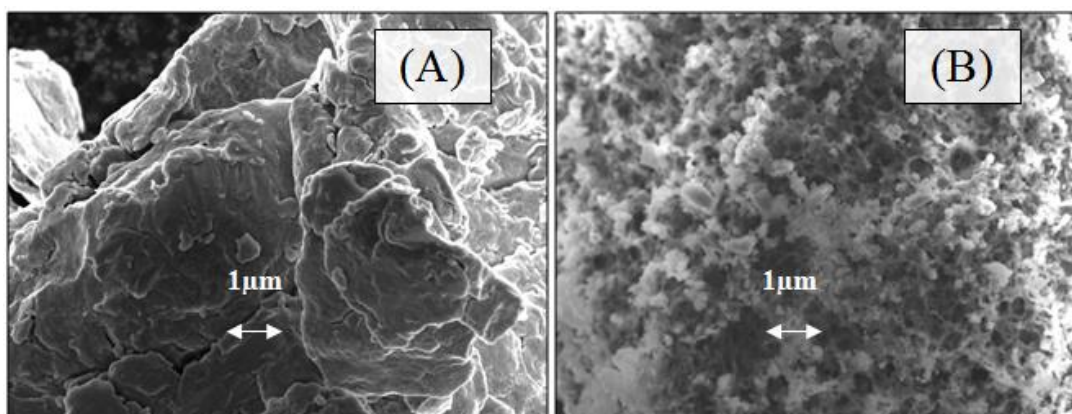


Figure 4.5. SEM images of (A) fresh and (B) used ZVI ($\text{pH}_0 = 3.5$)

Table 4.1. Iron leaching from tested solids

System	[Catalyst] ⁽¹⁾ g/L	[Fe] _{total} ⁽²⁾ mg/L	$\text{pH}_0 / \text{pH}_f$ ⁽³⁾	Iron leaching ⁽⁴⁾ mg/L
Fenton (Fe-MFI)	1	34	4.3 / 3.7	0.014
Fenton (ZVI)	0.056	56	4.3 / 4.3	0.009
Fenton (ZVI)	0.056	56	3.5 / 3.6	3.3

(1) Concentration of solid catalyst; (2) Corresponding total iron concentration; (3) pH of IBP solution / pH at the end of the experiment; (4) Concentration of total dissolved iron at the end of experiment

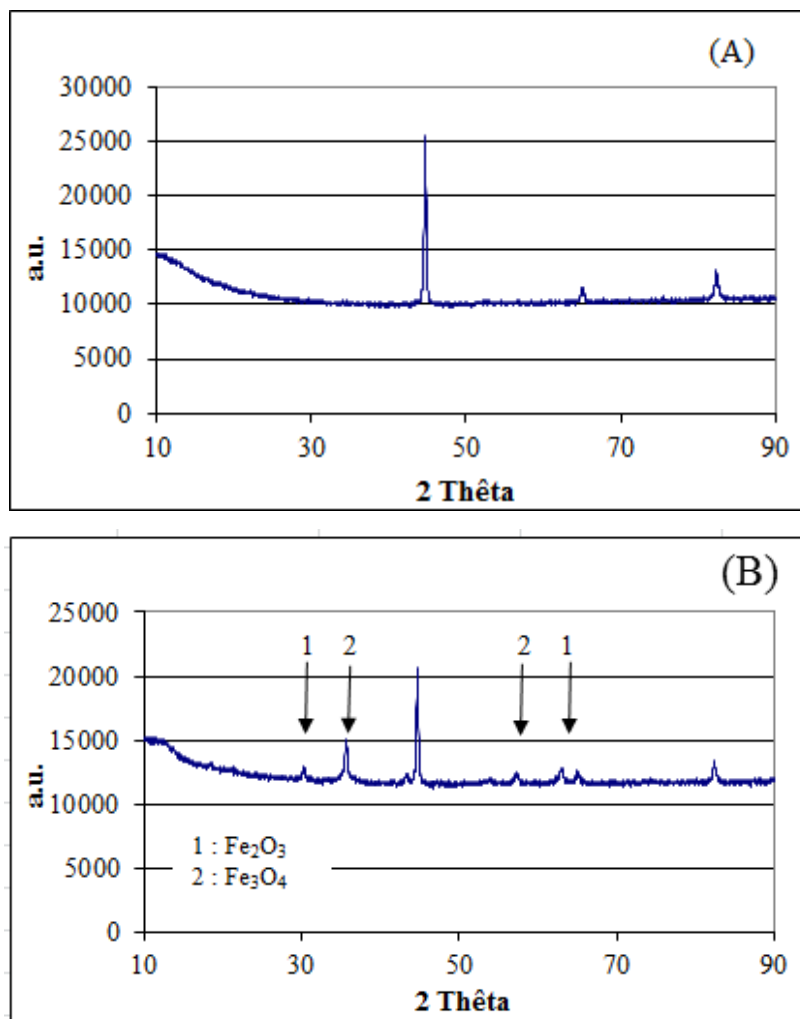


Figure 4.6. XRD analysis of (A) fresh and (B) used ZVI

On the contrary, ZVI surface became coarser due to the formation of numerous little clusters indicating a corroded surface (figures 4.5A and 4.5B). Estimation of elemental composition by EDX analysis also confirmed oxidation of ZVI surface, oxygen content increasing from 2.3% to 20.2%. According to XRD analysis (figure 4.6B), other diffraction peaks were observed at $2\theta = 30.03^\circ$ and 63.03° matching with maghemite (Fe_2O_3) pattern (PDF 39-1346), and at $2\theta = 35.69^\circ$ and 57.32° corresponding to magnetite (Fe_3O_4) (PDF 75-0449). These peaks were not present on the original particle spectrum (cf. figure 4.6A).

Evaluation by ICP-AES of dissolved iron concentration after reaction with ZVI showed that acidic condition caused significant iron leaching (3.3 mg/L *i.e.* 0.06 mM of Fe) from this catalyst (table 4.1). This concentration in solution is lower than that used for the homogenous reaction depicted in figure 4.3 and possible mechanism explaining the higher activity of this system with respect to ferrous salt is addressed in the next section.

4.1.4. Mechanisms of Fenton reaction over investigated catalysts

Fenton reaction with iron-containing solids can occur according to two main mechanisms, *i.e.*, a true heterogeneous one implying surface iron species and a homogeneous one induced by metal ions leached in the solution [65]. Due to acidification with H₂SO₄, significant iron leaching occurred from ZVI (3.3 mg/L) that should in fact be responsible for its catalytic activity at pH₀ 3.5. Under acid (and H₂O₂) addition, ZVI was corroded and released Fe²⁺ into the solution which subsequently reacted with H₂O₂ and generated •OH as per homogeneous Fenton mechanism (reactions R.4.1 to R.4.3). Several authors [85,138,203] proposed that a fast reduction of Fe³⁺ to Fe²⁺ should occur on Fe⁰ surface, which was mentioned as the main advantage of ZVI over iron salt catalyst, but could be limited by the availability of Fe⁰ on the surface [203]. In any case, a continuous release of iron in solution should lead to a better utilization than addition at once.

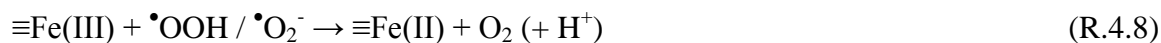


(notation \equiv indicates species on catalyst surface)

Conversely, real heterogeneous Fenton reaction seemed to occur on Fe-MFI catalyst owing to its low iron leaching (0.014 mg/L). As described in chapter 1, true heterogeneous Fenton is based on the activity of iron species (Fe^{II} and Fe^{III}) present on the catalyst surface, which lead to radical [70,75] and/or non-radical mechanisms [50,65,74] according to the following reactions:

Radical mechanism (involving hydroxyl radical •OH):





Non-radical mechanism (involving high-valent iron species **Fe(IV)**):



In order to evaluate the contribution of free radicals in Fenton reaction catalyzed by Fe-MFI, a complementary experiment was carried out with and without methanol (CH_3OH) as radical scavenger ($[\text{CH}_3\text{OH}] = 50 \text{ mM}$, *i.e.* 500 times higher than molar concentration of IBP). In this experiment, methanol was injected after adsorption step (at the same time as the injection of H_2O_2). Experimental conditions were kept similar ($[\text{H}_2\text{O}_2] = 6.4 \text{ mM}$, $T = 25^\circ\text{C}$, $\text{pH}_0 = 4.3$), except that Fe-MFI concentration was set to higher level (4.8 g/L). High Fe-MFI concentration should increase IBP removal efficiency and facilitates the evaluation of the radical scavenger effect. From [figure 4.7](#), it can be seen that the presence of excess methanol reduced IBP removal yield from 88% to 23% (with similar H_2O_2 consumption of about 80%) after 3 h. This result is in contrast to the homogeneous Fenton reaction for which complete inhibition was observed in the presence of methanol (see [§ 3.1.4](#)). However, methanol might have scavenged only radicals within the liquid bulk, so that this residual activity could be explained either from a parallel non-radical mechanism or a radical one but involving adsorbed IBP.

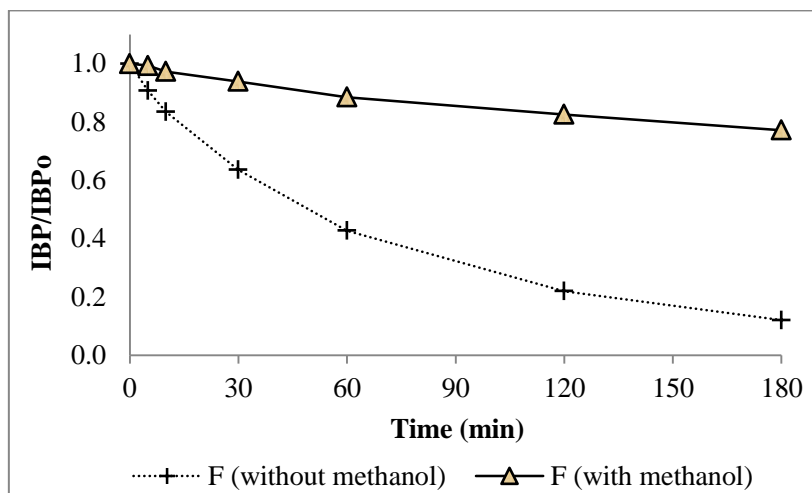


Figure 4.7. Effect of methanol on heterogeneous Fenton oxidation of IBP over Fe-MFI
 ([IBP]₀ = 20 mg/L, [Fe-MFI] = 4.8 g/L, [H₂O₂]₀ = 6.4 mM, T = 25°C)

As abovementioned, the presence of different iron active species (*i.e.* ≡Fe(III) and Fe²⁺) may be responsible for the different initial catalytic activity observed in heterogeneous and homogeneous systems. Moreover, while in homogeneous reaction dissolved ferrous ions directly react with H₂O₂ to form [•]OH, the heterogeneous reaction involves several serial steps including H₂O₂ diffusion into the catalyst pores to the active sites, chemisorption of H₂O₂ onto ≡Fe(III) sites to form ≡Fe(III)(H₂O₂) surface complex (R.4.5), dissociation of this ferric complex into ≡Fe(II) species (R.4.6) and reaction between ≡Fe(II) and H₂O₂ to generate [•]OH (R.4.7). Subsequently, [•]OH might attack IBP adsorbed on the zeolite framework and/or in the bulk solution [68]. Since the half-life of [•]OH radical is only a few nanoseconds and its migration distance is only a few micro-meters [65], reaction with IBP in bulk solution might be in fact limited on the most external surface of Fe-MFI catalyst.

The catalytic activity of iron-containing zeolite catalyst is thus not only influenced by the iron content, but also metal dispersion, type of iron species [191], intensity of Brønsted-lewis acid sites [86], and possibly pore size distribution and particle size [177,277] if diffusional limitations are involved.

Due to its negligible iron leaching (and thus truly heterogeneous catalytic mechanism), Fe-MFI was selected for further investigation on heterogeneous Fenton oxidation.

4.2. PARAMETRIC STUDY

Prior to evaluate possible sono- and/or photo-activation of the heterogeneous Fenton reaction, a parametric study was first carried out to investigate the effect of catalyst concentration, hydrogen peroxide concentration, pH and temperature. Except in the last two cases, the pH of the IBP solution was not modified and the temperature was set to 25°C. As abovementioned, a preliminary adsorption step (120 min) was conducted in order to discriminate IBP removal by adsorption and oxidation.

4.2.1. Effect of solid catalyst concentration

In this study, concentration of Fe-MFI was varied in between 1 and 4.8 g/L, which should correspond to 0.13 – 0.62 mM of accessible iron. This investigated range was thus larger than for the homogeneous reaction, thanks to iron immobilization allowing easy catalyst separation and recycling. In these conditions, increasing Fe-MFI concentration was always found beneficial for both IBP and TOC removal (figures 4.8A and 4.8B).

IBP degradation was well fitted by a first-order kinetic law, resulting in: $k_{1\text{g/L}} = 0.0014 \text{ min}^{-1}$ ($R^2=0.9741$), $k_{3\text{g/L}} = 0.0071 \text{ min}^{-1}$ ($R^2=0.9984$), $k_{4.8\text{g/L}} = 0.0139 \text{ min}^{-1}$ ($R^2=0.9976$). There was thus no plateauing of the oxidation rate when increasing the catalyst concentration, which excludes any significant radical scavenging effect from surface iron species. The fact that rate constants did not strictly increase proportionally with respect to the Fe-FMI concentration could make suspect a possible role of the pollutant adsorption inducing nonlinear effects.

The effect of solid catalyst concentration could be explained by a higher amount of active sites for H_2O_2 decomposition, as confirmed by the increased oxidant consumption (figure 4.8C). Note however that it was higher than in the homogeneous reaction (1.7 mM or 26% with 1 g/L of Fe-MFI vs. 0.85 mM or 13% with $[\text{Fe}^{2+}] = 0.134 \text{ mM}$), despite the conversion of IBP was much lower. According to the literature, higher H_2O_2 consumption in the heterogeneous system could be attributed to the decomposition of H_2O_2 to water and oxygen on the zeolite surface [84].

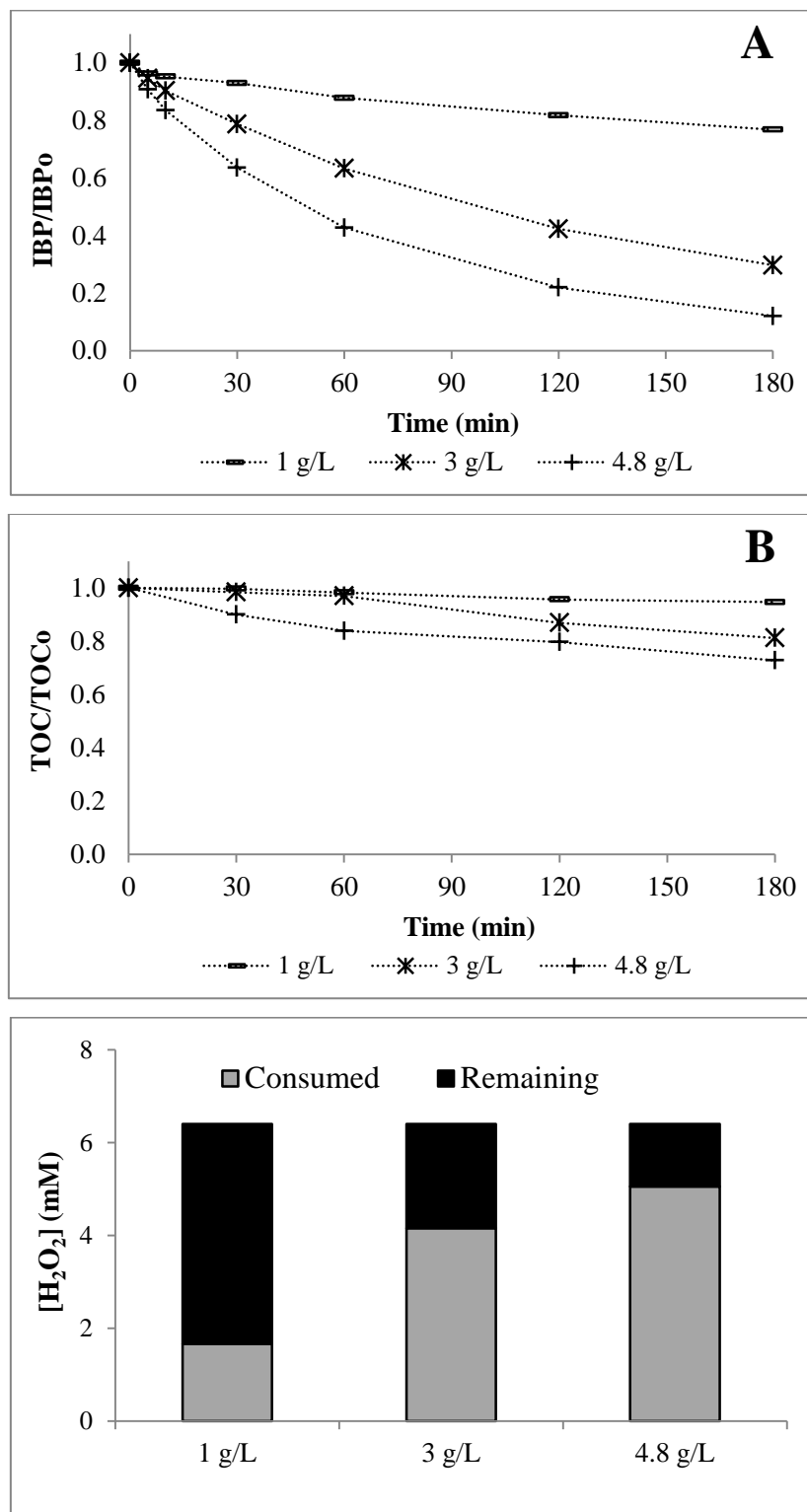


Figure 4.8. Effect of Fe-MFI concentration on Fenton oxidation: evolution of (A) IBP and (B) TOC concentration, and (C) H₂O₂ consumption ([IBP]₀ = 20 mg/L, [Fe-MFI] = 1 – 4.8 g/L, [H₂O₂]₀ = 6.4 mM, pH₀ = 4.3, T = 25°C)

The observed trends were consistent with previous studies using Fe-ZSM5 catalyst. Olmos et al. [191] and Makhotkina et al. [190] reported that increasing catalyst concentration improved the oxidation of acetone and MTBE, even at very high concentrations (5-25 and 5-70 g/L of Fe-ZSM5, respectively).

4.2.2. Effect of H₂O₂ concentration

As seen in chapter 3 for the homogeneous systems, an optimal dosage is expected for the oxidant, due to the scavenging of •OH provoked by a too large excess. On the other hand, iron containing zeolite decomposing part of H₂O₂ into water and oxygen, it should shift this optimum to a higher value. In this study, the catalyst concentration was set at 4.8 g/L and three levels of H₂O₂ concentration were tested - 1.6, 6.4 and 22.4 mM - corresponding to 0.5, 2 and 7 times the stoichiometric amount needed for complete mineralization of IBP. It should be recalled that for sono- and photo-oxidation (without catalyst) the optimal H₂O₂ concentration lay in between the last two values.

As depicted in [figure 4.9A](#), IBP oxidation rate increased with H₂O₂ dosage on the whole investigated range due to the abovementioned effect of Fe-FMI. Moreover the first-order rate constant was found proportional to the concentration of oxidant: $k_{1.6 \text{ mM}} = 0.0029 \text{ min}^{-1}$ ($R^2=0.9678$), $k_{6.4 \text{ mM}} = 0.0139 \text{ min}^{-1}$ ($R^2=0.9976$), $k_{22.4 \text{ mM}} = 0.0411 \text{ min}^{-1}$ ($R^2=0.9983$).

H₂O₂ effect was however somewhat different regarding TOC removal. Increasing H₂O₂ concentration from 1.6 mM to 6.4 mM enhanced TOC conversion from 11% to 27%, but further increase to 22.4 mM resulted in only a slight positive effect (28% of mineralization), mainly due to some levelling off after 60 min. This kind of plateau in TOC removal profile was also observed by previous studies [163,165,167]. It might result from the complexation of iron active sites by oxidation intermediates, that hampered Fenton cycle [167], or to the formation of intermediates exhibiting slower rate constants for radical attack (especially small organic compounds, such as carboxylic acids [36]). Moreover, under excess of H₂O₂ higher iron leaching concentration was observed (0.1 mg/L of Fe at 22.4 mM H₂O₂ vs. 0.048 mg/L at 6.4 mM H₂O₂) – which might be the result of higher complexation of surface iron. Note also that similar amount of H₂O₂ was consumed -5.1 mM vs. 6.5 mM - when starting with either 6.4 mM or 22.4 mM, respectively ([figure 4.9C](#)). These results confirmed that a too large excess was useless to further improve IBP mineralization.

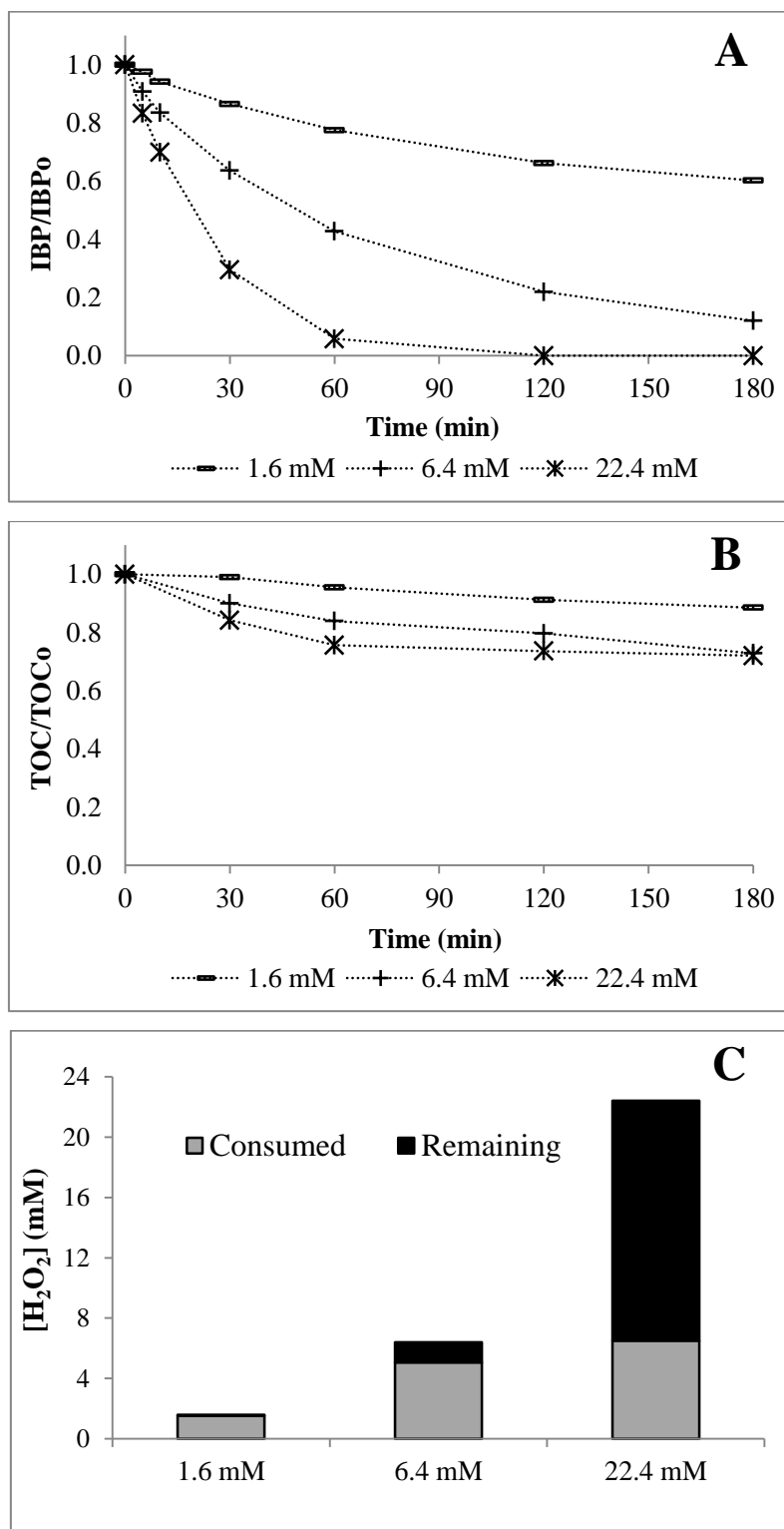


Figure 4.9. Effect of H₂O₂ concentration on Fenton oxidation over Fe-MFI: evolution of (A) IBP and (B) TOC concentration, and (C) H₂O₂ consumption ([IBP]₀ = 20 mg/L, [Fe-MFI] = 4.8 g/L, [H₂O₂] = 1.6 – 22.4 mM (0.5 – 7 times stoichiometric amount), pH₀ = 4.3, T = 25°C)

4.2.3. Effect of H₂O₂ / Fe molar ratio

Effect of Fenton reagent is usually investigated by varying iron concentration while keeping H₂O₂ concentration unchanged and vice versa. On the other hand, the molar ratio of H₂O₂ / Fe appears as a key parameter to control the performance of Fenton oxidation and optimum ratios between 10 – 50 have been reported in the literature [14, 32–36]. In order to evaluate this role, different amounts of H₂O₂ and Fe-MFI were tested for two different molar ratios matching lower and upper bounds of the interval. The corresponding experimental conditions are given in [table 4.2](#). Note that the molar ratio was calculated based on the corresponding concentration of accessible iron (instead of total iron) in the suspension as it should be more relevant.

Table 4.2. Experimental conditions for effect of H₂O₂ / Fe molar ratio

Experiment	Ratio	[H ₂ O ₂]	[Fe-MFI]	[Fe] ^c
	H ₂ O ₂ /Fe	(mM)	(g/L)	(mM)
R=48 ^a ;1x ^b	48	3.2	0.5	0.07
R=48;2x	48	6.4	1	0.13
R=10;1x	10	3.2	2.4	0.32
R=10;2x	10	6.4	4.8	0.64

^a R : ratio of molar [H₂O₂] / [Fe]

^b 1x, 2x : [H₂O₂] corresponds to 1 or 2 times the stoichiometric amount for pollutant mineralization

^c [Fe] : corresponding concentration of accessible iron in the slurry (according to CO chemisorption)

IBP and TOC time-concentration profiles exhibited in [figure 4.10A](#) and [figure 4.10B](#), respectively, seem to indicate that low H₂O₂ / Fe molar ratio (R) promoted faster oxidation than high value. For instance, after 3 hours of reaction, IBP conversion was more than 65% at R = 10, but less than 25% at R = 48. However, even higher IBP removal rate was achieved with 22.4 mM of H₂O₂ and 4.8 g/L of Fe-MFI (cf. [figure 4.9A](#)), *i.e.* for R = 35. Thus, the reaction performance could not in fact be reduced to this sole parameter for the investigated catalyst, probably due to non-radical decomposition of H₂O₂ over Fe-MFI.

In particular, the effect of increasing H₂O₂ concentration from 3.2 mM (1x) to 6.4 mM (2x) was more significant at low H₂O₂/Fe ratio. Due to the higher concentration of active surface species for H₂O₂ decomposition at R = 10, more than half of H₂O₂ was consumed by the reaction, while it was the reverse at R = 48 ([figure 4.10C](#)). Therefore oxidant concentration was more limiting in the first case.

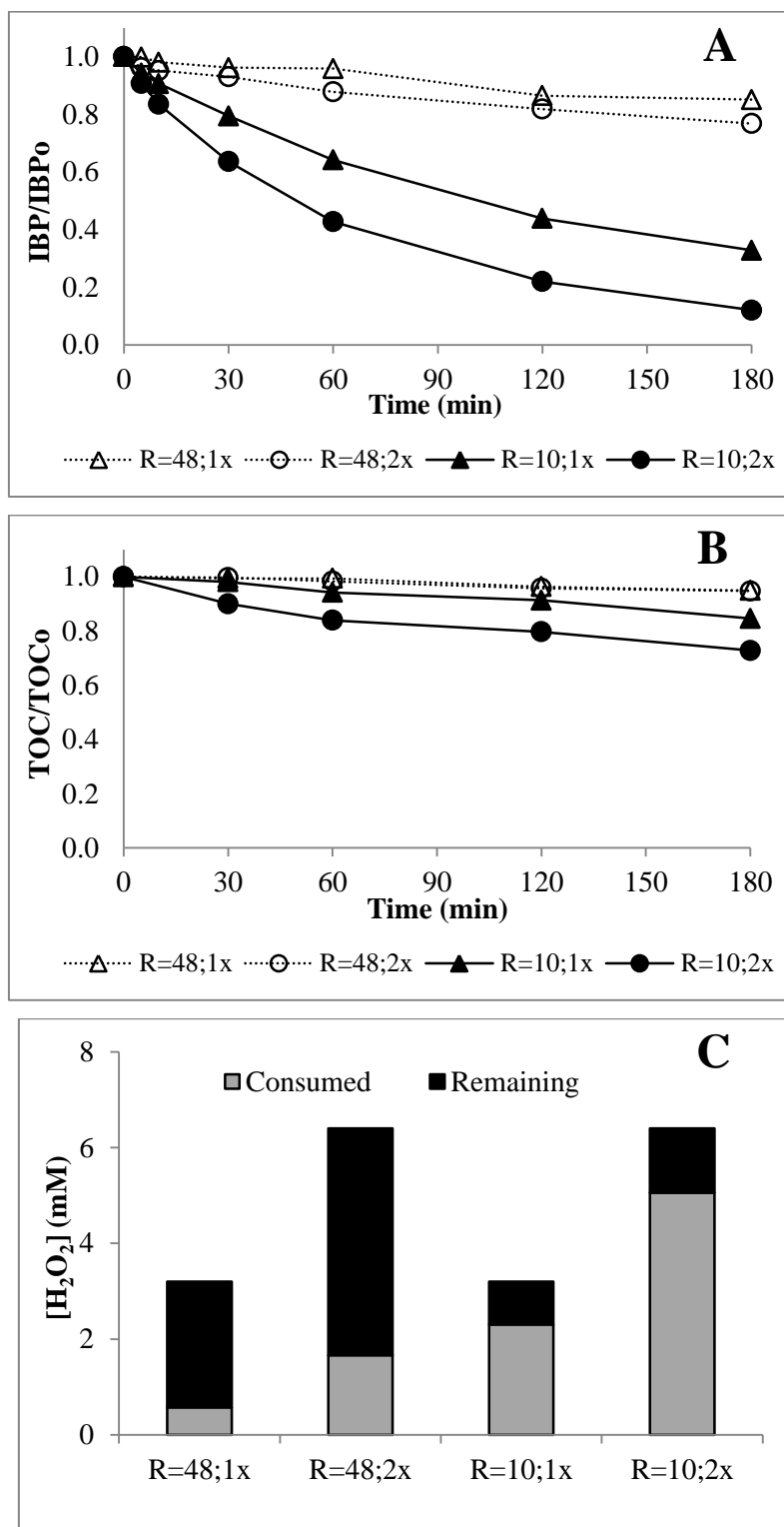


Figure 4.10. Effect of H₂O₂ / Fe molar ratio on Fenton oxidation over Fe-MFI: evolution of (A) IBP and (B) TOC concentration, and (C) H₂O₂ consumption ([IBP]₀ = 20 mg/L, R = 10 – 48, [Fe-MFI] = 0.5 – 4.8 g/L, [H₂O₂]₀ = 3.2 – 6.4 mM, pH₀ = 4.3, T = 25°C)

4.2.4. Effect of temperature

Based on Arrhenius law, it is expected that an increase in temperature leads to a faster generation of hydroxyl radicals by the Fenton reaction. On the other hand, it also increases the rate of wasteful reactions, and temperature effect thus depends on the respective activation energies. Previous studies in heterogeneous Fenton oxidation using Fe-ZSM5 catalyst reported that catalytic activity was improved by increasing temperature (from 10°C to 80°C) and no optimum value was observed [84,86,177,190].

Three levels of temperature, *i.e.* 15°C, 25°C and 45°C, were investigated here, resulting only in a marginal effect on IBP adsorption. A clear enhancement in terms of IBP oxidation rate constant ($k_{15^{\circ}\text{C}} = 0.0057 \text{ min}^{-1}$ ($R^2=0.9946$), $k_{25^{\circ}\text{C}} = 0.0139 \text{ min}^{-1}$ ($R^2=0.9976$), $k_{45^{\circ}\text{C}} = 0.0470 \text{ min}^{-1}$ ($R^2=0.9992$)) was observed at higher temperature (figure 4.11A), leading to an apparent activation energy of 53 kJ/mol. TOC conversion was also improved at higher temperature, but to a lesser extent than IBP conversion (figure 4.11B). As observed previously at the highest H₂O₂ concentration, the removal of TOC plateaued after 60 min for the experiment conducted at 45°C, so that mineralization yield still did not exceed 28%. It should be however noticed figure 4.11C that actually all H₂O₂ was consumed at the end of the experiment performed at 45°C, which in fact explained here why the reaction was stopped.

On the other hand, iron leaching was significantly higher at 45°C (0.21 mg/L of Fe) than at 25°C (0.048 mg/L) and 15°C (0.046 mg/L), and possible contribution of homogeneous contribution will be thus addressed in section 4.2.6. Even though dissolved iron is still below the standard limit for discharge (2 mg/L), metal loss should be minimized to limit catalyst deactivation upon recycling or continuous operation. From economical point of view, working under room temperature is better in industrial scale application. Therefore, room temperature was preferred for further investigation of Fe-MFI. Note however that under process conditions, the reaction could thus benefit from the temperature increase by ultrasound/light activation.

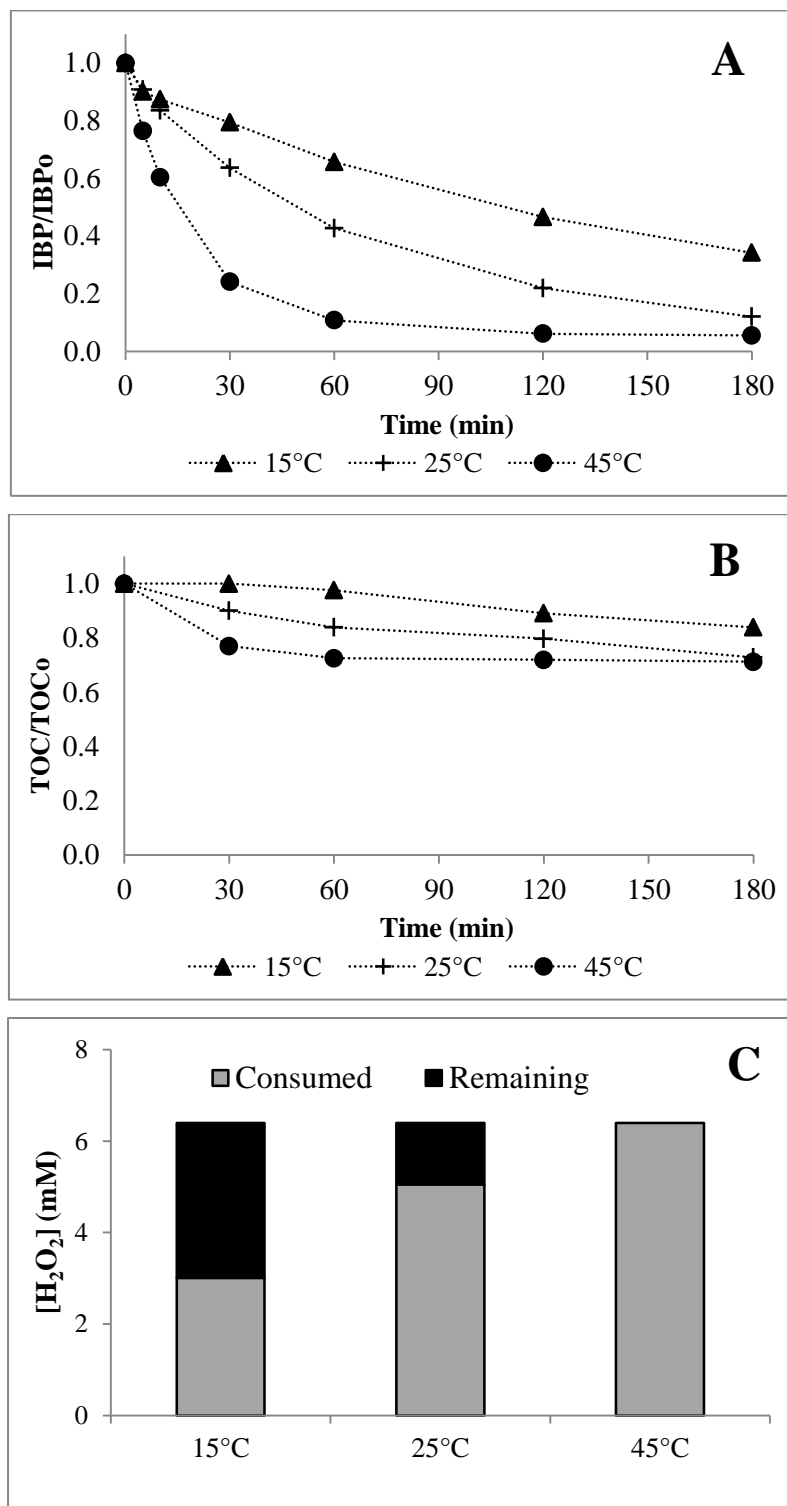


Figure 4.11. Effect of temperature on Fenton oxidation over Fe-MFI: evolution of (A) IBP and (B) TOC concentration, and (C) H₂O₂ consumption ([IBP]₀ = 20 mg/L, [Fe-MFI] = 4.8 g/L, [H₂O₂]₀ = 6.4 mM, pH₀ = 4.3, T = 15 – 45°C)

4.2.5. pH effect

Heterogenization of the Fenton system usually overcomes the classical problem of loss of iron catalyst and narrow pH range (pH = 2 – 4). However, several studies using Fe-ZSM5 catalyst reported that acidic conditions (pH = 3 – 4) were still necessary to obtain appreciable catalytic activity [86,177,190], while others indicated that this type of catalyst could work well under near-neutral pH (pH = 4 – 6) [84,163,165,167]. Velichkova et al. [165] observed that the oxidation rate of paracetamol over Fe-MFI was similar with or without preliminary acidification of the solution (at pH₀ 2.8), probably due to the zeolite ability to significantly lower the pH (from 5.5 to 3.6). As abovementioned, the acidity of Fe-MFI is due to the presence of Brønsted and Lewis acid sites on the zeolite [201].

The investigation of pH effect was here carried out close to neutral conditions (pH = 4 – 8) with or without controlled pH. This range was also chosen to mimic the pH of a real wastewater matrix which is usually buffered at circumneutral or slightly alkaline value [67,164,178,278]. The experimental conditions are given in [table 4.3](#) and the experiments were performed with 4.8 g/L of Fe-MFI.

Table 4.3. Experimental conditions for pH effect

Experiment	pH ₀	pH _i	pH _f	pH setting method
pH 4.3	4.3	3.3	3.2	Experiment was conducted with the synthetic IBP solution without pH adjustment
pH 6.0	6.0	3.3	3.2	pH of the solution was set to 6.0 using NaOH 1 M before contact with solid catalyst
pH 8.0	8.0	3.6	3.5	pH of the solution was set to 8.0 using NaOH 1 M before contact with solid catalyst
pH 7.0 (controlled)	7.0	7.0	7.0	pH of the solution was adjusted to 7 (± 0.2) using NaOH 1 M during the experiment

pH₀: initial pH of the solution, pH_i: pH of the solution after adsorption step, pH_f: pH of the solution at the end of reaction

Increasing the initial pH of the solution to 6 or 8 had negligible influence on IBP time-concentration profile, which was almost superimposed to that obtained without pH adjustment ([figure 4.12A](#)), and led to a small reduction of TOC conversion for the highest

value (figure 4.12B). In addition, similar IBP adsorption was also observed during the preliminary solid-liquid contacting phase. As abovementioned, these results could be explained by the ability of Fe-MFI to acidify the different solutions ($\text{pH}_0 = 4.3 - 8$) towards almost single pH value ($\text{pH}_i = 3.3 - 3.6$) during the adsorption step (table 4.3).

On the contrary, IBP adsorption was reduced from 25% to 5% and degradation kinetics was significantly hampered if the reaction was performed under a controlled pH of 7 by continuous addition of NaOH during the experiment: IBP removal rate was found 12 times slower ($k = 0.0012 \text{ min}^{-1}$) than under non-controlled pH, and final TOC abatement decreased from 27% to 7%. Under this condition, IBP was in ionic form and zeolite surface was negatively charged, thus leading to electrostatic repulsion. This observation provides support for the hypothesis that of $\bullet\text{OH}$ attack in heterogeneous Fenton oxidation of IBP mainly occurred on the catalyst surface.

Moreover, lower IBP and TOC conversions at pH 7 were not followed by lower H_2O_2 consumption, figure 4.12C. It is noteworthy to recall that the mixture of IBP and H_2O_2 (6.4 mM) was previously found to be stable at pH 8, as self-decomposition of H_2O_2 only occurs only at $\text{pH} > 10$ [279,280].

Similar trends were reported by Makhotkina et al. [190] for the wet peroxide oxidation of 1,1-dimethylhydrazine over Fe-ZSM5 catalyst: the molecule abatement was lower at neutral-alkaline pH ($\text{pH}=7-10$) compared to acidic pH ($\text{pH}=2-5$), while H_2O_2 consumption remained similar. The authors argued that different reaction mechanisms occurred depending on pH, as they measured different values of activation energy for the catalytic decomposition of H_2O_2 under alkaline (17 kJ/mol) and acidic (53 kJ/mol) conditions. The former value being closer to that observed in the presence of catalase (7 kJ/mol) or iron oxohydroxides (11 kJ/mol) than in the presence of transition metal ions (30–80 kJ/mol) where free-radical mechanism takes place, alkaline conditions were believed to favor non-radical decomposition route.

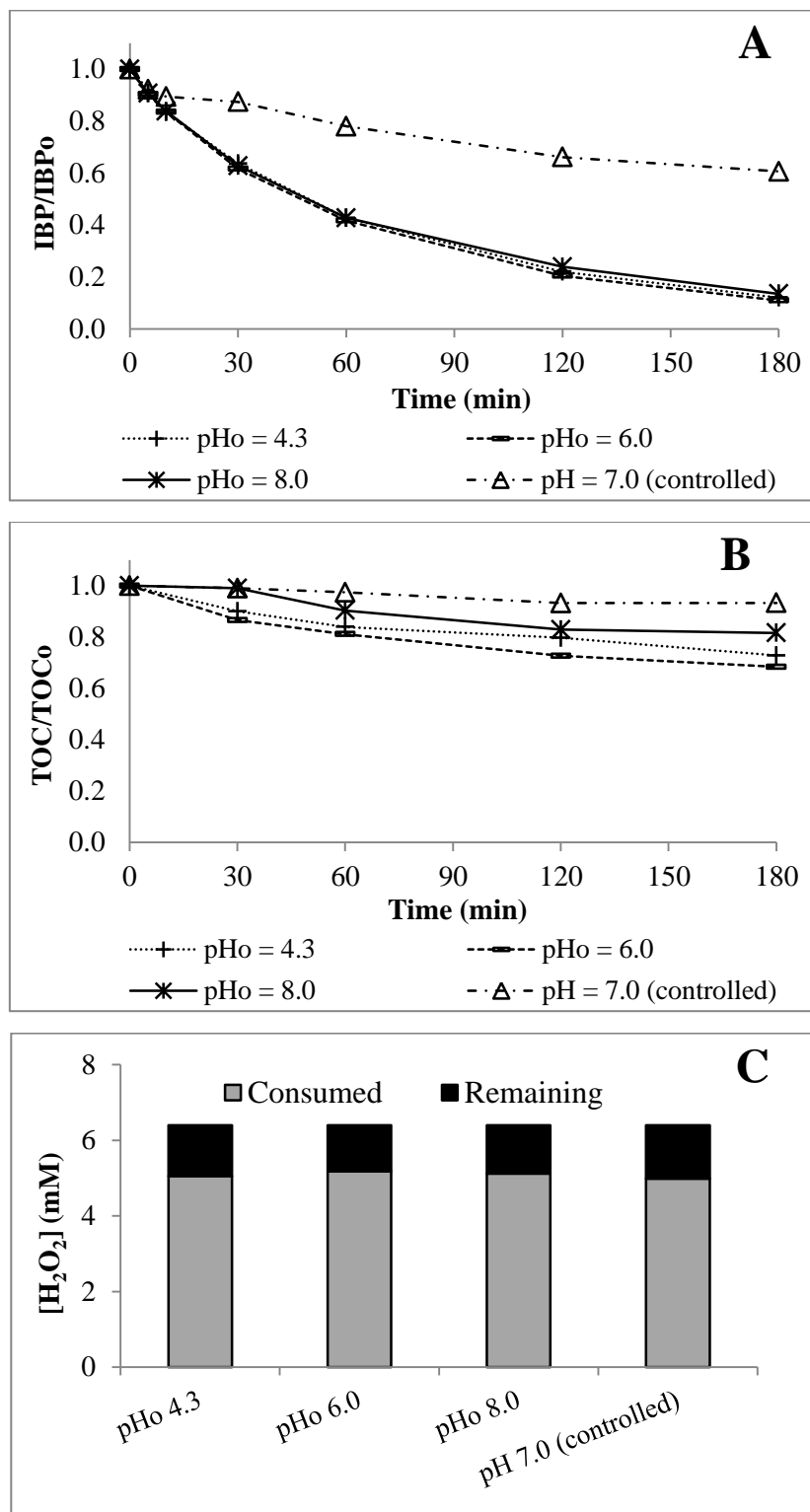


Figure 4.12. Effect of pH on Fenton oxidation over Fe-MFI: evolution of (A) IBP and (B) TOC concentration, and (C) H₂O₂ consumption ([IBP]₀ = 20 mg/L; [Fe-MFI] = 4.8 g/L, [H₂O₂]₀ = 6.4 mM, pH₀ = 4.3-8 or pH controlled at 7, T = 25°C)

Non-radical mechanism at neutral or alkaline pH, mediated by high-valent iron species, was also proposed by other researchers [50,65]. Note that in our case the zeolite support also

induced such mechanism [15]. An alternative explanation for this lower performance at pH 7 could lie in the reduction of $\bullet\text{OH}$ oxidation potential at neutral pH (2.8 V at pH 3 vs 1.9 V at pH 7 [177]).

Regarding iron leaching, increasing pH toward alkaline condition (pH controlled at 7) reduced the concentration of dissolved iron from 0.048 mg/L to 0.024 mg/L.

4.2.6. Activity of leached iron

Metal loss into the solution could initiate homogeneous Fenton reaction, whose contribution should depend not only on the concentration of dissolved iron, but also the nature of the corresponding species (for instance free or as complexes).

First, the concentration of leached iron in the present study (0.048 – 0.21 mg/L corresponding to 0.03 – 0.13 % of total iron content in Fe-ZSM5) was in the lower range compared to that measured in previous works with Fe-ZSM5 catalyst (0.040 – 4 mg/L or 0.4 – 7% of initial catalyst content) [84,162,163,165,167]. Iron leaching rate is influenced by many factors including pH, temperature, catalyst particle size, but also H_2O_2 concentration [84,177] and intermediates formed during reaction [165]. It should be also mentioned that commercial Fe-ZSM5 catalyst [163,165] is usually more stable than laboratory-prepared Fe-ZSM5 [84,162,167].

Nonetheless, despite these wide variations in dissolved iron concentration (0.04 – 4 mg/L), negligible contribution of homogeneous reaction was always reported when examined [84,162,165].

To verify this point in the present conditions, activity of the leachates was also examined. The suspensions collected after heterogeneous oxidation experiment at 25°C ([Fe] leached = 48 $\mu\text{g/L}$) and 45°C ([Fe] leached = 210 $\mu\text{g/L}$) - both at 4.8 g/L Fe-MFI and 6.4 mM H_2O_2 - were filtered on a 0.2 μm pore size membrane. Then the leachates were complemented with IBP and H_2O_2 to match previous initial conditions. [Figure 4.13A](#) and [figure 4.13B](#) compare the time-concentration profiles of IBP and TOC during Fenton oxidation with Fe-MFI catalyst and corresponding filtrate.

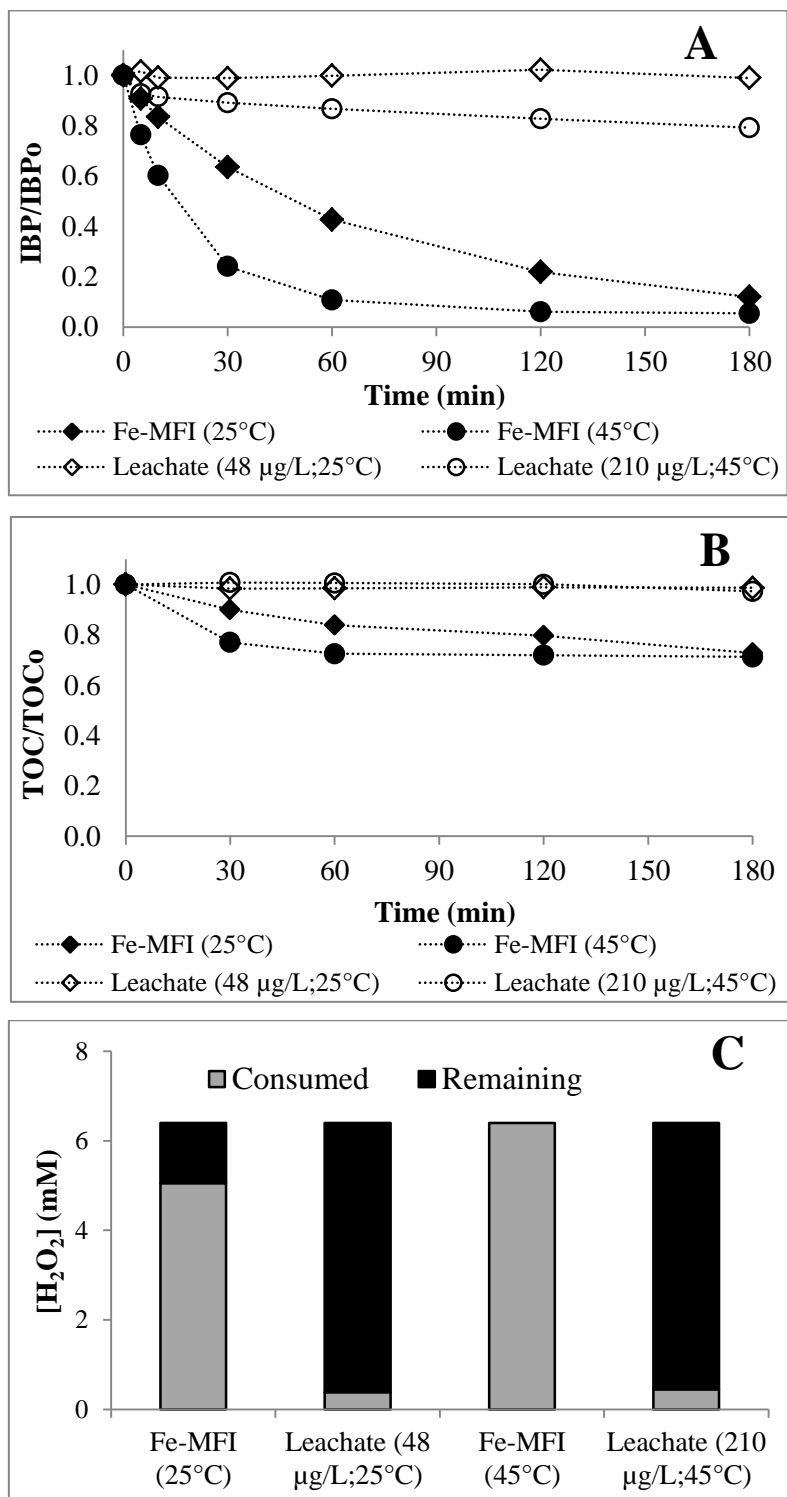


Figure 4.13. Activity of leachate for Fenton oxidation: evolution of (A) IBP and (B) TOC concentration, and (C) H₂O₂ consumption
 ([IBP]₀ = 20 mg/L, [Fe-MFI] = 4.8 g/L, [Fe]_{leachate} = 48 µg/L (25°C) and 210 µg/L (45°C), [H₂O₂]₀ = 6.4 mM, pH_{0 Fe-MFI*} = 4.3, pH_{0 leachate} = 3.2, T = 25°C and 45°C) (*before contact). Corresponding Fenton oxidations were recalled for comparison

In accordance with the previous studies, negligible IBP and TOC degradation was indeed observed with the leachate at 25°C, while only 21% conversion of IBP was observed for the other condition (210 µg/L of Fe at 45°C). In line with this result, only marginal H₂O₂ consumptions were measured (figure 4.13C), indicating that the amount of dissolved iron was too small to yield appreciable decomposition rate and/or the corresponding species exhibited negligible activity. This confirms that Fenton oxidation of IBP over Fe-MFI was mainly induced by surface iron species.

Highlights: heterogeneous Fenton processes

- ✓ *Catalytic activity of iron-containing zeolite of ZSM5 type (Fe-MFI) and zero-valent iron particles (ZVI) was compared.*
- ✓ *Fe-MFI catalyst was selected as it did not require preliminary acidification and led to very low iron leaching (<0.1 mg/L)*
- ✓ *IBP removal increased with increasing both Fe-MFI and H₂O₂ concentrations and temperature, but reduced under buffered-neutral pH*
- ✓ *Appreciable ibuprofen removal (88%) and mineralization (27%) were obtained in heterogeneous Fenton reaction performed under mild conditions (25°C, not controlled pH, 4.8 g/L of Fe-MFI, 2 times the stoichiometric amount of H₂O₂)*

4.3. HETEROGENEOUS SONO-FENTON PROCESSES

Besides the easiest recovery of the catalyst, heterogeneous Fenton oxidation also allows to operate at wider pH ranges than the homogeneous reaction. However its main drawback lies in significantly lower reaction rates as shown in § 4.1.2 and possible catalyst deactivation by reaction byproducts (such as oligomers formed at catalyst surface blocking the active surface) [45]. To overcome these issues, ultrasound irradiation can be used for chemical activation and continuous cleaning of the catalyst surface [122,192], as well as for improvement of active surface area due to particle size reduction [281]. In this section, coupling of heterogeneous Fenton oxidation (F) and ultrasound (US) called heterogeneous sono-Fenton oxidation (US/F) was studied. In addition to the operating parameters of the Fenton reaction, different US characteristics were varied, namely density, intensity, frequency and application mode. As for homogeneous processes, 20 kHz was chosen as reference ultrasound frequency.

4.3.1. Investigation of 20 kHz sono-Fenton oxidation

4.3.1.1. Effect of catalyst particles on sonolysis

First, to better assess the effect of ultrasound on heterogeneous systems, a preliminary test was performed to investigate the possible influence of Fe-MFI particles on sonolysis at 20 kHz in the absence of oxidant.

Previous studies conducted at higher frequencies (80-200 kHz) reported contradictory conclusions for particles in the 5-15 μm range (0.1 – 1% solid content): no effect [105], detrimental [282] or positive one [283]. Indeed, regardless of the particle type (active or inert), solid can either provide additional nuclei for cavitation improving the generation of radicals [192,284] or attenuate the sound waves involving a decrease in the net energy transferred into the system [129]. Ultrasound attenuation in slurry depends upon the size of the particles with respect to the sound wavelength ($\lambda = c/f$ with c the sound velocity ~ 1500 m/s in water). Scattering effect is important when the particle radius (R_p) is of the same order of magnitude or higher than the sound wavelength, while viscous loss dominates in the reverse case [123]. Nonetheless, under cavitation conditions, the effect of bubbles might be higher than that of solid.

On the other hand, solid particles can act as adsorbent for the target molecule or as catalyst to further decompose hydrogen peroxide generated by ultrasound. As shown in figure 4.14, conversion of IBP and TOC was found very similar with 4.8 g/L of Fe-MFI or without particles, indicating they had no effect on sonolysis process. Negligible attenuation of US is consistent considering the mean size of the particles ($d_{43} = 7.9 \mu\text{m}$) - much lower than λ (7.5 cm at 20 kHz) - and the rather low concentration of the slurry (about 0.5%). Concentration of H_2O_2 generated by US ($0.41 \mu\text{M}/\text{min}$) was also too low for heterogeneous Fenton mechanism to superimpose.

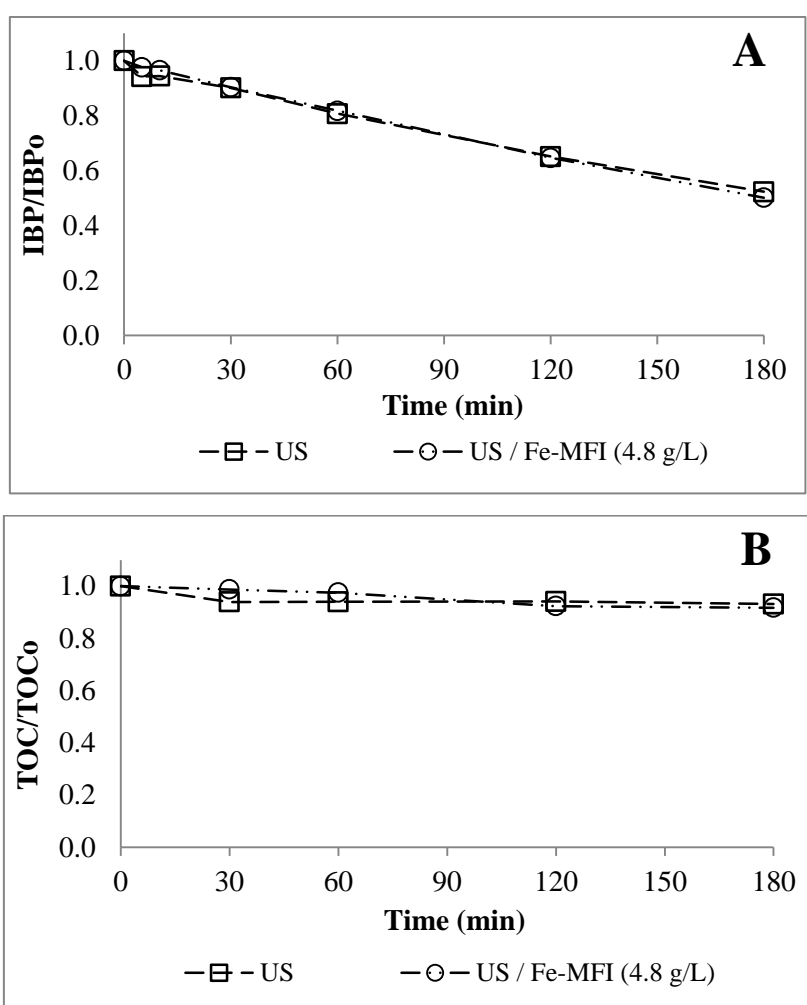


Figure 4.14. Effect of Fe-MFI on sonolysis: evolution of (A) IBP and (B) TOC concentration. ($[\text{IBP}]_0 = 20 \text{ mg}/\text{L}$, $[\text{Fe-MFI}] = 4.8 \text{ g}/\text{L}$, $\text{pH}_0 = 4.3$, $T = 25^\circ\text{C}$, $f_{\text{US}} = 20 \text{ kHz}$, $D_{\text{US}} = 50 \text{ W}/\text{L}$)

4.3.1.2. Comparison of Fenton and sono-Fenton oxidation with Fe/MFI

The effect of 20 kHz ultrasound as activation technique for heterogeneous Fenton reaction was investigated under the following reaction conditions: $\text{pH}_0 = 4.3$, $T = 25^\circ\text{C}$ (controlled), $[\text{H}_2\text{O}_2]_0 = 6.4 \text{ mM}$, $[\text{Fe-MFI}] = 1 \text{ g/L (-)}$ and 4.8 g/L (+) , using $D_{\text{US}} = 50 \text{ W/L}$. As depicted in [figure 4.15](#), ultrasound irradiation had only marginal effect on Fenton oxidation for the highest solid concentration. Under sonication, the first order rate constant for IBP oxidation (k) only increased from 0.0139 (F(+)) to $0.0159 \text{ min}^{-1} \text{ (US/F(+))}$. In this case, the overall process was dominated by the Fenton reaction, that produced $\cdot\text{OH}$ faster than ultrasound ($k_{\text{US}} = 0.0035 \text{ min}^{-1}$).

On the other hand, apparent additive effect between US and Fenton reaction was observed at catalyst concentration of 1 g/L , resulting for IBP oxidation into: $k_{\text{US/F}} = 0.0059 \text{ min}^{-1}$ vs. $k_{\text{F}} = 0.0014 \text{ min}^{-1}$ and k_{US} (or $k_{\text{US/6.4 mM H}_2\text{O}_2}$) = 0.0038 min^{-1} . In the same way, TOC conversion by the coupling process (14%) was close to the sum of individual Fenton oxidation (5%) and sonolysis (7%). Similar H_2O_2 consumption was observed in both cases (26% in Fenton vs. 27% in sono-Fenton), discarding any enhancement of the reaction as it was observed for the homogeneous system (cf. [§ 3.2.2](#)).

The benefit of hybridizing heterogeneous Fenton oxidation with US is still a matter of discussion, because some studies reported a synergistic interaction [64,105,119,122,130,175], while others indicated only minor effects [127–129]. Moreover, when a synergistic effect was observed, activation of heterogeneous catalyst was only concluded in some cases [105,122,175]. Absence of synergistic effect in the present study could be ascribed to limited iron surface (re)activation, negligible contribution of iron leaching and/or limited particle size reduction (discussed in details in [§ 4.6](#)).

To further investigate this coupling, a parametric study was conducted by varying ultrasound parameters: application mode, power intensity, power density and frequency. Heterogeneous sono-Fenton oxidation was then mainly performed at high catalyst concentration ($[\text{Fe-MFI}] = 4.8 \text{ g/L}$), considering the appreciable IBP removal under this condition.

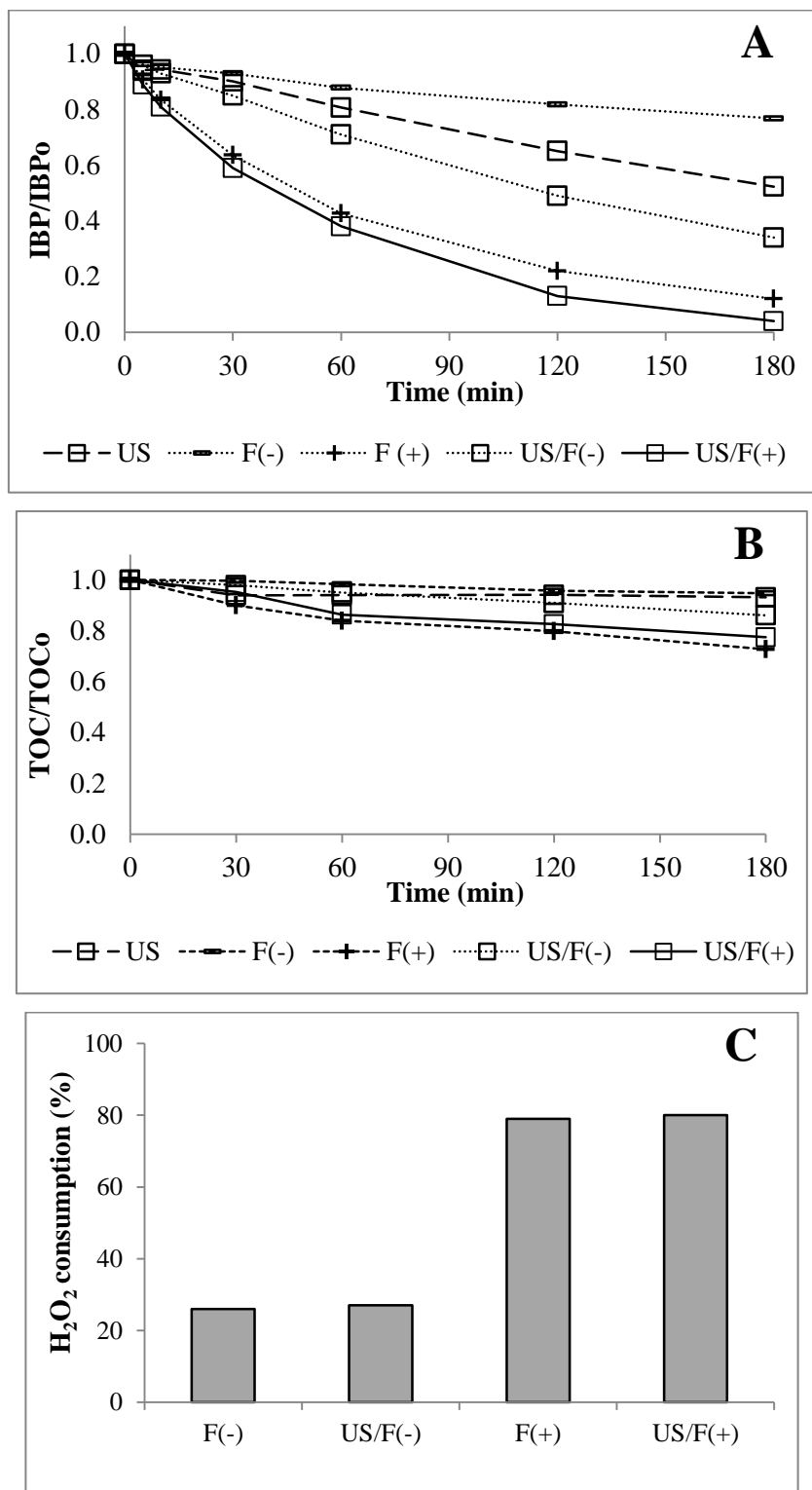


Figure 4.15. Comparison of Fenton and sono-Fenton oxidation with Fe-MFI: evolution of (A) IBP and (B) TOC concentration, and (C) H₂O₂ consumption ([IBP]₀ = 20 mg/L, pH₀ = 4.3, T = 25°C, [H₂O₂]₀ = 6.4 mM, [Fe-MFI] = 1 and 4.8 g/L, f_{US} = 20 kHz, D_{US} = 50 W/L)

4.3.2. Effect of US application mode

For applications where mechanical effects were mainly sought, like in sludge pretreatment, high power for a short time was found beneficial [253,285].

Previous studies on sono-Fenton process were performed in either continuous [81,82,106] or sequential (pulse) mode [117,121,127,130]. However, they rarely compared the effect of US operation mode with same applied specific energy (E_{US}).

In this study, effect of ultrasound application mode was firstly investigated by doubling the power input (100 W/L) with a cycle of 10 seconds US ON and 10 seconds US OFF, in order to get higher transient mechanical effects for the activation of the catalyst surface at similar energy consumption (540 kJ/kg). Actually, it didn't result in any measurable influence: IBP and TOC removal at the end of the reaction remained at 96% and 23%, respectively, [figure 4.16](#). Therefore, continuous mode was used for following experiments.

4.3.3. Effect of ultrasound intensity

Ultrasound intensity (I_{US}) or ultrasound power input per unit probe surface is one of the main parameters of ultrasound, as it is directly linked to the amplitude of the acoustic pressure. However, it is usually investigated by varying ultrasound power with the same probe [81,121,127] and more rarely by changing the emitter diameter. In this case, variation of US intensity was performed by changing probe diameter from 51 mm ($I_{US} = 2.45 \text{ W/cm}^2$) to 35 mm ($I_{US} = 5.2 \text{ W/cm}^2$), while the power density was kept constant at 50 W/L. Again, it didn't yield any increase of the pollutant conversion or mineralization, which could be the result of a reduced volume of the cavitation zone balancing locally enhanced effects ([figure 4.17](#)).

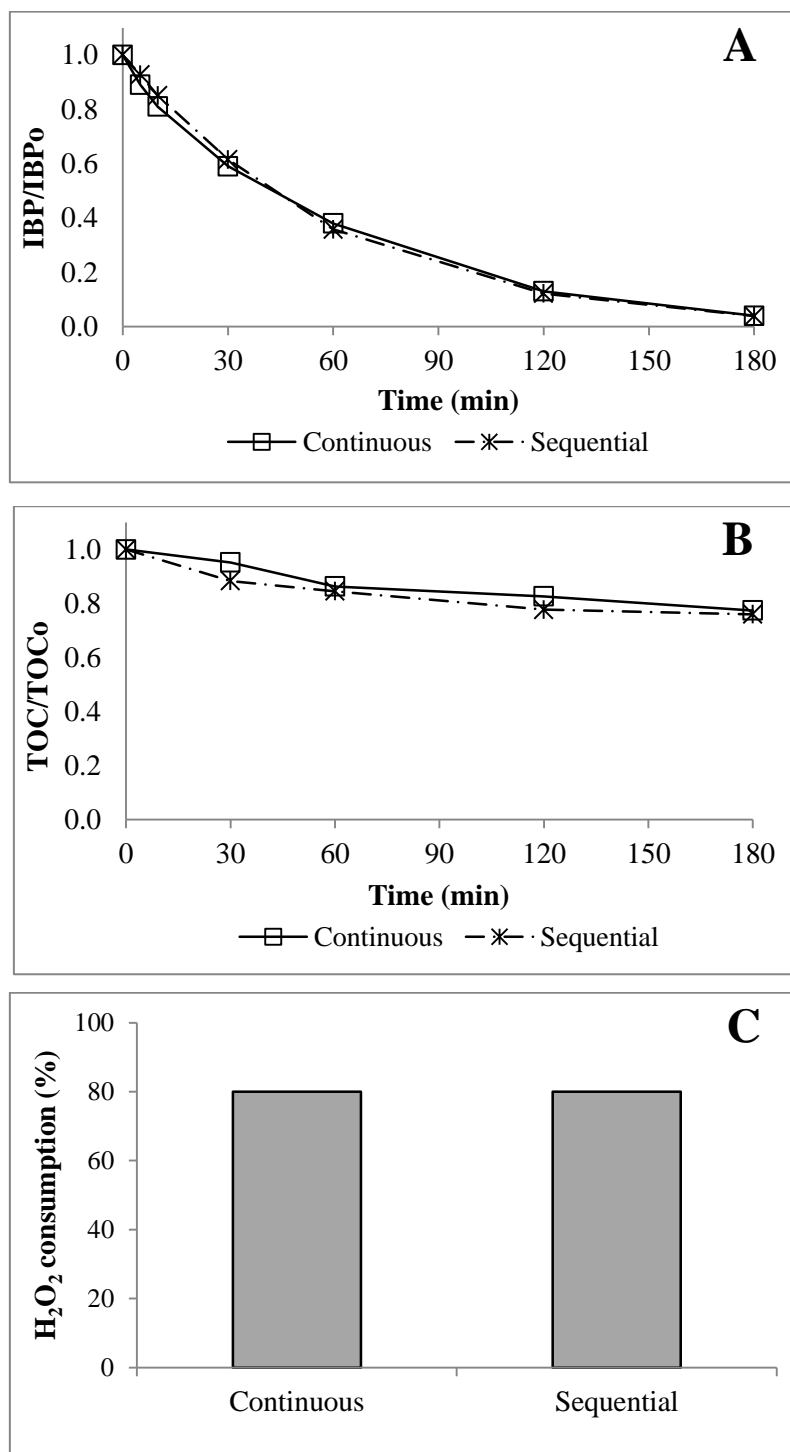


Figure 4.16. Effect of US application mode on sono-Fenton oxidation with Fe-MFI: evolution of (A) IBP and (B) TOC concentration, and (C) H₂O₂ consumption ([IBP]₀ = 20 mg/L, pH₀ = 4.3, T = 25°C, [H₂O₂]₀ = 6.4 mM, [Fe-MFI] = 4.8 g/L, f_{US} = 20 kHz, E_{US} = 540 kJ/kg, sequential mode: 10 s US ON / 10 s US OFF)

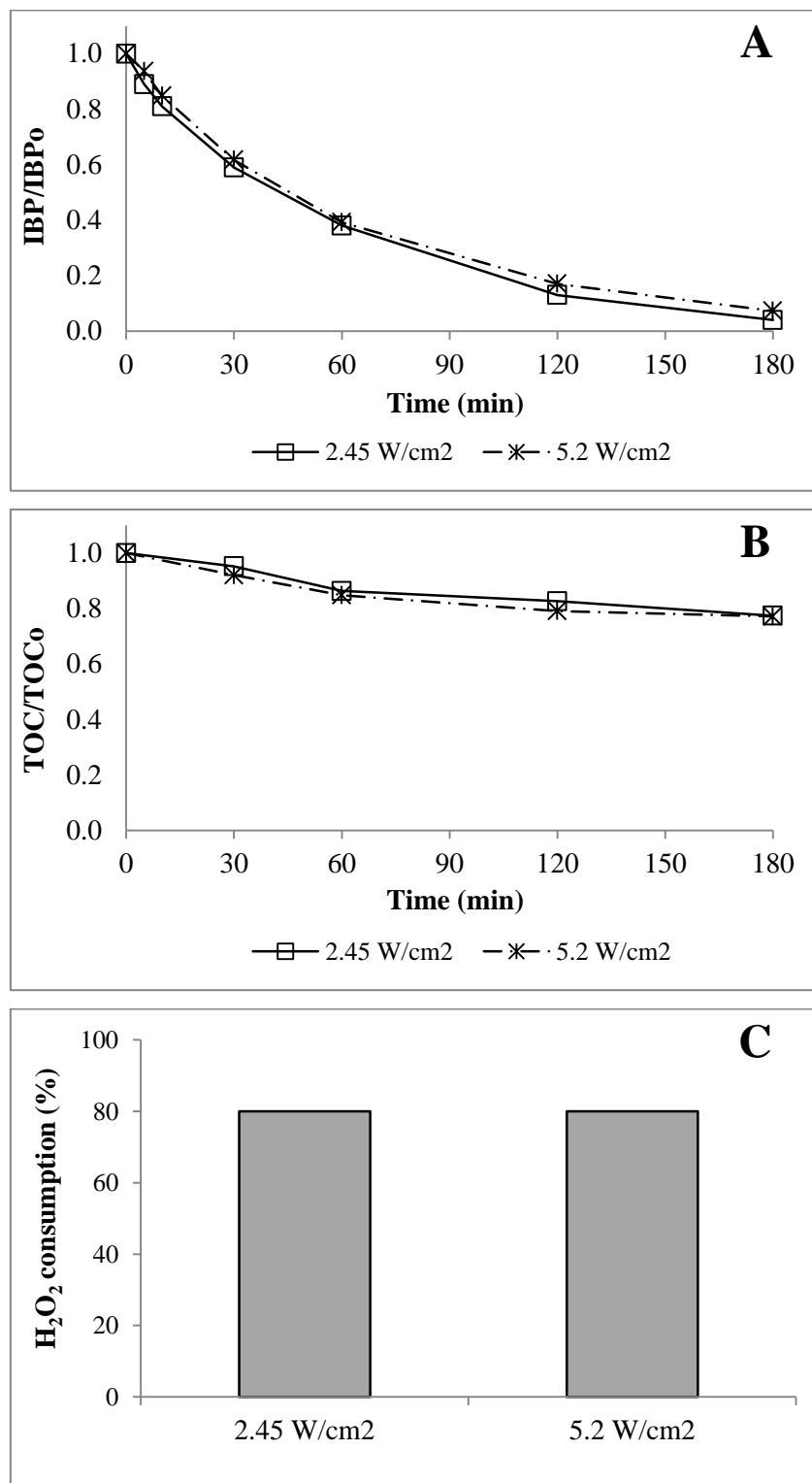


Figure 4.17. Effect of US intensity on Fenton oxidation with Fe-MFI: evolution of (A) IBP and (B) TOC concentration, and (C) H₂O₂ consumption ([IBP]₀ = 20 mg/L, pH₀ = 4.3, T = 25°C, [H₂O₂]₀ = 6.4 mM, [Fe-MFI] = 4.8 g/L, f_{US} = 20 kHz, I_{US} = 2.45 – 5.2 W/cm²)

4.3.4. Effect of ultrasound power density

The influence of a higher ultrasound density (D_{US}) was investigated by comparing sono-Fenton results at 50 W/L (US(-)) and 100 W/L (US(+)), corresponding to specific energy (E_{US}) of 540 kJ/kg and 1080 kJ/kg, respectively. It should be noted that this range of E_{US} is similar to that used in previous works ($E_{US} = 500 - 1000$ kJ/kg) [81,117,120,127]. For these tests, 1 and 4.8 g/L of Fe-MFI were successively used (denoted F(-) and F(+)) (table 4.4).

Figure 4.18A and figure 4.18B put into evidence a slight increase in IBP and TOC removal when doubling D_{US} . However, IBP oxidation rate constant increased by 50% maximum (table 4.4), while the improvement of final TOC conversion did not exceed 27%. Similarly, up to 7% higher consumption of H_2O_2 was measured at $D_{US} = 100$ W/L.

Moreover, it can be seen that the enhancement in catalytic activity was clearer at high Fe-MFI concentration (condition US(+)/F(+)). This might be due to a higher contact between $\bullet OOH$ and $\equiv Fe(III)$ leading to catalyst surface activation according to Eq. R.4.12 – 4.14 [71]:



The limited improvement at 100 W/L also explains why the sequential application mode of US (§ 4.3.2) or the twice increase in US intensity at same E_{US} (§ 4.3.3) had only low effect on sono-Fenton efficiency. Accounting for higher energy consumption versus relatively low enhancement in terms of IBP and TOC removal, continuous application of this high power input may be not economical.

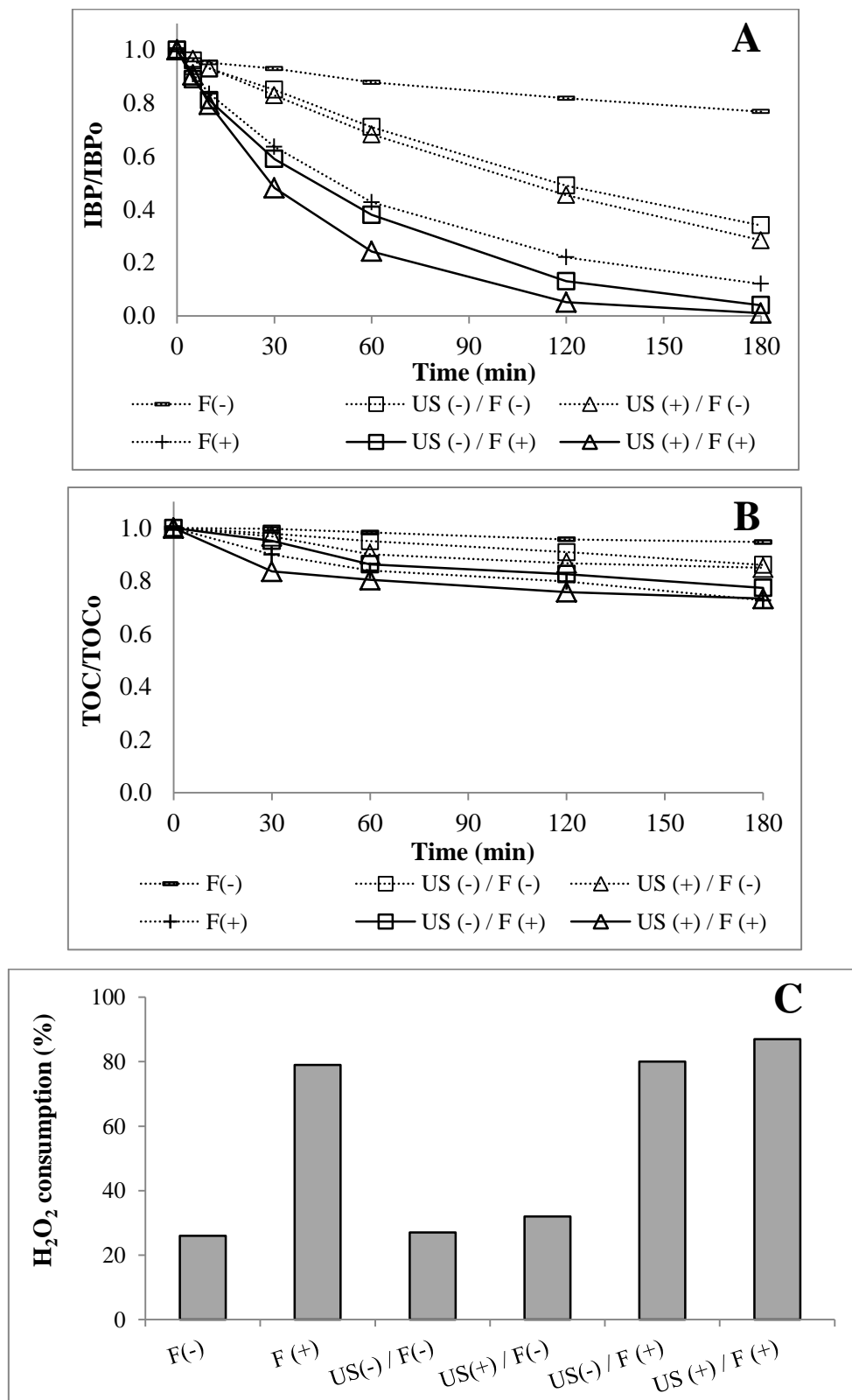


Figure 4.18. Effect of US density on Fenton oxidation with Fe/MFI: evolution of (A) IBP and (B) TOC concentration, and (C) H₂O₂ consumption ([IBP]₀ = 20 mg/L, pH₀ = 4.3, T = 25°C, [H₂O₂]₀ = 6.4 mM, [Fe-MFI] = 1 and 4.8 g/L, D_{US} = 50 – 100 W/L, f_{US} = 20 kHz)

Table 4.4. Effect of ultrasound power density on IBP degradation

Process	D_{US} (W/L)	[Fe-MFI] (g/L)	IBP removal (%)	TOC removal (%)	H ₂ O ₂ Cons. (%)	k IBP (min ⁻¹)	SF*
US(-)	50	-	48	7	-	0.0035	-
US(+)	100	-	58	7	-	0.0048	-
F(-)	-	1	23	5	26	0.0014	-
F(+)	-	4.8	88	27	79	0.0139	-
US(-)/F(-)	50	1	66	14	27	0.0059	1.2
US(+)/F(-)	100	4.8	72	15	32	0.0069	1.1
US(-)/F(+)	50	1	96	23	80	0.0159	0.9
US(+)/F(+)	100	4.8	99	27	87	0.0239	1.3

Other parameters remained constant: [IBP]₀ = 20 mg/L, [H₂O₂]₀ = 6.4 mM, pH₀ = 4.3, T = 25°C, f_{US} = 20 kHz; *E.3.1 (cf. § 3.2.4)

4.3.5. Effect of ultrasound frequency

While the increase in US frequency promotes the generation of hydroxyl radicals, decreasing the sonication frequency should enhance mixing, mass transfer, dispersion and disaggregation of solid catalyst particles, as well as increase the surface defects or active sites on the catalyst surface [243].

In the presence of 4.8 g/L of Fe-MFI, varying sound frequency from 12 to 862 kHz only marginally improved IBP and TOC removal rates (figures 4.19A and 4.19B). Slightly reduced degradation at 12 kHz vs. 20 kHz discarded any activation of the catalyst surface by US mechanical effects, probably because the particles (about 8 μm mean diameter) were small as compared to the size of the cavitation bubbles (Sauter diameter of 10 to 50 μm at 20 kHz [96]). This is also consistent with the negligible evolution of particle size, morphology or iron content reported under ultrasound in § 4.6.

Moreover, in any case, the reaction probably didn't suffer from high enough limitations by internal or external mass transfer to see low frequency sonication bring any improvement on the whole process. Consumption of H₂O₂ at the end of reaction was also the same under 12 and 20 kHz (figure 4.19C). In sole sonolysis, rate constant of IBP removal was multiplied by a factor 3 between 20 and 862 kHz (cf. § 3.1.2.4), leading to a value (0.0102 min⁻¹ at 862 kHz) comparable to that of Fenton oxidation (0.0139 min⁻¹). However, additive effects were hardly seen in coupling processes even under high frequency (k_{US(862 kHz)/F} = 0.0174 min⁻¹).

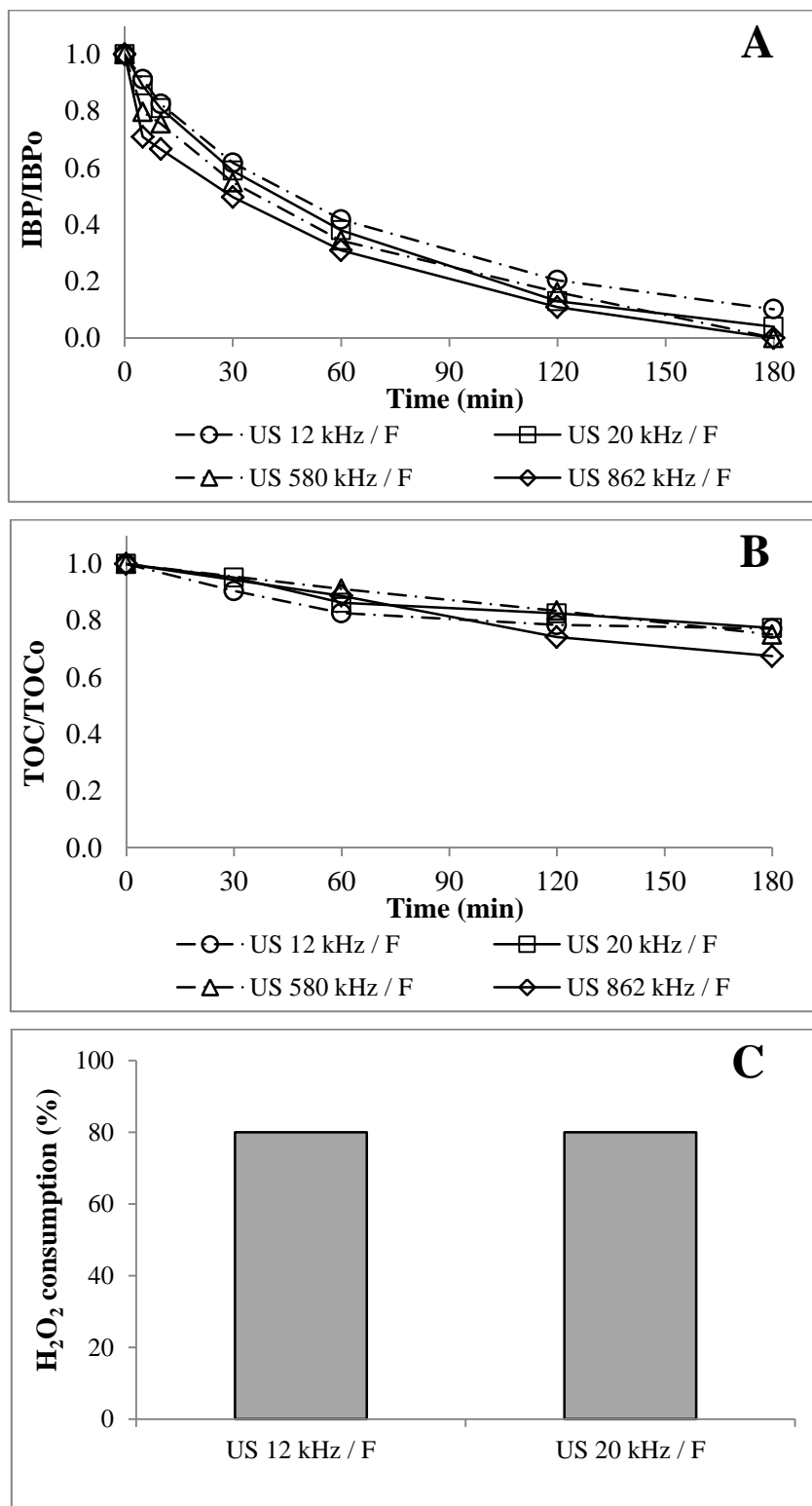


Figure 4.19. Effect of sound frequency on sono-Fenton oxidation with Fe-MFI: evolution of (A) IBP and (B) TOC concentration, and (C) H₂O₂ consumption ([IBP]₀ = 20 mg/L, pH₀ = 4.3, T = 25°C, [H₂O₂]₀ = 6.4 mM, [Fe-MFI] = 4.8 g/L, D_{US} = 50 W/L, f_{US} = 12 – 862 kHz)

4.4. HETEROGENEOUS PHOTO-FENTON PROCESSES

As shown in chapter 3 (§ 3.2.3), ultraviolet (UV) and visible (Vis) light irradiation emitted by LP Hg and xenon lamp can be used to enhance homogeneous Fenton oxidation process. In this section, coupling of heterogeneous Fenton oxidation and light irradiation (UV from LP Hg lamp or Vis from Xe lamp) called heterogeneous photo-Fenton processes (LP Hg/F or Xe/F) was also examined (using loop reactor configuration).

4.4.1. Heterogeneous photo-Fenton oxidation under UV light (LP Hg lamp)

Activation of heterogeneous Fenton oxidation by light irradiation was firstly evaluated at 254 nm (using LP Hg lamp). Experiments were carried out at different Fe-MFI concentrations: 1 g/L and 4.8 g/L (denoted as (-) and (+), respectively), while other parameters remained constant (pH₀ 4.3 and 25°C). The results of photolysis (LP Hg), photo-oxidation (LP Hg/H₂O₂) and “dark” heterogeneous Fenton (F) are also recalled in [figure 4.20](#) for comparison purpose.

Ibuprofen degradation rate was significantly improved when shifting from “dark” to photo-assisted Fenton oxidation ([figure 4.20A](#)). Same trend was observed for TOC at 1 g/L of Fe-MFI, while F(+) and LP Hg/F(+) achieved almost same TOC conversion after 3 hours ([figure 4.20B](#)). On the other hand, degradation profiles by LP Hg/Fenton and LP Hg/H₂O₂ were found very similar suggesting that direct photolysis of hydrogen peroxide was the dominant process even at the highest catalyst concentration.

Furthermore, it is worth noting that in fact IBP removal rate decreased with an increase in catalyst concentration. Indeed, the rate constants for LP Hg/H₂O₂, LP Hg/F(-) and LP Hg/F(+) process were 0.0664 min⁻¹ (R²=0.9954), 0.0578 min⁻¹ (R²=0.9987) and 0.0411 min⁻¹ (R²=0.9970), respectively. In these conditions, UV light scattering/absorption caused by the presence of Fe-MFI particles seemed to overweigh their catalytic effect, thus reducing the effectiveness of radical production.

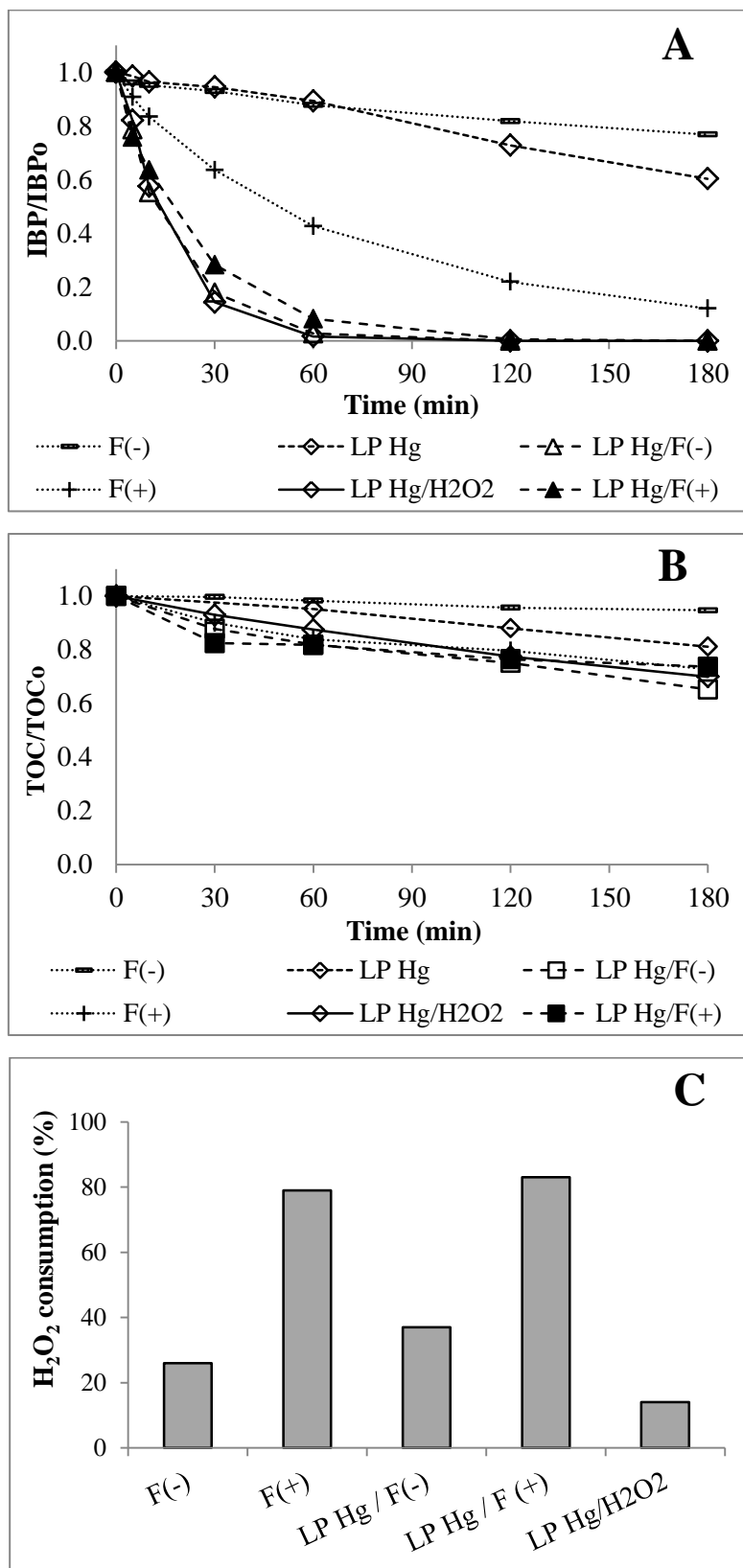


Figure 4.20. Photo-Fenton oxidation with Fe-MFI under UV light and comparison with separate processes: evolution of (A) IBP and (B) TOC concentration, and (C) H₂O₂ consumption ([IBP]₀ = 20 mg/L, [Fe-MFI] = 1 and 4.8 g/L, [H₂O₂] = 6.4 mM, pH₀ = 4.3, T = 25°C, UV lamp: LP Hg 6W)

Consumption of H_2O_2 for F(-), LP Hg/ H_2O_2 and LP Hg/F(-) was 26%, 14% and 37%, indicating not more than additive effect, and higher TOC removal in LP Hg/F(-) (35%) than F(-) (5%) at similar H_2O_2 consumption could be attributed to LP Hg/ H_2O_2 process (30%). On the other hand, LP Hg /F(+) and F(+) showed similar H_2O_2 consumption (79% vs. 83%) mainly due to the zeolite (figure 4.20C). Therefore, photo-activation/regeneration of the catalyst was not visible in the present conditions.

Among previous studies investigating photo-Fenton oxidation with Fe-ZSM5 catalyst [80,162,163,165,167], only one clearly concluded to an activation of the sole heterogeneous reaction by UV light [163], while some others indicated noticeable contribution of iron leaching (homogeneous photo-Fenton reaction) [165] or a prominent role of UV/ H_2O_2 reaction [167].

4.4.2. Heterogeneous photo-Fenton oxidation under visible light (Xe lamp)

In order to limit the contribution of photolysis of H_2O_2 , another set of photo-Fenton experiments were conducted under visible light using xenon lamp. Results are depicted in figure 4.21. In these conditions, the improvement in IBP degradation rate was much lower than under UV light: overall rate constants of 0.0019 and 0.0159 min^{-1} were measured for Xe/F(-) and Xe/F(+), respectively, as compared to 0.0014 and 0.0139 min^{-1} for F(-) and F(+). On the other hand, Xe/ H_2O_2 mechanism – despite very slow – could contribute for a rate constant value up to 0.0017 min^{-1} (in the absence of solid particles). Therefore, all together, photo-activation of the heterogeneous reaction was only marginal, even at high Fe-MFI concentration. Probably, photons might not reach active iron sites located within the zeolite porous structure, limiting the activation effect to the most outer particle surface.

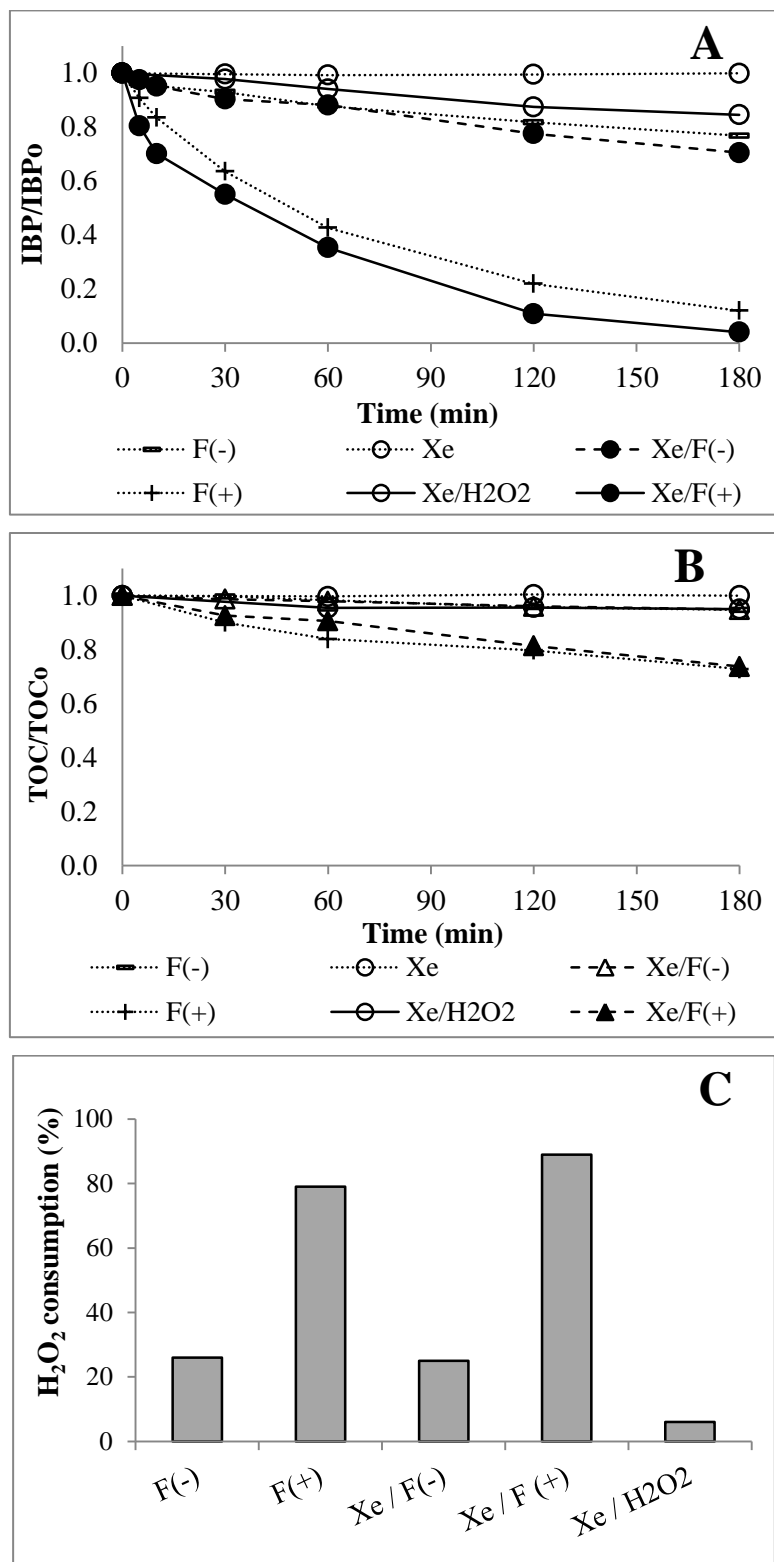


Figure 4.21. Photo-Fenton oxidation with Fe-MFI under Vis light and comparison with separate processes: evolution of (A) IBP and (B) TOC concentration and (C) H₂O₂ consumption ([IBP]₀ = 20 mg/L, [Fe-MFI] = 1 and 4.8 g/L, [H₂O₂]₀ = 6.4 mM, pH₀ = 4.3, T = 25°C, Vis lamp: Xenon 150W)

4.5. HETEROGENEOUS SONO-PHOTO-FENTON PROCESSES

Despite the very limited activation of heterogeneous process by ultrasound or light irradiation observed in this study (cf. § 4.3 and 4.4), the efficacy of the coupled sono-photo-Fenton oxidation process was also evaluated with 1 g/L of Fe-MFI (to limit light attenuation effects). Two experiments were performed, one with the LP Hg lamp (figure 4.22) and the other with the Xe lamp (figure 4.23), while low frequency ultrasound was applied in both cases (with $D_{US} = 50$ W/L, based here on the whole treated volume of 1.5 L).

From figure 4.22A, it can be seen that IBP degradation by US/LP Hg/F was slightly faster than LP Hg/F. Moreover, some enhancement of H_2O_2 consumption was indeed observed (figure 4.22C, 37% in LP Hg/F vs. 50% in US/LP Hg/F). The influence of US on LP Hg/ H_2O_2 process being negligible (cf. chapter 3, § 3.2.1), a promotion of homogeneous photo-Fenton process by increased iron leaching could be suspected. Nonetheless, addition of ultrasound on LP Hg/F did not result in any measurable improvement of TOC conversion (figure 4.22B). This is consistent with the limited mineralization observed by ultrasound itself (cf. chapter 3, § 3.1.2). In all cases, LP Hg/ H_2O_2 process being much more effective than US and Fenton oxidation at selected Fe-MFI concentration, it was the dominant mechanism.

Sono-photo-Fenton oxidation process under visible light irradiation (figure 4.23) showed different trends than under UV light. Indeed, sono-photo(Vis)-Fenton oxidation (US/Xe/F) was found very similar to sono-Fenton (US/F) regarding both IBP and TOC conversion. H_2O_2 consumption at the end of reaction was also almost the same in both cases, discarding any contribution of photo-mediated process initiated by visible light.

Comparison with literature is rather difficult because heterogeneous sono-photo-Fenton process is still rarely studied. Zhong et al. [175] reported that the removal of acid orange 7 by sono-photo-Fenton oxidation with $Fe_2O_3/SBA-15$ catalyst at $f_{US}=20$ kHz and $\lambda_{UV}=254$ nm corresponded to the sum of sono-Fenton and photo-Fenton contributions. On the other hand, under similar conditions ($Fe_2O_3/SBA-15$ catalyst, $f_{US}=20$ kHz), but UVA irradiation, Segura et al. [120] observed that photo-Fenton oxidation dominated the coupled process for phenol remediation. Based on all these results, the advantage of combining both ultrasound and light irradiation with heterogeneous Fenton oxidation seems rather questionable. The efficacy of the heterogeneous sono-photo-Fenton process does not seem to exceed the sum of sono-Fenton and photo-Fenton processes, and in some cases, as observed here, one process takes over the other depending on light irradiation wavelength.

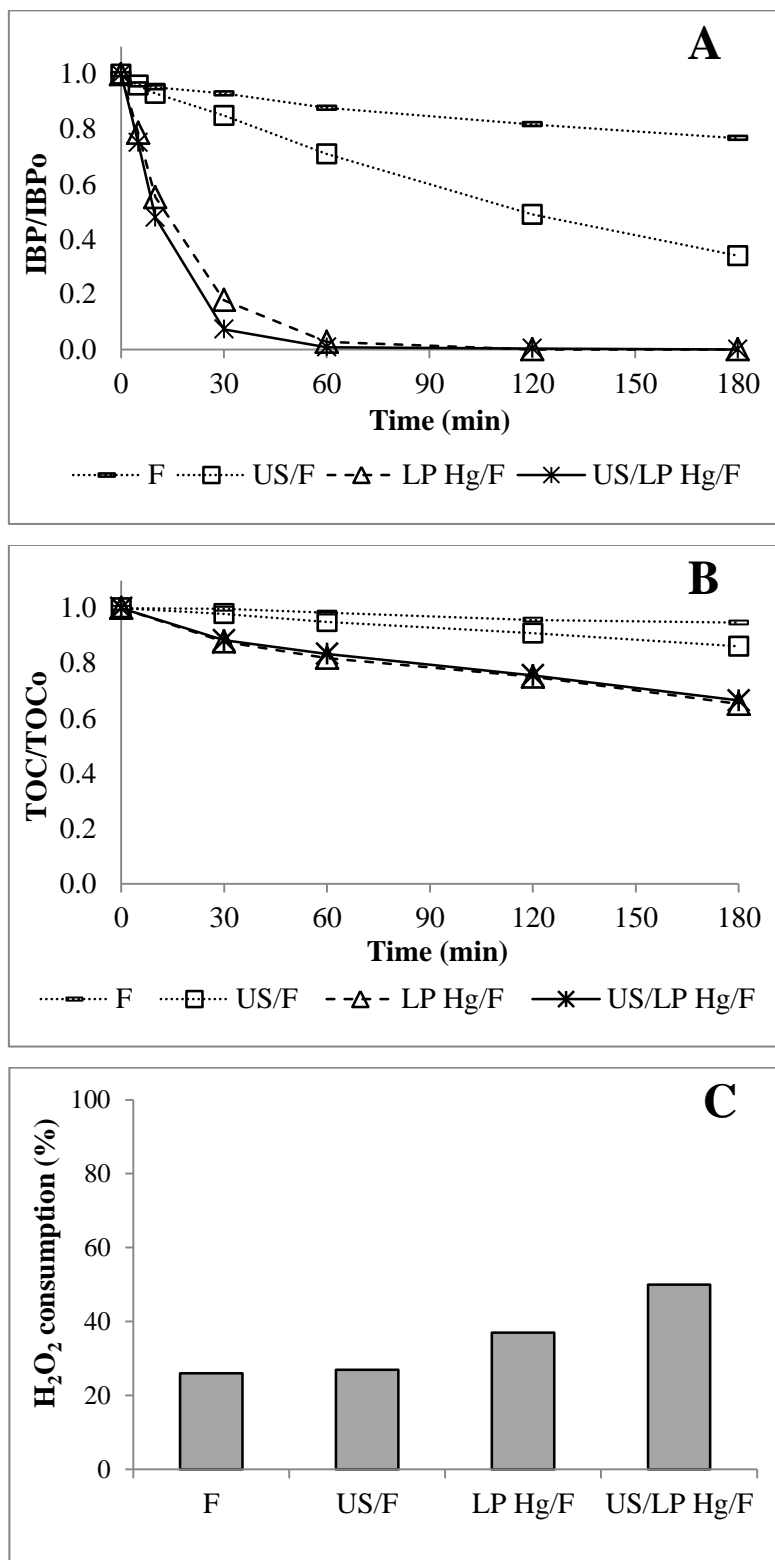


Figure 4.22. Sono-photo-Fenton oxidation with Fe-MFI under UV light and 20 kHz US, and comparison with other Fenton-based processes: evolution of (A) IBP and (B) TOC concentration, and (C) H₂O₂ consumption ([IBP]₀ = 20 mg/L, [Fe-MFI] = 1 g/L, [H₂O₂]₀ = 6.4 mM, pH₀ = 4.3, T = 25°C, f_{US} = 20 kHz, D_{US} = 50W/L, UV lamp: LP Hg 6 W)

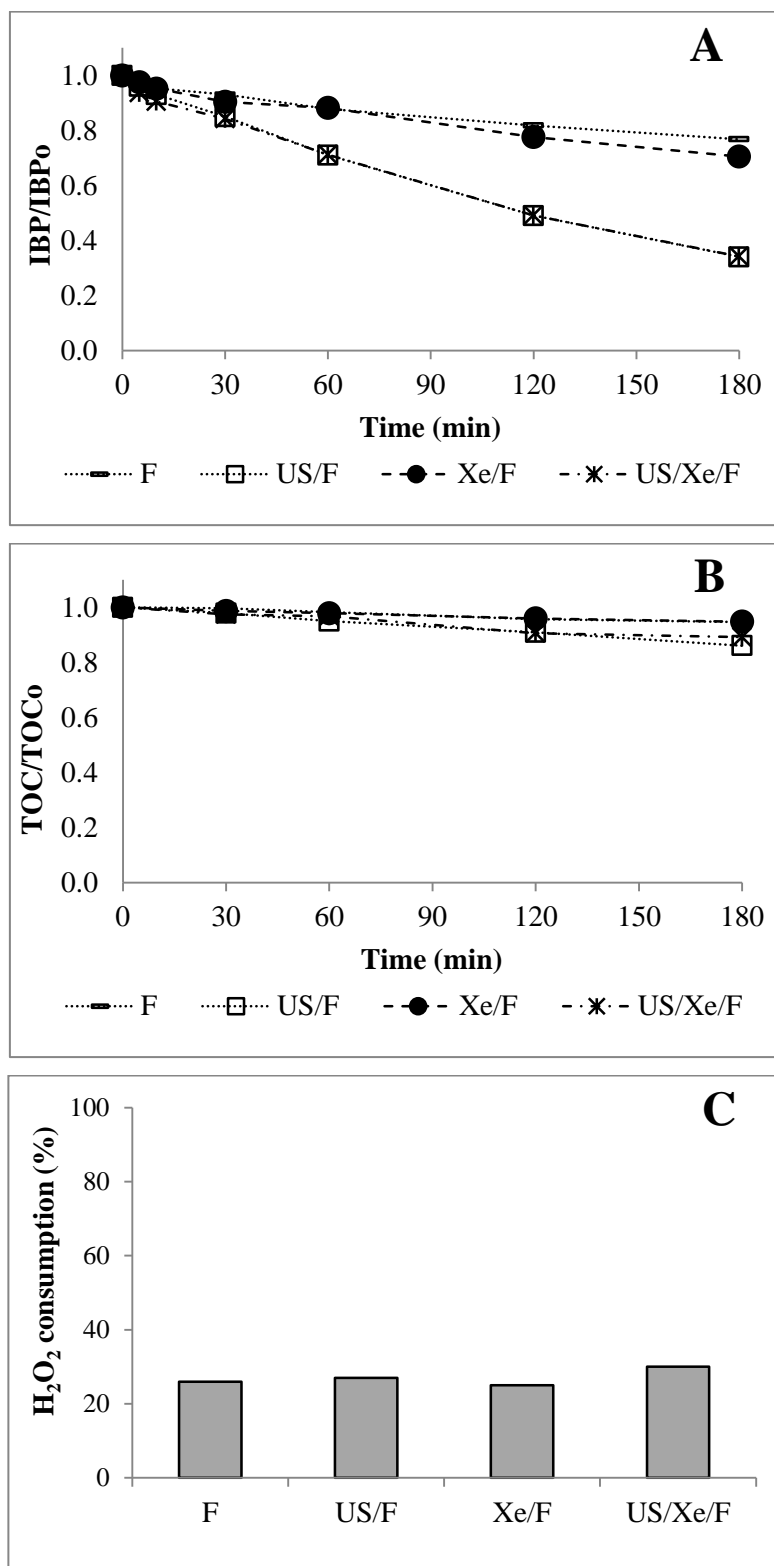


Figure 4.23. Sono-photo-Fenton oxidation with Fe-MFI under Vis light and 20 kHz US, and comparison with other Fenton-based processes: evolution of (A) IBP and (B) TOC concentration, and (C) H₂O₂ consumption ([IBP]₀ = 20 mg/L, [Fe-MFI] = 1 g/L, [H₂O₂]₀ = 6.4 mM, pH₀ = 4.3, T = 25°C, f_{US} = 20 kHz, D_{US} = 50W/L, Vis lamp: Xenon 150 W)

4.6. EVOLUTION OF THE HETEROGENEOUS CATALYST AFTER (SONO-, PHOTO-)FENTON OXIDATION

4.6.1. Particle size distribution

Under ultrasound irradiation, the collapse of cavitation bubbles near particle surface generates liquid microjets with a velocity of about 100 m/s [286]. These microjets can increase mass transfer rate (diffusion of substrates to/from the catalyst surface), can cause erosion (surface cleaning and/or leaching) or even fragmentation of the particles, improving the apparent catalytic reaction rate [120,122,175,287].

The size distribution of Fe-MFI particles after Fenton, photo-Fenton and sono-Fenton oxidation was evaluated and compared with that of fresh one (figure 4.24).

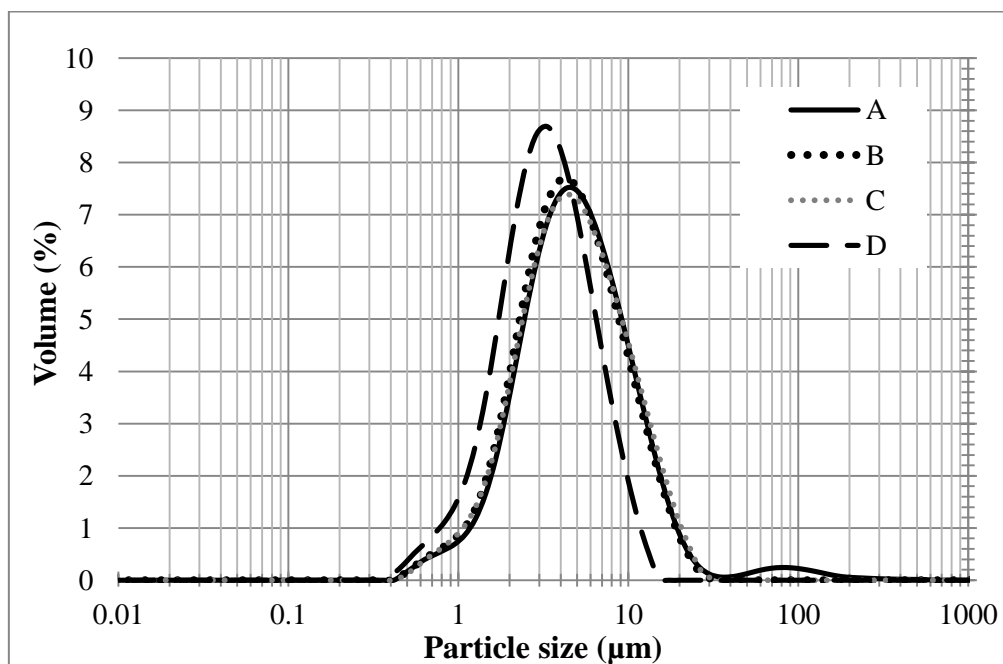


Figure 4.24. Fe-MFI particle size distribution: (A) before reaction, (B) after Fenton, (C) after photo-Fenton, (D) after sono-Fenton oxidation

As expected, the results showed that the particle size distribution before and after Fenton and photo-Fenton oxidation was similar, while a reduction of the mean size was observed after sono-Fenton oxidation (d_{43} shifted from 7.9 µm to 4.1 µm). However, catalyst fragmentation under sonication observed in this study was less remarkable compared to the previous studies (showing particle size reduced from hundreds to tens of microns) [120,175]. According to the literature [287], erosion and fragmentation by ultrasound are strongly

dependent on the size of particles size vs. the size of cavitation bubbles, which is frequency-dependent [95,288]. Since the diameter of cavitation bubbles at 20 kHz is tens of microns [96,289], mechanical effects would mainly concern larger particles ($> 200 \mu\text{m}$) [287].

4.6.2. Catalyst morphology and iron content

As abovementioned (see § 4.2.6), iron leaching from the solid catalyst is an important issue because it can result into progressive loss of activity, additional homogeneous oxidation mechanism and supplementary post-treatment to lower the dissolved metal concentration below acceptable level if too high. Since ultrasound application may affect the catalyst stability, iron leaching in the coupling processes was also evaluated. First, SEM and EDX analysis showed no major modification of the catalyst morphology (figure 4.25) and surface iron content after Fenton ($3.3 \pm 1.0\%$) and sono-Fenton process ($3.4 \pm 1.1\%$). This result is in accordance with the study of Queirós et al. [177] who reported that the morphology and elemental composition of Fe-ZSM5 catalyst were not modified after Fenton or sono-Fenton oxidation. Note that the catalyst used in photo-Fenton oxidation was not examined since no further change was expected with respect to Fenton reaction.

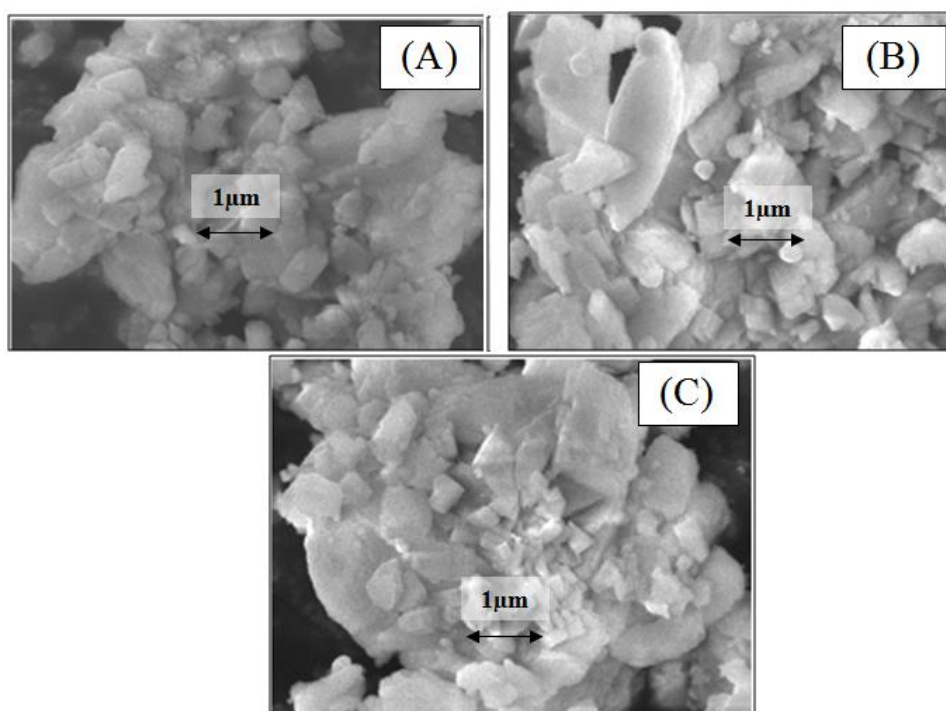


Figure 4.25. SEM images of (A) fresh and used Fe-MFI from (B) Fenton and (C) sono-Fenton oxidation

Concentrations of dissolved iron after Fenton oxidation, with and without activation are summarized in [table 4.5](#). It can be seen that iron leaching remained very low in all cases ($\leq 0.3\%$ of the total iron amount). As expected, for Fenton and sono-Fenton oxidation, dissolved iron concentration increased with Fe-MFI concentration, and higher leaching was observed under increasing US. In both cases, these effects were however rather limited.

Table 4.5. Iron leaching after 180 minutes of heterogeneous (sono-, photo-)Fenton oxidation

Process	D_{US} W/L	λ nm	[Fe-MFI] g/L	Iron leaching	
				mg/L	% of initial solid content ^a
Adsorption	-	-	1	0.009	0.03
F(-)	-	-	1	0.014	0.04
F(+)	-	-	4.8	0.048	0.03
US(-)/F(-)	50	-	1	0.028	0.08
US(+)/F(-)	100	-	1	0.048	0.14
US(-)/F(+)	50	-	4.8	0.054	0.03
US(+)/F(+)	100	-	4.8	0.082	0.05
LP Hg/F(-)	-	254	1	0.085	0.25
LP Hg/F(+)	-	254	4.8	0.079	0.05
Xe/F(-)	-	360-740	1	0.023	0.07
Xe/F(+)	-	360-740	4.8	0.056	0.03
US(-)/LP Hg/F(-)	50	254	1	0.095	0.28
US(-)/Xe/F(-)	50	360-740	1	0.048	0.14

^a Iron content in fresh Fe-MFI determined from ICP-AES analysis of acid leachate

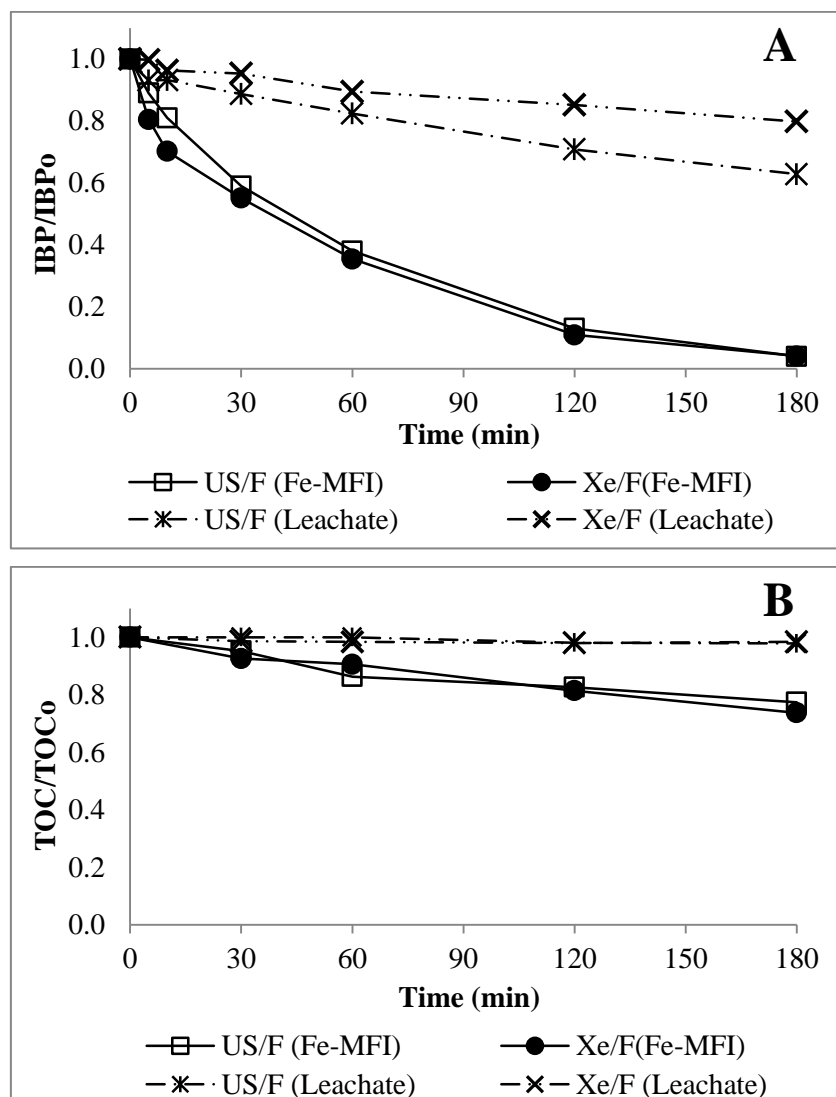
Interestingly, higher iron leaching was also observed in photo-Fenton as compared to Fenton oxidation. There are two possible explanations for this observation: first, ferrous iron resulting from the photo-reduction of ferric species on the catalyst surface is more soluble [155,154]; second, the formation of reaction intermediates (*e.g.* carboxylic acids), able to complex surface iron species, would promote metal dissolution [290,291]. Considering higher mineralization yield obtained in LP Hg/Fenton than in Xe/Fenton (cf. [§ 4.4](#)), the latter explanation seems to be more plausible.

In all cases, iron concentrations in solution (0.009 – 0.095 mg/L) were much below admissible value (2 mg/L) and also much smaller than those used for the homogeneous tests (1.8-7.5 mg/L). Thus marginal catalytic contribution from iron leaching is expected, as already seen in [§ 4.2.6](#) for Fenton only. This is checked for ultrasound and light activated reaction in the following paragraph.

4.6.3. Activity of leached iron in sono-Fenton and photo(Vis)-Fenton oxidation

Filtrates from sono-Fenton (with $f_{US} = 20$ kHz, $D_{US} = 50$ W/L) and photo-Fenton oxidation (with Xe lamp) at high Fe-MFI concentration (4.8 g/L) were re-used after adjustment of IBP and H_2O_2 concentration as described in § 4.2.6.

Figure 4.26 compares the time-concentration profiles of IBP and TOC during sono-Fenton and photo-Fenton oxidation with Fe-MFI catalyst and corresponding filtrate (no solid). It indicates that activity of leached iron in sono-Fenton (0.054 mg/L) and photo-Fenton (0.056 mg/L) was indeed negligible, as degradation of IBP observed in leaching tests was due to sonolysis alone and photolysis of H_2O_2 , respectively. In addition, H_2O_2 consumption was also very low compared to that observed for the heterogeneous system.



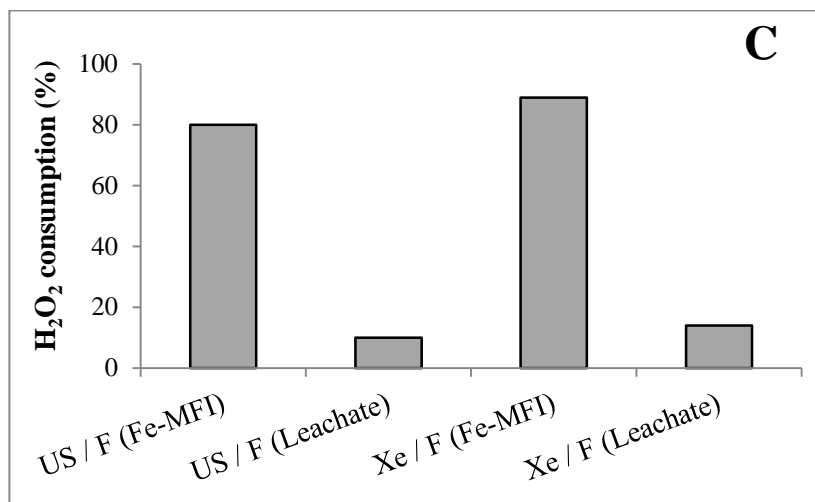


Figure 4.26. Leaching tests of sono-Fenton and photo-Fenton oxidation: evolution of (A) IBP and (B) TOC concentration and (C) H₂O₂ consumption
 ([IBP]₀ = 20 mg/L, [Fe_{leachate}] = 54 µg/L (US/F) and 56 µg/L (Xe/F), [H₂O₂]₀ = 6.4 mM, pH_{leachate} = 3.2, T = 25°C, f_{US} = 20 kHz, D_{US} = 50 W/L, Vis lamp: Xenon 150 W). Sono-Fenton and photo-Fenton oxidation results over Fe-MFI (4.8 g/L) were recalled for comparison

4.6.4. Effect of ultrasound and light irradiation on residual carbon content

Catalyst surface cleaning effect by ultrasound is still rarely reported in literature. Only some studies reported that the enhancement of sonocatalysis process was due to catalyst surface cleaning by ultrasound [122,292]. Part of IBP molecules were preliminary adsorbed on Fe-MFI and might undergo degradation either in adsorbed phase or after desorption during oxidation. In this section, carbon contents of Fe-MFI catalyst after selected experiments such as adsorption only, Fenton oxidation, and coupled processes with 1 g/L of catalyst were calculated using following equation:

$$X_{TOC} (\%) = \frac{TOC_{AD}^L + TOC_{AD}^S - TOC_{OX}^L - TOC_{OX}^S}{TOC_{AD}^L + TOC_{AD}^S} \quad (E.4.1)$$

Where TOC_{AD}^L and TOC_{AD}^S are the concentration of TOC in liquid and solid phase after adsorption (mg/L) and TOC_{OX}^L and TOC_{OX}^S are the concentration of TOC in liquid and solid phase after oxidation (mg/L).

As shown in [figure 4.27](#), TOC reduction in solid phase was found to be insignificant during Fenton oxidation, even under ultrasound and light irradiation: carbon content on Fe-MFI varied from 0.35% after preliminary adsorption (in rather good agreement with IBP

adsorbed amount shown in figure 4.1) to 0.28% in best conditions. This is an expected result for F, US/F or Vis/F performed with 1 g/L Fe-MFI as corresponding TOC removal in liquid phase was also relatively low. For UV-assisted processes for which up to 35% of TOC conversion was achieved in solution, this might be explained by a higher affinity of reaction intermediates for the zeolite. Evaluation of overall mineralization yield (based on both liquid and solid phases) shows that in this condition TOC removal would be overestimated by less than 15% if based on liquid phase only. Note that it was not possible to determine the residual carbon content for the experiments with 4.8 g/L of catalyst, because the theoretical carbon content after adsorption (0.08% according to figure 4.1) was below the detection limit (0.1%).

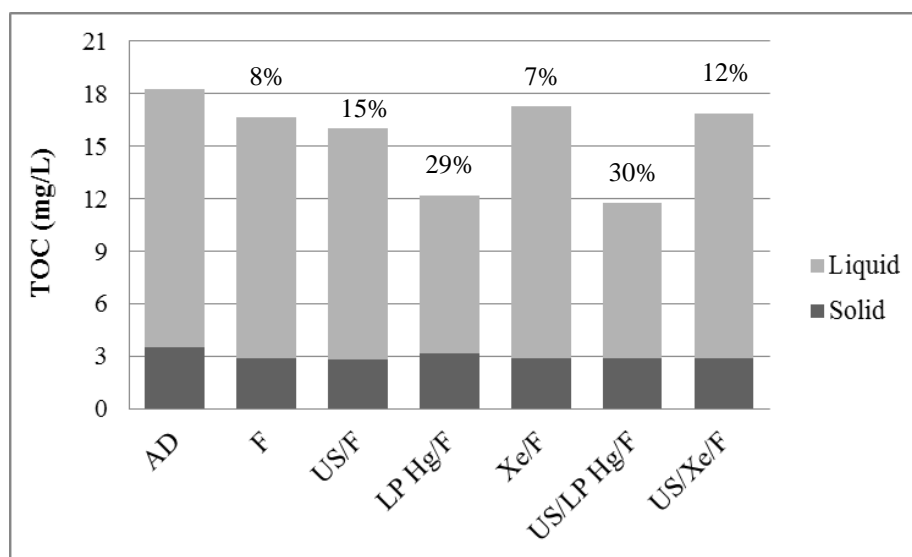


Figure 4.27. Carbon speciation after adsorption, Fenton oxidation and coupled processes ($[\text{IBP}]_0 = 20 \text{ mg/L}$, $[\text{Fe-MFI}] = 1 \text{ g/L}$, $[\text{H}_2\text{O}_2] = 6.4 \text{ mM}$, $\text{pH}_0 = 4.3$, $T = 25^\circ\text{C}$; US(-): $f_{\text{US}} = 20 \text{ kHz}$, $D_{\text{US}} = 50 \text{ W/L}$, UV: LP Hg lamp 6W, Vis: Xe lamp 150 W). Overall mineralization yield accounting for both liquid and solid phases is given above each bar

Highlights: heterogeneous (sono-)(photo-)Fenton processes

- ✓ Contrarily to the homogeneous Fenton, synergistic interaction between (ultra)sound/light and heterogeneous Fenton reaction was not observed.
- ✓ Absence of activation effect could be due to: limited interaction between ultrasound/light and Fe-MFI active surface and/or marginal catalyst modification under ultrasound and light irradiation and/or insignificant mass transfer limitation

4.7. EVALUATION OF TRANSFORMATION PRODUCTS

Transformation products during heterogeneous Fenton oxidation using Fe-MFI and ZVI (under acidic condition), as well as during sono-Fenton oxidation (Fe-MFI catalyst), were examined. As mentioned previously in chapter 3, analysis of samples was carried out by LC-HRMS and interpretation of intermediate evolution was only qualitative.

Oxidation intermediates were essentially the same as those observed in homogeneous Fenton reaction, but were not always detected (for instance some di-hydroxylated IBP derivatives). Therefore same degradation pathways could be hypothesized (cf. § 3.3, figure 3.26 for detailed scheme), except direct photo-degradation because light irradiation was not used in this case.

As in chapter 3, the evolution of four key transformation products, TP1A (1-hydroxy-IBP), TP1B (2-hydroxy-IBP), TP4 (4-isobutylacetophenone) and TP5 (TP4 isomer), was monitored during heterogeneous processes. With Fe-MFI catalyst, for which contribution of homogeneous reaction was negligible, formation and degradation of TP1A and TP1B occurred at slow rates (figures 4.28 and 4.29, respectively). Furthermore, despite limited effect of ultrasound on TOC removal in US(-)/F(+), its presence was found beneficial for the degradation of these products. Conversely, both formation and removal of TP1A and TP1B were much faster during Fenton oxidation with ZVI, due to significant leached iron which efficiently catalyzed the reaction. However, the occurrence of these compounds differed from what observed with ferrous salt ($\text{FeSO}_4 \cdot 7\text{H}_2\text{O}$), for which only the other mono-hydroxylated derivatives were detected. This would thus deserve further investigation.

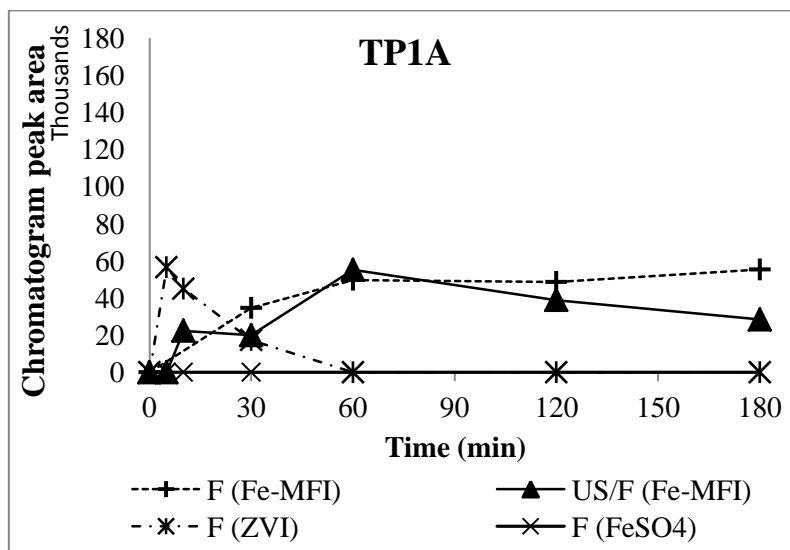


Figure 4.28. Evolution of TP1A concentration during heterogeneous Fenton-based processes (results of homogeneous Fenton reaction with ferrous iron salt were recalled for comparison purpose) ($\text{pH}_0_{\text{Fe-MFI}} = 4.3$; $\text{pH}_0_{\text{ZVI}} = 3.5$; $\text{pH}_0_{\text{FeSO}_4} = 2.6$)

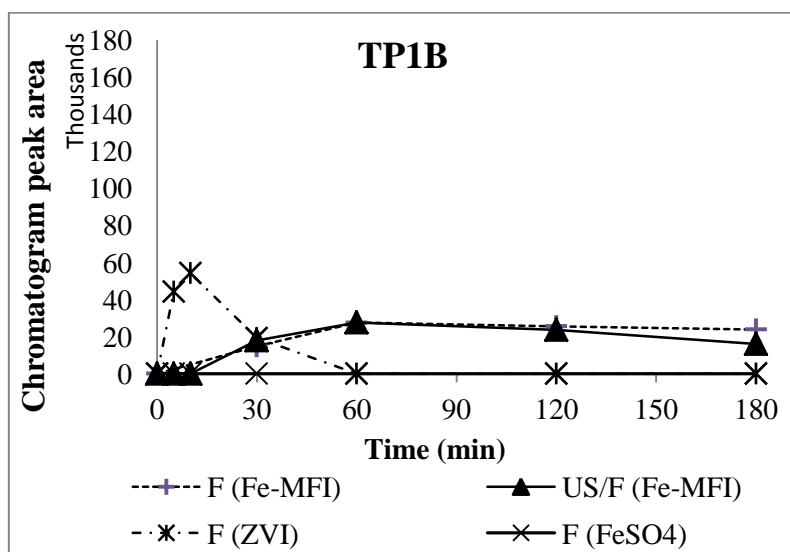


Figure 4.29. Evolution of TP1B concentration during heterogeneous Fenton-based processes (results of homogeneous Fenton reaction with ferrous iron salt were recalled for comparison purpose) ($\text{pH}_0_{\text{Fe-MFI}} = 4.3$; $\text{pH}_0_{\text{ZVI}} = 3.5$; $\text{pH}_0_{\text{FeSO}_4} = 2.6$)

Likewise, higher amounts of TP4 and TP5 were formed with ZVI than Fe-MFI, but they were also fast removed (in less than 1 hour) in the former case (figures 4.30 and 4.31, respectively). As for TP1A and TP1B, US helped the degradation of these intermediates, which differed from homogeneous process where sonolysis mainly promoted their formation.

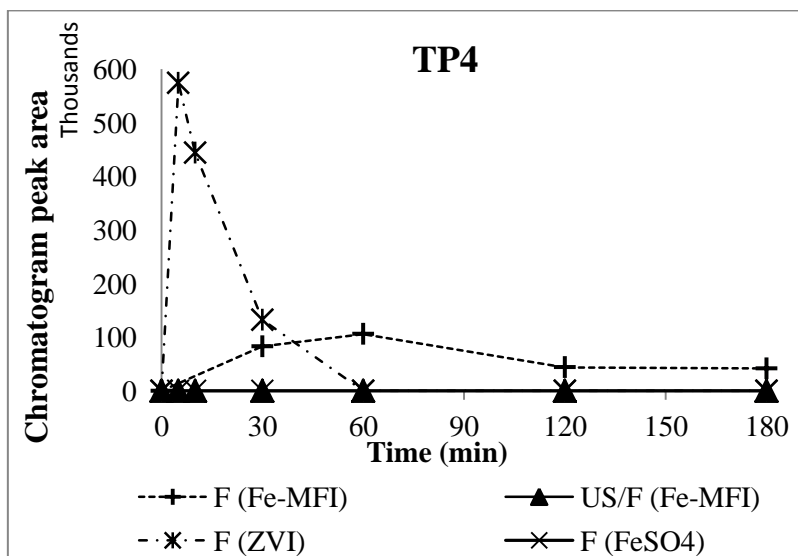


Figure 4.30. Evolution of TP4 concentration during heterogeneous Fenton-based processes (results of homogeneous Fenton reaction with ferrous iron salt were recalled for comparison purpose) ($\text{pH}_0_{\text{Fe-MFI}} = 4.3$; $\text{pH}_0_{\text{ZVI}} = 3.5$; $\text{pH}_0_{\text{FeSO}_4} = 2.6$)

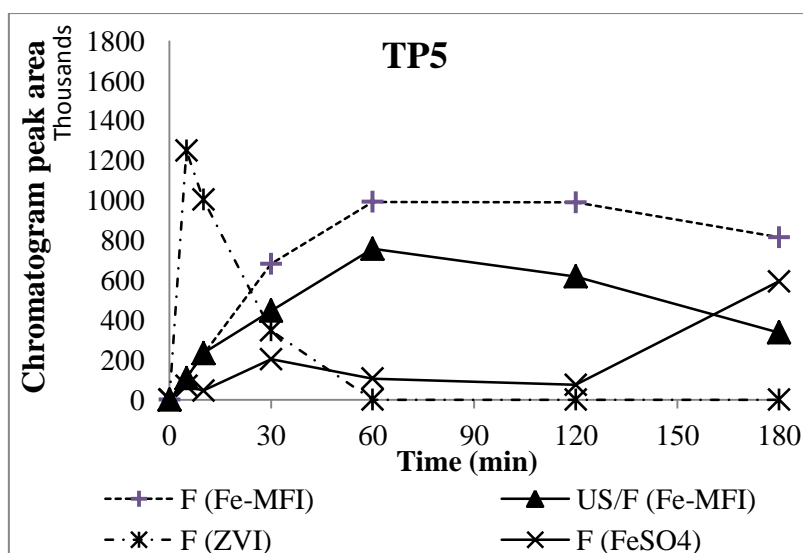


Figure 4.31. Evolution of TP5 concentration during heterogeneous Fenton-based processes (results of homogeneous Fenton reaction with ferrous iron salt were recalled for comparison purpose) ($\text{pH}_0_{\text{Fe-MFI}} = 4.3$; $\text{pH}_0_{\text{ZVI}} = 3.5$; $\text{pH}_0_{\text{FeSO}_4} = 2.6$)

According to these findings and previous results in chapter 3, different effects of activation processes may induce this contrasted behavior of specific intermediates and more specific studies are needed to explain the mechanisms involved in each process and their effects on the transformation/degradation pathway.

4.8. EFFECT OF WATER MATRIX

Contrarily to the homogeneous Fenton oxidation, heterogeneous Fenton (F) oxidation of IBP was performed in wastewater (WW) without pH adjustment. The result showed a high reduction of IBP degradation rate constant, from 0.0139 min^{-1} to 0.0016 min^{-1} (figure 4.32A). According to the literature [273,293], organic and inorganic compounds in wastewater may affect the heterogeneous reaction by (i) fouling the catalyst pores, (ii) poisoning the catalyst active sites (iron active sites forming complexes with organic and/or inorganic compounds), (iii) scavenging hydroxyl radicals and (iv) increasing the pH value, which could lower the catalyst activity. The latter effect seems to be predominant since the acidic zeolite was not able to reduce the pH to acidic condition due to the presence of natural buffer in WW matrix (in WW, pH value was only reduced from 8 to 7 after contact with Fe-MFI).

What is more, pH effect was evidenced by comparing Fenton oxidation performed in DW at a controlled pH of 7 (DW pH 7) and in WW matrix (figure 4.32). As described previously in § 4.2.5, alkaline pH solution can affect heterogeneous Fenton oxidation by limiting the interaction between ibuprofen and catalyst (repulsion between ionic form of IBP ($\text{pK}_a = 3.97$) and negatively charged Fe-MFI surface ($\text{pH}_{\text{pzc}} = 2.9$)), by reducing the oxidation potential of hydroxyl radical or by changing the reaction mechanism from radical to non-radical one.

Nonetheless, IBP oxidation was still slower in WW matrix than in DW at pH 7. One possible explanation is catalyst fouling or poisoning. At the end of adsorption step, adsorption of organic and inorganic compounds on Fe-MFI was indeed higher in WW matrix (21 mg/L of TC and 18 mg/L of IC adsorbed) than in DW matrix (4 mg/L of TC and no IC adsorbed). Nevertheless, these adsorbed compounds seemed not to affect the available active sites since similar H_2O_2 consumption was observed (figure 4.32C), excluding possible fouling or poisoning effect. Therefore lower IBP removal could be rather attributed to the scavenging effect of carbonate and bicarbonate ions present in WW matrix.

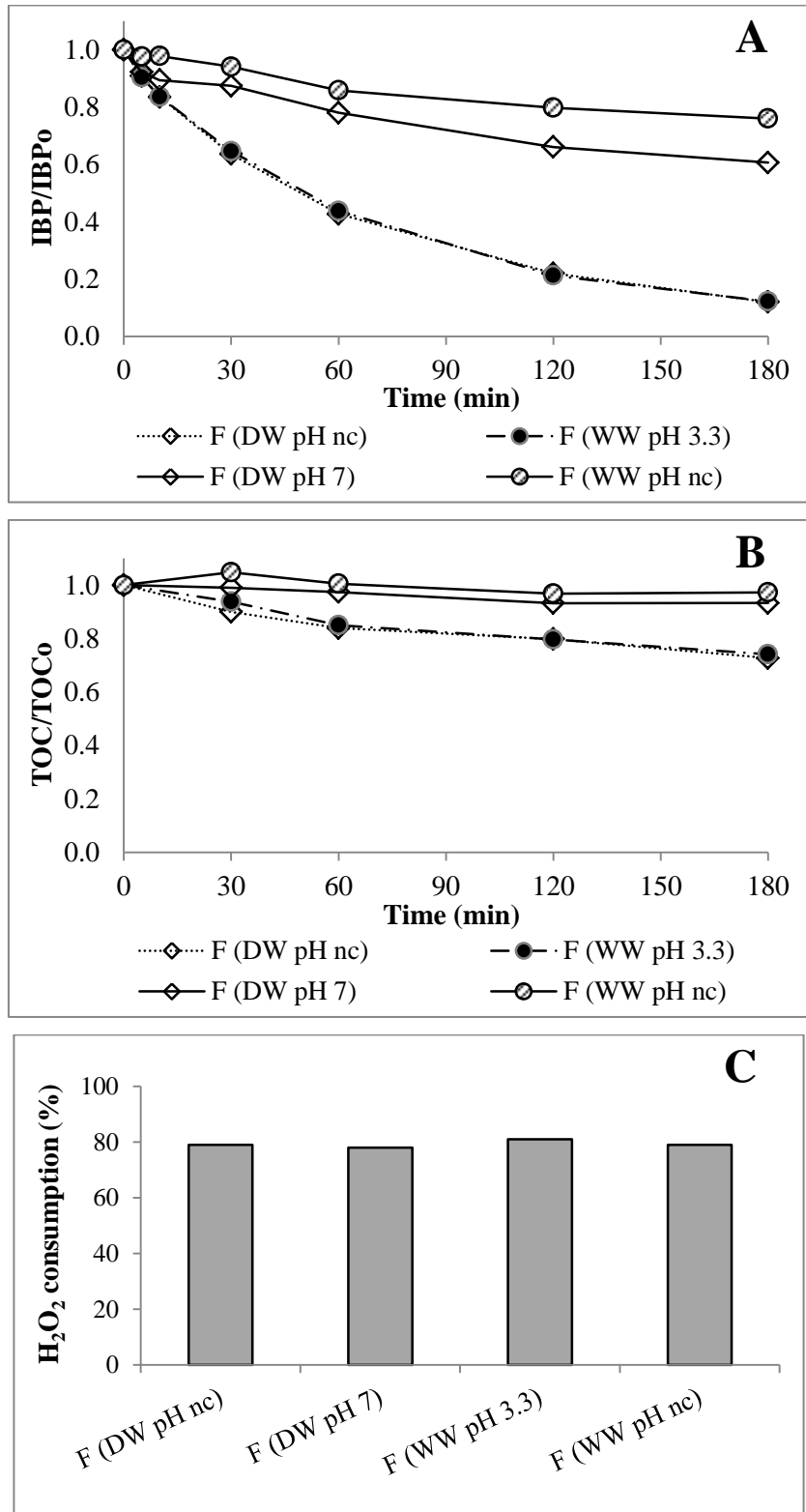


Figure 4.32. Effect of WW matrix on heterogeneous Fenton process: evolution of (A) IBP and (B) TOC concentration, and (C) H₂O₂ consumption ([IBP]₀ = 20 mg/L, [Fe-MFI] = 4.8 g/L, [H₂O₂]₀ = 6.4 mM, pH nc: pH not controlled, T = 25°C)

In order to confirm the dominant role of pH in WW matrix, a supplementary experiment was conducted in WW matrix whose initial pH was set to 3.3 (adjusted with 1 M H₂SO₄, denoted as WW pH 3.3). This pH value matched the value reached in DW after contact with Fe-MFI. Such acidification should maintain the catalytic activity of the heterogeneous catalysis and at the same time lower the inorganic carbon content. As shown in [figure 4.32A](#), at pH₀ = 3.3, similar IBP removal was indeed obtained in DW and WW matrix. Similar role of pH was observed for mineralization yield. Under non controlled pH, TOC removal by Fenton oxidation was reduced from 27% (DW pH nc) to 3% (WW pH nc), but the efficacy of the process could be normalized by preliminary acidification (WW pH 3.3) ([figure 4.32B](#)). In addition, it should be mentioned that the acidification step caused more iron leached into solution (0.081 mg/L for WW pH nc vs. 0.250 mg/L for WW pH 3.3).

Despite ultrasound had only a marginal effect on heterogeneous Fenton oxidation using high Fe-MFI concentration (4.8 g/L) in DW (cf. [figure 4.18](#)), sono-Fenton oxidation was also tested in WW matrix without pH adjustment. Regarding IBP, additive effect between ultrasound and heterogeneous Fenton oxidation at 4.8 g/L of catalyst was clearly observed in WW matrix ([figure 4.33](#)): IBP removal rate constant increased from 0.0016 min⁻¹ in sonolysis or Fenton oxidation to 0.0038 min⁻¹ in sono-Fenton oxidation. Because Fenton oxidation itself was significantly hampered, ultrasound irradiation then took significant part in the degradation process.

Accounting for measurement uncertainty, TOC removal in sono-Fenton (US/F) process showed hardly more than additive effect of ultrasound and Fenton oxidation, as the corresponding mineralization yields were 9%, 2% and 3% and respectively ([figure 4.33B](#)).

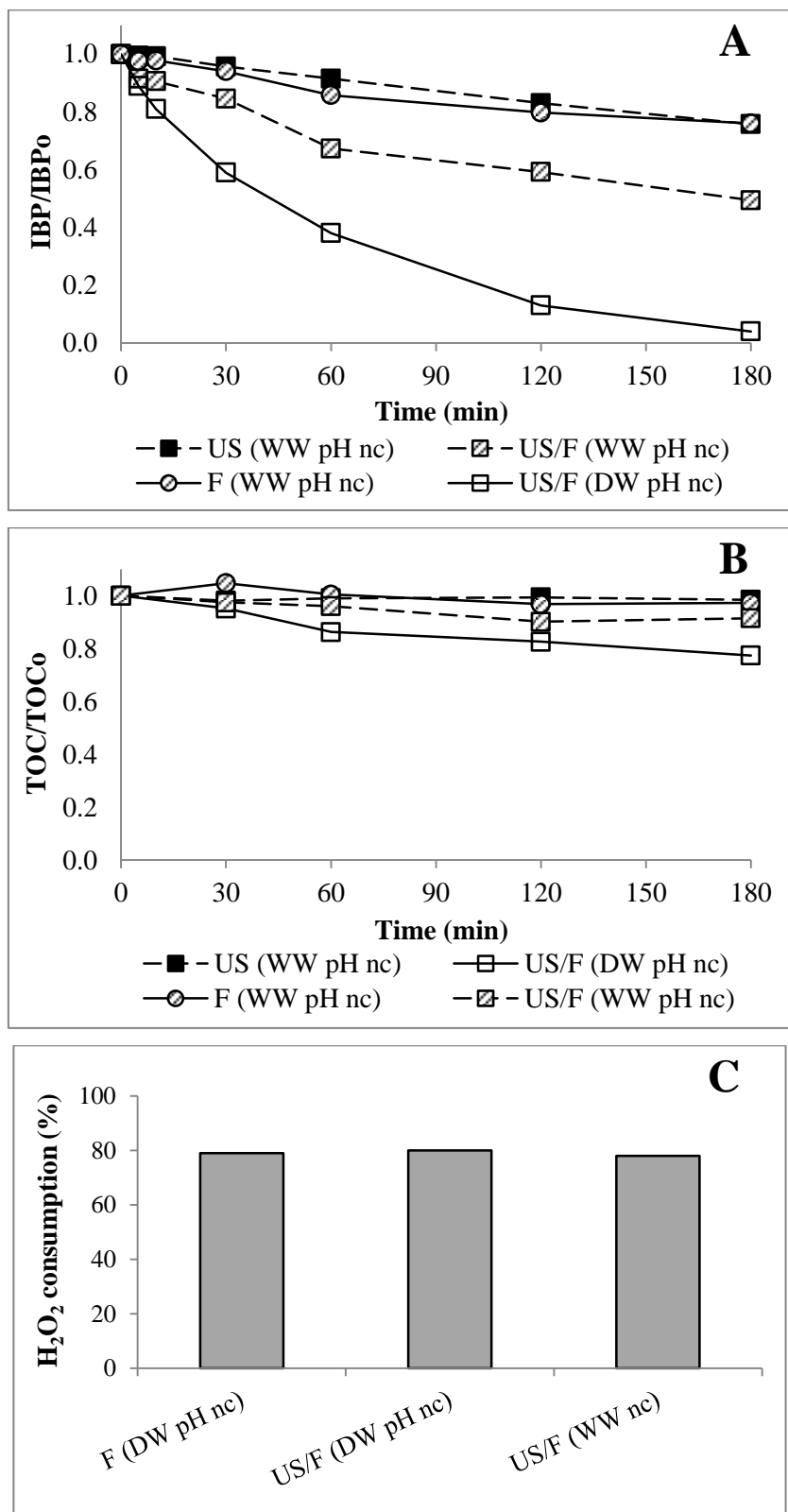


Figure 4.33. Effect of WW matrix on heterogeneous sono-Fenton process: evolution of (A) IBP and (B) TOC concentration, and (C) H₂O₂ consumption ([IBP]₀ = 20 mg/L, [Fe-MFI] = 4.8 g/L, [H₂O₂]₀ = 6.4 mM, pH nc: pH not controlled, T = 25°C, D_{US} = 50 W/L, f_{US} = 20 kHz)

In order to evaluate the effects of WW matrix and ultrasound on the catalyst textural properties, nitrogen porosimetry was performed, whose results are given in table 4.6. In all cases, BET surface area (S_{BET}) and microporous volume of the catalyst were only slightly reduced after use (by 10% maximum) and the effect was a little increased in WW matrix. This porosity reduction may be attributed to the deposition of organic and inorganic compounds from WW matrix or from IBP and its degradation products.

Table 4.6. Effect of WW matrix and ultrasound irradiation on catalyst BET surface area and porosity

Process	S_{BET} (m^2/g)	V_{meso} (cm^3/g)	V_{micro} (cm^3/g)	V_{tot} (cm^3/g)
Fresh Fe-MFI	329	0.050	0.130	0.180
F (DW)	310	0.052	0.123	0.175
F (WW)	297	0.051	0.118	0.169
US/F (DW)	308	0.055	0.122	0.177
US/F (WW)	298	0.052	0.118	0.170

Heterogeneous photo-Fenton oxidation was not evaluated in WW matrix as photo-activation of Fe-MFI catalyst was not observed in DW.

4.9. CONCLUSIONS

Two iron based catalysts were assessed for the catalytic wet peroxide oxidation of ibuprofen: iron-containing zeolite of ZSM5 type (Fe-MFI) and zero-valent iron particles (ZVI). Both catalysts were able to promote Fenton reaction. However, preliminary acidification was necessary to activate ZVI, while Fe-MFI catalyst was directly active by lowering the pH of the solution. Evaluation of used catalyst morphology and iron leaching revealed that the activity of ZVI was due to metal ions leached in the solution, while Fe-MFI promoted a true heterogeneous reaction implying surface iron species. This catalyst was thus selected for further investigation.

Parametric study of Fenton oxidation using Fe-MFI showed that ibuprofen removal rate was improved when increasing the concentrations of catalyst and hydrogen peroxide, as well as temperature. On the other hand, increase of solution pH towards (buffered) alkaline condition reduced the removal yield.

Contrarily to the homogeneous Fenton process (catalyzed by ferrous sulfate) where regeneration of ferrous ion could be promoted, activation of heterogeneous Fenton reaction by ultrasound or light irradiation appeared to be very limited. By coupling Fenton oxidation on Fe-MFI and ultrasound, only additive effect was observed at low catalyst concentration, while Fenton reaction was predominant at high Fe-MFI concentration. In the combined process of Fenton reaction with light irradiation, photo-peroxide oxidation (UV/H₂O₂) was the prevailing mechanism under UV light (LP Hg lamp), whilst the effect of visible light (emitted by xenon lamp) was found to be marginal.

Despite the limited synergy with ultrasound and light irradiation, heterogeneous Fenton oxidation catalyzed by Fe-MFI appeared to be a promising technique for ibuprofen removal in water. Under mild operating conditions (25°C, 4.8 g/L of Fe-MFI, 2 times the stoichiometric amount of H₂O₂), up to 88% of ibuprofen and 27% of TOC were removed after 3 hours of reaction. Moreover, this appreciable performance was also followed by very low iron leaching of about 0.05 mg/L. In wastewater matrix, heterogeneous Fenton oxidation of ibuprofen was however hampered, mainly due to buffered alkaline pH neutralizing Fe-MFI acidic sites. Therefore, preliminary acidification would still be required to maintain this performance. Only minor modifications of the catalyst after reaction (regarding particle size, morphology, iron content, and specific surface area) proved it could suit for continuous water treatment process coupled with ultrafiltration membrane.

This page is intentionally left blank

CONCLUSIONS AND PERSPECTIVES

This page is intentionally left blank

The aim of this study was to investigate the effect of (high / low frequency) (ultra)sound and (ultraviolet / visible) light irradiation for (re)activation of (homogeneous / heterogeneous) catalysts in Fenton reaction. Ibuprofen (IBP), one of the most frequently detected pharmaceuticals in water resources, was chosen as model molecule for this study. Both homogeneous and heterogeneous reaction have been extensively investigated and discussed in chapters 3 and 4, respectively. Compared to previous studies, complete work on the evaluation of synergistic effect of coupling processes was carried out by studying the separate processes and their exhaustive combinations. Moreover, a large set of parameters was varied, including irradiation wavelength range for both ultrasound and light, as well as concentration of oxidant and catalyst. At each stage dedicated studies or analyses were performed to get an insight of involved mechanisms by using various radical scavengers, examining the activity of leached iron, analyzing transformation products, pH and matrix effects, etc.

First, without additional oxidant (or catalyst), (ultra)sound alone (US) yielded moderate IBP degradation rates on the whole investigated frequency range (12 – 862 kHz), while effect of light irradiation appeared highly wavelength dependent: fast degradation under ultraviolet but no effect under visible light ([see following table](#)). This dependence is clearly related to direct photolysis, while US acts through free radical formation, like Fenton reactive systems. In addition, it should be mentioned that UV-Vis/H₂O₂ process (using MP Hg lamp 150 W) was very effective for the degradation and mineralization of IBP. Compared to other tested processes, the remarkable performance of this process could be ascribed to both high power and wide UV-C spectral emission of the lamp inducing very effective direct photolysis and photo-decomposition of H₂O₂.

Detailed comparison between homogeneous and heterogeneous systems was based on results obtained at same available iron content (0.13 mM), and a representative set of data is reported on the figure below, including reference experiments conducted without Fenton's reagent, under US or Vis irradiation.

Then, main point of this global comparison was the huge difference at the very beginning of the reaction (< 5 min) in between the results of homogeneous Fenton oxidation (IBP conversion > 60%) and that of heterogeneous counterparts (IBP conversion < 7%). At same available iron, all homogeneous Fenton-based processes started much faster, whatever the type of activation applied. However, after this fast initial step, performance of classical Fenton system drastically stepped down, due to formation of various ferric species (including

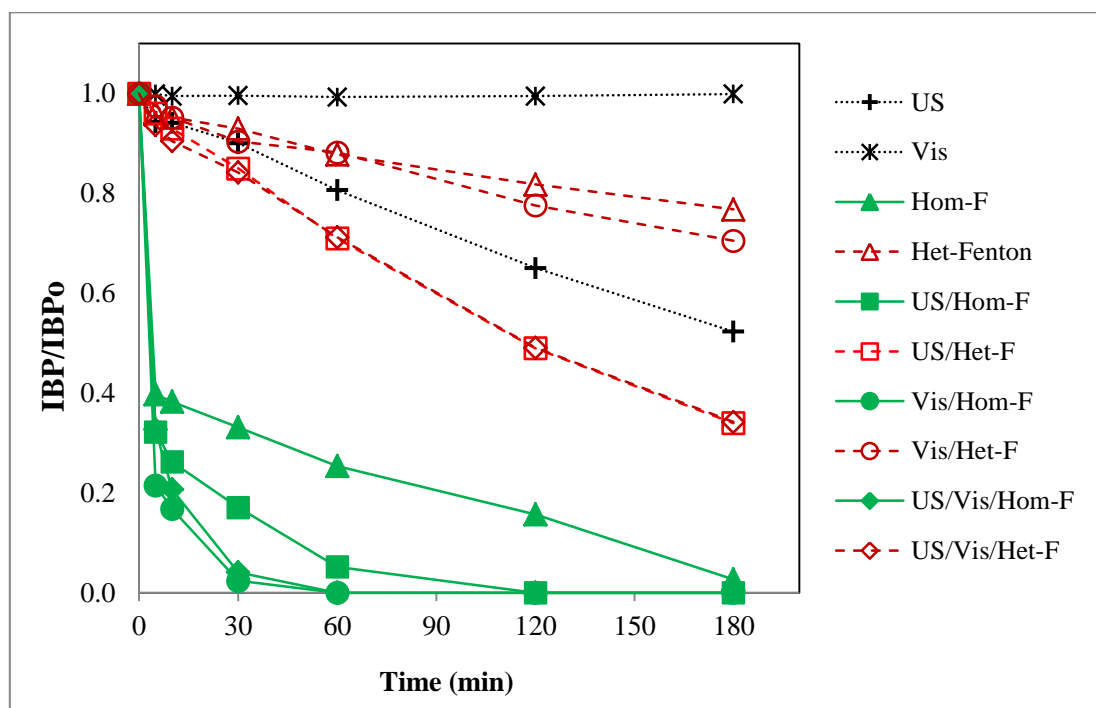
CONCLUSIONS AND PERSPECTIVES

complexes). As expected, both US and UV/Vis irradiations were able to regenerate homogeneous catalyst.

Summary of the principal results in homogeneous and heterogeneous processes

Processes	[Fe] (mM)	[H ₂ O ₂] (mM)	IBP Removal (%)		IBP constant rate (min ⁻¹)	TOC Removal (%) t=180 min	H ₂ O ₂ Conso (%) t=180 min	Interaction effect
			t=5 min	t=180 min				
Non-catalytic processes								
Ultrasound (US)	-	-	6	48	0.0035	7	-	
Ultraviolet (UV)	-	-	1	40	0.0028	19	-	
Visible (Vis)	-	-	0	0	0	0	-	
UV-Vis	-	-	23	100	0.0567	45	-	
UV/H ₂ O ₂	-	-	18	100	0.0664	30	14	
Vis/H ₂ O ₂	-	-	1	15	0.0009	5	6	
UV-Vis/H ₂ O ₂	-	-	49	100	0.2610	97	99	
Fenton processes								
Hom-F	0.033	1.6	25	35	NA	6	7	
Hom-F	0.134	6.4	60	97	NA	9	13	
Het-F	0.134	6.4	4	23	0.0014	5	26	
Het-F	0.643	6.4	9	88	0.0139	27	79	
Sono-Fenton processes								
US /Hom-F	0.033	1.6	25	89	NA	12	10	Additive
US /Hom-F	0.134	6.4	68	100	NA	39	44	Synergistic
US /Het-F	0.134	6.4	4	66	0.0059	14	27	Additive
US /Het-F	0.643	6.4	11	96	0.0159	23	80	No synergy
Photo-Fenton processes								
UV/Hom-F	0.134	6.4	79	100	NA	82	99	Synergistic
Vis/Hom-F	0.033	1.6	23	76	NA	15	15	Synergistic
Vis/Hom-F	0.134	6.4	79	100	NA	59	80	Synergistic
UV/Het-F	0.134	6.4	21	100	0.0578	35	37	No synergy
UV/Het-F	0.643	6.4	24	100	0.0411	26	83	No synergy
Vis/Het-F	0.134	6.4	3	30	0.0019	5	25	No synergy
Vis/Het-F	0.643	6.4	20	96	0.0159	26	89	Additive
Sono-photo-Fenton processes								
US/Vis/Hom-F	0.033	1.6	28	100	NA	17	25	Synergistic
US/Vis/Hom-F	0.134	6.4	67	100	NA	62	76	No synergy
US/Vis/Het-F	0.134	6.4	6	66	0.0058	11	30	No synergy

US(20 kHz, 50 W/L); UV(LP Hg lamp 6 W); Vis(Xenon lamp 150 W); UV-Vis(MP Hg lamp 150W); NA: not applicable due to steep change of slope



Comparison of homogeneous and heterogeneous process: IBP concentration-time profiles ($[IBP]_0 = 20$ mg/L, $[H_2O_2]_0 = 6.4$ mM, $[Fe^{2+}]_0 = 0.134$ mM or $[Fe-MFI] = 1$ g/L, $T = 25^\circ C$, $pH_0 = 2.6$ or 4.3 , $f_{US} = 20$ kHz, $D_{US} = 50W/L$, lamp = 150W Xe (Vis))

With regard to the negligible effect of direct photolysis under visible light (Vis), a remarkable synergistic effect was observed in photo(Vis)-Fenton process, for which nearly complete conversion of IBP was obtained in 30 min instead of 180 minutes (see Vis/Hom-F vs. Hom-F in figure). Likewise higher mineralization yield (TOC removal) and H_2O_2 consumption were always observed under coupled homogeneous processes (see table).

On the contrary, the expected activation by ultrasound or light irradiation of heterogeneous Fenton reaction (Het-F) catalyzed by Fe-ZSM5 catalyst (Fe-MFI) appeared to be very limited, wherein no more than additive effect was observed (see table). In heterogeneous system, IBP removal rates fitted well first-order kinetics indicating that Fe-MFI catalyst was not suffering significant deactivation during the reaction. Extensive catalyst analysis before and after reaction using SEM-EDX, nitrogen porosimetry, laser diffraction and ICP-AES (for lixiviate) also showed no significant modification in catalyst properties. Thus, benefit from US or UV/Vis irradiation for active surface reactivation is questionable. Moreover, in these conditions of rather slow kinetics, higher external mass transfer or particle disruption due to ultrasound would not be useful. On the other hand, contrasted results on

light irradiation effect would drive further work towards a more detailed investigation of light propagation in suspensions.

Despite the limited synergy with US and UV/Vis, heterogeneous Fenton reaction catalyzed by Fe-MFI is still a promising oxidation process considering its stability and activity, yielding more than 25% of TOC removal after 3 hours of reaction in 0.5% slurry. In addition, this appreciable performance obtained without acidification was also followed by very low iron leaching of about 0.05 mg/L, well above discharge limit (2 mg/L), leading to potential economical process.

To check more relevant conditions of application, efficacy of simple or combined processes was also tested in wastewater effluent matrix. All photo-based oxidation processes (UV, UV/H₂O₂, Vis/Hom-F) were inhibited, probably due to light attenuation, while preliminary acidification was essential to counterbalance the alkaline buffered pH effect of wastewater matrix and maintain the performance of ultrasound and Fenton-based processes. These results showed that water matrix must be taken into account to select the optimum process and determine the operating conditions for practical use. In addition, the influence of different molecules on process interaction would have to be considered, as well as that of pollutant concentration as wastewaters to be treated are less concentrated.

Regarding the net synergistic effect in homogeneous system, further studies should consider the optimization of coupled US/Vis/Hom-F process with the aim of achieving mineralization level required to remove (most of) the toxicity of the treated sample under relatively low reagent concentration (iron catalyst and H₂O₂) and low energy consumption. On the other hand, effect of US and UV/Vis activation on heterogeneous Fenton reaction should be further investigated by comparing several iron-containing solids. In any case, Fe-MFI is already a good candidate for testing in continuous water treatment process in association with membrane filtration. This type of continuous membrane process would be even more promising with a slowly dissolving iron catalyst as ZVI by optimizing solid iron content to obtain both activity and iron concentration below discharge limit.

REFERENCES

- [1] ANSM, Analyse des ventes de médicaments en France en 2012, (2013). http://ansm.sante.fr/var/ansm_site/storage/original/application/796352eff0e9119cca0ea5bbd898353a.pdf (accessed January 30, 2017).
- [2] ANSES, Campagne nationale d'occurrence des résidus de médicaments dans les eaux destinées à la consommation humaine, 2011.
- [3] T. Deblonde, C. Cossu-Leguille, P. Hartemann, Emerging pollutants in wastewater: a review of the literature., *Int. J. Hyg. Environ. Health.* 214 (2011) 442–8. doi:10.1016/j.ijheh.2011.08.002.
- [4] A. Ziylan, N.H. Ince, The occurrence and fate of anti-inflammatory and analgesic pharmaceuticals in sewage and fresh water: Treatability by conventional and non-conventional processes, *J. Hazard. Mater.* 187 (2011) 24–36.
- [5] J. Quintana, S. Weiss, T. Reemtsma, Pathways and metabolites of microbial degradation of selected acidic pharmaceutical and their occurrence in municipal wastewater treated by a membrane bioreactor, *Water Res.* 39 (2005) 2654–2664. doi:10.1016/j.watres.2005.04.068.
- [6] L. Berthod, D.C. Whitley, G. Roberts, A. Sharpe, R. Greenwood, G.A. Mills, Quantitative structure-property relationships for predicting sorption of pharmaceuticals to sewage sludge during waste water treatment processes, *Sci. Total Environ.* 579 (2017) 1512–1520. doi:10.1016/j.scitotenv.2016.11.156.
- [7] M. Carballa, F. Omil, J.M. Lema, Removal of cosmetic ingredients and pharmaceuticals in sewage primary treatment, *Water Res.* 39 (2005) 4790–4796. doi:10.1016/j.watres.2005.09.018.
- [8] M.M. Huber, S. Korhonen, T. a Ternes, U. von Gunten, Oxidation of pharmaceuticals during water treatment with chlorine dioxide., *Water Res.* 39 (2005) 3607–17. doi:10.1016/j.watres.2005.05.040.
- [9] Y. Mao, X. Wang, X. Guo, H. Yang, Y.F. Xie, Characterization of haloacetaldehyde and trihalomethane formation potentials during drinking water treatment, *Chemosphere.* 159 (2016) 378–384. doi:10.1016/j.chemosphere.2016.05.088.
- [10] M.J. Ahmed, Adsorption of non-steroidal anti-inflammatory drugs from aqueous solution using activated carbons: Review, *J. Environ. Manage.* 190 (2017) 274–282. doi:10.1016/j.jenvman.2016.12.073.
- [11] A. Vona, F. di Martino, J. Garcia-Ivars, Y. Picó, J.-A. Mendoza-Roca, M.-I. Iborra-Clar, Comparison of different removal techniques for selected pharmaceuticals, *J. Water Process Eng.* 5 (2015) 48–57. doi:10.1016/j.jwpe.2014.12.011.
- [12] J. Rivera-Utrilla, M. Sánchez-Polo, M.Á. Ferro-García, G. Prados-Joya, R. Ocampo-Pérez, Pharmaceuticals as emerging contaminants and their removal from water. A review, *Chemosphere.* 93 (2013) 1268–1287.
- [13] J. Wang, S. Wang, Removal of pharmaceuticals and personal care products (PPCPs) from wastewater: A review, *J. Environ. Manage.* 182 (2016) 620–640. doi:10.1016/j.jenvman.2016.07.049.
- [14] M.S.U. Rehman, N. Rashid, M. Ashfaq, A. Saif, N. Ahmad, J.-I. Han, Global risk of pharmaceutical contamination from highly populated developing countries, *Chemosphere.* 138 (2015) 1045–1055. doi:10.1016/j.chemosphere.2013.02.036.
- [15] M. Winkler, Selective degradation of ibuprofen and clofibrac acid in two model river

REFERENCES

- biofilm systems, *Water Res.* 35 (2001) 3197–3205. doi:10.1016/S0043-1354(01)00026-4.
- [16] World Health Organization, Pharmaceuticals in drinking water, 2012.
- [17] E.R. Cooper, T.C. Siewicki, K. Phillips, Preliminary risk assessment database and risk ranking of pharmaceuticals in the environment., *Sci. Total Environ.* 398 (2008) 26–33. doi:10.1016/j.scitotenv.2008.02.061.
- [18] Z. Shu, J.R. Bolton, M. Belosevic, M.G. El Din, Photodegradation of emerging micropollutants using the medium-pressure UV/H₂O₂ Advanced Oxidation Process., *Water Res.* 47 (2013) 2881–9. doi:10.1016/j.watres.2013.02.045.
- [19] J.L. Packer, J.J. Werner, D.E. Latch, K. McNeill, W.A. Arnold, Photochemical fate of pharmaceuticals in the environment: Naproxen, diclofenac, clofibrac acid, and ibuprofen, *Aquat. Sci.* 65 (2003) 342–351. doi:10.1007/s00027-003-0671-8.
- [20] M. Bergheim, R. Gminski, B. Spangenberg, M. Dębiak, A. Bürkle, V. Mersch-Sundermann, et al., Recalcitrant pharmaceuticals in the aquatic environment: a comparative screening study of their occurrence, formation of phototransformation products and their in vitro toxicity, *Environ. Chem.* 11 (2014) 431–444.
- [21] A. Azzouz, E. Ballesteros, Influence of seasonal climate differences on the pharmaceutical, hormone and personal care product removal efficiency of a drinking water treatment plant, *Chemosphere.* 93 (2013) 2046–2054.
- [22] M. Farré, D. Asperger, L. Kantiani, S. González, M. Petrovic, D. Barceló, Assessment of the acute toxicity of triclosan and methyl triclosan in wastewater based on the bioluminescence inhibition of *Vibrio fischeri.*, *Anal. Bioanal. Chem.* 390 (2008) 1999–2007. doi:10.1007/s00216-007-1779-9.
- [23] L. Lishman, S.A. Smyth, K. Sarafin, S. Kleywegt, J. Toito, T. Peart, et al., Occurrence and reductions of pharmaceuticals and personal care products and estrogens by municipal wastewater treatment plants in Ontario, Canada., *Sci. Total Environ.* 367 (2006) 544–58. doi:10.1016/j.scitotenv.2006.03.021.
- [24] F. Méndez-Arriaga, S. Esplugas, J. Giménez, Degradation of the emerging contaminant ibuprofen in water by photo-Fenton., *Water Res.* 44 (2010) 589–95.
- [25] C. Bouissou-Schurtz, P. Houeto, M. Guerbet, M. Bachelot, C. Casellas, A.-C. Mauclair, et al., Ecological risk assessment of the presence of pharmaceutical residues in a French national water survey, *Regul. Toxicol. Pharmacol.* 69 (2014) 296–303. doi:10.1016/j.yrtph.2014.04.006.
- [26] C. Carlsson, A.-K. Johansson, G. Alvan, K. Bergman, T. Kühler, Are pharmaceuticals potent environmental pollutants?: Part I: Environmental risk assessments of selected active pharmaceutical ingredients, *Sci. Total Environ.* 364 (2006) 67–87. doi:http://dx.doi.org/10.1016/j.scitotenv.2005.06.035.
- [27] M.S. Kostich, A.L. Batt, J.M. Lazorchak, Concentrations of prioritized pharmaceuticals in effluents from 50 large wastewater treatment plants in the US and implications for risk estimation., *Environ. Pollut.* 184C (2013) 354–359. doi:10.1016/j.envpol.2013.09.013.
- [28] D. Pascoe, W. Karntanut, C.T. Müller, Do pharmaceuticals affect freshwater invertebrates? A study with the cnidarian *Hydra vulgaris*, *Chemosphere.* 51 (2003) 521–528. doi:10.1016/S0045-6535(02)00860-3.
- [29] L. Heckmann, A. Callaghan, H. Hooper, R. Connon, T. Hutchinson, S. Maund, et al., Chronic toxicity of ibuprofen to *Daphnia magna*: Effects on life history traits and population dynamics, *Toxicol. Lett.* 172 (2007) 137–145. doi:10.1016/j.toxlet.2007.06.001.
- [30] N. Pounds, S. Maclean, M. Webley, D. Pascoe, T. Hutchinson, Acute and chronic effects of ibuprofen in the mollusc *Planorbis carinatus* (Gastropoda: Planorbidae),

REFERENCES

- Ecotoxicol. Environ. Saf. 70 (2008) 47–52. doi:10.1016/j.ecoenv.2007.07.003.
- [31] B. Quinn, F. Gagné, C. Blaise, An investigation into the acute and chronic toxicity of eleven pharmaceuticals (and their solvents) found in wastewater effluent on the cnidarian, *Hydra attenuata*, *Sci. Total Environ.* 389 (2008) 306–314. doi:10.1016/j.scitotenv.2007.08.038.
- [32] S. Han, K. Choi, J. Kim, K. Ji, S. Kim, B. Ahn, et al., Endocrine disruption and consequences of chronic exposure to ibuprofen in Japanese medaka (*Oryzias latipes*) and freshwater cladocerans *Daphnia magna* and *Moina macrocopa*., *Aquat. Toxicol.* 98 (2010) 256–64. doi:10.1016/j.aquatox.2010.02.013.
- [33] F. Méndez-Arriaga, R.A. Torres-Palma, C. Pétrier, S. Esplugas, J. Gimenez, C. Pulgarin, Mineralization enhancement of a recalcitrant pharmaceutical pollutant in water by advanced oxidation hybrid processes, *Water Res.* 43 (2009) 3984–3991.
- [34] O. Legrini, E. Oliveros, A.M. Braun, Photochemical processes for water treatment, *Chem. Rev.* 93 (1993) 671–698. doi:10.1021/cr00018a003.
- [35] S. Navalon, M. Alvaro, H. Garcia, Heterogeneous Fenton catalysts based on clays, silicas and zeolites, *Appl. Catal. B Environ.* 99 (2010) 1–26.
- [36] M. Pera-Titus, V. García-Molina, M. a Baños, J. Giménez, S. Esplugas, Degradation of chlorophenols by means of advanced oxidation processes: a general review, *Appl. Catal. B Environ.* 47 (2004) 219–256. doi:10.1016/j.apcatb.2003.09.010.
- [37] M. Klavarioti, D. Mantzavinos, D. Kassinos, Removal of residual pharmaceuticals from aqueous systems by advanced oxidation processes., *Environ. Int.* 35 (2009) 402–17. doi:10.1016/j.envint.2008.07.009.
- [38] N. Sabri, K. Hanna, V. Yargeau, Chemical oxidation of ibuprofen in the presence of iron species at near neutral pH, *Sci. Total Environ.* 427–428 (2012) 382–389.
- [39] S.-P. Sun, X. Zeng, A.T. Lemley, Nano-magnetite catalyzed heterogeneous Fenton-like degradation of emerging contaminants carbamazepine and ibuprofen in aqueous suspensions and montmorillonite clay slurries at neutral pH, *J. Mol. Catal. A Chem.* 371 (2013) 94–103. doi:10.1016/j.molcata.2013.01.027.
- [40] F. Méndez-Arriaga, R.A. Torres-Palma, C. Pétrier, S. Esplugas, J. Gimenez, C. Pulgarin, Ultrasonic treatment of water contaminated with ibuprofen, *Water Res.* 42 (2008) 4243–4248.
- [41] R. Xiao, Z. He, D. Diaz-Rivera, G.Y. Pee, L.K. Weavers, Sonochemical degradation of ciprofloxacin and ibuprofen in the presence of matrix organic compounds, *Ultrason. Sonochem.* 21 (2014) 428–435.
- [42] R.K. Szabó, C. Megyeri, E. Illés, K. Gajda-Schranz, P. Mazellier, A. Dombi, Phototransformation of ibuprofen and ketoprofen in aqueous solutions., *Chemosphere.* 84 (2011) 1658–63. doi:10.1016/j.chemosphere.2011.05.012.
- [43] J. Madhavan, F. Grieser, M. Ashokkumar, Combined advanced oxidation processes for the synergistic degradation of ibuprofen in aqueous environments., *J. Hazard. Mater.* 178 (2010) 202–8.
- [44] J.C.C. da Silva, J.A.R. Teodoro, R.J. de C.F. Afonso, S.F. Aquino, R. Augusti, Photolysis and photocatalysis of ibuprofen in aqueous medium: characterization of by-products via liquid chromatography coupled to high-resolution mass spectrometry and assessment of their toxicities against *Artemia salina*., *J. Mass Spectrom.* 49 (2014) 145–53. doi:10.1002/jms.3320.
- [45] J. Choina, H. Kosslick, C. Fischer, G.-U. Flechsig, L. Frunza, A. Schulz, Photocatalytic decomposition of pharmaceutical ibuprofen pollutions in water over titania catalyst, *Appl. Catal. B Environ.* 129 (2013) 589–598. doi:10.1016/j.apcatb.2012.09.053.
- [46] F. Méndez-Arriaga, S. Esplugas, J. Giménez, Photocatalytic degradation of non-

REFERENCES

- steroidal anti-inflammatory drugs with TiO₂ and simulated solar irradiation., *Water Res.* 42 (2008) 585–94.
- [47] S. Loaiza-Ambuludi, M. Panizza, N. Oturan, A. Özcan, M.A. Oturan, Electro-Fenton degradation of anti-inflammatory drug ibuprofen in hydroorganic medium, *J. Electroanal. Chem.* 702 (2013) 31–36. doi:10.1016/j.jelechem.2013.05.006.
- [48] C. Zwiener, Oxidative treatment of pharmaceuticals in water, *Water Res.* 34 (2000) 1881–1885. doi:10.1016/S0043-1354(99)00338-3.
- [49] A. Ziylan, N.H. Ince, Catalytic ozonation of ibuprofen with ultrasound and Fe-based catalysts, *Catal. Today.* (2014). doi:10.1016/j.cattod.2014.03.002.
- [50] R. Gonzalez-Olmos, F. Holzer, F.-D. Kopinke, A. Georgi, Indications of the reactive species in a heterogeneous Fenton-like reaction using Fe-containing zeolites, *Appl. Catal. A Gen.* 398 (2011) 44–53. doi:10.1016/j.apcata.2011.03.005.
- [51] M.Y. Ghaly, G. Härtel, R. Mayer, R. Haseneder, Photochemical oxidation of p-chlorophenol by UV/H₂O₂ and photo-Fenton process. A comparative study, *Waste Manag.* 21 (2001) 41–47. doi:10.1016/S0956-053X(00)00070-2.
- [52] I. Michael, A. Achilleos, D. Lambropoulou, V.O. Torrens, S. Pérez, M. Petrović, et al., Proposed transformation pathway and evolution profile of diclofenac and ibuprofen transformation products during (sono)photocatalysis, *Appl. Catal. B Environ.* 147 (2014) 1015–1027.
- [53] M.A. Miranda, I. Morera, F. Vargas, M.J. Gómez-Lechón, J.V. Castell, In vitro assessment of the phototoxicity of anti-inflammatory 2-arylpropionic acids, *Toxicol. Vitro.* 5 (1991) 451–455. doi:10.1016/0887-2333(91)90071-K.
- [54] G. Ruggeri, G. Ghigo, V. Maurino, C. Minero, D. Vione, Photochemical transformation of ibuprofen into harmful 4-isobutylacetophenone: pathways, kinetics, and significance for surface waters., *Water Res.* 47 (2013) 6109–21. doi:10.1016/j.watres.2013.07.031.
- [55] E. Illés, E. Takács, A. Dombi, K. Gajda-Schrantz, G. Rácz, K. Gonter, et al., Hydroxyl radical induced degradation of ibuprofen., *Sci. Total Environ.* 447 (2013) 286–92. doi:10.1016/j.scitotenv.2013.01.007.
- [56] E. Neyens, J. Baeyens, A review of classic Fenton's peroxidation as an advanced oxidation technique, *J. Hazard. Mater.* 98 (2003) 33–50.
- [57] V. Kavitha, K. Palanivelu, The role of ferrous ion in Fenton and photo-Fenton processes for the degradation of phenol., *Chemosphere.* 55 (2004) 1235–43. doi:10.1016/j.chemosphere.2003.12.022.
- [58] F. Velichkova, C. Julcour-Lebigue, B. Koumanova, H. Delmas, Heterogeneous Fenton oxidation of paracetamol using iron oxide (nano)particles, *J. Environ. Chem. Eng.* 1 (2013) 1–9. doi:10.1016/j.jece.2013.09.011.
- [59] H.J.H. Fenton, Oxidation of tartaric acid in the presence of iron, *J. Chem. Soc.* 889 (1894) 899–910.
- [60] A. Babuponnusami, K. Muthukumar, A review on Fenton and improvements to the Fenton process for wastewater treatment, *J. Environ. Chem. Eng.* 2 (2013) 557–572.
- [61] A.Y. Sychev, V.G. Isak, Iron compounds and the mechanisms of the homogeneous catalysis of the activation of O₂ and H₂O₂ and of the oxidation of organic substrates, *Russ. Chem. Rev.* 64 (1995) 1105.
- [62] J. De Laat, H. Gallard, Catalytic decomposition of hydrogen peroxide by Fe(III) in homogeneous aqueous solution: mechanism and kinetic modeling, *Environ. Sci. Technol.* 33 (1999) 2726–2732.
- [63] J.J. Pignatello, E. Oliveros, A. MacKay, Advanced Oxidation Processes for Organic Contaminant Destruction Based on the Fenton Reaction and Related Chemistry, *Crit. Rev. Environ. Sci. Technol.* 36 (2006) 1–84. doi:10.1080/10643380500326564.

REFERENCES

- [64] Y. Segura, F. Martínez, J.A. Melero, R. Molina, R. Chand, D.H. Bremner, Enhancement of the advanced Fenton process (Fe⁰/H₂O₂) by ultrasound for the mineralization of phenol, *Appl. Catal. B Environ.* 113–114 (2012) 100–106. doi:10.1016/j.apcatb.2011.11.024.
- [65] J. He, X. Yang, B. Men, D. Wang, Interfacial mechanisms of heterogeneous Fenton reactions catalyzed by iron-based materials: A review, *J. Environ. Sci.* (2016). doi:10.1016/j.jes.2015.12.003.
- [66] Y. Ahmed, Z. Yaakob, P. Akhtar, Degradation and mineralization of methylene blue using a heterogeneous photo-Fenton catalyst under visible and solar light irradiation, *Catal. Sci. Technol.* 6 (2016) 1222–1232. doi:10.1039/C5CY01494H.
- [67] S. Rahim Pouran, A.R. Abdul Aziz, W.M.A. Wan Daud, Review on the main advances in photo-Fenton oxidation system for recalcitrant wastewaters, *J. Ind. Eng. Chem.* 21 (2015) 53–69. doi:10.1016/j.jiec.2014.05.005.
- [68] E.G. Garrido-Ramírez, B.K. Theng, M.L. Mora, Clays and oxide minerals as catalysts and nanocatalysts in Fenton-like reactions — A review, *Appl. Clay Sci.* 47 (2010) 182–192. doi:10.1016/j.clay.2009.11.044.
- [69] P. V Nidheesh, Heterogeneous Fenton catalysts for the abatement of organic pollutants from aqueous solution: a review, *RSC Adv.* 5 (2015) 40552–40577. doi:10.1039/C5RA02023A.
- [70] S. Lin, M.D. Gurol, Catalytic Decomposition of Hydrogen Peroxide on Iron Oxide: Kinetics, Mechanism, and Implications, *Environ. Sci. Technol.* 32 (1998) 1417–1423. doi:10.1021/es970648k.
- [71] X. Xue, K. Hanna, M. Abdelmoula, N. Deng, Adsorption and oxidation of PCP on the surface of magnetite: Kinetic experiments and spectroscopic investigations, *Appl. Catal. B Environ.* 89 (2009) 432–440. doi:10.1016/j.apcatb.2008.12.024.
- [72] X. Zeng, A.T. Lemley, Fenton Degradation of 4,6-Dinitro-o-cresol with Fe²⁺-Substituted Ion-Exchange Resin, *J. Agric. Food Chem.* 57 (2009) 3689–3694. doi:10.1021/jf900764q.
- [73] S. Zha, Y. Cheng, Y. Gao, Z. Chen, M. Megharaj, R. Naidu, Nanoscale zero-valent iron as a catalyst for heterogeneous Fenton oxidation of amoxicillin, *Chem. Eng. J.* 255 (2014) 141–148. doi:10.1016/j.cej.2014.06.057.
- [74] A.L.-T. Pham, C. Lee, F.M. Doyle, D.L. Sedlak, A silica-supported iron oxide catalyst capable of activating hydrogen peroxide at neutral pH values., *Environ. Sci. Technol.* 43 (2009) 8930–5. doi:10.1021/es902296k.
- [75] K. Rusevova, R. Köferstein, M. Rosell, H.H. Richnow, F.-D. Kopinke, A. Georgi, LaFeO₃ and BiFeO₃ perovskites as nanocatalysts for contaminant degradation in heterogeneous Fenton-like reactions, *Chem. Eng. J.* 239 (2014) 322–331. doi:10.1016/j.cej.2013.11.025.
- [76] W.C. Bray, M.H. Gorin, Ferryl ion, a compound of tetravalent iron, *J. Am. Chem. Soc.* 54 (1932) 2124–2125. doi:10.1021/ja01344a505.
- [77] I. Fecheté, Y. Wang, J.C. Védrine, The past, present and future of heterogeneous catalysis, *Catal. Today.* 189 (2012) 2–27. doi:10.1016/j.cattod.2012.04.003.
- [78] M.D.G. de Luna, R.M. Briones, C.-C. Su, M.-C. Lu, Kinetics of acetaminophen degradation by Fenton oxidation in a fluidized-bed reactor, *Chemosphere.* 90 (2013) 1444–1448. doi:10.1016/j.chemosphere.2012.09.003.
- [79] R.P. Cavalcante, L. da Rocha Sandim, D. Bogo, A.M.J. Barbosa, M.E. Osugi, M. Blanco, et al., Application of Fenton, photo-Fenton, solar photo-Fenton, and UV/H₂O₂ to degradation of the antineoplastic agent mitoxantrone and toxicological evaluation, *Environ. Sci. Pollut. Res.* 20 (2013) 2352–2361.
- [80] H. Kusić, N. Koprivanac, I. Selanec, Fe-exchanged zeolite as the effective

REFERENCES

- heterogeneous Fenton-type catalyst for the organic pollutant minimization: UV irradiation assistance., *Chemosphere*. 65 (2006) 65–73. doi:10.1016/j.chemosphere.2006.02.053.
- [81] M. Siddique, R. Farooq, G.J. Price, Synergistic effects of combining ultrasound with the Fenton process in the degradation of Reactive Blue 19, *Ultrason. Sonochem.* 21 (2014) 1206–12.
- [82] C. Wang, Y. Shih, Degradation and detoxification of diazinon by sono-Fenton and sono-Fenton-like processes, *Sep. Purif. Technol.* 140 (2015) 6–12. doi:10.1016/j.seppur.2014.11.005.
- [83] M. Velásquez, I.P. Santander, D.R. Contreras, J. Yáñez, C. Zaror, R.A. Salazar, et al., Oxidative degradation of sulfathiazole by Fenton and photo-Fenton reactions, *J. Environ. Sci. Heal. Part A*. 49 (2014) 661–670. doi:10.1080/10934529.2014.865447.
- [84] G. Centi, S. Perathoner, T. Torre, M.G. Verduna, Catalytic wet oxidation with H₂O₂ of carboxylic acids on homogeneous and heterogeneous Fenton-type catalysts, *Catal. Today*. 55 (2000) 61–69. doi:10.1016/S0920-5861(99)00226-6.
- [85] T. Zhou, Y. Li, J. Ji, F.-S. Wong, X. Lu, Oxidation of 4-chlorophenol in a heterogeneous zero valent iron/H₂O₂ Fenton-like system: Kinetic, pathway and effect factors, *Sep. Purif. Technol.* 62 (2008) 551–558. doi:10.1016/j.seppur.2008.03.008.
- [86] A. Cihanoglu, G. Gündüz, M. Dükkancı, Degradation of acetic acid by heterogeneous Fenton-like oxidation over iron-containing ZSM-5 zeolites, *Appl. Catal. B Environ.* 165 (2015) 687–699. doi:10.1016/j.apcatb.2014.10.073.
- [87] D.E. Hughes, W.L. Nyborg, Cell Disruption by Ultrasound: Streaming and other activity around sonically induced bubbles is a cause of damage to living cells, *Sci.* 138 (1962) 108–114. doi:10.1126/science.138.3537.108.
- [88] T.J. Mason, J.P. Lorimer, *Applied sonochemistry: the uses of power ultrasound in chemistry and processing*. 2002, John Wiley & Sons, Ltd., 1991.
- [89] N.T. Le, C. Julcour-Lebigue, H. Delmas, An executive review of sludge pretreatment by sonication, *J. Environ. Sci. (China)*. 37 (2015) 139–53. doi:10.1016/j.jes.2015.05.031.
- [90] Y.G. Adewuyi, *Sonochemistry: Environmental Science and Engineering Applications*, *Ind. Eng. Chem. Res.* 40 (2001) 4681–4715. doi:10.1021/ie010096l.
- [91] S. Pilli, P. Bhunia, S. Yan, R.J. LeBlanc, R.D. Tyagi, R.Y. Surampalli, Ultrasonic pretreatment of sludge: a review, *Ultrason. Sonochem.* 18 (2011) 1–18.
- [92] J. González-García, V. Sáez, I. Tudela, M.I. Díez-García, M. Deseada Esclapez, O. Louisnard, Sonochemical treatment of water polluted by chlorinated organocompounds. A review, *Water*. 2 (2010) 28–74. doi:10.3390/w2010028.
- [93] Y. Ma, Short review : Current trends and future challenges in the application of sono-Fenton oxidation for wastewater treatment, *Sustain. Environ. Res.* 22 (2012) 271–278.
- [94] J.P. Lorimer, T.J. Mason, *Sonochemistry. Part 1—The physical aspects*, *Chem. Soc. Rev.* 16 (1987) 239–274. doi:10.1039/CS9871600239.
- [95] Y.L. Pang, A.Z. Abdullah, S. Bhatia, Review on sonochemical methods in the presence of catalysts and chemical additives for treatment of organic pollutants in wastewater, *Desalination*. 277 (2011) 1–14.
- [96] F. Burdin, N.A. Tsochatzidis, P. Guiraud, A.M. Wilhelm, H. Delmas, Characterisation of the acoustic cavitation cloud by two laser techniques, *Ultrason. Sonochem.* 6 (1999) 43–51. doi:10.1016/S1350-4177(98)00035-2.
- [97] Z. Frontistis, D. Mantzavinos, Sonodegradation of 17 α -ethynylestradiol in environmentally relevant matrices: Laboratory-scale kinetic studies, *Ultrason. Sonochem.* 19 (2012) 77–84.
- [98] I. Gültekin, N.H. Ince, Ultrasonic destruction of bisphenol-A: the operating

REFERENCES

- parameters, *Ultrason. Sonochem.* 15 (2008) 524–9.
- [99] G.T. Güyer, N.H. Ince, Degradation of diclofenac in water by homogeneous and heterogeneous sonolysis, *Ultrason. Sonochem.* 18 (2011) 114–119.
- [100] I. Quesada-Peñate, C. Julcour-Lebigue, U.J. Jáuregui-Haza, A.M. Wilhelm, H. Delmas, Sonolysis of levodopa and paracetamol in aqueous solutions, *Ultrason. Sonochem.* 16 (2009) 610–616.
- [101] R. Xiao, D. Diaz-Rivera, L.K. Weavers, Factors Influencing Pharmaceutical and Personal Care Product Degradation in Aqueous Solution Using Pulsed Wave Ultrasound, *Ind. Eng. Chem. Res.* 52 (2013) 2824–2831.
- [102] S.-H. Kim, Q. Tian, J. Fang, S. Sung, Removal of 17- β estradiol in water by sonolysis, *Int. Biodeterior. Biodegradation.* 102 (2015) 11–14. doi:10.1016/j.ibiod.2015.03.017.
- [103] M. Goel, H. Hongqiang, A.S. Mujumdar, M.B. Ray, Sonochemical decomposition of volatile and non-volatile organic compounds-a comparative study, *Water Res.* 38 (2004) 4247–4261.
- [104] H.-M. Hung, M.R. Hoffmann, Kinetics and Mechanism of the Sonolytic Degradation of Chlorinated Hydrocarbons: Frequency Effects, *J. Phys. Chem. A.* 103 (1999) 2734–2739. doi:10.1021/jp9845930.
- [105] J. Liang, S. Komarov, N. Hayashi, E. Kasai, Improvement in sonochemical degradation of 4-chlorophenol by combined use of Fenton-like reagents., *Ultrason. Sonochem.* 14 (2007) 201–207.
- [106] G. Cruz-González, K. Gonzalez-Labrada, Y. Milian-Rodriguez, I. Quesada-Peñate, J. Colín-Luna, J. Ramírez-Muñoz, et al., Enhancement of paracetamol degradation by sono-Fenton process, *Int. J. Chem. Mater. Environ. Res.* 2 (2015) 37–45.
- [107] I.D. Manariotis, H.K. Karapanagioti, C. V. Chrysikopoulos, Degradation of PAHs by high frequency ultrasound, *Water Res.* 45 (2011) 2587–2594. doi:10.1016/j.watres.2011.02.009.
- [108] E. De Bel, C. Janssen, S. De Smet, H. Van Langenhove, J. Dewulf, Sonolysis of ciprofloxacin in aqueous solution: Influence of operational parameters, *Ultrason. Sonochem.* 18 (2011) 184–189. doi:10.1016/j.ultsonch.2010.05.003.
- [109] A.M. Lastre-Acosta, G. Cruz-González, L. Nuevas-Paz, U.J. Jáuregui-Haza, A.C.S.C. Teixeira, Ultrasonic degradation of sulfadiazine in aqueous solutions, *Environ. Sci. Pollut. Res.* 22 (2015) 918–925.
- [110] Z. Eren, N.H. Ince, Sonolytic and sonocatalytic degradation of azo dyes by low and high frequency ultrasound, *J. Hazard. Mater.* 177 (2010) 1019–1024. doi:10.1016/j.jhazmat.2010.01.021.
- [111] V. Naddeo, V. Belgiorno, D. Kassinos, D. Mantzavinos, S. Meric, Ultrasonic degradation, mineralization and detoxification of diclofenac in water: Optimization of operating parameters, *Ultrason. Sonochem.* 17 (2010) 179–185. doi:10.1016/j.ultsonch.2009.04.003.
- [112] M. Sivakumar, A.B. Pandit, Ultrasound enhanced degradation of Rhodamine B: optimization with power density, *Ultrason. Sonochem.* 8 (2001) 233–240. doi:10.1016/S1350-4177(01)00082-7.
- [113] B. Neppolian, H. Jung, H. Choi, J.H. Lee, J.-W. Kang, Sonolytic degradation of methyl tert-butyl ether: the role of coupled Fenton process and persulphate ion, *Water Res.* 36 (2002) 4699–4708.
- [114] L. Jih-Gaw, M. Ying-Shih, Oxidation of 2-chlorophenol in water by ultrasound/Fenton method, *J. Environ. Eng.* 126 (2000) 130–137.
- [115] S. Papoutsakis, S. Miralles-Cuevas, N. Gondrexon, S. Baup, S. Malato, C. Pulgarin, Coupling between high-frequency ultrasound and solar photo-Fenton at pilot scale for the treatment of organic contaminants: an initial approach., *Ultrason. Sonochem.* 22

REFERENCES

- (2015) 527–34. doi:10.1016/j.ultsonch.2014.05.003.
- [116] P. Vaishnave, A. Kumar, R. Ameta, P.B. Punjabi, S.C. Ameta, Photo oxidative degradation of azure-B by sono-photo-Fenton and photo-Fenton reagents, *Arab. J. Chem.* (2012). doi:10.1016/j.arabjc.2010.12.019.
- [117] D.H. Bremner, R. Molina, F. Martínez, J.A. Melero, Y. Segura, Degradation of phenolic aqueous solutions by high frequency sono-Fenton systems (US–Fe₂O₃/SBA-15–H₂O₂), *Appl. Catal. B Environ.* 90 (2009) 380–388. doi:10.1016/j.apcatb.2009.03.028.
- [118] P.R. Gogate, S. Mujumdar, A.B. Pandit, A Sonophotocatalytic Reactor for the Removal of Formic Acid from Wastewater, *Ind. Eng. Chem. Res.* 41 (2002) 3370–3378. doi:10.1021/ie010711i.
- [119] R. Huang, Z. Fang, X. Yan, W. Cheng, Heterogeneous sono-Fenton catalytic degradation of bisphenol A by Fe₃O₄ magnetic nanoparticles under neutral condition, *Chem. Eng. J.* 197 (2012) 242–249. doi:10.1016/j.cej.2012.05.035.
- [120] Y. Segura, R. Molina, F. Martínez, J. a Melero, Integrated heterogeneous sono-photo Fenton processes for the degradation of phenolic aqueous solutions., *Ultrason. Sonochem.* 16 (2009) 417–24. doi:10.1016/j.ultsonch.2008.10.004.
- [121] H. Zhang, H. Fu, D. Zhang, Degradation of CI Acid Orange 7 by ultrasound enhanced heterogeneous Fenton-like process, *J. Hazard. Mater.* 172 (2009) 654–660.
- [122] B. Neppolian, J.-S. Park, H. Choi, Effect of Fenton-like oxidation on enhanced oxidative degradation of para-chlorobenzoic acid by ultrasonic irradiation., *Ultrason. Sonochem.* 11 (2004) 273–9. doi:10.1016/j.ultsonch.2003.11.001.
- [123] M. Su, M. Xue, X. Cai, Z. Shang, F. Xu, Particle size characterization by ultrasonic attenuation spectra, *Particuology.* 6 (2008) 276–281. doi:10.1016/j.partic.2008.02.001.
- [124] A. Khataee, P. Gholami, B. Vahid, S.W. Joo, Heterogeneous sono-Fenton process using pyrite nanorods prepared by non-thermal plasma for degradation of an anthraquinone dye, *Ultrason. Sonochem.* 32 (2016) 357–370. doi:10.1016/j.ultsonch.2016.04.002.
- [125] E. Villaroel, J. Silva-Agredo, C. Petrier, G. Taborda, R.A. Torres-Palma, Ultrasonic degradation of acetaminophen in water: Effect of sonochemical parameters and water matrix, *Ultrason. Sonochem.* 21 (2014) 1763–1769.
- [126] R.A. Torres, G. Sarantakos, E. Combet, C. Pétrier, C. Pulgarin, Sequential helio-photo-Fenton and sonication processes for the treatment of bisphenol A, *J. Photochem. Photobiol. A Chem.* 199 (2008) 197–203.
- [127] D.H. Bremner, S. Di Carlo, A.G. Chakinala, G. Cravotto, Mineralisation of 2,4-dichlorophenoxyacetic acid by acoustic or hydrodynamic cavitation in conjunction with the advanced Fenton process., *Ultrason. Sonochem.* 15 (2008) 416–9. doi:10.1016/j.ultsonch.2007.06.003.
- [128] J. Madhavan, P.S.S. Kumar, S. Anandan, M. Zhou, F. Grieser, M. Ashokkumar, Ultrasound assisted photocatalytic degradation of diclofenac in an aqueous environment., *Chemosphere.* 80 (2010) 747–52. doi:10.1016/j.chemosphere.2010.05.018.
- [129] M. Dükkancı, M. Vinatoru, T.J. Mason, The sonochemical decolourisation of textile azo dye Orange II: effects of Fenton type reagents and UV light., *Ultrason. Sonochem.* 21 (2014) 846–53.
- [130] C.-H. Weng, V. Huang, Application of Fe⁰ aggregate in ultrasound enhanced advanced Fenton process for decolorization of methylene blue, *J. Ind. Eng. Chem.* 28 (2015) 153–160. doi:10.1016/j.jiec.2015.02.010.
- [131] M. Cai, J. Su, G. Lian, X. Wei, C. Dong, H. Zhang, et al., Sono-advanced Fenton decolorization of azo dye Orange G: Analysis of synergistic effect and mechanisms,

REFERENCES

- Ultrason. Sonochem. 31 (2016) 193–200. doi:10.1016/j.ultsonch.2015.12.017.
- [132] J. Herney-Ramirez, M. a. Vicente, L.M. Madeira, Heterogeneous photo-Fenton oxidation with pillared clay-based catalysts for wastewater treatment: A review, *Appl. Catal. B Environ.* 98 (2010) 10–26. doi:10.1016/j.apcatb.2010.05.004.
- [133] T. Oppenländer, *Photochemical purification of water and air, advanced oxidation processes: Principles, reaction mechanisms, reactor concepts*, 2003. doi:10.1002/9783527610884.
- [134] K. Loubière, M. Oelgemöller, T. Aillet, O. Dechy-Cabaret, L. Prat, Continuous-flow photochemistry: A need for chemical engineering, *Chem. Eng. Process. Process Intensif.* 104 (2016) 120–132. doi:10.1016/j.cep.2016.02.008.
- [135] F.H. Li, K. Yao, W.Y. Lv, G.G. Liu, P. Chen, H.P. Huang, et al., Photodegradation of Ibuprofen Under UV–Vis Irradiation: Mechanism and Toxicity of Photolysis Products, *Bull. Environ. Contam. Toxicol.* 94 (2015) 479–483. doi:10.1007/s00128-015-1494-8.
- [136] H.D. Burrows, M. Canle L, J.A. Santaballa, S. Steenken, Reaction pathways and mechanisms of photodegradation of pesticides, *J. Photochem. Photobiol. B Biol.* 67 (2002) 71–108. doi:10.1016/S1011-1344(02)00277-4.
- [137] S. Parsons, *Advanced Oxidation Processes for Water and Wastewater Treatment*, 2004.
- [138] S. Na, C. Jinhua, M. Cui, J. Khim, Sonophotolytic diethyl phthalate (DEP) degradation with UVC or VUV irradiation, *Ultrason. Sonochem.* 19 (2012) 1094–1098.
- [139] P. Iovino, S. Chianese, S. Canzano, M. Prisciandaro, D. Musmarra, Degradation of Ibuprofen in Aqueous Solution with UV Light: the Effect of Reactor Volume and pH, *Water, Air, {&} Soil Pollut.* 227 (2016) 1–9. doi:10.1007/s11270-016-2890-3.
- [140] H.-S. Son, J.-K. Im, K.-D. Zoh, A Fenton-like degradation mechanism for 1,4-dioxane using zero-valent iron (Fe⁰) and UV light., *Water Res.* 43 (2009) 1457–63. doi:10.1016/j.watres.2008.12.029.
- [141] M.G. Gonzalez, E. Oliveros, M. Wörner, A.M. Braun, Vacuum-ultraviolet photolysis of aqueous reaction systems, *J. Photochem. Photobiol. C Photochem. Rev.* 5 (2004) 225–246. doi:10.1016/j.jphotochemrev.2004.10.002.
- [142] A. Lopez, A. Bozzi, G. Mascolo, J. Kiwi, Kinetic investigation on UV and UV/H₂O₂ degradations of pharmaceutical intermediates in aqueous solution, *J. Photochem. Photobiol. A Chem.* 156 (2003) 121–126. doi:10.1016/S1010-6030(02)00435-5.
- [143] I. Kim, H. Tanaka, Photodegradation characteristics of PPCPs in water with UV treatment, *Environ. Int.* 35 (2009) 793–802. doi:10.1016/j.envint.2009.01.003.
- [144] B.C. Faust, J. Hoigné, Photolysis of Fe (III)-hydroxy complexes as sources of OH radicals in clouds, fog and rain, *Atmos. Environ. Part A. Gen. Top.* 24 (1990) 79–89. doi:10.1016/0960-1686(90)90443-Q.
- [145] H.-J. Benkelberg, P. Warneck, Photodecomposition of Iron(III) hydroxo and sulfato complexes in aqueous solution: wavelength dependence of OH and SO₄⁻ quantum Yields, *J. Phys. Chem.* 99 (1995) 5214–5221. doi:10.1021/j100014a049.
- [146] C. Lee, J. Yoon, Determination of quantum yields for the photolysis of Fe(III)-hydroxo complexes in aqueous solution using a novel kinetic method., *Chemosphere.* 57 (2004) 1449–58. doi:10.1016/j.chemosphere.2004.07.052.
- [147] S.G. Behar B, Photochemical evolution of oxygen from certain aqueous solutions, *Pubmed.* 154 (1966) 1012–1013.
- [148] F. Torrades, M. Pérez, H.D. Mansilla, J. Peral, Experimental design of Fenton and photo-Fenton reactions for the treatment of cellulose bleaching effluents., *Chemosphere.* 53 (2003) 1211–20. doi:10.1016/S0045-6535(03)00579-4.
- [149] A. Safarzadeh-Amiri, J.R. Bolton, S.R. Cater, Ferrioxalate-mediated photodegradation of organic pollutants in contaminated water, *Water Res.* 31 (1997) 787–798.

REFERENCES

- doi:10.1016/S0043-1354(96)00373-9.
- [150] E.M. Rodríguez, B. Núñez, G. Fernández, F.J. Beltrán, Effects of some carboxylic acids on the Fe(III)/UVA photocatalytic oxidation of muconic acid in water, *Appl. Catal. B Environ.* 89 (2009) 214–222. doi:10.1016/j.apcatb.2008.11.030.
- [151] T.D. Waite, F.M.M. Morel, Photoreductive dissolution of colloidal iron oxides in natural waters, *Environ. Sci. Technol.* 18 (1984) 860–868. doi:10.1021/es00129a010.
- [152] D.A. Nichela, J.A. Donadelli, B.F. Caram, M. Haddou, F.J. Rodriguez Nieto, E. Oliveros, et al., Iron cycling during the autocatalytic decomposition of benzoic acid derivatives by Fenton-like and photo-Fenton techniques, *Appl. Catal. B Environ.* 170–171 (2015) 312–321. doi:10.1016/j.apcatb.2015.01.028.
- [153] C.H. Langford, J.H. Carey, The charge transfer photochemistry of the hexaaquoiron(III) ion, the chloroheptaquoiron(III) ion, and the μ -dihydroxo dimer explored with *tert*-butyl alcohol scavenging, *Can. J. Chem.* 53 (1975) 2430–2435.
- [154] F. Martínez, G. Calleja, J.A. Melero, R. Molina, Heterogeneous photo-Fenton degradation of phenolic aqueous solutions over iron-containing SBA-15 catalyst, *Appl. Catal. B Environ.* 60 (2005) 181–190. doi:10.1016/j.apcatb.2005.03.004.
- [155] N. Wang, T. Zheng, G. Zhang, P. Wang, A review on Fenton-like processes for organic wastewater treatment, *J. Environ. Chem. Eng.* (2016). doi:10.1016/j.jece.2015.12.016.
- [156] G.B. Ortiz de la Plata, O.M. Alfano, A.E. Cassano, 2-Chlorophenol degradation via photo Fenton reaction employing zero valent iron nanoparticles, *J. Photochem. Photobiol. A Chem.* 233 (2012) 53–59. doi:10.1016/j.jphotochem.2012.02.023.
- [157] F. Yuan, C. Hu, X. Hu, J. Qu, M. Yang, Degradation of selected pharmaceuticals in aqueous solution with UV and UV/H₂O₂, *Water Res.* 43 (2009) 1766–1774. doi:10.1016/j.watres.2009.01.008.
- [158] D.H. Funai, F. Didier, J. Giménez, S. Esplugas, P. Marco, A. Machulek, Photo-Fenton treatment of valproate under UVC, UVA and simulated solar radiation, *J. Hazard. Mater.* 323 (2017) 537–549.
- [159] J. Sun, J. Feng, S. Shi, Y. Pi, M. Song, Y. Shi, Degradation of the antibiotic sulfamonomethoxine sodium in aqueous solution by photo-Fenton oxidation, *Chinese Sci. Bull.* 57 (2012) 558–564. doi:10.1007/s11434-011-4887-z.
- [160] B. Iurascu, I. Siminiceanu, D. Vione, M.A. Vicente, A. Gil, Phenol degradation in water through a heterogeneous photo-Fenton process catalyzed by Fe-treated laponite., *Water Res.* 43 (2009) 1313–22. doi:10.1016/j.watres.2008.12.032.
- [161] J. Feng, X. Hu, P.L. Yue, H.Y. Zhu, G.Q. Lu, Discoloration and mineralization of Reactive Red HE-3B by heterogeneous photo-Fenton reaction., *Water Res.* 37 (2003) 3776–84. doi:10.1016/S0043-1354(03)00268-9.
- [162] M.B. Kasiri, H. Aleboyeh, A. Aleboyeh, Degradation of Acid Blue 74 using Fe-ZSM5 zeolite as a heterogeneous photo-Fenton catalyst, *Appl. Catal. B Environ.* 84 (2008) 9–15. doi:10.1016/j.apcatb.2008.02.024.
- [163] F. Duarte, L.M. Madeira, Fenton- and Photo-Fenton-Like Degradation of a Textile Dye by Heterogeneous Processes with Fe/ZSM-5 Zeolite, *Sep. Sci. Technol.* 45 (2010) 1512–1520. doi:10.1080/01496395.2010.487452.
- [164] R. Gonzalez-Olmos, M.J. Martin, A. Georgi, F.-D. Kopinke, I. Oller, S. Malato, Fe-zeolites as heterogeneous catalysts in solar Fenton-like reactions at neutral pH, *Appl. Catal. B Environ.* 125 (2012) 51–58. doi:10.1016/j.apcatb.2012.05.022.
- [165] F. Velichkova, H. Delmas, C. Julcour, B. Koumanova, Heterogeneous Fenton and photo-Fenton oxidation for paracetamol removal using iron containing ZSM-5 zeolite as catalyst, *AIChE J.* (2016) n/a--n/a. doi:10.1002/aic.15369.
- [166] I. Grčić, S. Papić, K. Žižek, N. Koprivanac, Zero-valent iron (ZVI) Fenton oxidation

REFERENCES

- of reactive dye wastewater under UV-C and solar irradiation, *Chem. Eng. J.* 195–196 (2012) 77–90. doi:10.1016/j.cej.2012.04.093.
- [167] M. Aleksić, H. Kušić, N. Koprivanac, D. Leszczynska, A.L. Božić, Heterogeneous Fenton type processes for the degradation of organic dye pollutant in water — The application of zeolite assisted AOPs, *Desalination*. 257 (2010) 22–29. doi:10.1016/j.desal.2010.03.016.
- [168] R. a Torres, C. Pétrier, E. Combet, F. Moulet, C. Pulgarin, Bisphenol A mineralization by integrated ultrasound-UV-iron (II) treatment., *Environ. Sci. Technol.* 41 (2007) 297–302.
- [169] J. Madhavan, P.S. Sathish Kumar, S. Anandan, F. Grieser, M. Ashokkumar, Degradation of acid red 88 by the combination of sonolysis and photocatalysis, *Sep. Purif. Technol.* 74 (2010) 336–341. doi:10.1016/j.seppur.2010.07.001.
- [170] H. Katsumata, T. Kobayashi, S. Kaneco, T. Suzuki, K. Ohta, Degradation of linuron by ultrasound combined with photo-Fenton treatment, *Chem. Eng. J.* 166 (2011) 468–473. doi:10.1016/j.cej.2010.10.073.
- [171] L.J. Xu, W. Chu, N. Graham, Degradation of di-n-butyl phthalate by a homogeneous sono-photo-Fenton process with in-situ generated hydrogen peroxide, *Chem. Eng. J.* 240 (2013) 541–547.
- [172] J. Madhavan, F. Grieser, M. Ashokkumar, Sonophotocatalytic degradation of paracetamol using TiO₂ and Fe³⁺, *Sep. Purif. Technol.* 103 (2013) 114–118. doi:10.1016/j.seppur.2012.10.003.
- [173] J. Madhavan, P.S. Sathish Kumar, S. Anandan, F. Grieser, M. Ashokkumar, Sonophotocatalytic degradation of monocrotopos using TiO₂ and Fe³⁺, *J. Hazard. Mater.* 177 (2010) 944–9. doi:10.1016/j.jhazmat.2010.01.009.
- [174] S. Chakma, V.S. Moholkar, Investigations in synergism of hybrid advanced oxidation processes with combinations of sonolysis + Fenton process + UV for degradation of bisphenol A, *Ind. Eng. Chem. Res.* 53 (2014) 6855–6865.
- [175] X. Zhong, S. Royer, H. Zhang, Q. Huang, L. Xiang, S. Valange, et al., Mesoporous silica iron-doped as stable and efficient heterogeneous catalyst for the degradation of C.I. Acid Orange 7 using sono-photo-Fenton process, *Sep. Purif. Technol.* 80 (2011) 163–171. doi:10.1016/j.seppur.2011.04.024.
- [176] C. Sirtori, A. Zapata, W. Gernjak, S. Malato, A. Lopez, A. Agüera, Solar photo-Fenton degradation of nalidixic acid in waters and wastewaters of different composition. Analytical assessment by LC-TOF-MS., *Water Res.* 45 (2011) 1736–44. doi:10.1016/j.watres.2010.11.023.
- [177] S. Queirós, V. Morais, C.S.D. Rodrigues, F.J. Maldonado-Hódar, L.M. Madeira, Heterogeneous Fenton's oxidation using Fe/ZSM-5 as catalyst in a continuous stirred tank reactor, *Sep. Purif. Technol.* 141 (2015) 235–245. doi:10.1016/j.seppur.2014.11.046.
- [178] Y. Segura, F. Martínez, J.A. Melero, J.L.G. Fierro, Zero valent iron (ZVI) mediated Fenton degradation of industrial wastewater: Treatment performance and characterization of final composites, *Chem. Eng. J.* 269 (2015) 298–305. doi:10.1016/j.cej.2015.01.102.
- [179] W. Chu, K.H. Chan, C.Y. Kwan, K.Y. Choi, Degradation of atrazine by modified stepwise-Fenton's processes., *Chemosphere.* 67 (2007) 755–61. doi:10.1016/j.chemosphere.2006.10.039.
- [180] A.C.-K. Yip, F.L.-Y. Lam, X. Hu, Chemical-Vapor-Deposited Copper on Acid-Activated Bentonite Clay as an Applicable Heterogeneous Catalyst for the Photo-Fenton-like Oxidation of Textile Organic Pollutants, *Ind. Eng. Chem. Res.* 44 (2005) 7983–7990. doi:10.1021/ie050647y.

REFERENCES

- [181] I.-H. Yoon, G. Yoo, H.-J. Hong, J. Kim, M.G. Kim, W.-K. Choi, et al., Kinetic study for phenol degradation by ZVI-assisted Fenton reaction and related iron corrosion investigated by X-ray absorption spectroscopy, *Chemosphere*. 145 (2016) 409–415. doi:10.1016/j.chemosphere.2015.11.108.
- [182] C.K. Duesterberg, S.E. Mylon, T.D. Waite, pH Effects on Iron-Catalyzed Oxidation using Fenton's Reagent, *Environ. Sci. Technol.* 42 (2008) 8522–8527. doi:10.1021/es801720d.
- [183] M. Pérez, Fenton and photo-Fenton oxidation of textile effluents, *Water Res.* 36 (2002) 2703–2710. doi:10.1016/S0043-1354(01)00506-1.
- [184] E. Elmolla, M. Chaudhuri, Optimization of Fenton process for treatment of amoxicillin, ampicillin and cloxacillin antibiotics in aqueous solution., *J. Hazard. Mater.* 170 (2009) 666–72. doi:10.1016/j.jhazmat.2009.05.013.
- [185] M.S. Saghafinia, S.M. Emadian, M. Vossoughi, Performances Evaluation of Photo-Fenton Process and Sonolysis for the Treatment of Penicillin G Formulation Effluent, *Procedia Environ. Sci.* 8 (2011) 202–208. doi:10.1016/j.proenv.2011.10.033.
- [186] R. Bauer, H. Fallmann, The Photo-Fenton Oxidation --- A cheap and efficient wastewater treatment method, *Res. Chem. Intermed.* 23 (1997) 341–354. doi:10.1163/156856797X00565.
- [187] N. Koprivanac, H. Kusic, AOP as an Effective tool for the Minimization of Hazardous Organic Pollutants in Colored Wastewater; Chemical and Photochemical Processes;, in: *Hazard. Mater. Wastewater Treat. Remov. Anal.*, 2006: pp. 149–199.
- [188] European Commission, Council Directive 76/464/EEC, (2006). http://ec.europa.eu/environment/water/water-dangersub/lib_dang_substances.htm.
- [189] F. Velichkova, Vers un procédé Fenton hétérogène pour le traitement en continu d'eau polluée par des polluants pharmaceutiques, (2014). <http://ethesis.inp-toulouse.fr/archive/00002806/> (accessed December 1, 2016).
- [190] O.A. Makhotkina, E.V. Kuznetsova, S.V. Preis, Catalytic detoxification of 1,1-dimethylhydrazine aqueous solutions in heterogeneous Fenton system, *Appl. Catal. B Environ.* 68 (2006) 85–91. doi:10.1016/j.apcatb.2006.07.008.
- [191] R. Gonzalez-Olmos, U. Roland, H. Toufar, F.-D. Kopinke, A. Georgi, Fe-zeolites as catalysts for chemical oxidation of MTBE in water with H₂O₂, *Appl. Catal. B Environ.* 89 (2009) 356–364. doi:10.1016/j.apcatb.2008.12.014.
- [192] P.R. Gogate, Treatment of wastewater streams containing phenolic compounds using hybrid techniques based on cavitation: a review of the current status and the way forward, *Ultrason. Sonochem.* 15 (2008) 1–15.
- [193] M. Dükkanci, G. Gündüz, S. Yilmaz, R. V. Prihod'ko, Heterogeneous Fenton-like degradation of Rhodamine 6G in water using CuFeZSM-5 zeolite catalyst prepared by hydrothermal synthesis., *J. Hazard. Mater.* 181 (2010) 343–50. doi:10.1016/j.jhazmat.2010.05.016.
- [194] T. Mason, J. Lorimer, *Applied Sonochemistry: Uses of Power Ultrasound in Chemistry and Processing*, 2002.
- [195] B. Darsinou, Z. Frontistis, M. Antonopoulou, I. Konstantinou, D. Mantzavinos, Sono-activated persulfate oxidation of bisphenol A: Kinetics, pathways and the controversial role of temperature, *Chem. Eng. J.* 280 (2015) 623–633. doi:10.1016/j.cej.2015.06.061.
- [196] K. Rusevova, F.-D. Kopinke, A. Georgi, Nano-sized magnetic iron oxides as catalysts for heterogeneous Fenton-like reactions-Influence of Fe(II)/Fe(III) ratio on catalytic performance., *J. Hazard. Mater.* 241–242 (2012) 433–40. doi:10.1016/j.jhazmat.2012.09.068.
- [197] L. Szpyrkowicz, C. Juzzolino, S.N. Kaul, A Comparative study on oxidation of

REFERENCES

- disperse dyes by electrochemical process, ozone, hypochlorite and fenton reagent, *Water Res.* 35 (2001) 2129–2136. doi:10.1016/S0043-1354(00)00487-5.
- [198] L. Wang, J. Yang, Y. Li, J. Lv, J. Zou, Removal of chlorpheniramine in a nanoscale zero-valent iron induced heterogeneous Fenton system: Influencing factors and degradation intermediates, *Chem. Eng. J.* 284 (2016) 1058–1067. doi:10.1016/j.cej.2015.09.042.
- [199] X.-R. Xu, X.-Y. Li, X.-Z. Li, H.-B. Li, Degradation of melatonin by UV, UV/H₂O₂, Fe²⁺/H₂O₂ and UV/Fe²⁺/H₂O₂ processes, *Sep. Purif. Technol.* 68 (2009) 261–266. doi:10.1016/j.seppur.2009.05.013.
- [200] B.G. Kwon, D.S. Lee, N. Kang, J. Yoon, Characteristics of p-chlorophenol oxidation by Fenton's reagent, *Water Res.* 33 (1999) 2110–2118. doi:10.1016/S0043-1354(98)00428-X.
- [201] J. Weitkamp, Zeolite and catalysis, *Solid State Ionics.* 131 (2000) 175–188. doi:http://dx.doi.org/10.1016/S0167-2738(00)00632-9.
- [202] Y.G. Adewuyi, *Sonochemistry in Environmental Remediation. 2. Heterogeneous Sonophotocatalytic Oxidation Processes for the Treatment of Pollutants in Water*, *Environ. Sci. Technol.* 39 (2005) 8557–8570. doi:10.1021/es0509127.
- [203] L. Gomathi Devi, S. Girish Kumar, K. Mohan Reddy, C. Munikrishnappa, Photo degradation of methyl orange an azo dye by advanced Fenton process using zero valent metallic iron: influence of various reaction parameters and its degradation mechanism., *J. Hazard. Mater.* 164 (2009) 459–67. doi:10.1016/j.jhazmat.2008.08.017.
- [204] W. Najjar, S. Azabou, S. Sayadi, A. Ghorbel, Catalytic wet peroxide photo-oxidation of phenolic olive oil mill wastewater contaminants, *Appl. Catal. B Environ.* 74 (2007) 11–18. doi:10.1016/j.apcatb.2007.01.007.
- [205] T. Sivasankar, V.S. Moholkar, Mechanistic approach to intensification of sonochemical degradation of phenol, *Chem. Eng. J.* 149 (2009) 57–69. doi:10.1016/j.cej.2008.10.004.
- [206] E.A. Neppiras, Acoustic cavitation, *Phys. Rep.* 61 (1980) 159–251. doi:10.1016/0370-1573(80)90115-5.
- [207] H. Shemer, Y.K. Kunukcu, K.G. Linden, Degradation of the pharmaceutical metronidazole via UV, Fenton and photo-Fenton processes., *Chemosphere.* 63 (2006) 269–76. doi:10.1016/j.chemosphere.2005.07.029.
- [208] A. Tomašević, E. Kiss, S. Petrović, D. Mijin, Study on the photocatalytic degradation of insecticide methomyl in water, *Desalination.* 262 (2010) 228–234. doi:10.1016/j.desal.2010.06.019.
- [209] C. Lee, J. Yoon, Temperature dependence of hydroxyl radical formation in the hv/Fe³⁺/H₂O₂ and Fe³⁺/H₂O₂ systems., *Chemosphere.* 56 (2004) 923–34. doi:10.1016/j.chemosphere.2004.04.047.
- [210] L. Snyder, J. Kirkland, J. Dolan, *Introduction to Modern Liquid Chromatography 3rd Edition*, 2010.
- [211] ThermoFisher Scientific, *Mass Analyzer Technology Overview*, (2017). <https://www.thermofisher.com/fr/fr/home/industrial/mass-spectrometry/mass-spectrometry-learning-center/mass-spectrometry-technology-overview/mass-analyzer-technology-overview.html> (accessed January 22, 2017).
- [212] Shimadzu, *TOC-L TOC Analyzer : SHIMADZU*, (2014). <http://www.shimadzu.com/an/toc/lab/toc-l4.html> (accessed March 22, 2014).
- [213] J. Rodier, B. Legube, N. Merlet, R. Brunet, *L'analyse de l'eau - 9ème édition - Eaux naturelles, eaux résiduaires, eau de mer: Eaux naturelles, eaux résiduaires, eau de mer*, Dunod, 2009.
- [214] D.W. O'Sullivan, M. Tyree, The kinetics of complex formation between Ti(IV) and

REFERENCES

- hydrogen peroxide, *Int. J. Chem. Kinet.* 39 (2007) 457–461.
- [215] C. Boss, K. Fredeen, *Concepts, Instrumentation and Techniques in Inductively Coupled Plasma Optical Emission Spectrometry*, Perkin Elmer, 1997.
- [216] Purdue University, *Scanning Electron Microscope*, (2014). <https://www.purdue.edu/epps/rem/rs/sem.htm> (accessed January 24, 2017).
- [217] J.-Y. Park, Y.-J. Lee, P.K. Khanna, K.-W. Jun, J.W. Bae, Y.H. Kim, Alumina-supported iron oxide nanoparticles as Fischer–Tropsch catalysts: Effect of particle size of iron oxide, *J. Mol. Catal. A Chem.* 323 (2010) 84–90. doi:10.1016/j.molcata.2010.03.025.
- [218] S.G. Marchetti, M.V. Cagnoli, J.F. Bengoa, R.C. Mercader, A.A. Yeramían, Study of the Fe/Zeolite-L system Part II: CO and H₂ chemisorption behavior, *Appl Surf Sci.* 165 (2000) 100–108.
- [219] J.S. Noh, J.A. Schwarz, Estimation of the point of zero charge of simple oxides by mass titration, *J. Colloid Interface Sci.* 130 (1989) 157–164. doi:10.1016/0021-9797(89)90086-6.
- [220] BASF, *Ibuprofen 38 - Technical information*, (2010) 14. http://www.pharma-ingredients.basf.com/Statements/TechnicalInformations/EN/PharmaSolutions/03_030720e_Ibuprofen.pdfRjU6vmF4zaygPqx4HQCQ&usg=AFQjCNGtAs eHO35b7LLCTIPs4Qfg30zvLA&sig2=Djk-8JNE5hRssyO0b5Wi8A&bvm=bv.65788261,d.bGQ.
- [221] S. Miralles-Cuevas, A. Arqués, M.I. Maldonado, J. a. Sánchez-Pérez, S. Malato Rodríguez, Combined nanofiltration and photo-Fenton treatment of water containing micropollutants, *Chem. Eng. J.* 224 (2013) 89–95. doi:10.1016/j.cej.2012.09.068.
- [222] R. Andreozzi, Advanced oxidation processes (AOP) for water purification and recovery, *Catal. Today.* 53 (1999) 51–59. doi:10.1016/S0920-5861(99)00102-9.
- [223] G. Gonzalez, A. Sagarzazu, T. Zoltan, Influence of Microstructure in Drug Release Behavior of Silica Nanocapsules, *J. Drug Deliv.* 2013 (2013) 1–8. doi:10.1155/2013/803585.
- [224] E. Carmona, V. Andreu, Y. Picó, Occurrence of acidic pharmaceuticals and personal care products in Turia River Basin: From waste to drinking water, *Sci. Total Environ.* 484 (2014) 53–63. doi:10.1016/j.scitotenv.2014.02.085.
- [225] A.S. Mestre, J. Pires, J.M.F. Nogueira, A.P. Carvalho, Activated carbons for the adsorption of ibuprofen, *Carbon N. Y.* 45 (2007) 1979–1988. doi:10.1016/j.carbon.2007.06.005.
- [226] B. Thokchom, K. Kim, J. Park, J. Khim, Ultrasonically enhanced electrochemical oxidation of ibuprofen., *Ultrason. Sonochem.* 22 (2015) 429–36. doi:10.1016/j.ultsonch.2014.04.019.
- [227] S. Yalkowsky, Y. He, P. Jain, *Handbook of Aqueous Solubility Data*, Second Edition, 2010.
- [228] K.D. Ertel, R.A. Heasley, C. Koegel, A. Chakrabarti, J.T. Carstensen, Determination of ibuprofen vapor pressure at temperatures of pharmaceutical interest, *J. Pharm. Sci.* 79 (2016) 552. doi:10.1002/jps.2600790620.
- [229] R. Xiao, M. Noerpel, H. Ling Luk, Z. Wei, R. Spinney, Thermodynamic and kinetic study of ibuprofen with hydroxyl radical: A density functional theory approach, *Int. J. Quantum Chem.* 114 (2014) 74–83. doi:10.1002/qua.24518.
- [230] HERA, *Hydrogen Peroxide*, (2005). http://www.heraproject.com/files/36-f-05-shor_h2o2_version1.pdf.
- [231] Sigma-Aldrich, *H₂O₂*, (2017). <http://www.sigmaaldrich.com/catalog/product/sial/95294?lang=fr®ion=FR> (accessed February 10, 2017).

REFERENCES

- [232] Chemspider, Iron(II) sulfate heptahydrate, (n.d). <http://www.chemspider.com/Chemical-Structure.56413.html> (accessed February 10, 2017).
- [233] Chemical Book, Ferrous sulfate heptahydrate, (2016). http://www.chemicalbook.com/ChemicalProductProperty_EN_CB9232125.htm (accessed February 10, 2017).
- [234] S.M. Auerbach, K.A. Carrado, P.K. Dutta, Handbook of Zeolite Science and Technology, CRC Press, 2003.
- [235] S. Giannakis, S. Papoutsakis, E. Darakas, A. Escalas-Cañellas, C. Pétrier, C. Pulgarin, Ultrasound enhancement of near-neutral photo-Fenton for effective E. coli inactivation in wastewater, *Ultrason. Sonochem.* 22 (2015) 515–26.
- [236] T.J. Mason, J.P. Lorimer, D.M. Bates, Quantifying sonochemistry: Casting some light on a “black art,” *Ultrasonics.* 30 (1992) 40–42.
- [237] S. Song, L. Zhan, Z. He, L. Lin, J. Tu, Z. Zhang, et al., Mechanism of the anodic oxidation of 4-chloro-3-methyl phenol in aqueous solution using Ti/SnO₂-Sb/PbO₂ electrodes., *J. Hazard. Mater.* 175 (2010) 614–21. doi:10.1016/j.jhazmat.2009.10.051.
- [238] S.T. Martin, A.T. Lee, M.R. Hoffmann, Chemical mechanism of inorganic oxidants in the TiO₂/UV process: Increased rates of degradation of chlorinated hydrocarbons, *Environ. Sci. Technol.* 29 (1995) 2567–2573.
- [239] L. Xu, J. Wang, A heterogeneous Fenton-like system with nanoparticulate zero-valent iron for removal of 4-chloro-3-methyl phenol., *J. Hazard. Mater.* 186 (2011) 256–64. doi:10.1016/j.jhazmat.2010.10.116.
- [240] I. Oller, S. Malato, J.A. Sánchez-Pérez, Combination of advanced oxidation processes and biological treatments for wastewater decontamination-a review, *Sci. Total Environ.* 409 (2011) 4141–4166.
- [241] S.O. Ganiyu, E.D. van Hullebusch, M. Cretin, G. Esposito, M.A. Oturan, Coupling of membrane filtration and advanced oxidation processes for removal of pharmaceutical residues: A critical review, *Sep. Purif. Technol.* 156 (2015) 891–914.
- [242] F. Torrades, J. García-Montaño, Using central composite experimental design to optimize the degradation of real dye wastewater by Fenton and photo-Fenton reactions, *Dye. Pigment.* 100 (2014) 184–189. doi:10.1016/j.dyepig.2013.09.004.
- [243] M. V. Bagal, P.R. Gogate, Wastewater treatment using hybrid treatment schemes based on cavitation and Fenton chemistry: a review, *Ultrason. Sonochem.* 21 (2014) 1–14.
- [244] J.-W. Kang, H.-M. Hung, A. Lin, M.R. Hoffmann, Sonolytic Destruction of Methyl tert-Butyl Ether by Ultrasonic Irradiation: The Role of O₃, H₂O₂, Frequency, and Power Density, *Environ. Sci. Technol.* 33 (1999) 3199–3205. doi:10.1021/es9810383.
- [245] P.R. Gogate, Cavitation: an auxiliary technique in wastewater treatment schemes, *Adv. Environ. Res.* 6 (2002) 335–358. doi:10.1016/S1093-0191(01)00067-3.
- [246] INERIS, 1-hydroxy-ibuprofene, (2012). <http://www.ineris.fr/substances/fr/substance/2916> (accessed December 1, 2016).
- [247] INERIS, Données technico-économiques sur les substances chimiques en France : Ibuprofène, DRC-11-118962-11078A, 2011.
- [248] R. Xiao, D. Diaz-Rivera, Z. He, L.K. Weavers, Using pulsed wave ultrasound to evaluate the suitability of hydroxyl radical scavengers in sonochemical systems, *Ultrason. Sonochem.* 20 (2013) 990–996.
- [249] P. Villegas-Guzman, J. Silva-Agredo, A.L. Giraldo-Aguirre, O. Flórez-Acosta, C. Petrier, R.A. Torres-Palma, Enhancement and inhibition effects of water matrices during the sonochemical degradation of the antibiotic dicloxacillin, *Ultrason. Sonochem.* 22 (2015) 211–219.

REFERENCES

- [250] P.R. Gogate, V.S. Sutkar, A.B. Pandit, Sonochemical reactors: Important design and scale up considerations with a special emphasis on heterogeneous systems, *Chem. Eng. J.* 166 (2011) 1066–1082.
- [251] M.A. Beckett, I. Hua, Impact of ultrasonic frequency on aqueous sonoluminescence and sonochemistry, *J. Phys. Chem. A.* 105 (2001) 3796–3802.
- [252] C. Pétrier, D. Casadonte, The sonochemical degradation of aromatic and chloroaromatic contaminants, *Adv. Sonochemistry.* 6 (2001) 92–108.
- [253] H. Delmas, N.T. Le, L. Barthe, C. Julcour-Lebigue, Optimization of hydrostatic pressure at varied sonication conditions – power density, intensity, very low frequency – for isothermal ultrasonic sludge treatment, *Ultrason. Sonochem.* 25 (2015) 51–59. doi:10.1016/j.ultsonch.2014.08.011.
- [254] G. V. Buxton, C.L. Greenstock, W.P. Helman, A.B. Ross, Critical review of rate constants for reactions of hydrated electrons, hydrogen atoms and hydroxyl radicals ($\cdot\text{OH}/\cdot\text{O}$ – in Aqueous Solution, *J. Phys. Chem. Ref. Data.* 17 (1988) 513–886. doi:10.1063/1.555805.
- [255] Pubchem, Hydrogen peroxide, (2017). https://pubchem.ncbi.nlm.nih.gov/compound/hydrogen_peroxide#section=Top (accessed January 16, 2016).
- [256] M.C. DeRosa, R.J. Crutchley, Photosensitized singlet oxygen and its applications, *Coord. Chem. Rev.* 233 (2002) 351–371. doi:10.1016/S0010-8545(02)00034-6.
- [257] B.A. Wols, C.H.M. Hofman-Caris, Review of photochemical reaction constants of organic micropollutants required for UV advanced oxidation processes in water., *Water Res.* 46 (2012) 2815–27. doi:10.1016/j.watres.2012.03.036.
- [258] M. Marković, M. Jović, D. Stanković, V. Kovačević, G. Roglić, G. Gojgić-Cvijović, et al., Application of non-thermal plasma reactor and Fenton reaction for degradation of ibuprofen, *Sci. Total Environ.* 505 (2015) 1148–55.
- [259] P.. Malik, S.. Saha, Oxidation of direct dyes with hydrogen peroxide using ferrous ion as catalyst, *Sep. Purif. Technol.* 31 (2003) 241–250. doi:10.1016/S1383-5866(02)00200-9.
- [260] S.A. Hamburger, P.B. McCay, Spin Trapping of Ibuprofen Radicals: Evidence That Ibuprofen is a Hydroxyl Radical Scavenger, *Free Radic. Res. Commun.* 9 (1990) 337–342. doi:10.3109/10715769009145692.
- [261] T.P. Kennedy, N. V Rao, W. Noah, J.R. Michael, M.H. Jafri, G.H. Gurtner, et al., Ibuprofen prevents oxidant lung injury and in vitro lipid peroxidation by chelating iron., *J. Clin. Invest.* 86 (1990) 1565–1573.
- [262] C.G. Joseph, G. Li Puma, A. Bono, D. Krishnaiah, Sonophotocatalysis in advanced oxidation process: a short review., *Ultrason. Sonochem.* 16 (2009) 583–9. doi:10.1016/j.ultsonch.2009.02.002.
- [263] L.J. Xu, W. Chu, N. Graham, Sonophotolytic degradation of dimethyl phthalate without catalyst: analysis of the synergistic effect and modeling., *Water Res.* 47 (2013) 1996–2004.
- [264] F. Zaviska, P. Drogui, E.M. El Hachemi, E. Naffrechoux, Effect of nitrate ions on the efficiency of sonophotochemical phenol degradation, *Ultrason. Sonochem.* 21 (2014) 69–75. doi:10.1016/j.ultsonch.2013.08.003.
- [265] M.P. Rayaroth, U.K. Aravind, C.T. Aravindakumar, Degradation of pharmaceuticals by ultrasound-based advanced oxidation process, *Environ. Chem. Lett.* 14 (2016) 259–290.
- [266] S. Loaiza-Ambuludi, M. Panizza, N. Oturan, M.A. Oturan, Removal of the anti-inflammatory drug ibuprofen from water using homogeneous photocatalysis, *Catal. Today.* 224 (2014) 29–33. doi:10.1016/j.cattod.2013.12.018.

REFERENCES

- [267] L.K. Weavers, F.H. Ling, M.R. Hoffmann, Aromatic Compound Degradation in Water Using a Combination of Sonolysis and Ozonolysis, *Environ. Sci. Technol.* 32 (1998) 2727–2733. doi:10.1021/es970675a.
- [268] M. Skoumal, R.M. Rodríguez, P.L. Cabot, F. Centellas, J.A. Garrido, C. Arias, et al., Electro-Fenton, UVA photoelectro-Fenton and solar photoelectro-Fenton degradation of the drug ibuprofen in acid aqueous medium using platinum and boron-doped diamond anodes, *Electrochim. Acta.* 54 (2009) 2077–2085. doi:10.1016/j.electacta.2008.07.014.
- [269] G. Caviglioli, P. Valeria, P. Brunella, C. Sergio, A. Attilia, B. Gaetano, Identification of degradation products of Ibuprofen arising from oxidative and thermal treatments, *J. Pharm. Biomed. Anal.* 30 (2002) 499–509. doi:10.1016/S0731-7085(02)00400-4.
- [270] L.E. Jacobs, R.L. Fimmen, Y.-P. Chin, H.E. Mash, L.K. Weavers, Fulvic acid mediated photolysis of ibuprofen in water., *Water Res.* 45 (2011) 4449–58. doi:10.1016/j.watres.2011.05.041.
- [271] J. V. Castell, M.J. Gomez-L., M.A. Miranda, I.M. Morera, Photolytic degradation of ibuprofen. Toxicity of the isolated photoproducts on fibroblasts and erythrocytes, *Photochem. Photobiol.* 46 (1987) 991–996. doi:10.1111/j.1751-1097.1987.tb04882.x.
- [272] H. Gong, W. Chu, S.H. Lam, A.Y.-C. Lin, Ibuprofen degradation and toxicity evolution during Fe²⁺/Oxone/UV process, *Chemosphere.* 167 (2017) 415–421. doi:10.1016/j.chemosphere.2016.10.027.
- [273] M. Tokumura, A. Sugawara, M. Raknuzzaman, M. Habibullah-Al-Mamun, S. Masunaga, Comprehensive study on effects of water matrices on removal of pharmaceuticals by three different kinds of advanced oxidation processes, *Chemosphere.* 159 (2016) 317–325. doi:10.1016/j.chemosphere.2016.06.019.
- [274] T.E. Doll, F.H. Frimmel, Photocatalytic degradation of carbamazepine, clofibric acid and iomeprol with P25 and Hombikat UV100 in the presence of natural organic matter (NOM) and other organic water constituents, *Water Res.* 39 (2005) 403–411. doi:10.1016/j.watres.2004.09.016.
- [275] M. Neamțu, D. Grandjean, A. Sienkiewicz, S. Le Faucheur, V. Slaveykova, J.J.V. Colmenares, et al., Degradation of eight relevant micropollutants in different water matrices by neutral photo-Fenton process under UV254 and simulated solar light irradiation – A comparative study, *Appl. Catal. B Environ.* 158 (2014) 30–37. doi:10.1016/j.apcatb.2014.04.001.
- [276] A.O. Yazaydin, R.W. Thompson, Molecular simulation of the adsorption of mtbe in silicalite, mordenite, and zeolite beta, *J. Phys. Chem. B.* 110 (2006) 14458–14462.
- [277] K.A. Sashkina, E.V. Parkhomchuk, N.A. Rudina, V.N. Parmon, The role of zeolite Fe-ZSM-5 porous structure for heterogeneous Fenton catalyst activity and stability, *Microporous Mesoporous Mater.* 189 (2014) 181–188. doi:10.1016/j.micromeso.2013.11.033.
- [278] L. Sanchez-Prado, R. Barro, C. Garcia-Jares, M. Llompарт, M. Lores, C. Petrakis, et al., Sonochemical degradation of triclosan in water and wastewater, 2008. doi:10.1016/j.ultsonch.2008.01.007.
- [279] O.B. Mathre, Destruction of cyanide in aqueous solutions, 1971.
- [280] E. Yazici, H. Deveci, Factors affecting decomposition of hydrogen peroxide, in: *Proc. XII Th Int. Miner. Process. Symp.*, 2010: pp. 609–616. doi:10.13140/RG.2.1.1530.0648.
- [281] J.K. Kim, F. Martinez, I.S. Metcalfe, The beneficial role of use of ultrasound in heterogeneous Fenton-like system over supported copper catalysts for degradation of p-chlorophenol, *Catal. Today.* 124 (2007) 224–231. doi:10.1016/j.cattod.2007.03.040.
- [282] G. Zhang, I. Hua, The impact of particulates on the aqueous sonication of

REFERENCES

- bromobenzene, *Chemosphere*. 46 (2002) 59–66. doi:10.1016/S0045-6535(01)00079-0.
- [283] J. Hartmann, P. Bartels, U. Mau, M. Witter, W. V Tümpling, J. Hofmann, et al., Degradation of the drug diclofenac in water by sonolysis in presence of catalysts., *Chemosphere*. 70 (2008) 453–61. doi:10.1016/j.chemosphere.2007.06.063.
- [284] A. Keck, E. Gilbert, R. Köster, Influence of particles on sonochemical reactions in aqueous solutions, *Ultrasonics*. 40 (2002) 661–665. doi:10.1016/S0041-624X(02)00195-6.
- [285] A. Grönroos, H. Kyllönen, K. Korpijärvi, P. Pirkonen, T. Paavola, J. Jokela, et al., Ultrasound assisted method to increase soluble chemical oxygen demand (SCOD) of sewage sludge for digestion, *Ultrason. Sonochem.* 12 (2005) 115–120. doi:10.1016/j.ultsonch.2004.05.012.
- [286] S.J. Doktycz, K.S. Suslick, Interparticle collisions driven by ultrasound, *Science* (80-.). 247 (1990) 1067–1069.
- [287] K.S. Suslick, S.J. Doktycz, E.B. Flint, On the origin of sonoluminescence and sonochemistry, *Ultrasonics*. 28 (1990) 280–290.
- [288] T. Leong, M. Ashokkumar, S. Kentish, The fundamentals of power ultrasound - A Review, *Acoust. Aust.* 39 (2011) 54–63.
- [289] T.J. Mason, *Practical sonochemistry: user's guide to applications in chemistry and chemical engineering*, E. Horwood, 1991.
- [290] M. Bobu, A. Yediler, I. Siminiceanu, S. Schulte-Hostede, Degradation studies of ciprofloxacin on a pillared iron catalyst, *Appl. Catal. B Environ.* 83 (2008) 15–23. doi:10.1016/j.apcatb.2008.01.029.
- [291] J. Deng, J. Jiang, Y. Zhang, X. Lin, C. Du, Y. Xiong, FeVO₄ as a highly active heterogeneous Fenton-like catalyst towards the degradation of Orange II, *Appl. Catal. B Environ.* 84 (2008) 468–473. doi:10.1016/j.apcatb.2008.04.029.
- [292] K.S. Suslick, D.J. Casadonte, Heterogeneous sonocatalysis with nickel powder, *J. Am. Chem. Soc.* 109 (1987) 3459–3461. doi:10.1021/ja00245a047.
- [293] P. Forzatti, Catalyst deactivation, *Catal. Today*. 52 (1999) 165–181. doi:10.1016/S0920-5861(99)00074-7.

APPENDIX

This page is intentionally left blank

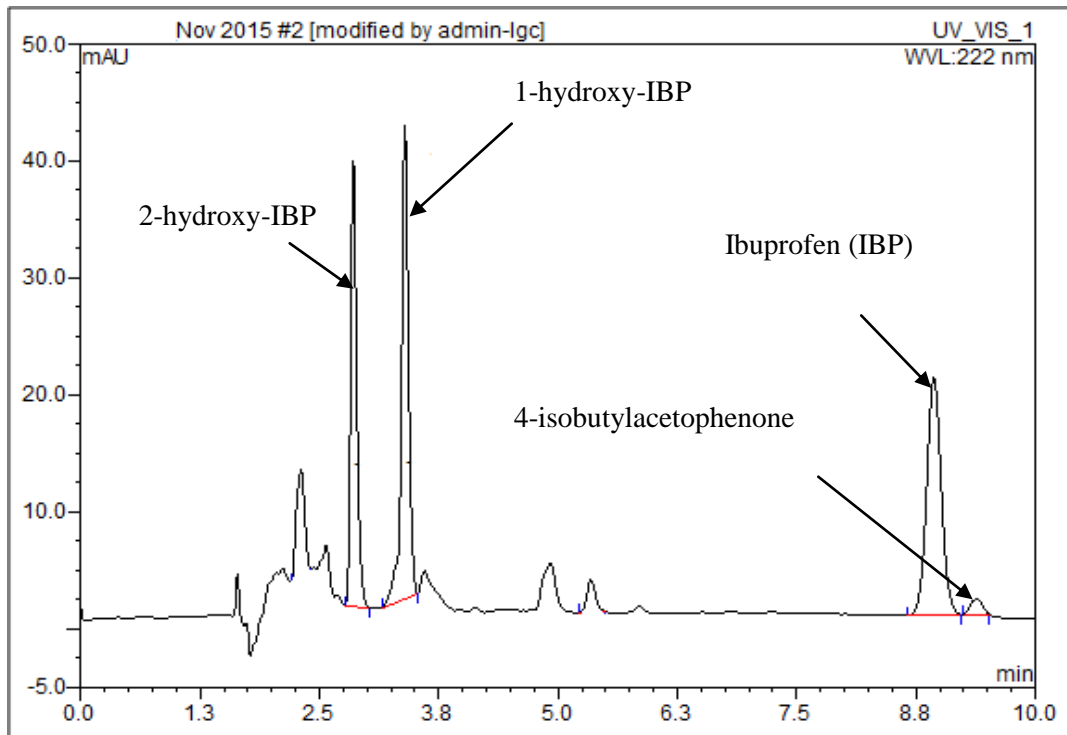


Figure I. Separation of IBP and transformation products by HPLC/UV

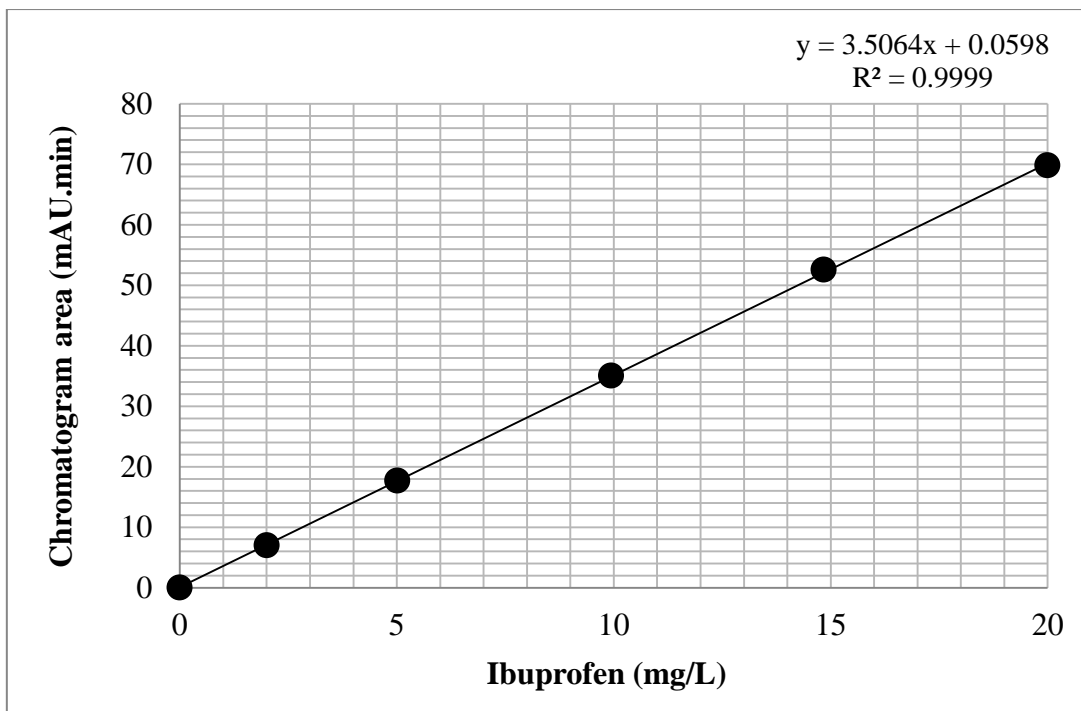


Figure II. Calibration curve of ibuprofen

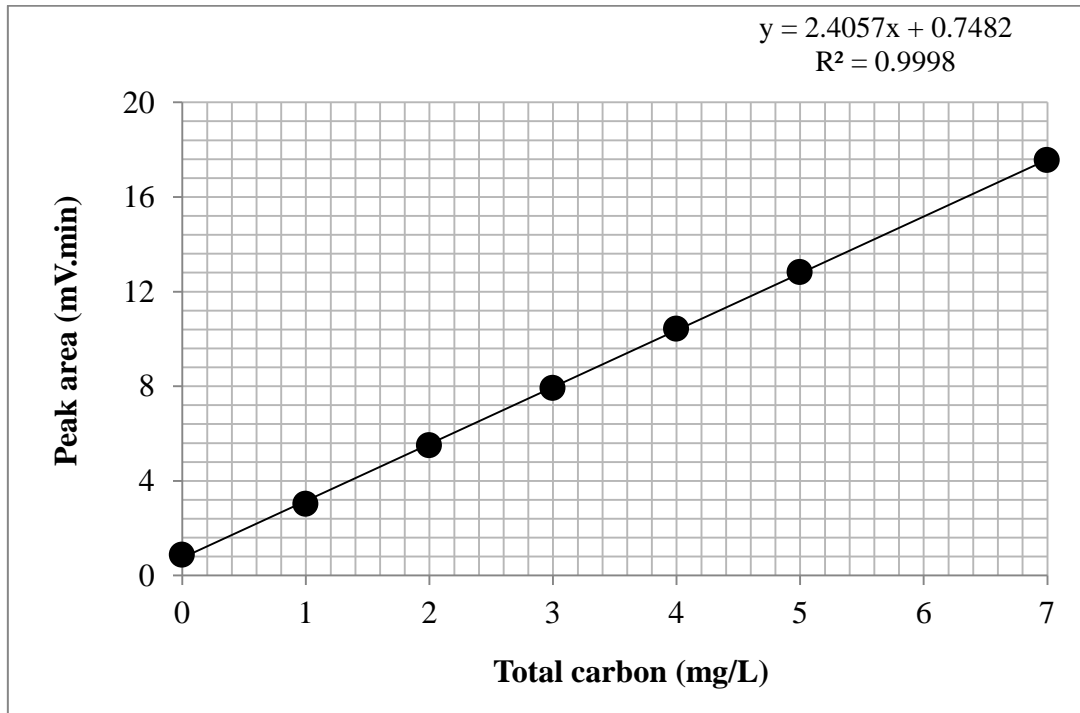


Figure III. Calibration curve of total carbon (TC)

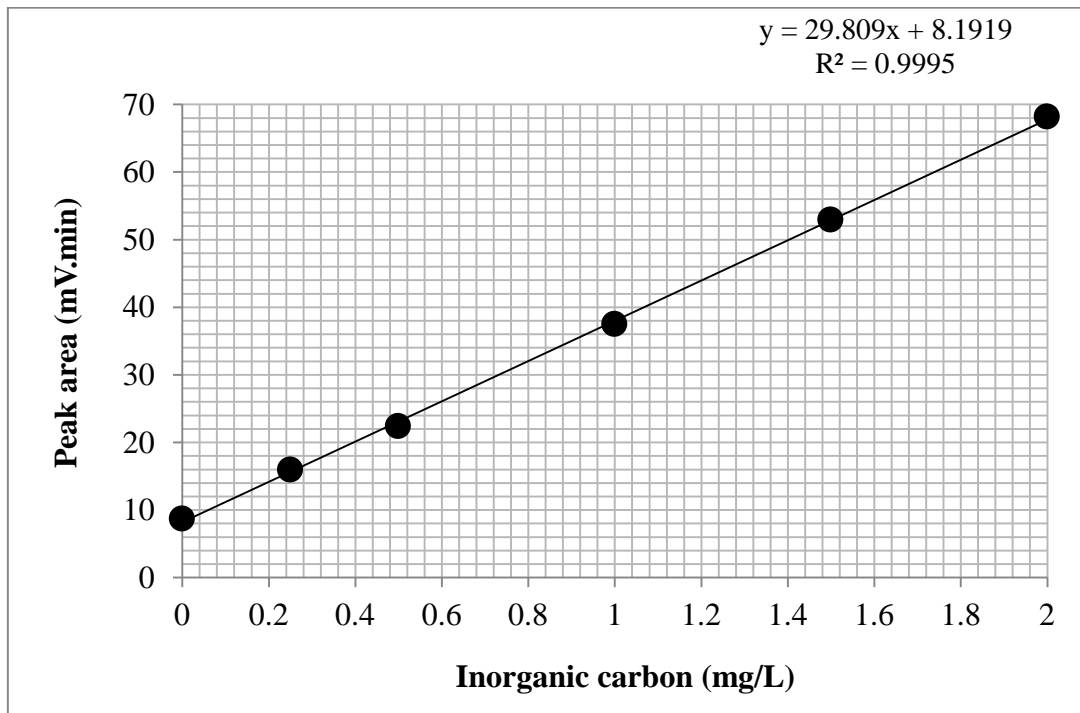


Figure IV. Calibration curve of inorganic carbon (IC)

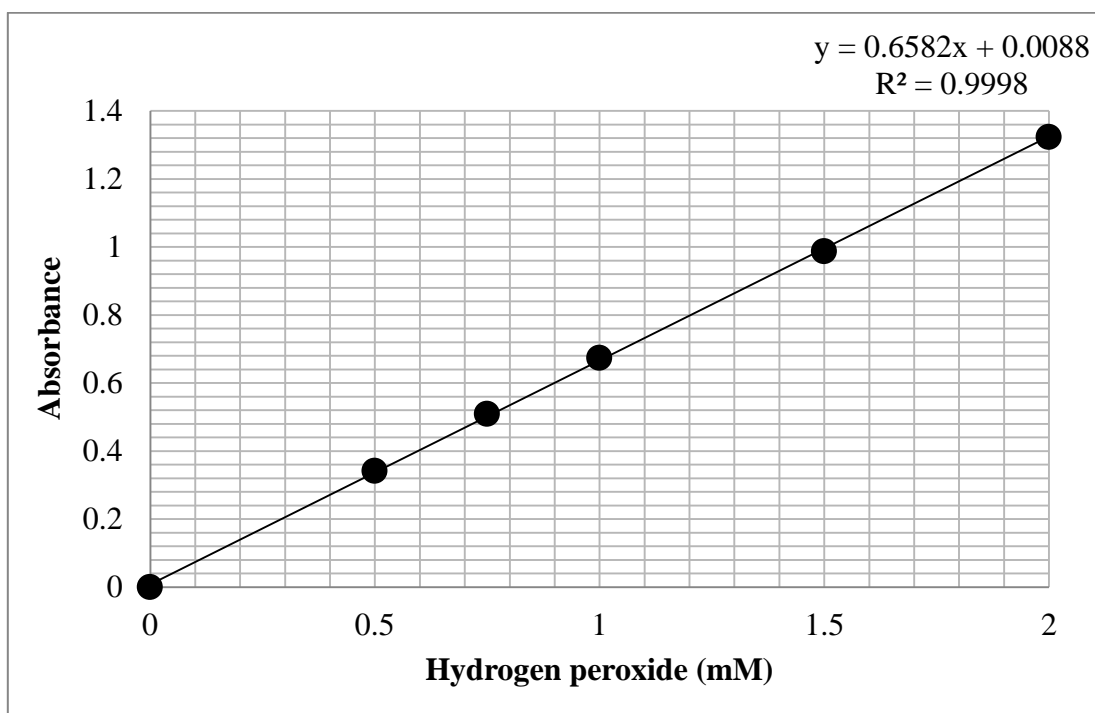


Figure V. Calibration curve of hydrogen peroxide (H_2O_2)

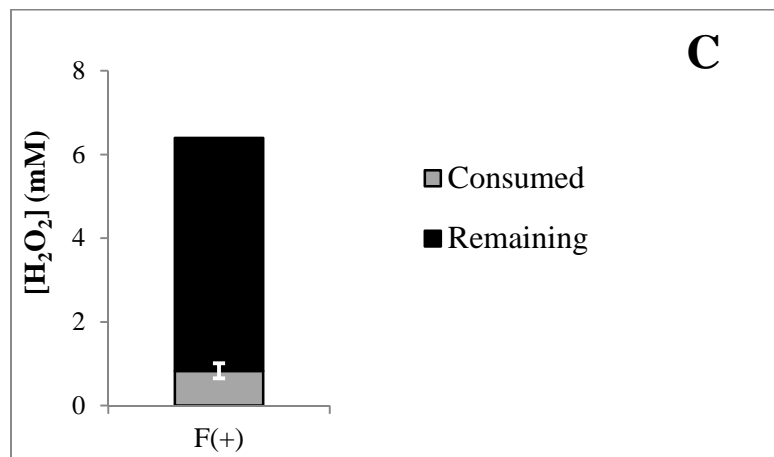
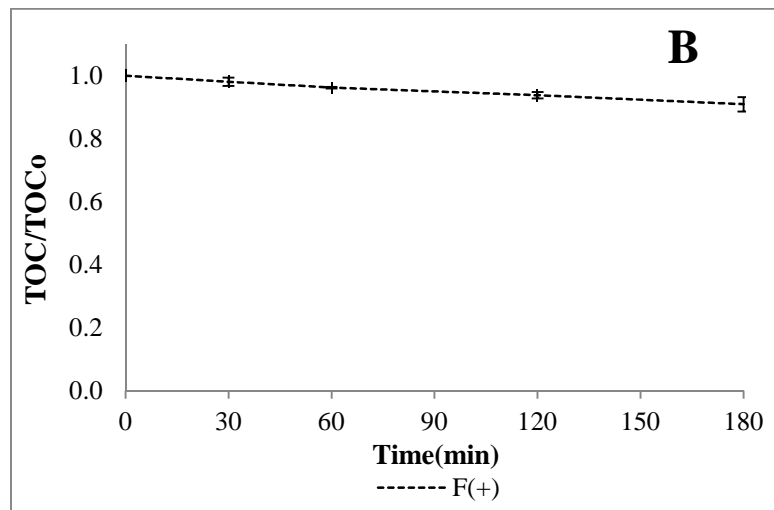
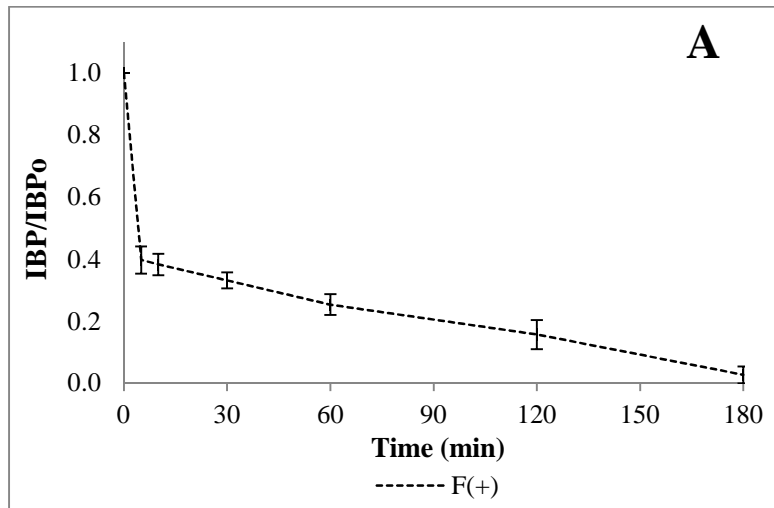


Figure VI. Example of experiment with error bars
 Degradation of IBP by Fenton oxidation: (A) IBP and (B) TOC concentration-time profiles, and (C)
 H₂O₂ consumption
 ([IBP]₀ = 20 mg/L, pH₀ = 2.6, T = 25°C, [Fe²⁺]₀ = 0.134 mM and [H₂O₂]₀ = 6.4 mM)